The Development and Application of Microelectrochemical Sensors for Real-Time Neurochemical Monitoring of Biological Markers of Oxidative Stress

A thesis submitted by

Michelle M. Doran B.Sc. (Hons.)

to

Maynooth University

For the degree of Doctor of Philosophy

Based on the research carried out in the

Department of Chemistry, Faculty of Science and Engineering,

Maynooth University, Maynooth, Co Kildare

Under the supervision of

Prof. John.P. Lowry and Dr. Niall. J. Finnerty

And direction of

Head of Department: Dr. John Stephens

December 2016

Table of Contents

Chapter 1: Introduction

Chapter 2: Theory

Chapter 3: Experimental

Chapter 4: Development

Chapter 6: NO and O_2 Monitoring in PD Model

Declaration

This thesis has not been submitted before, in whole or in part, to this or any other University for any degree, and except where otherwise stated, is the original work of the author. The research on the development of the superoxide biosensor was supervised by Dr. Niall J. Finnerty. All *in-vivo* research work was supervised by Prof. John P. Lowry

Signed: _____

Michelle Doran

To Mam and Dad

Acknowledgments

Firstly I would like to thank my supervisors Prof. John Lowry and Dr. Niall Finnerty. John thank you for providing me with this wonderful opportunity to be part of your research group. I am grateful for all the guidance, support and encouragement you provided me with over the past four years. A special thanks for all the patience and help during the last few months with the correcting and proof reading of this thesis. Niall thank you for all your help and direction and for answering the millions of questions I asked. Your enthusiasm and support throughout the research was much appreciated. I was privileged to have such fantastic supervision which made the writing of this thesis possible for that I am truly appreciative.

This research was funded by the Irish Research Council (Project No: RS/2012/152) and Maynooth University John and Pat Hume Scholarships and these are gratefully acknowledged.

A special thanks to all the people in our research group that I have worked with over the years: Keeley, Andrea, Saidhbhe, Fiachra, John, Gama, Michelle, Ken and Rachel. I was privileged to work with so many doctors the knowledge and enthusiasm each one of you have for our line of work is inspirational. Thank you for all the help, support and encouragement you provided me with over the years it's truly appreciated. I wish you all the very best in the future. Thanks to Caroline my only 4th year student sorry for the 'horrible' project. You were always there to listen, to provide encouragement and you brightened many a day with your mammy's baking. Thanks to Karen who always provided the lab with an endless supply of mints and soap. Your help and encouragement were much appreciated.

Thanks to all the academic staff, technicians, Noel, Carol and Donna. I am very grateful for all the help and support you gave me throughout my journey in Maynooth. Thanks to all the postgrads and postdocs in the Chemistry department. Firstly, thanks to everyone I shared the write-up room with Andrew, Justine, Chris, Ross and Matthew for all the help and encouragement and the chatting when a break was needed. To Jessica who showed me what happens when you leave your computer unlocked in the write-up room. Thanks to Collette for all the Thursday lunches, coffees and walks and the support and encouragement you gave me. I have had a fantastic experience in Maynooth and I was lucky to share this experience with Sam, Jessica, Emer, Harlei, Michelle Q, Alice, Lucy, Muhib, Mark G, Mark K, Michelle K, Xiang, Nan and Aoife over the past four years. Thanks for all the nights out, cinema trips,

lunches, chats and laughs and for the friendships I am very grateful and I wish each one of you every success and happiness in everything you do or wish to do in the future.

Thank you to all my friends especially Ali, Niamh, Michelle, Rachael, Jen and Sam. I am so grateful for your willingness to provide a distraction with the Saturday nights out, lunches, cinema trips and trips away over the years. Thanks a million for the constant encouragement and support you gave me throughout this process. I am blessed and privileged to have such amazing friends that have helped me throughout my studies.

Special thanks to my family who have supported me throughout my studies. To my mam and dad for the constant support, love and encouragement you provided me with over the years I am grateful for always taking an interest in everything I did without them I would not have been able to achieve this goal. To my sisters, Therese and Louise thank you for your support, kindness, love and encouragement. For all the shopping trips, cinema trips, holidays and walks and for always being there for a chat or to listen especially when I needed it most. To my brother Matthew who has the ability to make me laugh on a daily basis with his insightful conversations. Your encouragement and support is much appreciated.

Finally, these four year spent in Maynooth have been fantastic and ones that I will always remember with fond memories. Thanks to everyone who made this experience so enjoyable and if I have forgotten anyone in this I will thank you in person.

Abbreviations

5HIAA	5-Hydroxyindoleactic Acid
5HT	5-Hydroxytyramine
AA	Ascorbic Acid
ANOVA	Analysis of Variance
AUC	Area Under the Curve
BSA	Bovine Serum Albumin
CNS	Central Nervous System
CPA	Constant Potential Amperometry
DHAA	Dehydroascorbic Acid
DOPAC	3,4-Dihydroxyphenlacetic acid
eNOS	Endothelial nitric oxide synthase
ECF	Extracellular Fluid
FAD	Flavin adenine dinucleotide
GA	Glutaraldehyde
HVA	Homovanillic Acid
H_2O_2	Hydrogen Peroxide
HPLC	High Performance Liquid Chromatography
iNOS	Inducible nitric oxide synthase
K_M	Michaelis-Menten constant
LIVE	Long Term *In-Vivo* Electrochemistry
LOD	Limit of Detection
L-DOPA	L-3,4-dihydroxyphenylalaine
MAO	Monoamine Oxidase
MMA	Methyl Methacrylate
MD	Microdialysis
MPTP	1-methyl-4-phenyl-1,2,3,6-tetrahydropyridine
NADH	Nicotinamide adenine dinucleotide
NADPH	Nicotinamide adenine dinucleotide phosphate

nNOS	Neuronal nitric oxide synthase
NO	Nitric oxide
NOS	Nitric Oxide Synthase
N_2	Nitrogen
O_2	Oxygen
O_2^-	Superoxide
OH	Hydroxyl
$ONOO^-$	Peroxynitrite
o-PD	*o*-Phenylenediamine
PBS	Phosphate Buffer Saline
PD	Parkinson's Disease
PEI	Polyethyleneimine
PF-LHA	Perifrontal-Lateral Hypothalamic Area
PPD	Poly(*o*-phenylenediamine)
Pt	Platinum
RNS	Reactive Nitrogen Species
ROS	Reactive Oxygen Species
SCE	Saturated Calomel Electrode
SEM	Standard Error Mean
SNpc	Substantia Pars Compacta
Sty	Styrene
SOD	Superoxide Dismutase
UA	Uric Acid
V_{max}	Maximum enzymatic velocity
XOD	Xanthine Oxidase

Abstract

This thesis investigates methods of studying oxidative stress, particularly its role in Parkinson's disease (PD) with a specific focus on the substrates oxygen (O_2), nitric oxide (NO) and superoxide (O_2). The primary aim was the *in-vitro* development and characterisation of a new O_2^- biosensor suitable for neurochemical monitoring. This thesis also details the neurochemical monitoring of NO and O_2 in an animal model of PD utilising the technique of Long Term *In-Vivo* Electrochemistry (LIVE).

Chapter 1 provides an introduction to the brain, biosensors, the chemical reactivity and formation of reactive oxygen species (ROS) and reactive nitrogen species (RNS) in biological systems, and concurrently their role in oxidative stress and the manifestation of PD. Chapter 2 describes the background theory relevant to the research undertaken, while Chapter 3 details the analytical techniques and experimental methods used in the fabrication and characterisation of the various sensor types utilised throughout this research.

The results are divided into three chapters. The first of these, Chapter 4 discusses the development and characterisation of the O_2^- biosensor outlining the various steps undertaken in the optimisation of the biosensor design with respect to O_2^- sensitivity. Chapter 5 details the interferences in the O_2^- calibration process and the relevant modifications made to the biosensor in order to minimise these interferences in the *in-vivo* environment. This chapter also includes further *in-vitro* characterisation of the O_2^- biosensor determining the response time, limit of detection (LOD) and the biosensor's ability to reject endogenous electroactive interferences present in the brain.

Chapter 6 focuses on the electrochemical detection of NO and O_2 in a reserpine mediated animal model of PD. The specific focus of this chapter is to elucidate the role of oxidative/nitrosative stress in the etiology and pathophysiology of PD. Additionally, this chapter discusses the O_2/NO circadian/diurnal changes over any 24 hr period and shows preliminary results of the impact light reversal induces on striatal NO and O_2 levels. Finally, Chapter 7 concludes the thesis, discusses the main experimental outcomes of this research and highlights potential future investigations.

Chapter 1: Introduction

1.1. Introduction

The primary aim of this thesis is the development of a sensor that can detect, with appropriate sensitivity and selectivity, the reactive oxygen species (ROS) superoxide (O_2^-) in the mammalian brain. The development of this sensor is well recognised as a critical need as O_2^- is speculated to be involved in oxidative stress which leads to neurodegenerative diseases such as Parkinson's disease (PD) and several other pathological conditions.

The mammalian brain is a very complex organ that supports a wide range of functions including sensory input and processing, behavioural output or response, emotional response, memory and cognition. The brain is comprised of approximately 10^{11}-10^{12} neurons and by at least twice as many glial cells (Emerit *et al*., 2004). The neurons are the functional units of the central nervous system (CNS) and are comprised of three parts; dendrites, cell bodies and axons. These neurons function by sending and receiving messages to and from other nerve cells. The key process of neural function is the manner in which neurons influence one another through synaptic contacts. The three main parts of a synapse include the axon terminal, the membrane encasing the tip of the dendritic spine and the synaptic cleft (See Figure 1.1). The transfer of messages between neurons occurs through synaptic transmission, which releases a neurotransmitter, which carries the message from neuron to neuron. Synaptic transmission is a complex process consisting of four steps; synthesis, release, receptor action and inactivation. When an action potential is propagated on an axon terminal, a neurotransmitter is released from the presynaptic membrane into the synaptic cleft. The neurotransmitter diffuses by exocytosis across the cleft where it binds to transmitter–activated receptors on the postsynaptic membrane, after which the neurotransmitter is deactivated.

Glial cells provide physical and functional support in the CNS and there are three types; astrocytes, microglial and oligodendrocytes. The primary function of the astrocytes is to protect the neurons from the depolarising effects of high concentrations of potassium which accumulates during high rates of neuronal activity. They also function to maintain electrical neutrality (Feldman *et al.*, 1997). Microglial are the equivalent in the nervous system of monocytes and marcophages, scavenging any dead or damaged cells (Emerit *et al.*, 2004). Oligodendrocytes produce myelin sheaths that envelop groups of axons. This significantly increases the speed and efficacy of axonal conduction.

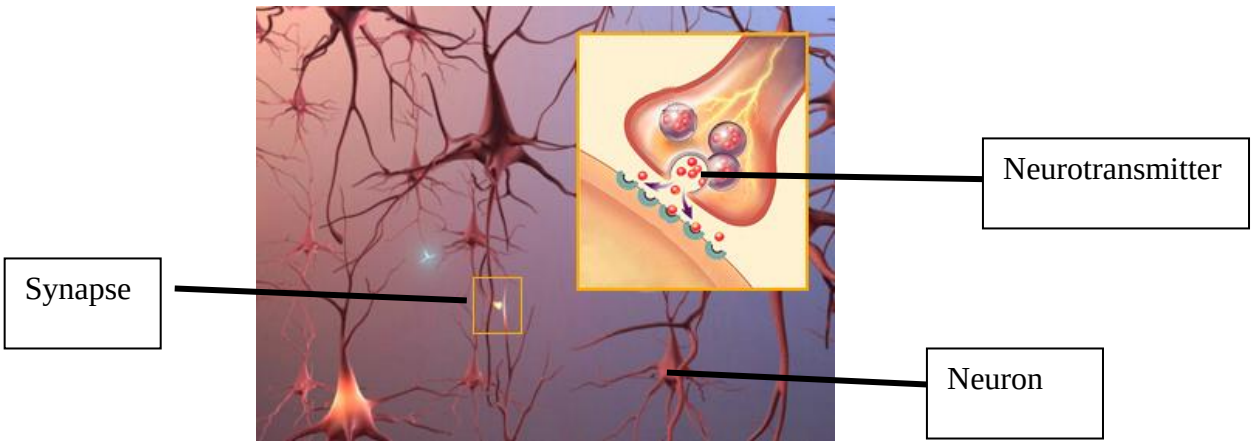

Figure 1.1.: An image displaying the structure of neurons and a synapse.

https://www.alz.org/braintour/synapses_neurotransmitters.asp

As outlined above, the brain is hugely complex and understanding the mechanisms underlying its function remains a challenge. A growing number of methodologies have been developed, including sampling, spectroscopic and electrochemical techniques, to study the neurochemical phenomena of the living brain.

1.2. Neurochemical Analysis

A number of techniques have been employed to determine the structure, metabolism and the role of neurochemicals in the brain. These include non-invasive techniques such as functional magnetic imaging (fMRI) (Austin *et al.*, 2003), positron emission tomography (PET) (Breier *et al.*, 1997) (Phelps, 2000), spectroscopic analyses, ^{1}H-NMR (Rothman *et al.*, 1993) (Mangia *et al*., 2003) (Shulman *et al.*, 1993) and ^{13}C-NMR (Gruetter *et al.*, 1998) (Rothman *et al.*, 1999) (Shen *et al.*, 1999). Other invasive techniques have also been developed including microdialysis (MD) (Miele and Fillenz, 1996) (Fray *et al.*, 1996) and long term *in-vivo* electrochemistry (LIVE) (O'Neill *et al.*, 1998) (O'Neill and Lowry, 2006).

The technique of MD facilitates the monitoring of neurotransmitters and other molecules in interstitial tissue fluid. This method is widely used for sampling and quantifying neurotransmitters, neuropeptides, and hormones in the brain and periphery (Chefer *et al.*, 2001). MD involves the implantation of a small probe into the brain which consists of a hollow tube and a semi permeable membrane. This membrane allows the passage of water and small

solutes (typically with molecular masses less than 20 kDa). On insertion of the probe into an external medium (i.e., tissue), substances at the outside surface of the dialysis membrane that are present in lower concentrations in the perfusate diffuse through the membrane into the perfusate. The perfusate slowly flows through the length of the dialysis probe into the outflow tubing where it can be collected for subsequent analyte quantification using for example high performance liquid chromatography (HPLC) and mass spectrometry (Shippenberg and Thompson, 2001). An advantage of this technique is that it provides a physical barrier between the perfusate and tissue, therefore limiting the tissue exposure to the flow of the perfusate. The selectivity of the technique and its ability to detect small concentrations of the relevant analyte are also beneficial. Conversely, MD also has drawbacks including poor temporal resolution, depletion around the probe area and also its large size limits the technique's use in smaller brain regions.

The first reports of voltammetry in the brain date back to 1958 when Clark used voltammetry to monitor oxygen (O_2) and glucose (Clark *et al.*, 1958) (Clark and Lyons, 1962). However, this technique is generally credited to the work by Adams *et al.* in 1973 (Kissinger *et al.*, 1973). Electrochemical techniques involve the application of a potential across an electrode-solution interface to oxidise or reduce species close to the electrode surface resulting in the generation of a Faradaic current (O'Neill, 1994). Several electrochemical techniques have been employed including cyclic voltammetry (CV), chronoamperometry, linear ramps, differential pulse amperometry (DPA) and constant potential amperometry (CPA). Voltammetry/Amperometry has been utilised to develop sensors for the detection of several electroactive species in the extracellular fluid (ECF) including O_2 (Bolger and Lowry, 2005) (Bolger *et al.*, 2011(b)), nitric oxide (NO) (Brown *et al.*, 2005), homovanillic acid (O'Neill and Fillenz, 1985(b)), ascorbic acid (AA) (O'Neill and Fillenz, 1985(a)) (Boutelle *et al.*, 1989), uric acid (UA) (O'Neill, 1990), dopamine (Robinson *et al.*, 2003) (Zachek *et al.*, 2008) and 5-hydroxytryptamine (5-HT) (Kristensen *et al.*, 1987*)* (Jackson *et al.*, 1995) (Wu *et al.*, 2003). However, in order to extend its application to the detection of electroinactive species (eg. glucose, lactate, glutamate) biosensors have been developed.

1.3. Biosensors

Biosensors provide a mediated system for the detection of electroinactive species in the brain. Therefore, as O_2^- is not electroactive, the development of a O_2^- biosensor is required for its detection and is the primary aim of this thesis. Chapter 4 details the various steps involved in the development of a sensitive and selective biosensor suitable for the *in-vivo* monitoring of O_2^-. A biosensor is defined as a self-contained integrated device incorporating a biological recognition element in close proximity to an electrochemical transduction element (Wilson and Gifford, 2005) (Thévenot *et al.*, 2001). A biosensor consists of three main parts; the biological recognition element, transducer and the signal processing system (Ronkainen *et al*., 2010) (Yoo and Lee, 2010). The biological recognition element, typically a protein, peptide or oligonucleide, translates information from the biochemical domain, usually the target analyte concentration into a chemical or physical output signal with a defined sensitivity. The transducer converts the signal from the recognition system into a measurable signal, while the signal processing system converts the signal into a readable form (Yoo and Lee, 2010) (Thévenot *et al.*, 2001). Biosensors can be classified as electrochemical, optical, thermometric, piezoelectric or magnetic depending on the transducer utilised (Newman and Setford, 2006).

Enzymatic biosensors are the most thoroughly investigated sensors in the biosensor field. The immobilisation of the enzyme component onto the metal electrode is achieved by various strategies including entrapment, physical adsorption and chemical bonding (Wilson and Thévenot, 1989). Enzymatic biosensors usually employ an analyte-specific molecular recognition element which enhances the sensitivity and selectivity of the sensor.

Amperometric enzyme electrodes can be divided into three categories; first, second and third generation devices. A first generation sensor monitors the consumption of O_2 (Clark and Lyons, 1962) or the production of hydrogen peroxide (H_2O_2) (Lowry and O'Neill, 1994). These sensors have limitations due to fluctuations in response to O_2 and interference from electroactive species as a result of the large potential required for the oxidation of H_2O_2. Second generation biosensors use a low overpotential and replace the O_2 required in the enzymatic reaction with a redox mediator (El Atrash and O'Neill, 1995) (Cass *et al.*, 1984). Problems associated with these devices include leaching of the untethered mediator from the enzyme layer, toxicity in biological tissues and redox interferences (McMahon *et al.*, 2007). Third generation biosensors are based on direct electron transfer between the active centre of the redox enzymes and the electrode (Chaubey *et al.*, 2000) (Kulys *et al.*, 1980). This approach is extremely difficult for

oxidase enzymes as the distance between the flavin adenine dinucleotide (FAD) active site and the electrodes is such that direct electron transfer to the electrode takes place slowly, or not at all. However, third generation biosensors based on peroxidase and laccase enzymes have been developed (Radi *et al*., 2009) (Rodríguez-Delgado *et al*., 2015). Early reports of third generation biosensors using organic salt electrodes are now considered mediated systems (Lowry and O'Neill, 2005).

Biosensors have found applications in a diverse range of areas including biomedical studies, medical diagnostics, drug discovery, food safety, process control, environmental monitoring and are key components in HPLC detectors (Turner, 2013) (El Atrash and O'Neill, 1995). Biosensors used for neurochemical analysis, benefit from high temporal resolution and small size. The small diameter size (127-µm bare diameter, 203-µm coated diameter) of the Pt electrode used throughout the development of this biosensor is below the threshold for cellular damage *in-vivo*. This finding was established by measuring UA release as a result of glial reaction during perturbation of brain tissue by metal electrodes of varying diameters and demonstrated that 5T Pt wire showed no significant difference in the glial cell count measured at three different regions; near, mid and far from the 5T sensors (Duff and O'Neill, 1994).

1.4 Reactive Oxygen Species

Molecular O_2 is relatively unreactive, however, O_2 derivatives more prone to participate in chemical reactions are formed during aerobic metabolism and in the environment (see Figure 1.2). The primary ROS produced *in-vivo* is O_2^- by the univalent reduction of O_2. This radical has both reducing and oxidising properties, reacting predominantly with metal ions and iron-sulfur clusters. Other ROS include H_2O_2, peroxynitrite ($ONOO^-$), myeloperoxidase, carbonate radical, hydroxyl radical (OH) and also singlet oxygen (Kowaltowski *et al.*, 2009) (Bartosz, 2009).

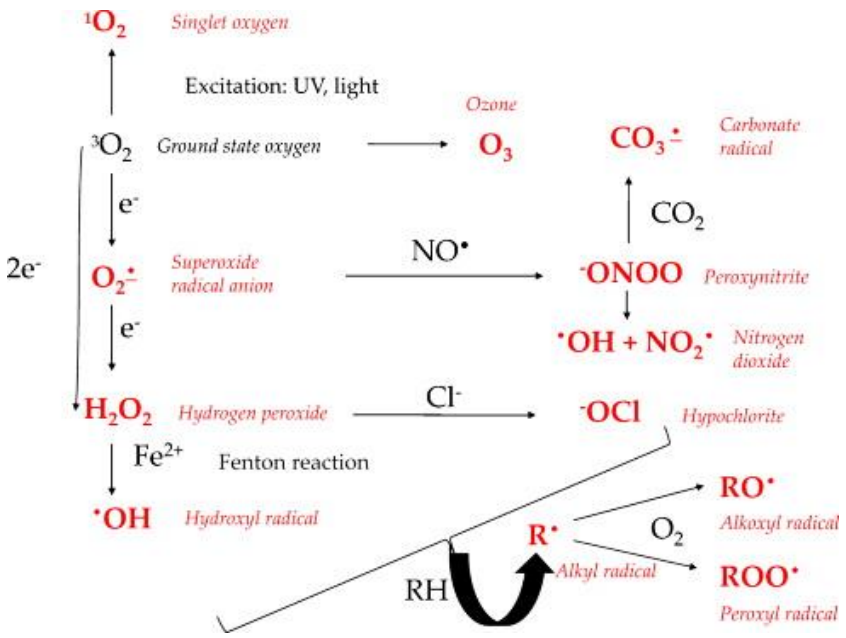

Figure 1.2: The main reactive oxygen species (Bartosz, 2009)

The respiratory chain produces O_2^- by the univalent reduction of molecular O_2. This process is mediated by enzymes such as xanthine oxidase (XOD) and nicotinamide adenine dinucleotide phosphate (NADPH) oxidase or non-enzymatically by redox reactive compounds (Dröge, 2002). Seven separate sites have been identified as sources of mitochondrial ROS production. These sites include complex 1 (siteIQ), complex III (site IIIQo), complex 1(site IF), complex II, glycerol 3-phosphate dehydrogenase, flavoprotein Q oxidoreductase, 2-oxoglutarate and pyruvate dehydrogenases. The latter three sites are poorly characterised in relation to the extent of O_2^- production (Brand, 2010) (Brand *et al.*, 2004). The majority of mitochondrial ROS generation occurs during the electron transport chain, therefore, the generation can occur at relatively high rates compared to cytosolic ROS production. The concentration of O_2^- is kept remarkably low in the *in-vivo* environment by the enzyme superoxide dimustase (SOD) (See Section 2.5.3). The brain contains a large quantity of this enzyme with ~0.5% of the soluble protein in the brain being Cu-Zn-SOD with an intracellular concentration of ~ 4–10 µM (Beckman and Koppenol, 1996).

Mitochondrial and cytosolic SOD regulate the levels of O_2^- by converting two O_2^- molecules into H_2O_2 and O_2. In biological tissues O_2^- can also undergo spontaneous dismutation producing H_2O_2 and singlet oxygen (Dröge, 2002). H_2O_2 has been implicated as an intracellular regulator of neuronal activity, growth and organelle function in brain cells. It also acts as a diffusional messenger for neuron-glia signalling and interneuronal communication which includes

regulation of synaptic transmission and plasticity (Rice, 2011). H_2O_2 is regulated by peroxidase enzymes, such as glutathione peroxidase which is cytosolic and mitochondrial (Rice, 2011), and catalase which is localised in intracellular peroxisomes (Dringen *et al*., 2005) (Cohen, 1994). Additional regulation of H_2O_2 is provided by thioredoxins, cellular thiols and peroxiredoxins which are abundant, however, they express lower catalytic efficiency to H_2O_2 compared to glutathione peroxidase or catalase (Rice, 2011) (Rhee *et al*., 2001) (Rhee, 2006). The tight regulation of H_2O_2 and O_2^- by an antioxidant system is important as highly reactive OH radicals can be formed by interaction of H_2O_2 with trace metal ions, particularly iron and copper which initiates lipid peroxidation (Brand *et al.*, 2004).

O_2^- can react with iron under *in-vivo* stress conditions, an excess of O_2^- results in the release of 'free iron' from iron-containing molecules (Jomova and Valko, 2011) (Valko *et al.*, 2006). The release of iron also has a negative impact on the [Fe_4-S_4] cluster-containing enzymes. Inactivation of these enzymes by O_2^- is a rapid process (rate constant estimated in the range 10^6 – 10^7 $M^{-1}s^{-1}$) leading to the oxidation of the iron–sulphur cluster. The oxidised protein binds with the Fe (III) more tightly so the protein releases Fe (II) ions. The released Fe (II) can participate in the Fenton reaction generating the highly reactive OH radicals (Fridovich, 1999) (Jomova and Valko, 2011).The iron catalysed Haber Weiss reaction is also another source of the OH radical. This reaction proceeds by the reaction of O_2^- with H_2O_2 where the O_2^- reduces the Fe rather than H_2O_2 (Kanti Das *et al.*, 2015).

The OH radical is highly reactive with a half-life in aqueous solutions of less than 1 ns (Pastor *et al.*, 2000). OH radicals formed *in-vivo* react in close proximity to the area of formation and have the ability to oxidise nucleic acids, proteins and phospholipids. The production of OH radicals close to DNA can have detrimental effects reacting with DNA bases or the deoxyribose backbone of DNA to produce damaged bases or strand breaks (Jomova and Valko, 2011). The most abundant *in-vivo* production of the OH radical occurs when the M^{n+} is iron or copper, however, this reaction has also been demonstrated using chromium, cobalt and other metals (Valko *et al.*, 2006). Conversely, the significance of the Fenton/Haber Weiss reaction *in-vivo* is still not understood since iron is effectively sequestered by various metal-binding proteins, therefore, the iron concentration in cells is relatively small. The effective and proper chelation of iron *in-vivo* is important to avoid the harmful effects of this 'free iron' in the physiological and pathological formation of inflammatory disorders, neurodegeneration, cardiovascular and metabolic disorders (Kell, 2009).

1.5 Reactive Nitrogen Species

The term reactive nitrogen species (RNS) encompasses a diverse range of compounds with different and distinct properties, however, they have one unifying characteristic in that they are all derivatives of NO (Patel *et al*., 1999). NO is an uncharged lipophilic molecule that contains a single unpaired electron, which makes it reactive with other molecules such as O_2, glutathione and the O_2^- radicals (Drew and Leeuwenburgh, 2002). NO has a diverse range of functions including modulating blood flow, thrombosis and neural activity and it also serves as an intercellular messenger (Beckman and Koppenol, 1996). Another important role of NO is its involvement in host defence, being produced by macrophages as a cytotoxic agent in response to an inflammatory or immune stimulus (Dedon and Tannenbaum, 2004).

NO is produced within cells by the actions of a group of enzymes called nitric oxide synthases (NOS). There are three principle isoforms of the NOS enzyme; neuronal NOS (nNOS), endothelial NOS (eNOS) and inducible NOS (iNOS) (Lacza *et al*., 2006) (Ghafourifar and Cadenas, 2005) (Marletta, 1993). The NOS enzymes have very similar structures and all exhibit a bi-domain structure. The first site consists of a C–terminal reductase domain that contains binding sites for NADPH, FAD, flavin mononucleotide (FMN) which are linked by a calmodulin recognition site to a N terminal oxygenase domain containing binding sites for haem, BH_4 and L-arginine (Alderton *et al.*, 2001) (Guix *et al.*, 2005). Both eNOS and nNOS activation are dependent on the levels of calcium/calmodulin and NO is produced in a transient manner *(*Mungrue *et al*., 2003) (Drew and Leeuwenburgh, 2002). However, iNOS is independent of calcium levels producing NO at high concentrations for longer periods of time (Iadecola *et al*., 1995) (Dedon and Tannenbaum, 2004). L-Arginine is used by NOS to produce NO and citrulline in a process requiring NADPH and O_2 (see Figure 1.3). N-Hydroxyarginine is produced as an intermediate before being reoxidised to form citrulline and NO (Lacza *et al*., 2006) (Guix *et al.*, 2005).

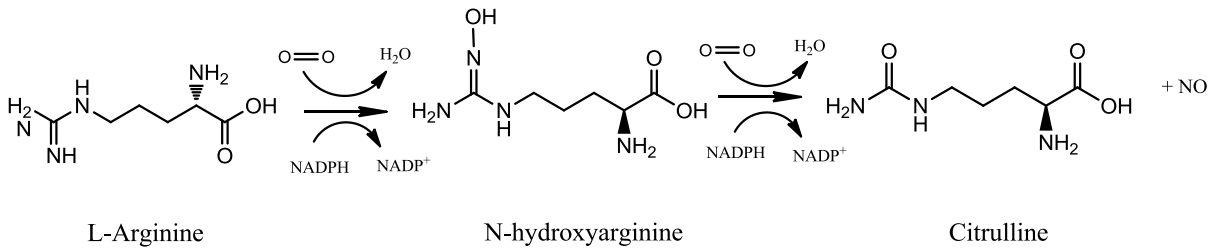

Figure 1.3.: A schematic illustrating the synthesis of NO by NOS.

NO is a relatively stable and non-reactive free radical and under normal physiological conditions exerts no toxic effects on cells. However, NO can react with O_2^- to produce a powerful oxidant, $ONOO^-$ with a rate constant near the diffusion controlled limit (Pryor and Squadrito, 1995) (Squadrito and Pryor, 1995) (Radi *et al.*, 2002) (Wink and Mitchell, 1998) (Estévez and Jordán, 2002). $ONOO^-$ formation occurs during ischemia-reperfusion injury, inflammation and neurodegenerative diseases, where NO and O_2^- levels are elevated and therefore is suggested to play a role in oxidative stress (Murphy, 1998). $ONOO^-$ can react directly with electron rich groups particularly sulfhydryls, iron sulphur centres, zinc-thiolates and the active-site sulfhydryl in tyrosine phosphate. $ONOO^-$ is very stable in solution, as a result of the cis-conformation which localises the negative charge over the entire molecule. The $ONOO^-$ anion reacts directly with molecules with a partial positive charge, reacting with carbon dioxide producing nitrosoperoxycarbonate as a transient intermediate that then rapidly decomposes to nitrogen dioxide and the carbonate radical (Pacher *et al.*, 2007). $ONOO^-$ can react with the active sites of SOD in a catalytic reaction which fails to inactivate the enzyme. It is hypothesised that the $ONOO^-$ is attracted by the same electrostatic field that draws the O_2^- anion to the active site with the copper centre essential for the nitrating activity of the enzyme (Beckman and Crow, 1993).

1.6. Oxidative Stress

For the past fifty years, oxidative stress has been increasingly recognised as a contributing factor in ageing, but its conceptual origins can be traced back to the 1950's (Hybertson *et al.*, 2011). Harham, in the 1950's articulated a 'free radical theory' of ageing, speculating that endogenous O_2 radicals were generated in cells and resulted in a pattern of damage. (Harman, 1955). Oxidative stress is described as an imbalance between the generation and elimination of ROS and RNS (Emerit *et al.*, 2004) (Simonian and Coyle, 1996). The human body produces O_2 free radicals and other ROS as by-products through numerous physiological and biochemical processes in the body (see Section 1.4 & Section 1.5), however, these radicals are primarily generated as a result of aerobic metabolism (Uttara *et al.*, 2009). The overproduction of ROS (arising either from mitochondrial electron-transport chain or excessive stimulation of NAD(P)H) results in oxidative stress, a deleterious process that can be an important mediator of damage to cell structures, including lipids, membranes, proteins and DNA (Valko *et al.*, 2007). This overproduction eventually leads to many chronic diseases such as atherosclerosis,

cancer, diabetes, rheumatoid arthritis, cardiovascular diseases, chronic inflammation, ageing and neurodegenerative diseases (Fridovich, 1999) (Uttara *et al.*, 2009).

The brain is highly vulnerable to oxidative damage by O_2 free radicals because of its high rate of metabolic activity, intensive production of reactive O_2 metabolites, relatively low antioxidant capacity, low mechanism activity, non-replicating nature of its neuronal cells and the high membrane surface to cytoplasm ratio (Evans, 1993) (Reiter, 1995) (Shohami *et al*., 1997). The main effector of the oxidative stress process in the brain is the neurotransmitter glutamate, primarily through the activation of its ionotropic receptors. The ionotropic receptors are characterised by their electrophysiological and pharmacological properties which include the kainic acid and N-methyl-D aspartate (NMDA) receptors (Gilgun-Sherki *et al*., 2001). The excitatory amino acids and neurotransmitters whose metabolism produces ROS, are unique in the brain as sources of oxidative stress. Other endogenous sources of ROS in the brain include enzymatic processes in which ROS are generated directly or indirectly (e.g. NOS, monoamine oxidase (MAO)) and various cells such as activated neutrophils. Exogenous sources of ROS include irradiation and pollutants which can cross the blood brain barrier, as well as xenobiotics and drugs (Shohami *et al.*, 1997).

Antioxidants are classified as exogenous (natural or synthetic) or endogenous compounds. Both remove free radicals, scavenging ROS or their precursors, inhibiting the formation of ROS and binding metal ions required for the catalysis of ROS generation and up-regulation of endogenous antioxidant defences. The antioxidant system can be classified into two major groups, enzymes and low molecular weight antioxidants. Enzymatic antioxidants include SOD, catalase, and glutathione peroxidase along with other supporting enzymes. Low molecular weight antioxidants can be further classified into indirect-acting antioxidants and direct-acting antioxidants. The direct-acting antioxidants are extremely important as a protective mechanism for oxidative stress (Uttara *et al.*, 2009) (Harman, 1955). These antioxidants include ascorbic and lipoic acids, polyphenols and carotenoids (Shohami *et al.*, 1997). The indirect-acting antioxidants, on the other hand, include mainly the chelating agents which prevent free radical generation, as they bind to the redox metal (Uttara *et al.*, 2009).

Cell death occurs by necrosis or apoptosis. In neurodegenerative diseases, apoptotic cell death is predominant. During this process, mitochondria play a major role and glutamatergic over stimulation (excitotoxicity) leads to increased neuronal calcium and apoptosis (Hybertson *et al.*, 2011). Many studies have considered the role of mitochondria in the pathogenesis of

neurodegenerative diseases, however, it is unclear whether mitochondria and oxidative stress are involved in the onset and progression of these diseases or whether they are consequences of neurodegeneration *(*Federico *et al.*, 2012). The next section discusses the role of oxidative stress in the pathogenesis of PD and the current therapies for the treatment of this neurodegenerative disease.

1.7. Parkinson's Disease

PD is the second most common neurodegenerative disease, primarily affecting people over 55 years (von Bohlen und Halbach, 2005). In about 95% of PD cases, there is no apparent genetic linkage, but in the rest of the cases the disease is hereditary (Dauer and Przedborski, 2003). PD was first reported by James Parkinson in 1817 when he published a monograph describing the clinical features of PD in six individuals. PD or Primary Parkinsonism is a neurological disorder that is characterised by any combination of six specific motoric features: tremor at rest, bradykinesia, rigidity, loss of postural reflexes, flexed posture and the freezing phenomenon (Fahn, 2003). Other non-motor symptoms such as sleep disorders, anxiety, depression, impulsivity, dementia and olfactory dysfunction can also be presented by PD patients.

Dopamine is a toxic neurotransmitter that has long been attributed to the pathogenesis of PD. The striatum receives its dopaminergic input from neurons of the substantia pars compacta (SNpc) via the nigrostriatal pathway (Betarbet *et al.*, 2002). Progressive degeneration of the dopamine containing neurons in the SNpc results in a substantial deficiency in striatal dopamine, which is thought to lead to many of the clinical symptoms of PD (Caudle *et al.*, 2008) (Valko *et al.*, 2007). The clinical signs of PD only appear when striatal dopamine is reduced by about 80% (Betarbet *et al.*, 2002) (Spina and Cohen, 1989).

The familial forms of PD are very infrequent with only about 5% of PD patients reporting a positive history. Six genes have been identified to be linked with heritable monogenic PD, while mutations and Lewis neuritis in SNCA and LRRK2 are responsible for autosomal-dominant PD. Mutations in Parkin, PINK1, DJ-1 and ATP132A account for PD that displays an autosomal recessive mode of inheritance (Klein and Schlossmacher, 2006). SNCA was the first gene to be associated with familial PD and usually patients develop early onset PD. The pathological hallmark of this disease is large cytoplasmic inclusions called Lewy bodies and

Lewy neuritis (Schiesling *et al*., 2008) (Emerit *et al.*, 2004). Parkin was the second identified PD gene and usually patients develop the disease in their thirties or forties. The Parkin protein functions as an E3 ubiquitin ligase in the process of ubiquitination. Post-mortem examinations show evidence of neuronal loss and gliosis in the SNpc, however, the brain is frequently lacking Lewy bodies (Klein and Schlossmacher, 2006).

These genetic factors are in accordance with epidemiological associations to PD. These associations consist of exposure to environmental toxins that act on the respiratory chain, such as pesticides, heavy metals and carbon monoxide, as well as neuroinflammation (Leão *et al.*, 2015). The presence of Lewy bodies in the dopaminergic neurons of SNpc, as well as the cortex and magnocellular basal forebrain nuclei are a pathological feature of PD. A major component of these Lewy bodies is a protein called α-synuclein (Spillantini *et al.*, 1997). The exact pathway of the involvement of the α-synuclein protein or its mutants in the degeneration remains unclear. One potential mechanism is an interaction between α–synuclein and cysolic dopamine, in particular the oxidative by-products of dopamine metabolism, which stabilises the pathogenic protofibril conformation of α-synuclein to inhibit its conversion to the nonpathogenic fibril (Caudle *et al.,* 2008).

Oxidative stress and mitochondrial dysfunction have also been strongly implicated in PD pathogenesis (Betarbet *et al.*, 2002). The link between mitochondrial dysfunction and PD was first discovered when a group of drug abusers developed PD symptoms after accidental exposure to 1-methyl-4-phenyl-1,2,3,6-tetrahydropyridine (MPTP) in the 1980's (Langston *et al*., 1983). The toxicity of MPTP is attributed to its ability to cross the blood brain barrier where it is metabolised to its active metabolite MPP^+ by MAO-B. MPP^+ is a complex I inhibitor, therefore this leads to the generation of large quantities of free radicals. MPP^+ is selectively taken up by dopaminergic neurons via its affinity for the dopamine transporter and therefore is selectively toxic to dopamine neurons (Tsang and Chung, 2009) (Javitch *et al.*, 1985) (Betarbet *et al*., 2002).

Dopamine synthesis primarily occurs at the neuronal terminal via the hydroxylation of tyrosine by tyrosine hydroxylase to form L-3,4-dihydroxyphenylalanine (L-DOPA). L-DOPA is then decarboxylated by aromatic acid decarboxylase to yield dopamine (Caudle *et al.,* 2008). Dopamine can autoxidise into dopamine quinone species or alternatively cytotoxic molecules including O_2^-, OH or H_2O_2 consequently leading to oxidative/nitrosative stress. Dopamine can be enzymatically deaminated by MAO into the metabolite 3,4-dihydroxyphenylacetic acid

(DOPAC) and H_2O_2 (see Equation 1.1) (Lotharius and Brundin, 2002) (Chinta and Andersen, 2008). Cellular free radical scavenging systems, including glutathione and SOD, scavenge ROS preventing these radicals from damaging cellular and mitochondrial structures. However, partial inhibition of complex I increases the quantity of ROS produced, usually overcoming these protective mechanisms (Betarbet *et al.*, 2002). A deficiency in glutathione, which results in the brain's inefficiency to clear H_2O_2 and also an increase in reactive iron promoting OH formation are also other sources of oxidative stress leading to cell death (Olanow and Tatton, 1999).

$$\text{Dopamine} + O_2 + H_2O \xrightarrow{\text{MAO}} H_2O_2 + NH_3 + \text{DOPAC} \qquad \textbf{Eqn 1.1}$$

Post-mortem findings of PD brains demonstrate that the systems decomposing OH radicals and other ROS are decreased substantially. It was demonstrated that the levels of glutathione are reduced and oxidative damage occurs to lipids, proteins and DNA, suggesting that the SNpc is in a state of oxidant stress (Ebadi *et al.*, 1996) (Olanow and Tatton, 1999). In PD, the iron content of the SNpc is elevated compared to controls with an increase of the Fe(III)/Fe(II) ratio from 2:1 to almost 1:2. This increases the overall iron content and Fe(II) enhances the conversion of H_2O_2 to OH leading to further oxidative stress (Chinta and Andersen, 2008). However, there is still considerable debate whether oxidative stress is the causative factor in the development of PD or whether it is as a result of a cascade of events initiated by some other influence such as mitochondrial impairment, inflammation, excitotoxicity and also the toxic effects of NO (Jenner, 2003) (Schapira and Jenner, 2011).

There are currently many therapies for the management of the motor symptoms and motor complications observed in PD. These therapies are based on a dopamine replacement strategy. However, alternative therapies such as anticholinergics, antiglutamatergic agents, MAO-B inhibitors or surgical procedures have also shown antiparkinsonian properties (Rascol *et al.*, 2003). The most effective drug to treat the motor symptoms of PD is L-DOPA (levodopa) and is regarded as the therapeutic 'gold standard' (Schapira *et al.*, 2009) (Lipski *et al.*, 2011). Levodopa/L-DOPA is orally administered and is usually combined with a DOPA-decarboxylase inhibitor to improve absorption and reduce peripheral metabolism. The majority of levodopa is metabolised in the liver and gut by 3-O-methyl transferase (COMT) to produce 3-O-methyldopa, which on accumulation can interfere with the brain penetration of L-DOPA.

COMT inhibitor drugs such as entacapone increase the amount of L-DOPA absorbed and maintained in the effective range for extended periods of time, therefore providing a reduced off-time and enhancing availability of the drug in the brain (Rascol *et al.*, 2003) (Schapira *et al.*, 2009).

L-DOPA is highly efficient in the initial treatment of PD by the direct replacement of dopamine. However, significant long-term complications of the administration of L-DOPA as a treatment for PD is the development of dyskinesia and motor complications due to the 'wearing off' effect of L-DOPA (Lipski *et al.*, 2011) (Schapira *et al.*, 2009). Other adverse side effects of the drug include nausea, hypertonia, vomiting and headache and these side effects are significantly more common on administration of higher doses of the drug (Group, 2004). Some evidence has suggested that treatment with L-DOPA may have a propensity to induce dopamine metabolism related oxidative stress (Lipski *et al.*, 2011) (Schapira *et al.*, 2009). *In-vitro* studies have demonstrated that L-DOPA is toxic in cell cultures via the process of oxidative stress (Lipski *et al.*, 2011). However, clinical trials in humans and studies conducted with animals, including rodents and primates, have failed to conclusively reveal a toxic effect following the administration of L-DOPA (Ferrario *et al.*, 2004) (Schapira *et al.*, 2009) (Group, 2004). The general consensus is that L-DOPA is not capable of stopping the progression of dopaminergic cell loss in the SNpc but can only slow the rate of PD progression. Currently none of the antiparkinsonian therapies offer a therapeutic strategy to manage patients with PD on a long-term basis; many motor and non-motor symptoms are resistant to current treatments with such treatments inducing adverse side effects and the quality of life and life expectancy remain abnormal (Rascol *et al.*, 2003). This fact necessitates the further development of novel PD therapeutic strategies.

1.8. Overview of Thesis

This thesis describes the *in-vitro* development of a O_2^- biosensor and also investigates the role of oxidative stress in the manifestation of PD. For this NO and O_2 sensors were implanted in the striatum and high and low doses of reserpine were administered.

Chapter 1 provides an introduction to the brain, biosensors, the chemical reactivity and formation of ROS and RNS in biological systems and concurrently their role in oxidative stress. This chapter also emphasises the harmful effects of oxidative stress with particular focus on its

role in the manifestation of PD. Chapter 2 describes the background theory that is relevant to the research undertaken, while Chapter 3 details the analytical techniques and experimental methods used in the fabrication and characterisation of the various sensor types utilised throughout the research. The results chapters commence with the development of the O_2^- biosensor (Chapter 4). This chapter outlines the steps undertaken in the optimisation of the biosensor design with respect to O_2^- sensitivity. Chapter 5 details the interferences in the O_2^- calibration and the relevant modifications made to the biosensor in order to minimise/eliminate these interferences in the *in-vivo* environment. Chapter 6 focuses on the electrochemical detection of NO and O_2 in a reserpine mediated model of PD. The specific focus of this chapter is to elucidate the role of oxidative/nitrosative stress in the etiology and pathophysiology of PD. Finally, Chapter 7 concludes the thesis and discusses the main experimental outcomes.

1.9. References

Alderton WK, Cooper CE and Knowles RG. (2001) Nitric oxide synthases: structure, function and inhibition. *Biochemical Journal* 357: 593-615.

Austin VC, Blamire AM, Grieve SM, *et al.* (2003) Differences in the BOLD fMRI response to direct and indirect cortical stimulation in the rat. *Magnetic Resonance in Medicine* 49: 838-847.

Bartosz G. (2009) Reactive oxygen species: Destroyers or messengers? *Biochemical Pharmacology* 77: 1303-1315.

Beckman JS and Crow JP. (1993) Pathological implications of nitric oxide, superoxide and peroxynitrite formation. *Biochemical Society Transactions* 21: 330-334.

Beckman JS and Koppenol WH. (1996) Nitric oxide, superoxide, and peroxynitrite: the good, the bad, and ugly. *American Journal of Physiology-Cell Physiology* 271: C1424-C1437.

Betarbet R, Sherer TB and Greenamyre JT. (2002) Animal models of Parkinson's disease. *BioEssays* 24: 308-318.

Bolger FB and Lowry JP. (2005) Brain Tissue Oxygen: *In Vivo* Monitoring with Carbon Paste Electrodes. *Sensors* 5: 473-487.

Bolger FB, McHugh SB, Bennett R, *et al.* (2011(b)) Characterisation of carbon paste electrodes for real-time amperometric monitoring of brain tissue oxygen. *Journal of Neuroscience Methods* 195: 135-142.

Boutelle MG, Svensson L and Fillenz M. (1989) Rapid changes in striatal ascorbate in response to tail-pinch monitored by constant potential voltammetry. *Neuroscience* 30: 11-17.

Brand MD. (2010) The sites and topology of mitochondrial superoxide production. *Experimental Gerontology* 45: 466-472.

Brand MD, Affourtit C, Esteves TC, *et al*. (2004) Mitochondrial superoxide: production, biological effects, and activation of uncoupling proteins. *Free Radical Biology and Medicine* 37: 755-767.

Breier A, Su T-P, Saunders R, *et al.* (1997) Schizophrenia is associated with elevated amphetamine-induced synaptic dopamine concentrations: Evidence from a novel positron emission tomography method. *Proceedings of the National Academy of Sciences* 94: 2569-2574.

Brown FO, Finnerty NJ, Bolger FB, *et al.* (2005) Calibration of NO sensors for *in-vivo* voltammetry: laboratory synthesis of NO and the use of UV–visible spectroscopy for

determining stock concentrations. *Analytical and Bioanalytical Chemistry* 381: 964-971.

Cass AEG, Davis G, Francis GD, *et al.* (1984) Ferrocene-mediated enzyme electrode for amperometric determination of glucose. *Analytical Chemistry* 56: 667-671.

Caudle WM, Colebrooke RE, Emson PC, *et al.* (2008) Altered vesicular dopamine storage in Parkinson's disease: a premature demise. *Trends in Neurosciences* 31: 303-308.

Chaubey A, Pande KK, Singh VS, *et al.* (2000) Co-immobilization of lactate oxidase and lactate dehydrogenase on conducting polyaniline films. *Analytica Chimica Acta* 407: 97-103.

Chefer VI, Thompson AC, Zapata A, *et al.* (2001) Overview of Brain Microdialysis. *Current Protocols in Neuroscience.* John Wiley & Sons, Inc.

Chinta SJ and Andersen JK. (2008) Redox imbalance in Parkinson's disease. *Biochimica et Biophysica Acta (BBA) - General Subjects* 1780: 1362-1367.

Clark LC and Lyons C. (1962) Electrode Systems for Continuous Monitoring in Cardiovascular Surgery. *Annals of the New York Academy of Sciences* 102: 29-45.

Clark LC, Misrahy G and Fox RP. (1958) Chronically Implanted Polarographic Electrodes. *Journal of Applied Physiology* 13: 85-91.

Cohen G. (1994) Enzymatic/Nonenzymatic Sources of Oxyradicals and Regulation of Antioxidant Defensesa. *Annals of the New York Academy of Sciences* 738: 8-14.

Dauer W and Przedborski S. (2003) Parkinson's Disease: Mechanisms and Models. *Neuron* 39: 889-909.

Dedon PC and Tannenbaum SR. (2004) Reactive nitrogen species in the chemical biology of inflammation. *Archives of Biochemistry and Biophysics* 423: 12-22.

Drew B and Leeuwenburgh C. (2002) Aging and the Role of Reactive Nitrogen Species. *Annals of the New York Academy of Sciences* 959: 66-81.

Dringen R, Pawlowski PG and Hirrlinger J. (2005) Peroxide detoxification by brain cells. *Journal of Neuroscience Research* 79: 157-165.

Dröge W. (2002) Free radicals in the physiological control of cell function. *Physiological Reviews* 82: 47-95.

Duff A and O'Neill RD. (1994) Effect of Probe Size on the Concentration of Brain Extracellular Uric Acid Monitored with Carbon Paste Electrodes. *Journal of Neurochemistry* 62: 1496-1502.

Ebadi M, Srinivasan SK and Baxi MD. (1996) Oxidative stress and antioxidant therapy in Parkinson's disease. *Progress in Neurobiology* 48: 1-19.

El Atrash SS and O'Neill RD. (1995) Characterisation *in vitro* of a naphthoquinone-mediated glucose oxidase-modified carbon paste electrode designed for neurochemical analysis *in vivo*. *Electrochimica Acta* 40: 2791-2797.

Emerit J, Edeas M and Bricaire F. (2004) Neurodegenerative diseases and oxidative stress. *Biomedicine & Pharmacotherapy* 58: 39-46.

Estévez AG and Jordán J. (2002) Nitric oxide and superoxide, a deadly cocktail. *Annals of the New York Academy of Sciences* 962: 207-211.

Evans P. (1993) Free radicals in brain metabolism and pathology. *British Medical Bulletin* 49: 577-587.

Fahn S. (2003) Description of Parkinson's disease as a clinical syndrome. *Annals of the New York Academy of Sciences* 991: 1-14.

Federico A, Cardaioli E, Da Pozzo P, *et al.* (2012) Mitochondria, oxidative stress and neurodegeneration. *Journal of the Neurological Sciences* 322: 254-262.

Feldman RS, Meyer JS, Quenzer LF, *et al.* (1997) *Principles of Neuropsychopharmacology*: Sinauer Associates Sunderland.

Ferrario JE, Taravini IRE, Mourlevat S, *et al.* (2004) Differential gene expression induced by chronic levodopa treatment in the striatum of rats with lesions of the nigrostriatal system. *Journal of Neurochemistry* 90: 1348-1358.

Fray A, Forsyth R, Boutelle M, *et al.* (1996) The mechanisms controlling physiologically stimulated changes in rat brain glucose and lactate: a microdialysis study. *The Journal of Physiology* 496: 49.

Fridovich I. (1999) Fundamental Aspects of Reactive Oxygen Species, or What's the Matter with Oxygen? *Annals of the New York Academy of Sciences* 893: 13-18.

Ghafourifar P and Cadenas E. (2005) Mitochondrial nitric oxide synthase. *Trends in Pharmacological Sciences* 26: 190-195.

Gilgun-Sherki Y, Melamed E and Offen D. (2001) Oxidative stress induced-neurodegenerative diseases: the need for antioxidants that penetrate the blood brain barrier. *Neuropharmacology* 40: 959-975.

Group TPS. (2004) Levodopa and the Progression of Parkinson's Disease. *New England Journal of Medicine* 351: 2498-2508.

Gruetter R, Seaquist ER, Kim S, *et al.* (1998) Localized *in vivo* 13C-NMR of glutamate metabolism in the human brain: initial results at 4 tesla. *Developmental Neuroscience* 20: 380-388.

Guix FX, Uribesalgo I, Coma M, *et al.* (2005) The physiology and pathophysiology of nitric oxide in the brain. *Progress in Neurobiology* 76: 126-152.

Harman D. (1955) Aging: a theory based on free radical and radiation chemistry.

Hybertson BM, Gao B, Bose SK, *et al.* (2011) Oxidative stress in health and disease: The therapeutic potential of Nrf2 activation. *Molecular Aspects of Medicine* 32: 234-246.

Iadecola C, Zhang F, Xu S, *et al.* (1995) Inducible Nitric Oxide Synthase Gene Expression in Brain following Cerebral Ischemia. *Journal of Cerebral Blood Flow & Metabolism* 15: 378-384.

Jackson BP, Dietz SM and Wightman RM. (1995) Fast-scan cyclic voltammetry of 5-hydroxytryptamine. *Analytical Chemistry* 67: 1115-1120.

Javitch JA, D'Amato RJ, Strittmatter SM, *et al.* (1985) Parkinsonism-inducing neurotoxin, N-methyl-4-phenyl-1,2,3,6 -tetrahydropyridine: uptake of the metabolite N-methyl-4-phenylpyridine by dopamine neurons explains selective toxicity. *Proceedings of the National Academy of Sciences* 82: 2173-2177.

Jenner P. (2003) Oxidative stress in Parkinson's disease. *Annals of Neurology* 53: S26-S38.

Jomova K and Valko M. (2011) Advances in metal-induced oxidative stress and human disease. *Toxicology* 283: 65-87.

Kanti Das T, Wati MR and Fatima-Shad K. (2015) Oxidative Stress Gated by Fenton and Haber Weiss Reactions and Its Association With Alzheimer's Disease. *Arch Neurosci* 2: e20078.

Kell DB. (2009) Iron behaving badly: inappropriate iron chelation as a major contributor to the aetiology of vascular and other progressive inflammatory and degenerative diseases. *BMC Medical Genomics* 2: 1.

Kissinger PT, Hart JB and Adams RN. (1973) Voltammetry in brain tissue — a new neurophysiological measurement. *Brain Research* 55: 209-213.

Klein C and Schlossmacher MG. (2006) The genetics of Parkinson disease:implications for neurological care. *Nat Clin Pract Neuro* 2: 136-146.

Kowaltowski AJ, de Souza-Pinto NC, Castilho RF, *et al.* (2009) Mitochondria and reactive oxygen species. *Free Radical Biology and Medicine* 47: 333-343.

Kristensen EW, Kuhr WG and Wightman RM. (1987) Temporal characterization of perfluorinated ion exchange coated microvoltammetric electrodes for *in vivo* use. *Analytical Chemistry* 59: 1752-1757.

Kulys JJ, Samalius AS and Švirmickas GJS. (1980) Electron exchange between the enzyme active center and organic metal. *FEBS Letters* 114: 7-10.

Lacza Z, Pankotai E, Csordás A, *et al.* (2006) Mitochondrial NO and reactive nitrogen species production: Does mtNOS exist? *Nitric Oxide* 14: 162-168.

Langston JW, Ballard P, Tetrud JW, *et al.* (1983) Chronic parkinsonism in humans due to a product of meperidine-analog synthesis. *Science* 219: 979-980.

Leão AHFF, Sarmento-Silva AJ, Santos JR, *et al.* (2015) Molecular, Neurochemical, and Behavioral Hallmarks of Reserpine as a Model for Parkinson's Disease: New Perspectives to a Long-Standing Model. *Brain Pathology* 25: 377-390.

Lipski J, Nistico R, Berretta N, *et al.* (2011) L-DOPA: a scapegoat for accelerated neurodegeneration in Parkinson's disease? *Progress in Neurobiology* 94: 389-407.

Lotharius J and Brundin P. (2002) Pathogenesis of parkinson's disease: dopamine, vesicles and [alpha]-synuclein. *Nat Rev Neurosci* 3: 932-942.

Lowry J and O'Neill R. (2005) Neuroanalytical chemistry *in-vivo* using biosensors. *Encyclopedia of Sensors*: 501-524.

Lowry JP and O'Neill RD. (1994) Partial characterization *in vitro* of glucose oxidase-modified poly(phenylenediamine)-coated electrodes for neurochemical analysis *in vivo*. *Electroanalysis* 6: 369-379.

Mangia S, Garreffa G, Bianciardi M, *et al.* (2003) The aerobic brain: lactate decrease at the onset of neural activity. *Neuroscience* 118: 7-10.

Marletta MA. (1993) Nitric oxide synthase structure and mechanism. *Journal of Biological Chemistry* 268: 12231-12234.

McMahon CP, Rocchitta G, Kirwan SM, *et al.* (2007) Oxygen tolerance of an implantable polymer/enzyme composite glutamate biosensor displaying polycation-enhanced substrate sensitivity. *Biosensors and Bioelectronics* 22: 1466-1473.

Miele M and Fillenz M. (1996) *In-vivo* determination of extracellular brain ascorbate. *Journal of Neuroscience Methods* 70: 15-19.

Mungrue IN, Bredt DS, Stewart DJ, *et al.* (2003) From molecules to mammals: what's NOS got to do with it? *Acta Physiologica Scandinavica* 179: 123-135.

Murphy LJ. (1998) Reduction of Interference Response at a Hydrogen Peroxide Detecting Electrode Using Electropolymerized Films of Substituted Naphthalenes. *Analytical Chemistry* 70: 2928-2935.

Newman JD and Setford SJ. (2006) Enzymatic biosensors. *Molecular Biotechnology* 32: 249-268.

O'Neill RD. (1990) Uric acid levels and dopamine transmission in rat striatum: diurnal changes and effects of drugs. *Brain Research* 507: 267-272.

O'Neill RD. (1994) Microvoltammetric techniques and sensors for monitoring neurochemical dynamics *in vivo*. A review. *Analyst* 119: 767-779.

O'Neill RD and Fillenz M. (1985(a)) Circadian changes in extracellular ascorbate in rat cortex, accumbens, striatum and hippocampus: Correlations with motor activity. *Neuroscience Letters* 60: 331-336.

O'Neill RD and Fillenz M. (1985(b)) Detection of homovanillic acid *in vivo* using microcomputer-controlled voltammetry: Simultaneous monitoring of rat motor activity and striatal dopamine release. *Neuroscience* 14: 753-763.

O'Neill RD and Lowry JP. (2006) Voltammetry *In Vivo* for Chemical Analysis of the Living Brain. *Encyclopedia of Analytical Chemistry*. John Wiley & Sons, Ltd.

O'Neill RD, Lowry JP and Mas M. (1998) Monitoring brain chemistry *in vivo*: voltammetric techniques, sensors, and behavioral applications. *Critical Reviews in Neurobiology* 12: 69-128.

Olanow C and Tatton W. (1999) Etiology and pathogenesis of Parkinson's disease. *Annual Review of Neuroscience* 22: 123-144.

Pacher P, Beckman JS and Liaudet L. (2007) Nitric oxide and peroxynitrite in health and disease. *Physiological Reviews* 87: 315-424.

Pastor N, Weinstein H, Jamison E, *et al.* (2000) A detailed interpretation of OH radical footprints in a TBP-DNA complex reveals the role of dynamics in the mechanism of sequence-specific binding1. *Journal of Molecular Biology* 304: 55-68.

Patel RP, McAndrew J, Sellak H, *et al.* (1999) Biological aspects of reactive nitrogen species. *Biochimica et Biophysica Acta (BBA) - Bioenergetics* 1411: 385-400.

Phelps ME. (2000) Positron emission tomography provides molecular imaging of biological processes. *Proceedings of the National Academy of Sciences* 97: 9226-9233.

Pryor WA and Squadrito GL. (1995) The chemistry of peroxynitrite: a product from the reaction of nitric oxide with superoxide. *American Journal of Physiology-Lung Cellular and Molecular Physiology* 268: L699-L722.

Radi R, Cassina A, Hodara R, *et al.* (2002) Peroxynitrite reactions and formation in mitochondria. *Free Radical Biology and Medicine* 33: 1451-1464.

Radi AE, Muñoz-Berbel X, Cortina-Puig M, *et al.* (2009) A Third-Generation Hydrogen Peroxide Biosensor Based on Horseradish Peroxidase Covalently Immobilized on Electrografted Organic Film on Screen-Printed Carbon Electrode. *Electroanalysis* 21: 1624-1629.

Rascol O, Payoux P, Ory F, *et al.* (2003) Limitations of current Parkinson's disease therapy. *Annals of Neurology* 53: S3-S15.

Reiter RJ. (1995) Oxidative processes and antioxidative defense mechanisms in the aging brain. *The FASEB Journal* 9: 526-533.

Rhee SG. (2006) H_2O_2, a Necessary Evil for Cell Signaling. *Science* 312: 1882-1883.

Rhee SG, Kang SW, Chang TS, *et al.* (2001) Peroxiredoxin, a Novel Family of Peroxidases. *IUBMB Life* 52: 35-41.

Rice ME. (2011) H_2O_2: A Dynamic Neuromodulator. *The Neuroscientist* 17: 389-406.

Robinson DL, Venton BJ, Heien MLAV, *et al.* (2003) Detecting Subsecond Dopamine Release with Fast-Scan Cyclic Voltammetry *In-Vivo*. *Clinical Chemistry* 49: 1763-1773.

Rodríguez-Delgado MM, Alemán-Nava GS, Rodríguez-Delgado JM, *et al.* (2015) Laccase-based biosensors for detection of phenolic compounds. *TrAC Trends in Analytical Chemistry* 74: 21-45.

Ronkainen NJ, Halsall HB and Heineman WR. (2010) Electrochemical biosensors. *Chemical Society Reviews* 39: 1747-1763.

Rothman DL, Petroff O, Behar KL, *et al.* (1993) Localized 1H NMR measurements of gamma-aminobutyric acid in human brain *in vivo*. *Proceedings of the National Academy of Sciences* 90: 5662-5666.

Rothman DL, Sibson NR, Hyder F, *et al.* (1999) *In vivo* nuclear magnetic resonance spectroscopy studies of the relationship between the glutamate--glutamine neurotransmitter cycle and functional neuroenergetics. *Philosophical Transactions of the Royal Society of London. Series B: Biological Sciences* 354: 1165-1177.

Schapira AH and Jenner P. (2011) Etiology and pathogenesis of Parkinson's disease. *Movement Disorders* 26: 1049-1055.

Schapira AH, Emre M, Jenner P, *et al.* (2009) Levodopa in the treatment of Parkinson's disease. *European Journal of Neurology* 16: 982-989.

Schiesling C, Kieper N, Seidel K, *et al.* (2008) Review: Familial Parkinson's disease – genetics, clinical phenotype and neuropathology in relation to the common sporadic form of the disease. *Neuropathology and Applied Neurobiology* 34: 255-271.

Shen J, Petersen KF, Behar KL, *et al.* (1999) Determination of the rate of the glutamate/glutamine cycle in the human brain by *in vivo* 13C NMR. *Proceedings of the National Academy of Sciences* 96: 8235-8240.

Shippenberg TS and Thompson AC. (2001) Overview of Microdialysis. *Current Protocols in Neuroscience.* John Wiley & Sons, Inc.

Shohami E, Beit-Yannai E, Horowitz M, *et al*. (1997) Oxidative stress in closed-head injury: brain antioxidant capacity as an indicator of functional outcome. *Journal of Cerebral Blood Flow & Metabolism* 17: 1007-1019.

Shulman RG, Blamire AM, Rothman DL, *et al.* (1993) Nuclear magnetic resonance imaging and spectroscopy of human brain function. *Proceedings of the National Academy of Sciences of the United States of America* 90: 3127-3133.

Simonian N and Coyle J. (1996) Oxidative stress in neurodegenerative diseases. *Annual Review of Pharmacology and Toxicology* 36: 83-106.

Spillantini MG, Schmidt ML, Lee VM-Y, *et al.* (1997) α-Synuclein in Lewy bodies. *Nature* 388: 839-840.

Spina MB and Cohen G. (1989) Dopamine turnover and glutathione oxidation: implications for Parkinson disease. *Proceedings of the National Academy of Sciences* 86: 1398-1400.

Squadrito GL and Pryor WA. (1995) The formation of peroxynitrite *in vivo* from nitric oxide and superoxide. *Chemico-Biological Interactions* 96: 203-206.

Thévenot DR, Toth K, Durst RA, *et al.* (2001) Electrochemical biosensors: recommended definitions and classification1. *Biosensors and Bioelectronics* 16: 121-131.

Tsang AHK and Chung KKK. (2009) Oxidative and nitrosative stress in Parkinson's disease. *Biochimica et Biophysica Acta (BBA) - Molecular Basis of Disease* 1792: 643-650.

Turner APF. (2013) Biosensors: sense and sensibility. *Chemical Society Reviews* 42: 3184-3196.

Uttara B, Singh AV, Zamboni P, *et al.* (2009) Oxidative stress and neurodegenerative diseases: a review of upstream and downstream antioxidant therapeutic options. *Current Neuropharmacology* 7: 65-74.

Valko M, Leibfritz D, Moncol J, *et al.* (2007) Free radicals and antioxidants in normal physiological functions and human disease. *The International Journal of Biochemistry & Cell Biology* 39: 44-84.

Valko M, Rhodes CJ, Moncol J, *et al.* (2006) Free radicals, metals and antioxidants in oxidative stress-induced cancer. *Chemico-Biological Interactions* 160: 1-40.

von Bohlen und Halbach O. (2005) Modeling neurodegenerative diseases *in vivo* review. *Neurodegenerative Diseases* 2: 313-320.

Wilson GS and Gifford R. (2005) Biosensors for real-time *in vivo* measurements. *Biosensors and Bioelectronics* 20: 2388-2403.

Wilson GS and Thévenot DR. (1989) Unmediated amperometric enzyme electrodes. *Biosensors: Pratical Approach*: 1-17.

Wink DA and Mitchell JB. (1998) Chemical biology of nitric oxide: insights into regulatory, cytotoxic, and cytoprotective mechanisms of nitric oxide. *Free Radical Biology and Medicine* 25: 434-456.

Wu K, Fei J and Hu S. (2003) Simultaneous determination of dopamine and serotonin on a glassy carbon electrode coated with a film of carbon nanotubes. *Analytical Biochemistry* 318: 100-106.

Yoo EH and Lee SY. (2010) Glucose biosensors: an overview of use in clinical practice. *Sensors* 10: 4558-4576.

Zachek MK, Hermans A, Wightman RM, *et al.* (2008) Electrochemical dopamine detection: Comparing gold and carbon fiber microelectrodes using background subtracted fast scan cyclic voltammetry. *Journal of Electroanalytical Chemistry* 614: 113-120.

Chapter 2: Theory

2.1. Introduction

The *in-vitro* development and characterisation of a superoxide (O_2^-) biosensor suitable for *in vivo* use was the primary goal of this research. In order to achieve this goal constant potential amperometry (CPA) was utilised throughout the course of the research which is described in Section 2.4. As O_2^- is not electroactive its direct measurement is not feasible. Therefore, this thesis discusses the development of a first generation biosensor involving the incorporation of superoxide dismutase (SOD) onto a Pt surface producing electrochemically detectable hydrogen peroxide (H_2O_2). However, to facilitate this enzymatic reaction, XOD must be added to the phosphate buffer saline (PBS) and different concentrations of xanthine are added to the buffer solution in order to generate O_2^- which can then undergo dismutation to produce H_2O_2. The application and different types of biosensors are discussed in detail in Section 1.3.

The effectiveness and suitability of each of the O_2^- biosensor designs are described and compared by their response to the target substrate and interferent species using linear/non-linear regression and other statistical analysis. Non-linear regression includes fitting the experimental data to Michaelis-Menten kinetics, and determining the important parameters K_M, V_{max} and α which are used to describe the activity of immobilised enzymes towards a substrate and the electrodes deviation from ideal kinetics, is detailed in Section 2.5.2.

Two important parameters govern the electrochemical analysis used in this research; the theory of mass transport and the rate of electron transfer. In general, a reaction at the electrode surface involves the transformation of a dissolved oxidised species to a reduced form and this results in an electrochemical signal (see Section 2.2). The theory of mass transport is based on three main processes; migration, convection and diffusion and these processes are discussed in detail in Section 2.3.

2.2. Oxidation and Reduction

Electrochemical analysis is based on the reactions that take place at the electrode surface. CPA involves the application of a fixed potential between the working and the reference electrode, which results in the oxidation or reduction of the target species. The H_2O_2 produced by the enzymatic dismutation of O_2^- at the working electrode is oxidised upon the application of a suitable potential giving a proportional Faradic current. The reaction symbolising the oxidation and reduction of a species occurring at the active surface is described in Equation 2.1, where O and R represent the oxidised and reduced species, respectively, and n symbolises the number of electrons involved in the reaction.

$$O + ne^- \rightleftharpoons R \qquad 2.1$$

The two main processes which contribute to the rate of reaction include mass transport of the reactant to the active surface of the electrode and electron transfer. This type of reaction is defined as a faradaic process as the reaction is governed by Faraday's law (i.e. the amount of chemical reaction caused by the flow of current is proportional to the amount of electricity passed). Some processes are non-faradaic; adsorption and desorption are examples and in this instance the structure of the electrode–solution interface changes with applied potential (Bard and Faulkner, 2000).

At equilibrium (E_{eq}), i.e. no negative or positive potential is applied compared to the energy of the solution species and consequently no oxidation/reduction processes occur. The Fermi level (E_F) or highest energy level of the metal based working electrode is equal in energy to the highest occupied molecular orbital (HOMO) of the solution species. An electrical potential applied to a metal acts to increase or decrease the energy of the Fermi levels. The application of a positive potential greater than E_{eq} results in a decrease in the energy of the Fermi level. It is then energetically more favourable for electrons to move from the HOMO level of the solution species to the lower lying E_F of the metal. This process results in an oxidation reaction (see Figure 2.2). A reduction reaction occurs when a negative potential is applied relative to E_{eq}

and electrons move from the increased E_F of the metal to the lowest unoccupied molecular orbital (LUMO) level of the solution species (see Figure 2.1) (Fisher, 1996).

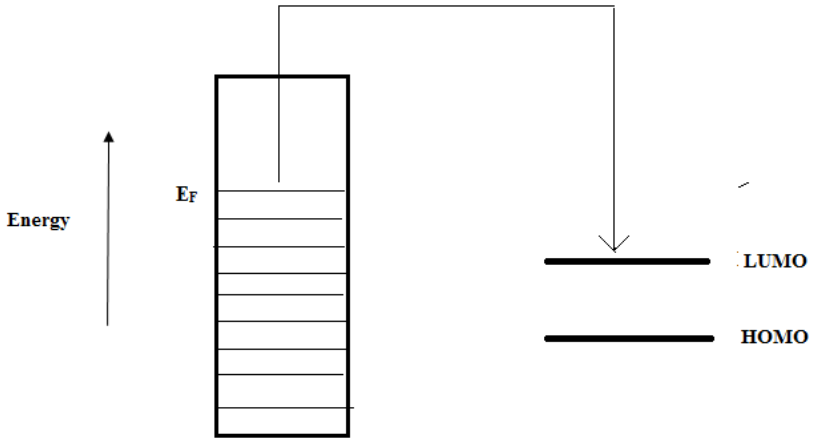

Figure 2.1: A schematic of a reduction reaction

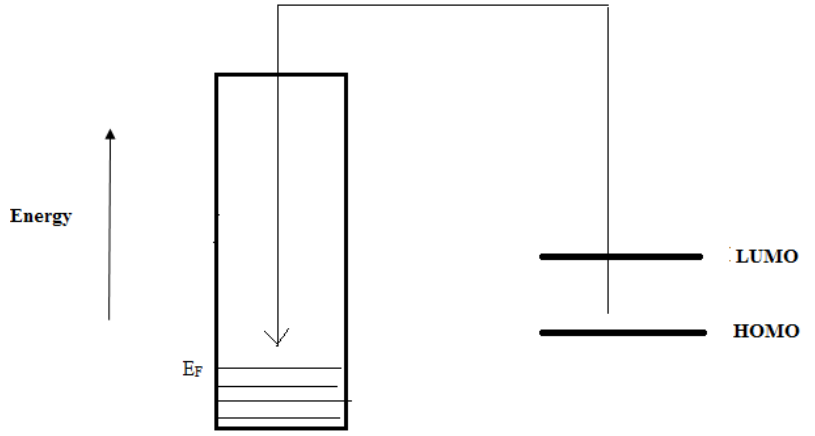

Figure 2.2: A schematic of an oxidation reaction

Additionally, upon application of a potential, a capacitance current arises as a result of the existence of opposing charges between the metal electrode and the target medium. This current is generated in the absence of any target analyte and all experimental data presented in this thesis is background subtracted to remove this capacitance current.

2.3. Mass Transport

Mass transport is a factor that affects the rate of reaction at the surface of an electrode. It is defined as the movement of substances from one place in solution to another. The experimentally measured current (I) is a direct indication of the rate of the electrochemical reaction and is represented by Faraday's law

$$I = nFAJ \qquad 2.2$$

Where (I) represents the current, n refers to the number of electrons, F is the Faraday constant, A is the area of the electrode (m^2) and J is the flux of the ions (mol m^{-2} s^{-1}).

The mass transport process is influenced by three main properties; migration, convection and diffusion.

2.3.1. Migration

The external electric field which exists at the electrode/solution interface as a result of a decrease in electrical potential between the two phases is capable of exerting an electrostatic force on charged species, therefore inducing the movement of ions away or to the electrode. This type of transport is defined as migration. Conversely, the migration effect is made negligible in this research by using an inert electrolyte (PBS, pH 7.4, Section 3.3.2.1) at larger quantities than the target species. In addition, the ionic strength of the electrolyte is high so λ, the Debye length is very small.

2.3.2. Convection

Movement due to convection occurs when a mechanical force acts on a solution. There are two types of convection; natural which arises from thermal gradients and/or density differences within the solution, and forced convection which is achieved by external forces such as stirring and bubbling (Fisher, 1996). *In-vitro* experiments introduce forced convection into the electrochemical cell by the use of a magnetic

stirrer alongside the addition of aliquots of substrate. However, this contribution can be neglected as the analysis of all calibration data was taken from the steady-state currents in a quiescent solution.

2.3.3. Diffusion

Diffusion arises from uneven concentration distributions and movement of molecules always occurs from an area of high concentration to a region of lower concentration. The rate of diffusion at a given point in the solution is dependent upon the concentration gradient and is governed by Fick's first law (see Equation 2.3) which states that the diffusional flux is proportional to the concentration

$$J = -D\frac{\partial c}{\partial x} \qquad \textbf{2.3}$$

J denotes the diffusional flux of the species, $\frac{\partial c}{\partial x}$ is the concentration gradient in direction x and D represents the diffusional coefficient. The negative sign signifies the material moving down a concentration gradient, i.e. moving from a region of higher concentration to a lower concentration.

Generally researchers are concerned with the change of concentration at a point as a function of time and this movement is described in Fick's second law of diffusion (see Equation 2.4).

$$\frac{\partial c}{\partial t} = D\frac{\partial^2 c}{\partial t^2} \qquad \textbf{2.4}$$

The progress of a reaction can result in the generation of a concentration gradient due to one of the species being consumed. However, in the case of microelectrodes which utilise very small diameters in the range of 5 – 300 μm (O'Neill *et al.*, 1998), currents

are small and minimal substrate is consumed, therefore a steady-state current is generated (i.e. $\frac{\partial c}{\partial t}$ = 0 no change in c with t).

For planar electrodes, which are uniformly available to species from the bulk solution, the variation of current with time is calculated from Fick's second law of diffusion, resulting in the generation of the Cottrell equation (Equation 2.5)

$$I = nFAJ = \frac{nFAD^{1/2}c_{\infty}}{(\pi t)^{1/2}} \qquad \textbf{2.5}$$

With I, the measured current at time t at the electrodes active site A being directly proportional to c_{∞}, the bulk concentration of the electroactive species. J is the flux, n denotes the number of electrons, D is the diffusion coefficient and F is the Faraday constant.

For any coordinated system a Laplace operator is substituted into Equation 2.3 to determine the flux for all electrode geometries which gives

$$J = -D\nabla^2 c \qquad \textbf{2.6}$$

and as a result, Fick's second law of diffusion for any geometry, becomes

$$\frac{\partial c}{\partial t} = D\nabla^2 c \qquad \textbf{2.7}$$

This research utilised cylinder electrodes so the laplacian operator is:

$$\frac{\partial^2}{\partial r^2} + (\frac{1}{r})(\frac{\partial}{\partial r}) \qquad \textbf{2.8}$$

In order to solve the above diffusion equations it is necessary to set conditions for the system to obey. These conditions include initial conditions (values at t = 0) and two boundary conditions.

Fick's first law for a species R at the electrode surface determines that the flux at the electrode, $J_R(0,t)$, is proportional to the current density, $\frac{i}{A}$.

$$-J_R(0,t) = \frac{i}{nFA} = D_R\left[\frac{\partial c_R(x,t)}{\partial x}\right]_{x=0} \qquad \textbf{2.9}$$

A is the surface area of the electrode, F is the Faraday constant, n is the number of electrons transferred and *i* is the current. The sum of the electrons transferred per unit time must be proportional to the concentration of R reaching the electrode surface over the specific time period.

2.4 Constant Potential Amperometry

Throughout this research project, the most commonly used electrochemical technique was CPA. This technique allows for the continuous monitoring of current by the application of a fixed potential where the redox reaction of the substrate of interest occurs (O'Neill, 1994). The application of a fixed potential during amperometric detection results in a negligible charging current, which minimises the background signal that adversely affects the limit of detection (LOD) (Ronkainen *et al.*, 2010). CPA allows for high temporal resolution to be achieved and also using sampling rates in the kHz range can resolve signals on a sub-millisecond timescale (Hermans, 2007). These characteristics make CPA an ideal technique for the *in-vitro*/*in-vivo* research discussed in this thesis.

Diffusion is considered to be the only mass transport form affecting CPA. In this instance, Equation 2.10 characterises the diffusion limits associated with the consumption of the analyte to produce a steady-state current (i_{ss})

$$i_{ss} = \frac{nFADC}{r} \qquad \textbf{2.10}$$

Where the i_{ss} is the steady-state current, n is the number of electrons, A is the area of the electrode, D is the diffusion coefficient, F is the Faraday constant, C is the concentration and r is the radius. However, other factors such as the geometry or the insulation thickness of the electrode have an effect on the steady-state current and therefore a geometric factor, G, is introduced into Equation 2.10:

$$i_{ss} = \frac{GnFADC}{r} \qquad \textbf{2.11}$$

The resulting current is directly proportional to the diffusion coefficient and the substrate concentration.

2.5 Enzymes

2.5.1 Introduction

Enzymes are efficient and selective biological catalysts; they increase the rate of reaction without themselves being used up in the process. The majority of enzymes are proteins and they are classified into six groups; oxidoreducatases, transferases, hydrolases, lyases, isomerases and ligases. These groups are classified based on the general class of organic chemical reaction that the enzyme catalyses. Enzymes are highly selective both in the reaction they catalyse and the substrates they act on, and the degree of substrate selectivity varies. Many enzymes exhibit stereoselectivity acting on only a single stereoisomer of the substrate. Reaction specificity is a key characteristic of enzymes and therefore the generation of wasteful by-products is very small (Horton *et al.*, 2002) (Berg *et al.*, 2002). Due to the selectivity of enzymes, they are highly desirable in the fabrication of biosensors. The use of the enzymes

superoxide dismutase (SOD) and xanthine oxidase (XOD) were essential in this research, for the development of a O_2^- biosensor.

Enzymes are constructed from long chains of amino acids which are folded into complex structures. The active site of an enzyme is the region that binds the substrates. The active site is a three-dimensional cleft or crevice that takes up a relatively small part of the total volume of the enzyme. The substrates are usually bound to the enzyme by multiple weak attractions with the specificity of substrate binding depending on the precisely defined arrangement of atoms in the active site (Berg *et al.*, 2002). Cu-Zn-SOD isolated from bovine erythrocytes is utilised throughout this thesis. It is a dimeric enzyme containing a Cu and a Zn ion, each subunit containing two active sites with each Cu ion coordinated by four histidine (His) residues in a distorted square-planar geometry (Carloni *et al.*, 1995).

2.5.2 Enzyme Kinetics

The primary function of enzymes is to enhance the rates of reactions so that they are compatible with the needs of the biological organism. The complex structure of enzymes leads to complex reaction mechanisms with many variables. A single substrate enzyme-catalysed reaction where one substrate binding site is present results in the following general enzyme equation which can be utilised to define the enzyme's kinetic activity.

$$E + S \underset{k_{-1}}{\overset{k_1}{\rightleftharpoons}} ES \underset{k_{-2}}{\overset{k_2}{\rightleftharpoons}} E + P \qquad \textbf{2.12}$$

E is the enzyme molecule, S is the substrate and P is the resulting product of the reaction. k_x refers to the rate constant for each specific reaction (x = 1, -1, 2, -2). The extent of the product formation is determined as a function of time. Initially, during the enzymatic reaction it is found that the concentration of the product is low and thus the reverse reaction of product to the enzyme-substrate complex, indicated by k_{-2}, is negligible. This yields the result shown in Equation 2.13

$$E + S \underset{k_{-1}}{\overset{k_1}{\rightleftharpoons}} ES \xrightarrow{k_2} E + P \qquad \textbf{2.13}$$

In 1913, Leonar Michaelis and Maud Menten proposed a simple model to account for the kinetic characteristics (Michaelis and Menten, 1913). The steady-state approximation can be applied to the formation and destruction of the enzyme-substrate complex which is the necessary intermediate of the enzyme catalysis. As a result the rate of change of [ES] with time is shown in Equation 2.14.

$$\frac{d[ES]}{dt} = k_1\,[E][S] - k_{-1}[ES] - k_2[ES] \qquad \textbf{2.14}$$

Where [E] is the concentration of unbound enzyme and [ES] is the concentration of the bound enzyme. Hence the total enzyme concentration $[E]_0$ can be substituted by,

$$\mathbf{[E] = [E]_0 - [ES]} \qquad \textbf{2.15}$$

Therefore,

$$\frac{d[ES]}{dt} = k_1\,[E]_0[S] - k_{-1}[ES][S] - k_{-1}\,[ES] - k_2[ES] \qquad \textbf{2.16}$$

Applying the steady-state approximation indicating the concentration of [ES] remains constant, setting $\frac{d[ES]}{dt} = 0$ gives:

$$k_1\,[E]_0[S] - k_{-1}[ES][S] - k_{-1}\,[ES] - k_2[ES] = 0 \qquad \textbf{2.17}$$

Using Equation 2.17 above, it is possible to isolate the concentration of the [ES] complex, yielding Equation 2.18

$$[ES] = \frac{[E]_0[S]}{[S] + \frac{k_{-1} + k_2}{k_1}} \qquad \textbf{2.18}$$

Michaelis and Menten replaced the $\frac{k_{-1}+k_2}{k_1}$ with K_M (Michaelis constant) to reduce Equation 2.18 to yield:

$$[ES] = \frac{[E]_0[S]}{[S] + K_M} \qquad \textbf{2.19}$$

K_M is an important characteristic of the [ES] interaction and is independent of enzyme and substrate concentrations. [ES] has been isolated as it governs the rate of reaction (v) and therefore the rate of formation of products, k_2, and is given by

$$\mathbf{v = k_2[ES]} \qquad \textbf{2.20}$$

Substituting into Equation 2.19 gives

$$v = \frac{k_2[E]_0[S]}{[S] + K_M} \qquad \textbf{2.21}$$

If the concentration of the substrate is very high compared to the enzyme then the enzyme will only exist as the complex ES and the rate of reaction can reach its maximal initial velocity, V_{max}. Thus, since [S] >> K_M and:

$$V_{max} = k_2[E]_0 \qquad \textbf{2.22}$$

then

$$v = \frac{V_{max}[S]}{[S] + K_M} \qquad \textbf{2.23}$$

Michaelis and Menten assumed that the substrate was usually present in higher concentrations than the enzyme. Therefore the initial substrate concentration $[S]_0$ is much greater than the initial enzyme concentration $[E]_0$. In this instance, $[S] = [S]_0$ and as a result Equation 2.23 becomes:

$$v = \frac{V_{max}[S]_0}{[S]_0 + K_M} \qquad \textbf{2.24}$$

When experimental values of v are plotted against $[S]_0$, as shown in Figure 2.3, we observe a rectangular hyperbola. From this graph we observe the V_{max} which is the maximal initial velocity, at a particular $[E]_0$. The K_m can also be calculated from the graph, when $v = \frac{V_{MAX}}{2}$

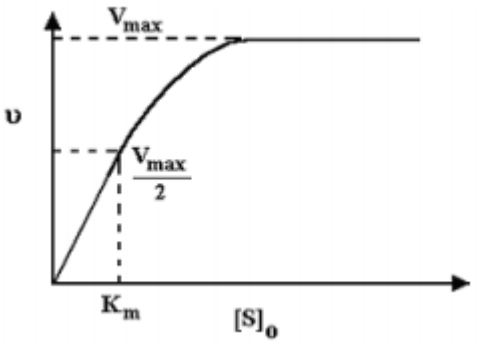

Figure 2.3: Graph of v against substrate concentration $[S]_0$ for a given enzyme concentration $[E]_0$ for a single substrate enzyme catalysed reaction from the Michaelis-Menten equation.

The Michaelis-Menten equation is a very useful analytical tool, because of its simplicity to make approximations, however, this equation fails to take account of specific circumstances. Some enzymes exhibit sigmoidal behaviour, rather than the hyperbolic curve seen in Figure 2.3, and in this case a deviation is made to the Michaelis-Menten equation. This kinetic behaviour is observed when more than one molecule of substrate binds to a single molecule of enzyme. However, when the enzyme binding sites are similar and independent the response will be hyperbolic as illustrated in Figure 2.3. In circumstances where a co-operative effect is observed, the binding of a substrate to one active site on the enzyme increases the affinity of other sites on the enzyme to bind more molecules of substrate - then sigmoidal kinetics is observed. For sigmoidal behaviour, deviations were made to ideal Michaelis-Menten kinetics and the Hill type equation was formulated (see Equation 2.25) by Lowry *et al.* (Lowry and O'Neill, 1994) (Lowry and O'Neill, 1992).

$$i = \frac{V_{max}}{1 + \left(\frac{K_M}{[S]}\right)^{\alpha}} \qquad \textbf{2.25}$$

Where i is the current observed from the oxidation of H_2O_2 at the surface of the electrode used to measure the rate of reaction. The α value acts as an indication of the deviation from ideal Michaelis-Menten kinetics, where an α value of 1 equates to ideal

behaviour. Conversely, an α value greater than 1 is indicative of sigmoidal behaviour indicating positive cooperativity.

2.5.3 Superoxide Dismutase

The discovery of SOD, has been termed the most important discovery of modern biology never to win a Nobel prize (Perry *et al.*, 2010). The ubiquitous SODs catalyse the dismutation of O_2^- to oxygen (O_2) and H_2O_2 at one of the fastest enzyme rates known with an enzymatic turnover of $\sim 10^6$ reactions per second (McCord, 2001) and therefore, are critical for protecting the cell against the toxic effects of the ROS species (Perry *et al*., 2010). Three types of SOD enzymes have been identified, all characterised by their prosthetic metal centre and their cellular localisation: Cu-Zn-SODs, Mn-SOD/Fe-SODs and Ni-SODs. However, they are all classified as SODs by virtue of their ability to catalyse the dismutation of O_2^- (Miller, 2012) (Perry *et al*., 2010) (Maier and Chan, 2002). A schematic representation of the common mechanism utilised by the SOD's to scavenge O_2^- is shown below in Figure 2.4.

Cu-Zn-SOD also known as SOD 1 is a 32 kDa dimer consisting of 153 amino acids that exist intracellularly (Maier and Chan, 2002). This relatively small protein constitutes a large fraction of total cell protein with an approximate *in-vivo* concentration of 10 µM (Rae *et al*., 1999). The active site of the oxidised form of SOD 1 has a Cu^{2+} ion coordinated in a distorted square pyramid by a solvent molecule and four His, with one acting as a ligand to a distorted tetrahedral Zn^{2+} coordinated by two other His and an aspartate (Asp^-) (Miller, 2004). SOD 1 is located primarily in astrocytes throughout the central nervous system (CNS), but is also detectable in neurons (Lindenau *et al*., 2000). The enzyme used throughout this thesis is Cu-Zn-SOD purified from bovine erythrocytes.

Mn-SOD called equivalently SOD 2 is a mitochondrial enzyme composed of a 96 kDa homotetramer which is localised in the mitochondrial matrix. Fe-SOD shows similar homology to Mn-SOD, however, this enzyme is usually absent in eukaryotes (Fukai and Ushio-Fukai, 2011). The active site of Mn/Fe-SOD is located between the N and C terminal domains and contains just one metal ion. The metal ion is coordinated in a strained trigonal bi-pyramidal geometry by four amino acid side chains, His 26, His

74, Asp 159 and His 163, and by one solvent molecule. The O_2^- reaches the active site through a funnel that uses electrostatics for guidance and has a narrow entrance to the active site allowing access for only smaller ions (Perry *et al.*, 2010). Mn-SOD is primarily located in neurons throughout the brain and spinal cord which is expected due to the high metabolic rate of these cells (Maier and Chan, 2002). However, Mn-SOD is only responsible for approximately 20% of SOD activity in the brain, whereas 80% is due to the Cu-Zn-SOD activity. Therefore, neuronal mitochondria seem to account for only a small proportion of the total SOD activity (Lindenau *et al.*, 2000).

The third class of SOD, Ni-SOD, originally identified in Streptomyces and cyanobacteria is characterised by the presence of a Ni metal centre (Youn *et al.*, 1996). Ni-SOD is a protein consisting of 120 amino acids. Access to the narrow active site channel is limited to O_2^- and a nearby group of conserved lysine residues aids electrostatic steering, while the tyrosine (Tyr9) functions as a gatekeeper (Perry *et al.*, 2010). However, there is no evidence that Ni-SOD is contained in gram-positive bacteria, archaea or eukaryotes other than green algae (Schmidt *et al.*, 2009) (Miller, 2012).

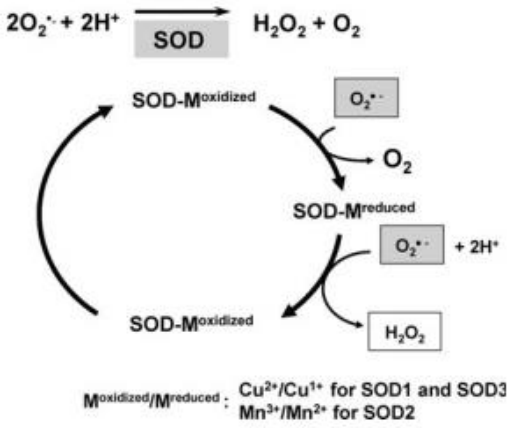

Figure 2.4: A schematic representation of the common mechanism of scavenging O_2^- by the SOD (Fukai and Ushio-Fukai, 2011).

2.5.4. Xanthine Oxidase

Milk XOD was originally described as aldehyde oxidase and since its discovery in 1912 has served as the benchmark for the whole class of complex metalloflavoproteins (Enroth *et al.*, 2000). Notably the enzyme xanthine oxidoreductase exists in two interconvertible forms; xanthine dehydrogenase and XOD. Corte and Stripe reported the first evidence of this enzyme originally in the form of xanthine dehydrogenase, but this enzyme can be converted under certain circumstances to XOD (Corte and Stirpe, 1972). This conversion occurs due to two mechanisms; the first by the oxidation of the sulfhydryl residues or by proteolysis.

XOD utilises xanthine and O_2 as a cofactor to produce uric acid (UA) and O_2^- (see Equation 2.26), therefore XOD can be postulated to be a major source of O_2^- intracellular production (Aitken *et al.*, 1993) (Kuppusamy and Zweier, 1989). Conversely, the native form of the enzyme xanthine dehydrogenase acts with xanthine but utilises nicotinamide adenine dinucleotide (NAD) as a cofactor for the reaction resulting in the formation of nicotinamide adenine dinucleotide phosphate (NADPH) and UA and this form of the enzyme is the predominant form in well organised tissues (Doehner and Landmesser, 2011):

$$\text{Xanthine} + H_2O + O_2 \xrightarrow{\text{XOD}} UA + O_2^- + 2H^+ \qquad \textbf{2.26}$$

The active form of the enzyme is a 290 kDa homodimer, with each subunit containing one molybdopterin cofactor, two spectroscopically distinct Fe_2S_2 centres and one flavin adenine dinucleotide (FAD) (Chung *et al.*, 1997) (Enroth *et al.*, 2000). Xanthine oxidoreductase enzymes have been isolated from a wide variety of organisms from bacteria to man (Enroth *et al.*, 2000); throughout this research XOD isolated from bovine milk was utilised. This enzyme was placed in the PBS (pH 7.4) and various aliquots of xanthine were injected into the electrochemical cell to generate O_2^-.

2.6 Hydrogen Peroxide

The use of Pt as an electrochemical catalyst for the oxidation of H_2O_2 in amperometric biosensors incorporating enzymes has been used extensively by many research groups (Lowry *et al.*, 1994) (O'Brien *et al.*, 2007) (Zain *et al.*, 2010) (Burmeister *et al.*, 2003) (Mitchell, 2004) (Parikh *et al.*, 2004). The H_2O_2 is generated by a specific enzyme reaction and the rate of oxidation is proportional to the analyte concentration (O'Neill *et al.*, 2004) (Hall *et al.*, 1998(a)). The oxidation process is well characterised as a two-electron transfer first proposed by Hickling and Wilson, and further investigated by Lingane and Lingane (Hickling and Wilson, 1951) (Lingane and Lingane, 1963). The mechanism is based on the formation of a thin Pt oxide with which the H_2O_2 acts to reduce, and then the current is attributed to the re-oxidation of the Pt (Hall *et al.*, 1998(b)). The mechanism of oxidation is detailed below (Hall *et al.*, 1998(b))

$$H_2O_2 + Pt(OH)_2 \rightleftharpoons Pt(OH)_2 . H_2O_2 \qquad \textbf{2.27}$$

$$Pt(OH)_2 . H_2O_2 \rightleftharpoons Pt + 2H_2O + O_2 \qquad \textbf{2.28}$$

$$Pt + 2H_2O \rightleftharpoons Pt(OH)_2 + 2H^+ + 2e^- \qquad \textbf{2.29}$$

The first two equations (Eqn 2.27, Eqn 2.28) detail the breakdown of this Pt oxidised complex into H_2O, O_2 and an unoxidised Pt. Equation 2.29 shows the re-oxidation of the Pt surface and it is the release of these two electrons that generates the current that is measured at the electrode surface.

2.7 Electropolymerisation of o-Phenylenediamine

Enzyme-based amperometric biosensors incorporating the permselective layer poly-*o*-phenylenediamine (PPD) have been manufactured for various analytes including glucose, glutamate and H_2O_2 (McMahon and O'Neill, 2005) (Lowry and O'Neill, 1994) (Malitesta *et al.*, 1990) (Wilson and Gifford, 2005) (O'Brien *et al.*, 2007). PPD can be deposited electrochemically from *o*-PD to produce a thin self-sealing insulating polymer on the Pt surface (Killoran and O'Neill, 2008). The film thickness of PPD grown under these experimental conditions are generally in the region of 10-35 nm (Malitesta *et al.*, 1990) (Myler *et al.*, 1997). PPD demonstrates beneficial traits being highly permeable to the enzyme generated H_2O_2 (Hamdi *et al.*, 2005) (Lowry and O'Neill, 1994) and effectively rejects larger interferent species such as ascorbic acid (AA) (Craig and O'Neill, 2003) (O'Neill *et al.*, 2008).

The structure of the insulating form of PPD is still not determined, however, two structures have been hypothesised (Prună and Brânzoi, 2012) . A ladder-like structure (Figure 2.5(A)) is proposed where the amino groups are condensed, within the benzene ring adjacent to each other along the polymer chain. Alternatively, an "open" 1,4-substituted benzenoid-quinoid structure (Figure 2.5(B)) has been assumed (Yano, 1995). Recent reports have determined that increased amino content is found when PPD is formed in neutral pH (Losito *et al*., 2003) suggesting that the PPD films formed in this research are of the "open" structure. Ullah *et al.* performed density functional theory (DFT) and time dependent (TD-DFT) calculations to gain insight into the structure of the PPD layer with both proposed structures investigated using the oligomer approach. This research proved to be inconclusive for identifying the dominant form of the structure, as both the Raman and IR results indicated a contribution from both structures. However, the UV-Vis spectra calculated using TD-DFT concluded that the real molecular structure of the PPD has a major contribution from the ladder structure and a small contribution from the open structure (Ullah *et al.*, 2013).

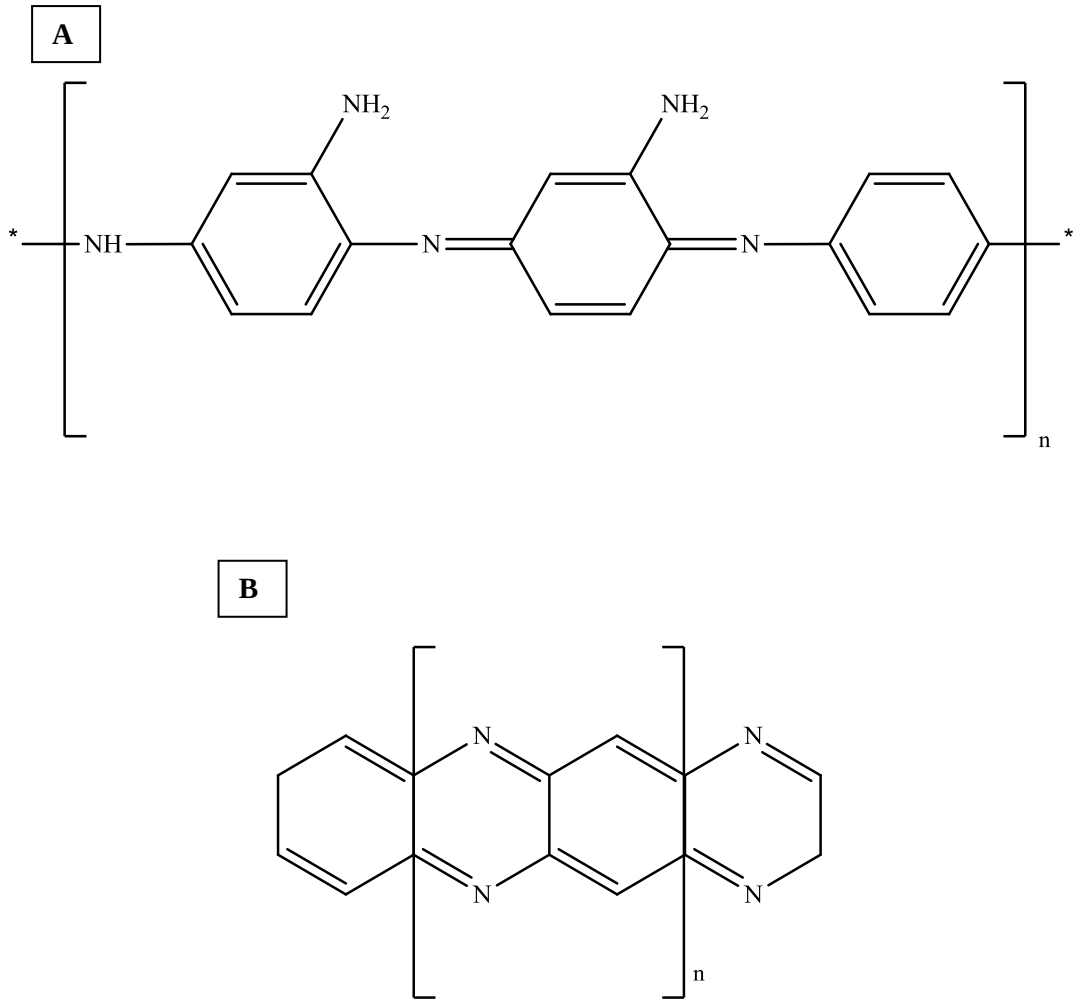

Figure 2.5: Possible structures for the polymeric form of o-PD (Sayyah *et al.*, 2009).

2.8 Ascorbic Acid

AA is a water soluble antioxidant essential for normal physiological function, with roles in the repair and growth of tissues and wound healing (Iqbal *et al.*, 2004). AA has been identified as an important antioxidant, enzyme cofactor and neuromodulator in the brain. The brain, spinal cord and adrenal glands have the highest AA concentration of all the tissues in the body and the total brain ascorbate levels are kept under strong homeostatic regulation (Rice, 2000). The AA concentration in the extracellular fluid (ECF) of the brain is approximately 500 µM (Miele and Fillenz, 1996).

This electroactive compound is readily oxidised at metal electrodes having an $E_{1/2}$ between -100 to +400 mV *vs.* SCE (O'Neill *et al.*, 1998). The mechanism for this reaction is a 2 e^- process resulting in the formation of L-dehydroascorbic acid. The hydrolysis of L-dehydroascorbic acid results in the production of an electro-inactive open chain product L-2,3-diketogulonic. The mechanism for this reaction is shown in Figure 2.6.

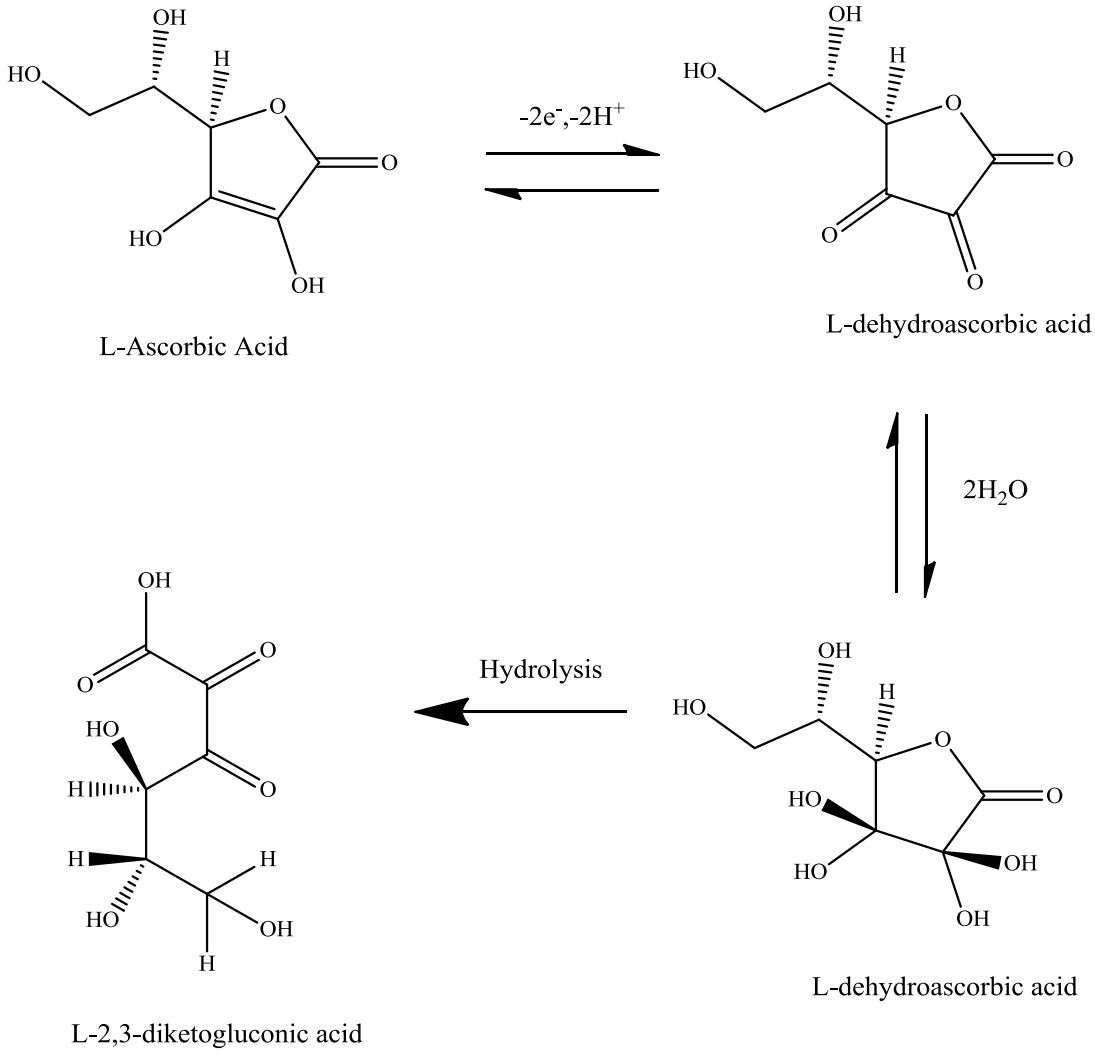

Figure 2.6: Reaction scheme for the oxidation of AA.

2.9 Data Analysis

All data was analysed after cessation of the experiments using linear or non-linear regression. The regression was applied after the average steady-state current value was obtained and this value was plotted on a graph of current response against substrate concentration.

2.9.1 Linear and Non-Linear Regression

Regression fitting involves finding a line or a curve which minimises the sum of the squares of the vertical distances of the points to the fitted line or curve. Linear regression is also known as the line of best fit. Linear regression fits were applied to AA, H_2O_2, NO and O_2 calibrations. Non-linear regression fits taking the form of the Michaelis-Menten equation and the modified Hill Type equation (see Section 2.5.2) were applied to enzymatic calibrations. On completion of the linear and non-linear regression, other statistical analysis tests were performed on the data sets in order to provide additional information and to enable comparisons to be drawn.

2.9.2 Statistical Analysis

Statistical analysis is carried out to determine if various data sets are significantly different. Throughout this research t-tests were employed as the method of analysis. Two forms of t-tests were utilised; unpaired t-tests and paired t-tests. Paired t-tests were performed on electrodes that differed only by post production intervention, for example stability over days or protein treatment. Unpaired t-tests were performed on electrodes that differed in their production method, for example different layering process or incorporation of different biosensor components. These t-tests were performed using GraphPad Prism and yielded a resulting P-value.

The assigned P-value is a probability, thus its value lies between $0 \leq P \leq 1$. It describes the statistical difference between two values and allows one to decide whether or not it is significantly different. The smaller the P-value the more likely it is to be significantly different. A confidence interval of 95% was used for these tests therefore, a P-value of < 0.05 was required to indicate a significant difference between the two

data sets involved. A P-value greater than 0.05 indicated no significant difference between the data sets involved.

The R^2 value, also known as the (coefficient of correlation)^2, is a measure of the goodness of fit of a data set to a line. It is a unitless value within the range $0 \leq R^2 \leq 1$. A value of 1 indicates a perfect fit, where all points lie directly on the line. A value of 0 indicates that there is no linear (non-linear) relationship between the X and Y values in the data set.

2.10 References

Aitken R, Buckingham D and Harkiss D. (1993) Use of a xanthine oxidase free radical generating system to investigate the cytotoxic effects of reactive oxygen species on human spermatozoa. *Journal of Reproduction and Fertility* 97: 441-450.

Bard AJ and Faulkner LR. (2000) *Electrochemical Methods: Fundamentals and Applications, 2nd Edition*: John Wiley & Sons.

Berg JM, Tymoczko JL and Stryer L. (2002) *Biochemistry, Fifth Edition*: W.H. Freeman.

Burmeister JJ, Palmer M and Gerhardt GA. (2003) Ceramic-based multisite microelectrode array for rapid choline measures in brain tissue. *Analytica Chimica Acta* 481: 65-74.

Carloni P, Bloechl PE and Parrinello M. (1995) Electronic structure of the Cu, Zn superoxide dismutase active site and its interactions with the substrate. *The Journal of Physical Chemistry* 99: 1338-1348.

Chung HY, Baek BS, Song SH, *et al*. (1997) Xanthine dehydrogenase/xanthine oxidase and oxidative stress. *Age* 20: 127-140.

Corte ED and Stirpe F. (1972) The regulation of rat liver xanthine oxidase. Involvement of thiol groups in the conversion of the enzyme activity from dehydrogenase (type D) into oxidase (type O) and purification of the enzyme. *Biochemical Journal* 126: 739-745.

Craig JD and O'Neill RD. (2003) Comparison of simple aromatic amines for electrosynthesis of permselective polymers in biosensor fabrication. *Analyst* 128: 905-911.

Doehner W and Landmesser U. (2011) Xanthine oxidase and uric acid in cardiovascular disease: clinical impact and therapeutic options. *Seminars in Nephrology*. Elsevier, 433-440.

Enroth C, Eger BT, Okamoto K, *et al.* (2000) Crystal structures of bovine milk xanthine dehydrogenase and xanthine oxidase: structure-based mechanism of conversion. *Proceedings of the National Academy of Sciences* 97: 10723-10728.

Fisher AC. (1996) *Electrode Dynamics*: Oxford University Press.

Fukai T and Ushio-Fukai M. (2011) Superoxide dismutases: role in redox signaling, vascular function, and diseases. *Antioxidants & Redox Signaling* 15: 1583-1606.

Hall SB, Khudaish EA and Hart AL. (1998(a)) Electrochemical oxidation of hydrogen peroxide at platinum electrodes. Part 1. An adsorption-controlled mechanism. *Electrochimica Acta* 43: 579-588.

Hall SB, Khudaish EA and Hart AL. (1998(b)) Electrochemical oxidation of hydrogen peroxide at platinum electrodes. Part II: effect of potential. *Electrochimica Acta* 43: 2015-2024.

Hamdi N, Wang J and Monbouquette HG. (2005) Polymer films as permselective coatings for H_2O_2-sensing electrodes. *Journal of Electroanalytical Chemistry* 581: 258-264.

Hermans A. (2007) *Fabrication and Applications of Dopamine-Sensitive Electrodes*: ProQuest.

Hickling A and Wilson W. (1951) The anodic decomposition of hydrogen peroxide. *Journal of The Electrochemical Society* 98: 425-433.

Horton H, Moran L, Ochs R, *et al.* (2002) *Principles of Biochemistry 3rd Edition*. Pearson Education

Iqbal K, Khan A and Khattak MMAK. (2004) Biological significance of ascorbic acid (Vitamin C) in human health–a review. *Pakistan Journal of Nutrition* 3: 5-13.

Killoran SJ and O'Neill RD. (2008) Characterization of permselective coatings electrosynthesized on Pt–Ir from the three phenylenediamine isomers for biosensor applications. *Electrochimica Acta* 53: 7303-7312.

Kuppusamy P and Zweier JL. (1989) Characterization of free radical generation by xanthine oxidase. Evidence for hydroxyl radical generation. *Journal of Biological Chemistry* 264: 9880-9884.

Lindenau J, Noack H, Possel H, *et al*. (2000) Cellular distribution of superoxide dismutases in the rat CNS. *Glia* 29: 25-34.

Lingane JJ and Lingane PJ. (1963) Chronopotentiometry of hydrogen peroxide with a platinum wire electrode. *Journal of Electroanalytical Chemistry (1959)* 5: 411-419.

Losito I, Palmisano F and Zambonin PG. (2003) o-Phenylenediamine Electropolymerization by Cyclic Voltammetry Combined with Electrospray Ionization-Ion Trap Mass Spectrometry. *Analytical Chemistry* 75: 4988-4995.

Lowry JP, McAteer K, El Atrash SS, *et al.* (1994) Characterization of Glucose Oxidase-Modified Poly(phenylenediamine)-Coated Electrodes *in vitro* and *in vivo*: Homogeneous Interference by Ascorbic Acid in Hydrogen Peroxide Detection. *Analytical Chemistry* 66: 1754-1761.

Lowry JP and O'Neill RD. (1992) Homogeneous mechanism of ascorbic acid interference in hydrogen peroxide detection at enzyme-modified electrodes. *Analytical Chemistry* 64: 453-456.

Lowry JP and O'Neill RD. (1994) Partial characterization *in vitro* of glucose oxidase-modified poly(phenylenediamine)-coated electrodes for neurochemical analysis *in vivo*. *ElectroAnalysis* 6: 369-379.

Maier CM and Chan PH. (2002) Book Review: Role of Superoxide Dismutases in Oxidative Damage and Neurodegenerative Disorders. *The Neuroscientist* 8: 323-334.

Malitesta C, Palmisano F, Torsi L, *et al.* (1990) Glucose fast-response amperometric sensor based on glucose oxidase immobilized in an electropolymerized poly(o-phenylenediamine) film. *Analytical Chemistry* 62: 2735-2740.

McCord JM. (2001) Analysis of Superoxide Dismutase Activity. *Current Protocols in Toxicology.* John Wiley & Sons, Inc.

McMahon CP and O'Neill RD. (2005) Polymer−Enzyme Composite Biosensor with High Glutamate Sensitivity and Low Oxygen Dependence. *Analytical Chemistry* 77: 1196-1199.

Michaelis L and Menten ML. (1913) Die kinetik der invertinwirkung. *Biochemistry* 49: 352.

Miele M and Fillenz M. (1996) *In vivo* determination of extracellular brain ascorbate. *Journal of Neuroscience Methods* 70: 15-19.

Miller AF. (2004) Superoxide dismutases: active sites that save, but a protein that kills. *Current Opinion in Chemical Biology* 8: 162-168.

Miller AF. (2012) Superoxide dismutases: Ancient enzymes and new insights. *FEBS Letters* 586: 585-595.

Mitchell KM. (2004) Acetylcholine and Choline Amperometric Enzyme Sensors Characterized i*n vitro* and i*n vivo*. *Analytical Chemistry* 76: 1098-1106.

Myler S, Eaton S and Higson SPJ. (1997) Poly(o-phenylenediamine) ultra-thin polymer-film composite membranes for enzyme electrodes. *Analytica Chimica Acta* 357: 55-61.

O'Neill RD. (1994) Microvoltammetric techniques and sensors for monitoring neurochemical dynamics *in vivo*. A review. *Analyst* 119: 767-779.

O'Neill RD, Lowry JP and Mas M. (1998) Monitoring brain chemistry *in vivo*: voltammetric techniques, sensors, and behavioral applications. *Critical Reviews in Neurobiology* 12: 69-128.

O'Brien K, Killoran S, O'Neill R, *et al*. (2007) Development and characterization *in vitro* of a catalase-based biosensor for hydrogen peroxide monitoring. *Biosensors and Bioelectronics* 22: 2994-3000.

O'Neill RD, Chang S-C, Lowry JP, *et al.* (2004) Comparisons of platinum, gold, palladium and glassy carbon as electrode materials in the design of biosensors for glutamate. *Biosensors and Bioelectronics* 19: 1521-1528.

O'Neill RD, Rocchitta G, McMahon CP, *et al*. (2008) Designing sensitive and selective polymer/enzyme composite biosensors for brain monitoring *in vivo*. *TrAC Trends in Analytical Chemistry* 27: 78-88.

Parikh V, Pomerleau F, Huettl P, *et al*. (2004) Rapid assessment of *in vivo* cholinergic transmission by amperometric detection of changes in extracellular choline levels. *European Journal of Neuroscience* 20: 1545-1554.

Perry JJP, Shin DS, Getzoff ED, *et al.* (2010) The structural biochemistry of the superoxide dismutases. *Biochimica et Biophysica Acta (BBA) - Proteins and Proteomics* 1804: 245-262.

Prună A and Brânzoi F. (2012) Electrochemical activity and microscopy of electrosynthesised poly(o-phenylenediamine) nanotubes. *Journal of Polymer Research* 19: 1-8.

Rae TD, Schmidt PJ, Pufahl RA, *et al*. (1999) Undetectable Intracellular Free Copper: The Requirement of a Copper Chaperone for Superoxide Dismutase. *Science* 284: 805-808.

Rice ME. (2000) Ascorbate regulation and its neuroprotective role in the brain. *Trends in Neurosciences* 23: 209-216.

Ronkainen NJ, Halsall HB and Heineman WR. (2010) Electrochemical biosensors. *Chemical Society Reviews* 39: 1747-1763.

Sayyah SM, El-Deeb MM, Kamal SM, *et al.* (2009) Electropolymerization of o-phenylenediamine on Pt-electrode from aqueous acidic solution: Kinetic, mechanism, electrochemical studies and characterization of the polymer obtained. *Journal of Applied Polymer Science* 112: 3695-3706.

Schmidt A, Gube M, Schmidt A, *et al.* (2009) In silico analysis of nickel containing superoxide dismutase evolution and regulation. *Journal of Basic Microbiology* 49: 109-118.

Ullah H, Shah A-u-HA, Ayub K, *et al*. (2013) Density Functional Theory Study of Poly(o-phenylenediamine) Oligomers. *The Journal of Physical Chemistry C* 117: 4069-4078.

Wilson GS and Gifford R. (2005) Biosensors for real-time *in vivo* measurements. *Biosensors and Bioelectronics* 20: 2388-2403.

Yano J. (1995) Electrochemical and structural studies on soluble and conducting polymer from o-phenylenediamine. *Journal of Polymer Science Part A: Polymer Chemistry* 33: 2435-2441.

Youn HD, Kim EJ, Roe JH, *et al*. (1996) A novel nickel-containing superoxide dismutase from Streptomyces spp. *Biochemical Journal* 318: 889-896.

Zain ZM, O'Neill RD, Lowry JP, *et al.* (2010) Development of an implantable d-serine biosensor for *in vivo* monitoring using mammalian d-amino acid oxidase on a poly(o-phenylenediamine) and Nafion-modified platinum–iridium disk electrode. *Biosensors and Bioelectronics* 25: 1454-1459.

Chapter 3: Experimental

3.1. Introduction

This chapter outlines the materials and methods used in the development and characterisation of a superoxide (O_2^-) biosensor *in-vitro*. The design of this sensor is based primarily, on previously designed Pt-based biosensors recently characterised in the research group. These biosensors have used styrene and methyl methacrylate (MMA) as an immobilisation matrix and used the dip adsorption method to incorporate the enzyme onto the Pt surface (Baker, 2013) (Bolger, 2007). The rejection of potential endogenous electroactive interferents by the application of an *o*-phenylenediamine (*o*-PD) layer has also previously been utilised in sensor designs (Lowry *et al.*, 1994) *(*Malitesta *et al.*, 1990) (Ryan *et al.*, 1997). This chapter also describes the design of the oxygen (O_2) and nitric oxide (NO) sensors utilised in an animal model of Parkinson's disease (PD). The O_2 sensor is a carbon paste electrode based on previous work carried out by Bolger *et al.* and Lowry *et al.* (Lowry *et al.*, 1996) (Bolger *et al.*, 2011(b)). The NO sensor is a Nafion®-modified Pt electrode which has been extensively characterised in the research group *(*Brown *et al.*, 2005) (Brown *et al.*, 2009) (Brown and Lowry, 2003).

Section 3.2 and Section 3.3 outlines the computer-based instrumentation, equipment and chemicals used throughout this project. Section 3.4 describes the manufacturing process of the different sensor types. The modifications to the O_2^- sensor are detailed in Section 3.5. The electrochemical set-up and the *in-vitro* experiments performed to characterise the various sensor types are described in Section 3.6. Section 3.7 gives details on the synthesis of NO and the use of UV spectrometry to determine the stock concentration. Finally, Section 3.8 provides details of the procedures performed in order to utilise these sensors in the *in-vivo* environment.

3.2 Computer-Based Instrumentation and Equipment

Throughout this research project, computer-based instrumentation was utilised in order to collect the experimental data. This instrumentation consisted of three main components; the computer, the PowerLab® interface system and the potentiostat. The function of each of these different components is outlined in the next section. The *in-vitro* experimental set-up is shown below in Figure 3.1.

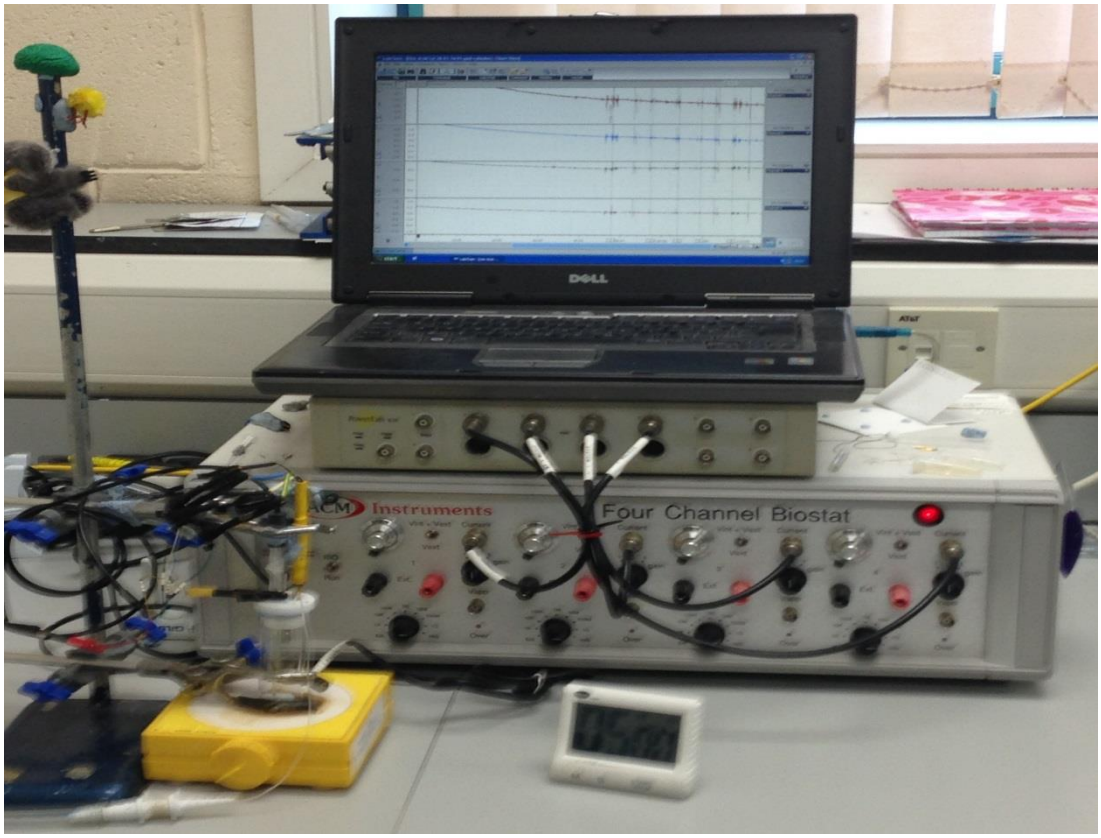

Figure 3.1: The *in-vitro* experimental set-up.

3.2.1 The Computer

A Dell Latitude D531 laptop running at 1.6 GHz was utilised for all *in-vitro* experiments. *In-vivo* data was attained using an iMAC operating with OS X and an Intel core 2 duo processor running at 2.4 GHz.

3.2.2 The PowerLab®

The PowerLab® is a data acquisition system comprising of hardware and software to record and display experimental data. These systems contain the digital-to-analogue converters (DAC) and the analogue-to-digital converters (ADC) which allow communication between the computer (digital) and the potentiostat/electrochemical cell (analogue). The system used throughout this research was an eight channel PowerLab® 8/30 from AD Instruments (see Figure 3.2).

Figure 3.2: An image of the PowerLab® 8/30 utilised in the research

3.2.3 The Potentiostat

The potentiostat used throughout this research was a 4-channel Biostat from ACM instruments (see Figure 3.3). The main function of the potentiostat is to apply a known potential to the working electrodes and to monitor the resulting current.

Figure 3.3: An image showing the potentiostat used in this project

3.2.4 Computer Programs

Constant potential amperometry (CPA) was carried out and analysed using LabChart 6 (AD Instruments, Oxford, UK.). All graphical and statistical analysis was performed using GraphPad Prism version 5.01 (GraphPad Software Inc., CA. USA). The former included linear regression and non-linear regression (fitting Michaelis-Menten enzymatic curves to the Hill-type equation), while statistical analysis consisted of paired and unpaired t-tests (See Section 2.9.1 and Section 2.9.2).

3.2.5 Supplementary Equipment

3.2.5.1 *In-Vitro* Equipment

Air-pump

The air pump used was a Rena Air 200 from RENA®, France.

Electronic Balance

Two electronic balances were used in this research; a three decimal place BP 210P and a four decimal place LA 230S, both supplied from Sartorius®, AG Gottingen, Germany.

Microscope

The microscope used in *in-vitro* electrode preparation was the stereo microscope SZ51 from Olympus America Inc. For *in-vivo* surgeries a SZ61 microscope (Olympus) was utilised.

pH meter

The pH meter used was the S20 Seveneasy ™ from Mettler-Toleda Switzerland and the CyberScan pH 510 from Eutech Instruments

Sonicator

The sonicator used was a Fisherbrand FB11002, Leicestershire, UK.

Vortex

The vortex used was a REAX Top Vortex supplied by Heidolph, Germany.

Magnetic Stirrer

The magnetic stirrer utilised was the Yellowline MST mini supplied by Lennox, Ireland.

Oven

A Binder ED 23 oven (Binder Scientific, Manchester, UK) was utilised for the production of the NO sensors.

3.2.5.2 *In-Vivo* Equipment

Anaesthetic Set-up

This set-up consisted of a vaporiser for induction and a Univentor 400 anaesthesia unit. The air pump in the system was a stellar S30 and the induction chamber used was a 1.4 L perspex box all supplied by AgnThos, Sweden. The entire anaesthetic set-up was contained within a laminar flow unit supplied by AirScience^{TM} and the induction chamber was contained within a fumehood.

Incubator

On completion of surgery, the animals were placed in a pre-heated Thermacage MKII heated incubator from Datesand Ltd, UK.

Stereotaxic Frame

The digital stereotaxic frame was sourced from Kopf Instruments.

3.3 Chemicals and Solutions

All chemicals were used as supplied unless otherwise stated. All solutions were prepared from doubly distilled, deionised water.

3.3.1 Chemicals

A list of the *in-vitro* and *in-vivo* chemicals utilised throughout this research project is shown below. The relevant supplier is also stated for each chemical.

3.3.1.1 Enzymes

Catalase	Sigma Aldrich
Superoxide Dismutase (SOD)	Sigma Aldrich
Xanthine oxidase (XOD)	Sigma Aldrich

3.3.1.2 Enzyme Substrate

Xanthine	Sigma Aldrich

3.3.1.3 *In-Vitro* Chemicals

3,4-Dihydroxypheylacetic acid	Sigma Aldrich
5-Hydroxyindoleacetic acid	Sigma Aldrich
5-Hydroxytryptomine (5-HT)	Sigma Aldrich
Acetone	Sigma Aldrich
Ascorbic Acid (AA)	Sigma Aldrich
Bovine Serum Albumin (Fraction V) (BSA)	Sigma Aldrich
Dehydroascorbic acid	Sigma Aldrich
Dopamine (DA)	Sigma Aldrich
Glutaraldehyde (GA)	Sigma Aldrich
Graphite powder	Sigma Aldrich

Homovanillic acid (HV)	Sigma Aldrich
Hydrogen Peroxide (30% w/w ACS reagent)	Sigma Aldrich
L-Cysteine	Sigma Aldrich
L-Glutathione	Sigma Aldrich
L-Tryptophan	Sigma Aldrich
L-Tyrosine	Sigma Aldrich
Methyl Methacrylate (MMA)	Sigma Aldrich
Nafion®	Sigma Aldrich
N-1-naphthyl-ethylenediamine (NEDD)	Sigma Aldrich
Nitrogen gas (N_2)	BOC Gases
Nitric oxide gas (NO)	In-house synthesis
Oxygen gas (O_2)	BOC Gases
o-Phenylenediamine (*o*-PD)	Sigma Aldrich
Polyethyleneimine (PEI)	Sigma Aldrich
Potassium hydroxide (KOH)	Sigma Aldrich
Potassium chloride (KCl)	Sigma Aldrich
Pyrogallol	Sigma Aldrich
Silicon oil	Aldrich Chemical
Sodium Chloride (NaCl)	Sigma Aldrich
Sodium Hydroxide (NaOH)	Sigma Aldrich
Sodium nitrite ($NaNO_2$)	Sigma Aldrich
Sodium Phosphate Monobasic Monohydrate ($NaH_2PO_4.H_2O$)	Sigma Aldrich
Styrene	Sigma Aldrich
Sulfanilamide (SULF)	Sigma Aldrich
Sulphuric acid (97%) (H_2SO_4)	Fischer Scientific
Uric Acid (UA)	Sigma Aldrich

3.3.1.4 *In-Vivo* Chemicals

Acetic Acid (100%) (CH_3COOH)	VWR
Buprenorphine hydrochloride (Tamgesic®)	Sigma Aldrich
Dentalon®	Hereaus Kulzer Gmbh
Isoflurane	Abbott Laboratories, IRL.
Sodium chloride (NaCl)	Sigma Aldrich
Reserpine	Sigma Aldrich

3.3.2 Solutions

All solutions were prepared on the day the experiment was carried out, unless otherwise stated. All solutions were dissolved in Millipore water (H_2O), unless stated otherwise. All solutions were prepared as stated below.

3.3.2.1 *In-Vitro* Solutions

Enzyme solutions

Superoxide Dismutase

Three enzyme solutions were used in the development of this biosensor. A 100 U, 200 U and 400 U solutions were prepared by dissolving 0.00036 g, 0.00072 g and 0.00144 g of SOD, respectively, in 1 mL of H_2O.

Xanthine Oxidase

One enzyme solution was used in the development of the O_2^- biosensor. A 0.002 U solution was prepared by adding 33.4 µL of XOD in 5 mL of PBS. This solution was made immediately before use.

Catalase

25 mg of catalase was dissolved in 1 mL of PBS. The solution was agitated until all the catalase had dissolved.

Enzyme Substrates

Xanthine

A 1 mM stock solution of xanthine was prepared by dissolving 0.0015 g of xanthine in 10 mL of H_2O. This required sonication for five minutes for complete dissolution yielding a cloudy solution.

General Solutions

Ascorbic Acid

A 0.1 M stock solution of AA was prepared by dissolving 0.176 g in 10 mL of H_2O.

Bovine serum albumin

For sensor designs 0.1% and 1% solutions of BSA were used. These solutions were prepared by dissolving 0.001 and 0.01 g of BSA in 1 mL of H_2O, respectively. The 0.01% solution of BSA was prepared by taking 0.1 mL of the 0.1% BSA solution and making this solution up to 1 mL in H_2O.

Carbon paste

250 µL of silicon oil was added to 0.71 g of graphite powder and this solution was thoroughly mixed together. This mixing process lasted approximately 3 hrs and was facilitated by the use of a pestle and mortar. This process ensured complete mixing of the two components.

Catalase-Glutaraldehyde (Cat-GA$_{0.25\%}$)

A Cat-GA (0.25%) solution was prepared by dissolving 25 mg of catalase in 1 mL of 0.25% GA solution.

Glutaraldehyde

Three concentrations of GA were investigated during the development process for the O_2^- biosensor; 0.05%, 0.5% and 1%. The 0.05%, 5% and 1% GA solutions were prepared by dissolving 2 µL, 20 µL and 40 µL, respectively, of 25% stock GA solution in 1 mL H_2O. The Catalase biosensor incorporated a 0.25% GA solution. This solution was prepared by dissolving 10 µL of GA in 1 mL of PBS.

Glutaraldehyde:BSA

This solution was prepared by dissolving 0.01 g of BSA in 0.5 mL H_2O. To this 20 µL of the 25% GA solution was added and the solution was made up with 1 mL of H_2O yielding a 1% w/v BSA and 0.5% v/v GA solution. This process is preferential as BSA added to GA results in immediate and irreversible cross-linking. A similar method was used to prepare a 0.1% w/v BSA and 0.5% v/v GA solution, however, 0.001 g of BSA was dissolved in 0.5 mL H_2O.

Neutral Griess Reagent

A reagent consisting of 0.4 mM NEDD and 0.017 mM SULF was prepared in 100 µM PBS (pH 7.4), containing 0.293 g SULF and 0.0104 g NEDD in 100 mL PBS.

Nitric Oxide

A stock solution of NO was prepared by bubbling the gas into H_2O and its subsequent concentration was determined by UV spectrometry.

o-Phenylenediamine

A 300 mM solution of *o*-PD was prepared by dissolving 0.324 g in 10 mL of N_2 saturated PBS. The solution was placed in a sonic bath and agitated with N_2 for approximately 10 minutes to ensure maximum dissolution.

Polyethyleneimine

Three concentrations of PEI were used during the development of this sensor; 1%, 2% and 3%. These solutions were prepared by dissolving 0.03125 g, 0.0625 g, 0.09375 g respectively of PEI (80% ethoxylated 35-40% solution in water) into 1 mL of H_2O.

Phosphate Buffer Saline

PBS was prepared by dissolving 8.9 g of NaCl, 0.15 M, 1.76 g of NaOH, 0.044 M and 6.06 g of $NaH_2PO_4.H_2O$, 0.044 M in 1 L of H_2O. The pH was adjusted to pH 7.4 if required using NaOH or $NaH_2PO_4.H_2O$.

Potassium Hydroxide

A 4 M KOH solution was prepared by dissolving 224 g of KOH in 1 L of H_2O.

Pyrogallol 5% alkaline

A 5% stock solution was prepared by dissolving 5 g of pyrogallol in 100 mL 4 M KOH.

Sodium nitrite

A saturated stock solution of $NaNO_2$ was prepared in H_2O.

Sulfuric Acid

A 6 M H_2SO_4 stock solution was prepared from a 97% H_2SO_4 commercial solution. 329 mL of H_2SO_4 was added with care to H_2O. This solution was made up to 1 L with H_2O.

Uric Acid

A stock solution of UA was prepared by the dissolution of 0.038 g in 10 mL of H_2O. This solution required sonication for 10 minutes for complete dissolution.

3.3.2.2 *In-Vivo* Solutions

Saline Solution

A 0.9% solution was prepared by dissolving 0.9 g NaCl in 100 mL H_2O.

Acetic Acid Solution

A 0.5% solution of CH_3COOH (Teixeira *et al.*, 2009) was prepared by dissolving 0.5 mL of 100% commercially available CH_3COOH in 100 mL of H_2O. This solution when prepared had an acidic pH of ~ 2.5. This pH would cause significant irritation to the animal so the pH was adjusted to a neutral pH of 7 prior to administration (Fernandes *et al.*, 2008).

Reserpine Solution

A 5 mg/kg solution was prepared by dissolving reserpine in a solution of 1 mL H_2O. Dissolution required agitation and the use of a sonic bath for ~ 10 minutes to yield a cloudy solution. This was injected in a volume of 1 mL.

A 0.1 mg/kg reserpine solution was prepared by dissolving 0.1 mg in 1 mL H_2O or 0.5% CH_3COOH solution (pH adjusted). Again, dissolution required agitation and the use of a sonic bath. This was injected in a volume based on the weight of the animal.

3.4 Electrode Preparation

3.4.1 Carbon Paste Electrode

Carbon paste electrodes were manufactured using 5 cm lengths of Teflon®-insulated silver wire (200-µm bare diameter, 270-µm coated diameter (8-T), Advent Research Materials, Suffolk, UK). The wire was carefully cut at both ends using a scalpel blade to create an even disc surface. 3 mm of the wire was exposed by removing the Teflon® from one end of the wire and the Teflon® was carefully pushed up the wire to create a 2 mm cavity. The 3 mm of exposed wire at the opposite end of the wire was then soldered into a gold clip for electrical conductivity and rigidity. The cavity was then packed with carbon paste (Section 3.3.2.1) by dipping the tip of the electrode into the paste and then using a bare length of silver wire the carbon paste was pushed into the cavity of the electrode. This process was repeated until the cavity was completely packed. A flat active surface at the tip of the electrode was obtained by gently tapping the electrode against a hard, flat surface.

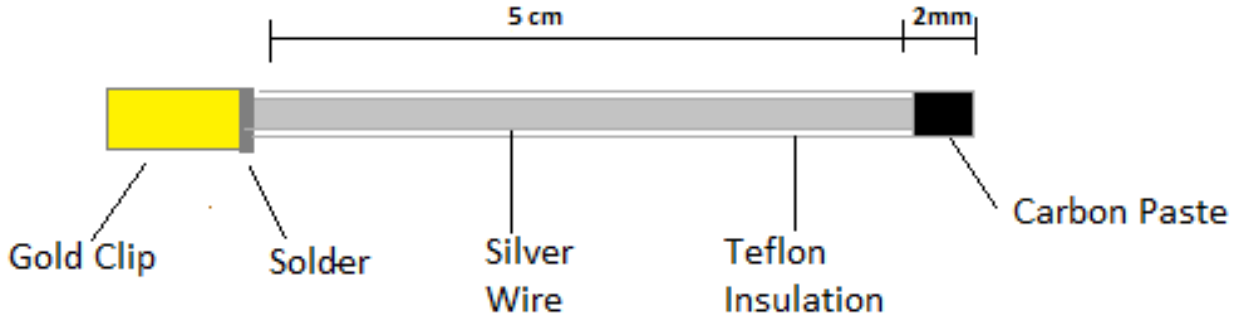

Figure 3.4. : A schematic representation of a carbon paste electrode.

3.4.2 Platinum Working Electrodes

The Pt electrodes were constructed using 6 cm of Teflon®-coated Pt/Ir (90%/10%) wire (127-µm bare diameter, 203-µm coated diameter (5T), Science Products GmbH, Hofheimer Straße 63, D-65719 Hofheim). A section of the Teflon® insulation was removed at one end of the wire which was then soldered into a gold clip providing both an electrical contact and rigidity. The active surface was created by carefully cutting the opposite end of the wire using a scalpel blade exposing a disc surface (See Figure 3.5(a)). A 1 mm cylinder Pt electrode was prepared in the same way as the Pt disc electrode, however, after the wire was soldered into a gold clip and a fresh disc surface was cut a 1 mm portion of the Teflon® coating was removed from the wire to expose a 1 mm active surface (see Figure 3.5(b)).

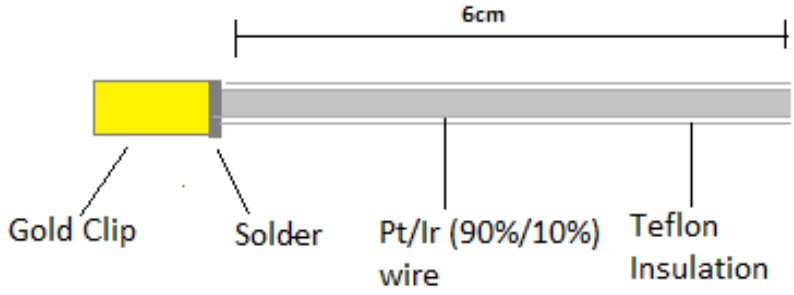

Figure 3.5(a): A schematic representation of a Pt/Ir disc electrode.

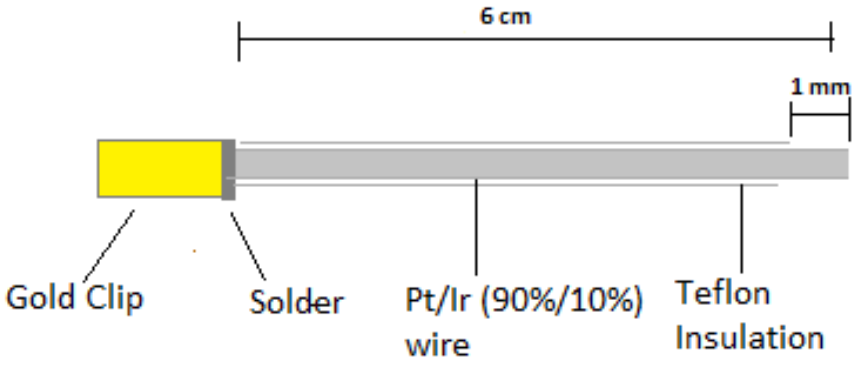

Figure 3.5(b): A schematic representation of a Pt/Ir 1 mm cylinder working electrode.

3.5 Electrode Modifications

3.5.1 Poly-*o*-phenylenediamine-modified electrodes

The electropolymerisation of *o*-PD onto the Pt electrodes was carried out in a three-electrode cell by applying a fixed potential of +700 mV *vs* SCE for 30 minutes. A 300 mM solution of *o*-PD was prepared as detailed in Section 3.3.2.1. As *o*-PD is easily oxidised in air the electrochemical cell was N_2 saturated and a N_2 atmosphere was maintained throughout the polymerisation process. Immediately, after polymerisation the electrodes were removed and rinsed in H_2O. The electrodes were allowed to dry at room temperature for at least three hrs before calibration or modification. This polymerisation process produced a thin self-sealing insulating polymer layer on the Pt surface.

3.5.2 Superoxide Biosensor

During the development of the O_2^- biosensor different variations in the manufacturing process were utilised. All sensors were polymerised with *o*-PD as described in Section 3.5.1 prior to modification unless otherwise stated. A list and description of each design is presented here. All modifications were allowed to dry overnight at 4^{o}C.

Development

Sty-(SOD)$_{1,2,5,10}$: A Pt-PPD 1 mm electrode was dipped into a pure solution of styrene followed by one, two, five or ten dip(s) into a solution of SOD. This was allowed to dry for four minutes at room temperature. The electrode was then re-dipped into the enzyme solution one, four or nine more time(s). Each dip coat of enzyme was given a four minute drying time

Sty-(SOD-GA)$_{2,5,10}$: A Pt-PPD 1 mm electrode was dipped into a pure solution of styrene followed immediately by a dip into a solution of SOD and a separate GA solution. This was allowed to dry for four minutes. The electrode was then sequentially

re-dipped into the enzyme and GA solution once more or a further four/nine times. Each dip series had a four minute drying time.

Sty-(SOD-BSA-GA)$_{2,5,10}$: A Pt-PPD 1 mm electrode was dipped into a pure solution of styrene followed immediately by a dip into a solution of SOD, a separate solution of BSA and a separate solution of GA. This was allowed to dry for four minutes. The electrode was then sequentially re-dipped into the enzyme, BSA and GA solutions once more or a further four/nine times. Each dip series had a four minute drying time.

Sty-(SOD-GA-PEI)$_{2,5,10}$: A Pt-PPD 1 mm electrode was dipped into a pure solution of styrene followed immediately by a dip into a solution of SOD, a separate solution of GA and a separate solution of PEI. This was given a four minute drying time at room temperature. The electrode was then sequentially re-dipped into the enzyme, GA and PEI solutions once more or a further four/nine times. Each dip series had a four minute drying time.

Sty-(SOD-BSA-GA-PEI)$_5$: A Pt-PPD 1 mm electrode was dipped into a pure solution of styrene followed immediately by a dip into a solution of enzyme, a separate solution of BSA, a separate solution of GA and a separate solution of PEI. This was given a four minute drying time at room temperature. The electrode was then sequentially re-dipped into the enzyme, BSA, GA and PEI solutions a further four times. Each dip series had a four minute drying time.

Sty-(SOD-BSA:GA-PEI)$_5$: A Pt-PPD 1 mm electrode was dipped into a pure solution of styrene followed immediately by a dip into a solution of enzyme, a solution of BSA and GA and a separate solution of PEI. This was given a four minute drying time. The electrode was then sequentially re-dipped into the enzyme, BSA:GA and PEI solutions a further four times. Each dip series had a four minute drying time.

MMA-(SOD-GA-PEI)$_5$: A Pt-PPD 1 mm electrode was dipped into a pure solution of MMA followed by a dip into a solution of SOD, a separate solution of GA and a separate solution of PEI. This was given a four minute drying time at room temperature. The electrode was then sequentially re-dipped into the enzyme, GA and PEI solutions a further four times. Each dip series had a four minute drying time.

Interference Designs

Pt-Catalase Biosensor: This catalase biosensor was prepared using the same procedure as previously developed and characterised in the research group (O'Brien *et al.*, 2007) (O' Riordan, 2013) A Cat-Ga$_{(0.25\%)}$ solution as described in 3.3.2.1 was prepared. The Pt-PPD sensor was placed in the catalase solution for an initial period of five minutes and the electrodes were subsequently allowed to air dry for five minutes. Following this drying period a further four dips of *ca.* 0.5 s duration were carried out with five minutes of air drying in between each immersion. The catalase solution was kept over ice during the modification to maintain the enzyme.

Sty: A Pt-PPD 1 mm electrode was dipped in a pure solution of styrene.

(GA)$_2$: A Pt-PPD 1 mm electrode was dipped into a GA solution. This was given a four minute drying time at room temperature. The electrode was sequentially re-dipped into the GA solution.

(PEI)$_2$: A Pt-PPD 1 mm electrode was dipped in a PEI solution. This was given a four minute drying time at room temperature. The electrode was sequentially re-dipped into the PEI solution

Sty-(GA-PEI)$_2$: A Pt-PPD 1 mm electrode was dipped into a pure solution of styrene, a separate solution of GA and a separate solution of PEI. This was given a four minute

drying time at room temperature. The electrode was sequentially re-dipped into the GA and PEI solutions.

Sty-(GA-PEI)$_5$: A Pt-PPD 1 mm electrode was dipped in a pure solution of styrene followed by a dip into a GA solution and a separate PEI solution. This was given a drying time of four minutes at room temperature. The electrode was sequentially re-dipped into the GA and PEI solution a further four times. Each dip series had a four minute drying time.

3.5.3. Nitric Oxide Sensor

The design of this sensor is based on previous work carried out in our research group (Brown and Lowry, 2003) (Brown *et al.*, 2009). The Nafion®-modified Pt disc electrodes were constructed using the method for manufacturing Pt electrodes detailed in Section 3.4.2. A pre-coat application method was employed to modify the surface of the Pt electrode. This method involved placing a fixed volume of Nafion® on a clock glass using a syringe. The application of a Nafion® droplet was allowed to air dry at room temperature for five minutes. Once the solvent had evaporated, further droplets of Nafion® were placed on top of the original droplet. This process was repeated five times yielding a localised concentrated layer of Nafion® which was then allowed to dry for ~ 30 minutes. After this, a final application of Nafion® was placed on top of the concentrated layer on the clock glass. The active surface of the electrode was then dipped through the concentrated layer of Nafion® on the clock glass and allowed to air dry for two minutes. The electrodes were then placed in the oven and annealed for five minutes at 210 °C. On completion of the annealing process, the electrode was further coated with another application of Nafion® following the same procedure. On cessation of the annealing process the electrodes were soldered into gold clips to provide an electrical contact and rigidity. A schematic representation of a NO sensor is depicted in Figure 3.6.

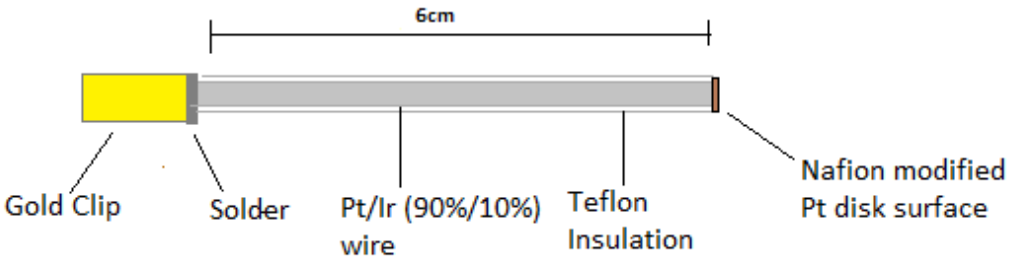

Figure 3.6: A schematic representation of a NO sensor.

3.5.4. Oxygen Sensors

Oxygen sensors used during this research were carbon paste electrodes which have previously been characterised and utilised by the research group for the detection of oxygen *in-vitro* and *in-vivo* (Bolger *et al.*, 2011(a)) (Bolger *et al.*, 2011(b)) (Bolger and Lowry, 2005) (Lowry *et al.*, 1996).

3.6 *In –Vitro* Electrochemical Experiments

3.6.1 Electrochemical Cell

The electrochemical cell used throughout this project was of in-house construction. It consisted of a 25 mL glass vial and a custom made Teflon® lid. The O_2^- calibrations were performed in a 10 mL pyrex beaker with a custom-made Teflon® lid. The Teflon® cap consisted of openings for the placement of the reference, auxiliary and working electrodes. In addition, there was an injection port for the addition of aliquots of analyte and a gas inlet. The reference electrode utilised was a saturated calomel electrode (SCE) which maintained a fixed potential against which the working electrode can be compared. The auxiliary electrode acts as a source or sink for electrons and silver wire was utilised to perform this role. The working electrode is the place where the electrochemical reaction takes place. All *in-vitro* calibrations were

performed in PBS (pH 7.4) at room temperature (21˚C - 23˚C) unless otherwise stated. A schematic of the electrochemical set-up is depicted below in Figure 3.7.

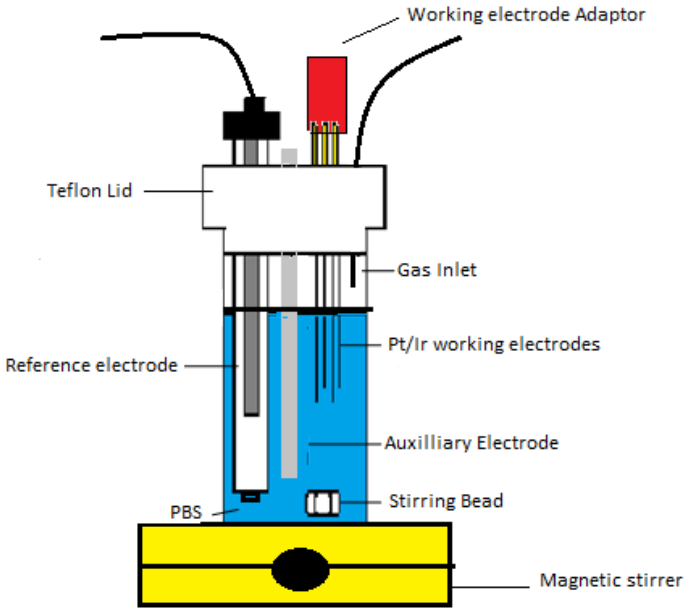

Figure 3.7: A schematic representation of the *in-vitro* electrochemical set-up.

3.6.2 Constant Potential Amperometry

CPA was utilised to calibrate all sensors. CPA involves the application of a fixed potential where the redox reaction of the substrate of interest takes place and allows for the continuous monitoring of current as a function of time (O'Neill, 1994). All O_2^- calibrations were performed at +700 mV *vs.* SCE. For the calibration of O_2 electrodes a potential of -650 mV *vs.* SCE was applied while for the NO sensors a potential of +900 mV *vs.* SCE was utilised. The fixed potential was applied to the working electrodes and the electrodes were given time to settle until the non-faradaic current reached a steady baseline current. When the desired baseline current was achieved, calibrations were performed which consisted of injecting a fixed volume of analyte into the buffer solution through the injection port. The solution was agitated for *ca.* 3-5 s using a magnetic stirring bead to help mix the solution and then the solution was allowed to reach a steady state before administration of a subsequent aliquot of analyte into the buffer solution.

3.6.3 Superoxide Calibrations

The O_2^- electrodes were placed in an electrochemical cell containing 0.002 U of xanthine oxidase (XOD). The electrodes were polarised at +700 mV *vs.* SCE and allowed to reach a steady-state prior to calibration. This usually required approximately 2-3 hrs. A freshly prepared solution of 1 mM xanthine (see Section 3.3.2.1) was then used and various aliquots were injected into the XOD solution. This solution was then agitated for *ca.* 3-5 s using a magnetic stirring bead to facilitate mixing. The current was recorded continuously and the solution was allowed to return to a steady-state before the administration of a subsequent aliquot of xanthine. The concentration range for the xanthine calibrations were:

0, 3, 6, 10, 20, 40, 60, 80, 100,200, 300, 400, 500, 600 µM

The combination of xanthine (0 – 600 µM) and XOD 0.002 U produced the O_2^- anion in a manner dependent on the concentration of xanthine. The univalent reduction of O_2 by XOD generating the O_2^- anion is dependent on pH. At pH 7.4, the yield of O_2^- was 28% of the total xanthine present in the reaction (Mesároš *et al.*, 1998). Therefore the concentrations for the O_2^- calibrations were:

0, 0.28, 0.84, 1.68, 2.80, 5.60, 11.20, 16.80, 22.40, 28, 56, 84, 112, 140, 154 µM

All experimental data in Chapter 4 (Development) is presented in terms of O_2^- concentration as SOD is immobilised on the Pt surface which facilitates the enzymatic reaction and the generation of H_2O_2. All experimental data in Chapter 5 (Interferences) is presented as a xanthine concentration unless otherwise stated.

3.6.4 Ascorbic Acid Calibrations

Standard AA calibrations were performed at a potential of +700 mV *vs.* SCE in a N_2 saturated cell under a N_2 atmosphere to maintain N_2 dissolution. The electrodes were allowed to reach a steady baseline current before the commencement of the calibration. Aliquots of a 0.1 M N_2 saturated AA stock solution (See Section 3.3.2.1) were injected into the buffer solution. The solution was stirred (*ca.* 3-5 s) using a magnetic stirring bead to uniformly mix the solution. The current was allowed to return to a steady-state before the administration of the next aliquot of AA. The concentration range for the AA calibrations were:

0, 200, 400, 600, 800, 1000 µM

AA calibrations performed on the NO sensors followed the same procedure, however, a potential of +900 mV was utilised. This potential was employed as it is the optimum potential for the oxidation of NO (Pallini *et al.*, 1998).

3.6.5 Uric Acid Calibrations

Standard UA calibrations were performed at a potential of +700 mV *vs.* SCE in a N_2 saturated cell under a N_2 atmosphere to maintain N_2 dissolution. Upon application of a potential, a capacitance current was instantly observed and the electrodes were allowed to reach a steady baseline current before commencement of the calibration. Aliquots of UA stock solution (see Section 3.3.2.1) were injected into the buffer solution. The solution was agitated for *ca.* 3-5 s to aid in the mixing process and the electrodes were allowed to return to a steady state current before the administration of subsequent aliquots of UA. The concentration range for the UA calibrations were:

0, 10, 20, 30, 40, 50, 60 µM

3.6.6 Oxygen Calibrations

The potential applied to the O_2 electrodes was -650 mV *vs.* SCE. The electrodes were allowed to settle before being calibrated. Various concentrations of O_2 were used. A *ca.* 0 µM concentration of O_2 was obtained by deoxygenating the cell utilising N_2 gas (Dixon *et al.*, 2002). A 240 µM concentration of O_2 was obtained by bubbling air through the buffer solution (Kanofsky, 1988). A 1200 µM concentration of O_2 was obtained by bubbling pure O_2 gas through the buffer solution until it was saturated (Lowry *et al.*, 1996). Each bubbling and quiescent period lasted approximately 30 minutes. The current was recorded continuously and the currents during the quiescent period were chosen for analysis.

To determine the O_2 sensitivity of electrodes at low physiological O_2 concentrations (0-125 µM) O_2 saturated PBS was utilised. PBS (20 mL) was placed in a glass cell using a syringe and this PBS was bubbled with N_2 for 30 minutes before commencement of the calibration - this ensured a 0% concentration of O_2. When the electrodes had reached a steady-state, standard aliquots (+416, +425, +434, +443 and +452 µL) of the saturated O_2 PBS solution were injected into the cell. The solution was agitated for *ca.* 3-5 s to facilitate mixing and the electrodes were allowed to return to a steady-state current before the administration of a subsequent aliquot. The concentration range for the O_2 calibrations were:

0, 25, 50, 75, 100, 125 µM

3.6.7 Nitric Oxide Calibrations

NO calibrations were performed at a potential of +900 mV *vs.* SCE in N_2 saturated PBS with a N_2 atmosphere. Aliquots of NO stock solution (see Section 3.3.2.1) were injected into the buffer solution. The solution was agitated for *ca.* 3-5 s to aid in the mixing process and the electrodes were allowed to return to a steady-state current before the administration of subsequent aliquots of analyte. The concentration range for the NO calibrations were:

0, 0.2, 0.4, 0.6, 0.8, 1.0 µM

3.6.8 Post Implantation Calibrations

Following removal of the headpiece, post *in-vivo* recording calibrations were carried out using the same procedure as detailed in Section 3.6.6 for O_2 sensors and Section 3.6.7 for NO sensors. The headpiece was connected to the potentiostat via the pedestal (see Figure 3.10).

3.7 Nitric Oxide Synthesis and UV Spectrometry

NO was synthesised in-house using an experimental method reported previously by our research group (Brown *et al.*, 2005). In summary, deoxygenated deionised water was placed in a round bottom flask which was then sealed with a rubber septum. The flask was then placed in a sonic bath for ten minutes and connected to the NO generation apparatus (see Figure 3.8). This round bottom flask was used for the collection of NO gas. The NO generation apparatus was purged with N_2 for at least 30 minutes prior to commencement of the synthesis. The use of 5% alkaline pyrogallol, and ensuring that all Quickfit joints were sealed with Parafilm, created an inert atmosphere for NO synthesis. NO gas was synthesised by the reaction of saturated $NaNO_2$ (see Section 3.3.2.1) with 6 M H_2SO_4 (See Section 3.3.2.1). The saturated $NaNO_2$ was introduced slowly into the H_2SO_4 and the reaction was stirred to facilitate the generation of NO. The gas was then passed through three Drescher bottles containing 4 M KOH (See Section 3.3.2.1) to remove any higher oxides and collected in the collection flask with the total process lasting *ca.* fifteen minutes.

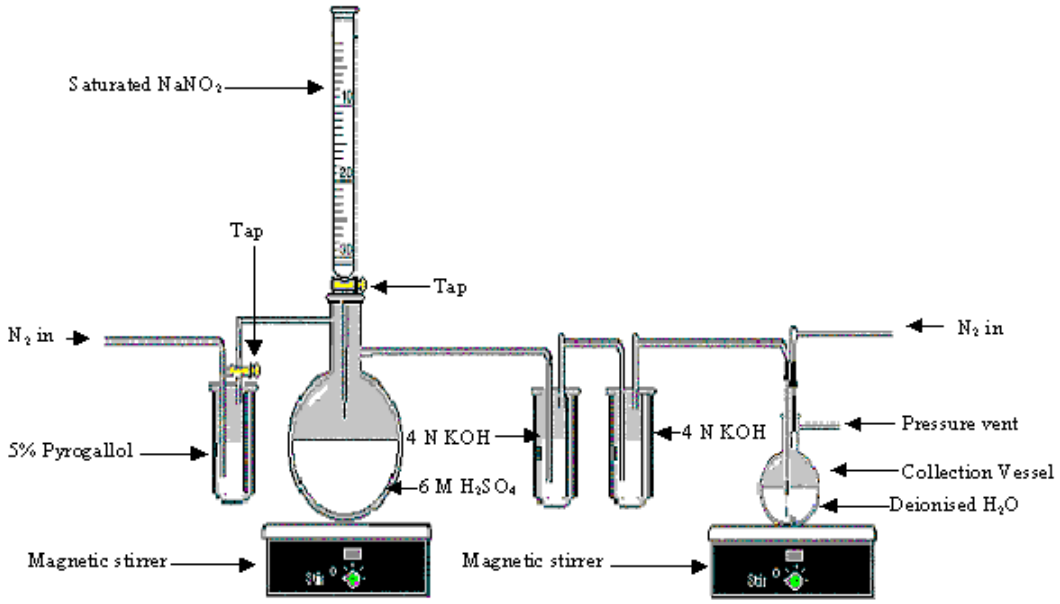

Figure 3.8: A schematic representation of the experimental set-up used to generate NO (Brown *et al.*, 2005).

UV spectrometry was carried out on completion of the NO synthesis to determine the stock concentration of NO. This procedure was described previously by Brown *et al.* (Brown *et al.*, 2005). Briefly, addition of NO to neutral griess reagent (see Section 3.3.2.1) under aerobic conditions results in a visible absorbance at 496 nm and the NO concentration is determined using the Beer Lambert Law.

3.8 *In-Vivo* Experiments

This section details the procedures and materials utilised for the implantation of different sensors in the brains of male Wistar rats. All experiments were conducted under license (B100/2205). All procedures were approved by Maynooth University Ethics Committee in accordance with the Council of the European Parliament Directive 2010/63/EU and Irish Statutory Instrument SI 543/2012. All *in-vivo* experiments were recorded continuously over a 24 hour period.

3.8.1 Subjects

The animals utilised in this *in-vivo* work were male Wistar rats. These animals were obtained from Charles River (UK Ltd., Manstin Rd.,Margate, Kent CT9 4LT UK). Animals typically weighted between 200-250 g on arrival. The animals were subject to regular handling and were group housed prior to surgery. They were housed in a temperature (17–23°C), humidity and light controlled (lights on 07:00, lights off 19:00) environment. Access to food and water was *ad libitum*.

3.8.2 Surgical Protocol

All surgical procedures were carried out under aseptic conditions. The surgical area and equipment were sterilised and all instruments were autoclaved prior to commencement of the surgery. The animal was anaesthetised in a perspex induction chamber using isoflurane (4 % in air; IsoFlo) for 4-5 minutes. Once the animal was anesthetised its weight was recorded and the top of the animal's head was shaved. The animal was transferred to a stereotaxic frame in a laminar flow hood and anaesthesia was maintained (1.5-3.0% in air depending on the level of pain during the surgery) using a nosepiece. The ear bars were placed into position and the animal's mouth was gently held shut with an elastic band to help maximise the effect of the isoflurane. A rectal temperature probe was inserted into the animal and normal physiological temperature was maintained using a heating pad under the animal. The area where the incision would be made was disinfected with an iodine solution and the animal was covered with a sterile surgical drape. Confirmation that the animal was under anaesthetic was carried out (checking tail and paw reflexes), prior to commencing the surgery.

An incision was then made along the anterior-posterior plane. The skull was exposed using sterile cotton swabs to push aside the tissue and four clamps were used to hold the incision open and to keep the surgical drape anchored during the surgery. The stereotaxic co-ordinates were referenced from the rat atlas of Paxinos and Watson (Paxinos and Watson, 2006). The anterior-posterior (A-P) and medial-lateral (M-L) co-ordinates were referenced from a zero-point, bregma, with positive A-P coordinates representing anterior to bregma, and positive M-L co-ordinates indicating the right

hemisphere. Dorsal Ventral (D-V) co-ordinates are referenced with respect to the dura with higher negative values indicating depth into the brain. All experiments were carried out in the striatum and the co-ordinates used were.

Table 3.1: Stereotaxic co-ordinates for electrode implantation in brain.

Brain Region	A-P	M-L	D-V
Striatum	+1.0 mm	± 2.5 mm	-5.0 mm

A permanent marker was used to mark the co-ordinates for the working electrodes, the reference electrode and for four support screws (one of which acts as the auxiliary electrode) arranged as in Figure 3.9. Each of the holes for the support screws were made using a hand-held drill and each screw was implanted immediately after each hole was drilled. Two bore holes were drilled for the working electrodes and the dura was pierced with a needle for *ca.* 5 s to provide a clear path for the implantation of the electrodes. The reference electrode was also put into place. The electrodes were then lowered into position.

A thin layer of loose cement (Dentalon Plus; Heraeus) was applied over the skull to hold all the electrodes in place. The cement was built up to the height of the screws and allowed to dry before the wires from the various electrodes were separated from the arms of the stereotaxic frame. The gold clips of each electrode were placed in the pedestal as in Figure 3.10 and cemented into place. The wires were then tidied into the centre of the headpiece and covered with cement until no wire was visible through the cement and there were no fissures for the animal to get a hold of. The top of the pedestal remained cement free to allow for the attachment of the cable connecting the electrodes to the potentiostat.

The animal was given a subcutaneous injection containing 0.9 mL saline (0.9 %) for rehydration and 0.1 mL buprenorphine (0.3 mg/mL; Buprecare) for postoperative analgesia and sedation. Two further subcutaneous injections of 1.0 mL saline each were given for rehydration alone. Finally, the scalp was sutured to allow the skin to heal around the headpiece. Anaesthesia was ceased and the animal was then removed

from the stereotaxic frame to be placed in a pre-warmed incubator until fully recovered. Animals were returned to their home bowl when sufficiently recovered and were assessed for good health.

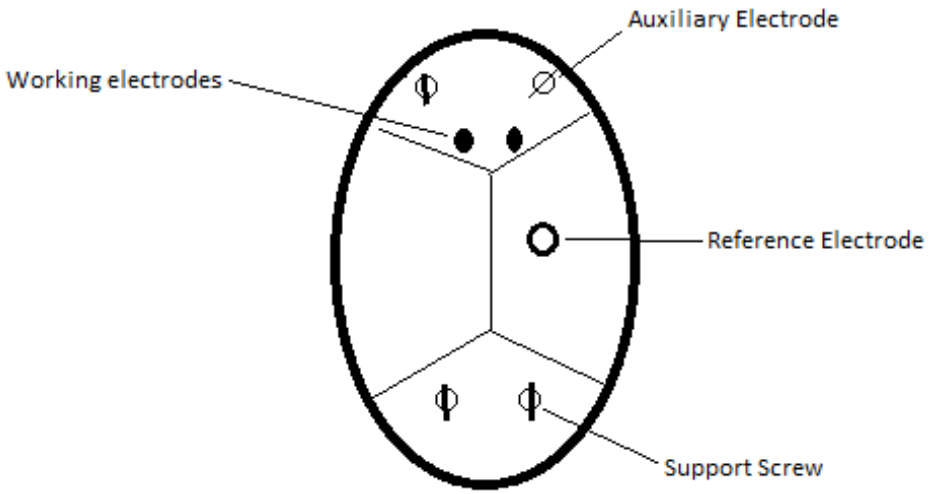

Figure 3.9: Schematic of typical orientation of drill holes for placement of skull screws, auxiliary electrode, reference electrode and working electrodes.

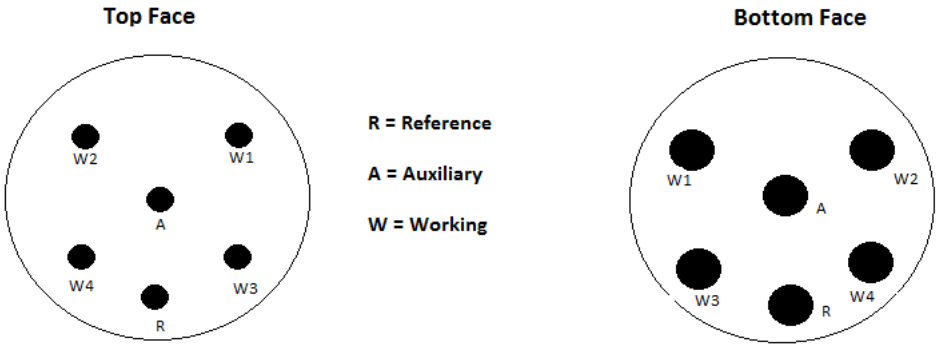

Figure 3.10: Schematic of the Teflon® pedestal used for *in-vivo* experiments.

3.8.3 *In-Vivo* Reference and Auxiliary Electrode

The auxiliary and reference electrode were constructed in a similar way to the carbon paste electrode (See Section 3.4.1). The reference potential provided by the silver wire implanted in brain tissue is similar to that of an SCE (O'Neill, 1993). The silver wire was soldered into the gold clip and epoxy was applied to the exposed area of the wire just above the clip to provide the electrodes with support and rigidity during surgery. The reference electrode was manufactured by exposing 3 mm of Teflon® from the opposite end of the wire and then the wire was bent leaving exposed wire at the tip (see Figure 3.11(A)) The auxiliary electrode was fabricated in the same way, however, the exposed bare wire was soldered onto a surgical screw (see Figure 3.11(B)).

A

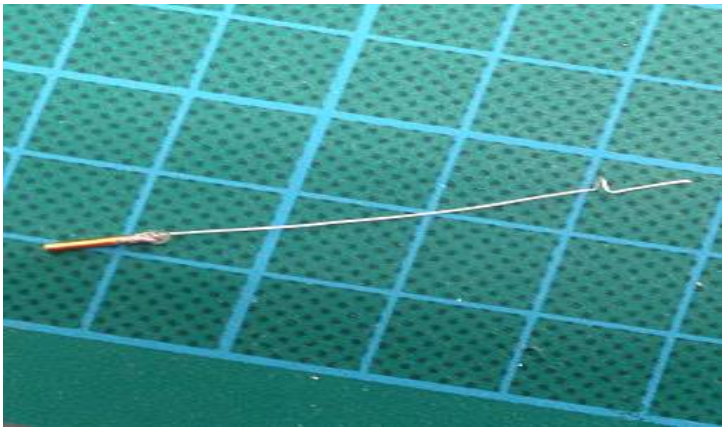

Figure 3.11(A): A schematic representation of a reference electrode.

B

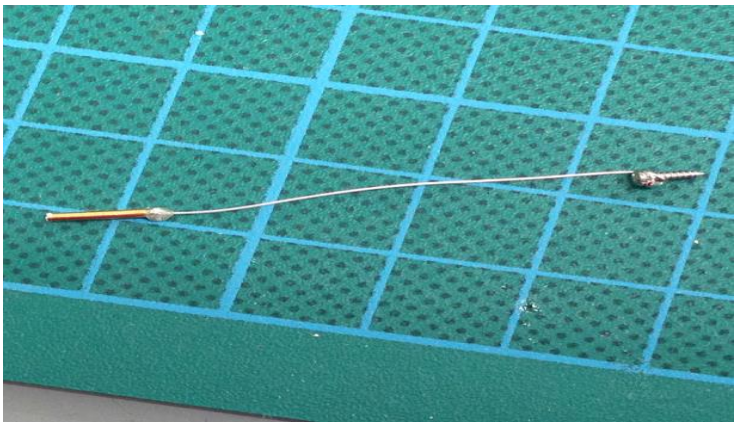

Figure 3.11(B): A schematic representation of an auxiliary electrode.

3.8.4: Continuous Monitoring

CPA was used to measure the response of the implanted electrodes during *in-vivo* experiments. Initial connection to the potentiostat involved connection of the insulated cable to the Teflon® pedestal which was then connected to the potentiostat. The appropriate potential was then applied to the electrodes ensuring a short interval between each application to rule out any cross-talk between each of the electrodes. Once the potential was applied, the electrodes were allowed to stabilise to a steady baseline level before commencement of any procedures.

3.8.5 In-Vivo Injections

3.8.5.1: Intraperitoneal Injection

Intraperitoneal (i.p.) injection was performed at a 45° angle into the peritoneal cavity which is located in the lower quadrant of the abdomen. The animal was positioned on its back and tilted so that no vital organs are present in the area that the injection is given.

3.8.5.2: Subcutaneous Injection

Subcutaneous (s.c.) injections are seldom painful to the subject unless the substance being administered causes irritation to the animal. The injection was administered into loose skin which is 'scruffed' on the back of the animal.

3.8.5.3: Termination

At the end of *in-vivo* experimentation, euthanasia was facilitated by administration of 1 mL of Euthatal (i.p). Expiration took *ca.* 10-20 minutes after the administration of the drug. The brains were removed following de-capitation and placed in a 10% formaldehyde solution for histology.

3.9 References

Baker KL. (2013) *The Development of Microelectrochemical Choline and Acetycholine Biosensors for Real-Time Neurochemical Monitoring*. Ph.D. Thesis, National University of Ireland, Maynooth.

Bolger FB. (2007) *The In-Vitro and In-Vivo Characterisation and Application of Real-Time Sensors and Biosensors for Neurochemical Studies of Brain Energy Metabolism*. Ph.D. Thesis, National University of Ireland, Maynooth.

Bolger FB, Bennett R and Lowry JP. (2011(a)) An *in vitro* characterisation comparing carbon paste and Pt microelectrodes for real-time detection of brain tissue oxygen. *Analyst* 136: 4028-4035.

Bolger FB and Lowry JP. (2005) Brain Tissue Oxygen: *In Vivo* Monitoring with Carbon Paste Electrodes. *Sensors* 5: 473-487.

Bolger FB, McHugh SB, Bennett R, *et al.* (2011(b)) Characterisation of carbon paste electrodes for real-time amperometric monitoring of brain tissue oxygen. *Journal of Neuroscience Methods* 195: 135-142.

Brown FO, Finnerty NJ, Bolger FB, *et al*. (2005) Calibration of NO sensors for *in-vivo* voltammetry: laboratory synthesis of NO and the use of UV–visible spectroscopy for determining stock concentrations. *Analytical and Bioanalytical Chemistry* 381: 964-971.

Brown FO, Finnerty NJ and Lowry JP. (2009) Nitric oxide monitoring in brain extracellular fluid: characterisation of Nafion®-modified Pt electrodes *in vitro* and *in vivo*. *Analyst* 134: 2012-2020.

Brown FO and Lowry JP. (2003) Microelectrochemical sensors for *in vivo* brain analysis: an investigation of procedures for modifying Pt electrodes using Nafion®. *Analyst* 128: 700-705.

Dixon BM, Lowry JP and O'Neill RD. (2002) Characterisation *in vitro* and *in vivo* of the oxygen dependence of an enzyme/polymer biosensor for monitoring brain glucose. *Journal of Neuroscience Methods* 119: 135-142.

Fernandes VS, Ribeiro AM, Melo TG, *et al.* (2008) Memory impairment induced by low doses of reserpine in rats: Possible relationship with emotional processing deficits in Parkinson disease. *Progress in Neuro-Psychopharmacology and Biological Psychiatry* 32: 1479-1483.

Kanofsky JR. (1988) Singlet oxygen production from the peroxidase-catalyzed oxidation of indole-3-acetic acid. *Journal of Biological Chemistry* 263: 14171-14175.

Lowry JP, Boutelle MG, O'Neill RD, *et al.* (1996) Characterisation of carbon paste electrodes *in vitro* for simultaneous amperometric measurement of changes in oxygen and ascorbic acid concentrations *in vivo*. *Analyst* 121: 761-766.

Lowry JP, McAteer K, El Atrash SS, *et al.* (1994) Characterisation of Glucose Oxidase-Modified Poly(phenylenediamine)-Coated Electrodes *in vitro* and *in vivo*: Homogeneous Interference by Ascorbic Acid in Hydrogen Peroxide Detection. *Analytical Chemistry* 66: 1754-1761.

Malitesta C, Palmisano F, Torsi L, *et al*. (1990) Glucose fast-response amperometric sensor based on glucose oxidase immobilized in an electropolymerized poly(o-phenylenediamine) film. *Analytical Chemistry* 62: 2735-2740.

Mesároš Š, Vaňková Ž, Grunfeld S, *et al*. (1998) Preparation and optimization of superoxide microbiosensor. *Analytica Chimica Acta* 358: 27-33.

O' Riordan SL. (2013) *Oxidative Stress Markers in Neurological Diseases and Disorders: Electrochemical Detection of Hydrogen Peroxide and Nitric Oxide* Ph.D. Thesis, National University of Ireland, Maynooth.

O'Neill RD. (1993) Sensor-tissue interactions in neurochemical analysis with carbon paste electrodes *in vivo*. *Analyst* 118: 433-438.

O'Neill RD. (1994) Microvoltammetric techniques and sensors for monitoring neurochemical dynamics *in vivo*. A review. *Analyst* 119: 767-779.

O'Brien K, Killoran S, O'Neill R, *et al*. (2007) Development and characterisation *in vitro* of a catalase-based biosensor for hydrogen peroxide monitoring. *Biosensors and Bioelectronics* 22: 2994-3000.

Pallini M, Curulli A, Amine A, *et al*. (1998) Amperometric nitric oxide sensors: a comparative study. *ElectroAnalysis* 10: 1010-1016.

Paxinos G and Watson C. (2006) *The Rat Brain in Stereotaxic Coordinates: Hard Cover Edition*: Elsevier Science.

Ryan MR, Lowry JP and O'Neill RD. (1997) Biosensor for Neurotransmitter L-Glutamic Acid Designed for Efficient Use of L-Glutamate Oxidase and Effective Rejection of Interference. *Analyst* 122: 1419-1424.

Teixeira AM, Reckziegel P, Müller L, *et al*. (2009) Intense exercise potentiates oxidative stress in striatum of reserpine-treated animals. *Pharmacology Biochemistry and Behavior* 92: 231-235.

Chapter 4:

Development

4.1 Introduction

Superoxide (O_2^-) is the primary reactive oxygen species (ROS) molecule and is generated as a reduced intermediate of molecular oxygen (O_2) (Tian *et al.*, 2006). O_2^- under normal physiological conditions has a very low and undetectable endogeneous concentration. O_2^- in biological samples lies within a narrow range of 50-200 nM (Mesároš *et al.*, 1998). The major source of O_2^- in cells is electron 'leakage' from electron transport chains in the mitochondria and in the endoplasmic reticulum (Maier and Chan, 2002). Under normal metabolic conditions these ROS are produced at a rate which is matched by the capacity of tissues to catabolise them (Wang *et al.*, 2013). However, when their production exceeds the body's natural ability to deal with this potentially cytotoxic species, a variety of pathological conditions may occur including stroke, cancer and neurodegeneration (McNeil and Manning, 2002). The quantification of the production of O_2^- anions is hard to achieve because of the natural ability of superoxide dismutase (SOD) to catalyse the dismutation of O_2 and their reactivity towards other small molecules. In summary, measuring O_2^- is problematic because of its low concentration, high reactivity and fleeting existence in the *in-vivo* environment (Wang *et al.*, 2014) (Ganesana *et al.*, 2012).

Electrochemical sensors for the detection of O_2^- have previously been developed by several research groups. Mesaros and coworkers have developed an amperometric O_2^- biosensor by the anodic polymerisation of pyrrole and concomitant immobilisation of SOD on Pt wire. The sensor was held at +700 mV and has a detection limit of 15 nM (Mesároš *et al.*, 1998). Manning *et al.* designed a sensor by covalently attaching cytochrome c to a gold working electrode through surface modification with DTSSP (3,3'-dithiobis(sulfosuccinimidylpropionate)). This molecule possesses a disulphide group for covalent attachment and the carboxyl groups to form amide linkages with the cytochrome c. The electrode was held at +100 mV and the detection limit was 10 nM (Manning *et al.*, 1998) (Manning and McNeil, 2011). Campanella *et al.* developed an O_2^- biosensor based on the SOD which is physically entrapped in a kappa-carrageenan gel membrane (Campanella *et al.*, 2000). The immobilised enzyme is then situated between the cellulose acetate membrane and a dialysis membrane and the whole assembly is fixed to the transducer by means of an O-ring. The Pt anode is then held at +650 mV.

Fabian *et al.* measured O_2^- *in-vivo* using a cytochrome c based platinised carbon electrode (Fabian *et al.*, 1995). This research demonstrated that this sensor was sensitive to changes in O_2^- levels and responsive to minute by minute changes in O_2^- levels during brain tissue injury and traumatic models of brain injury. Wang and co-workers developed a O_2^- sensor based on nitrilotriacetic acid (NTA) facilitated electron transfer of SOD on carbon fibre microelectrodes (Wang *et al.*, 2013). This sensor was utilised in the rat brain for the *in-vivo* monitoring of O_2^- during ischemia and reperfusion processes. However, few reports exist for measuring O_2^- levels *in-vivo* and its implication in the development of neurodegenerative disorders.

This chapter outlines the developmental steps undertaken to develop a sensitive and selective O_2^- biosensor for *in-vivo* neurochemical applications. The different immobilisation strategies used to incorporate SOD onto a Pt surface are discussed. The influence of stabilisers and cross-linkers are also investigated in terms of their use in conjunction with the enzyme and their effect on the sensor's sensitivity and kinetic parameters. The latter are compared in order to determine the best design for the optimal detection of O_2^-.

4.2 Experimental

All instrumentation and experimental software used in this chapter are described in Chapter 3, Section 3.2. All chemicals and solutions used are detailed in Section 3.3. The electrodes were constructed from a 1 mm Pt cylinder electrode as depicted in Section 3.4.2. The different biosensor designs developed and the manufacturing process associated with each design is explained in detail in Section 3.5.2.

All experimental data was collected using the cell set-up described in Section 3.6.1. All data was recorded in phosphate buffer saline (PBS) containing 0.002 U xanthine oxidase (XOD). Constant potential amperometry (CPA) was performed were the biosensor was held at + 700 mV as this potential has been determined to be optimal for the oxidation of hydrogen peroxide (H_2O_2) (Lowry *et al.*, 1994). Different aliquots of 1 mM xanthine (See Section 3.3.2.1) were injected into the electrochemical cell and a range of concentrations were used to compare the different biosensor designs. The combination of xanthine and XOD produced the O_2^- anion in a manner dependent on

the concentration of xanthine. The univalent reduction of XOD generating the O_2^- anion is dependent on pH. At pH 7.4, the yield of O_2^- was 28% of the total xanthine present in the reaction (See Section 3.6.3).

The data is reported as mean ± SEM where n denotes the number of electrodes used. The significance of difference observed was estimated using two-tailed t-tests. Paired tests were used when comparing data collected from the same electrode, unpaired tests were used for comparing data from different electrodes.

All calibration plots obeyed Michaelis-Menten Hill-type enzyme kinetics. The kinetic parameters V_{max}, K_m and sensitivity were used to compare the different biosensor designs. The Hill coefficient, α, reflects the deviation from ideal enzyme kinetics. These parameters are described in detail in Chapter 2, Section 2.5.2. Usually, a large K_m concentration is desirable as this coefficient defines the linear region slope, however, as the O_2^- concentration is so low *in-vivo* a low K_m concentration is desirable for this biosensor. Throughout this chapter the linear region slope is referred to as sensitivity.

4.3 Results and Discussion

This results section outlines the various steps involved in the development of the O_2^- biosensor. The primary focus was to find the best construction protocol that optimises the sensor's sensitivity.

4.3.1 Immobilisation

Different immobilisation strategies have been utilised in the development of biosensors and are a critical step in their design. The most common methods include entrapment within a membrane, cross linking, covalent bonding and physical adsorption (Mateo *et al.*, 2007) (Sassolas *et al.*, 2012) (Thévenot *et al.*, 2001). Entrapment involves the incorporation of an enzyme into a gel or a polymer. Electrochemical polymerisation is an attractive and convenient method used to immobilise enzymes on electrode surfaces. Electropolymerisation can utilise

conducting and non-conducting polymers. Typical conducting polymers include polypyrrole, polyaniline and polythiophene (Sassolas *et al*., 2012). A biosensor for hypoxanthine was developed by entrapment of XOD within a polyaniline film electropolymerised on a sodium montmorillonite–methyl viologen carbon-paste modified electrode. This biosensor works by electrocatalytic reduction of O_2 using cyclic voltammetry. The minimum detectable level is 0.8 μM *(*Hu *et al.*, 2000).

Biosensors incorporate immobilisers to assist in enzyme entrapment. Synthetic polymers such as styrene and methyl methacrylate have been used as immobilisers in the manufacture of biosensors. Polystyrene has been used as a solid support for protein immobilisation in enzyme–linked immunosorbent assays (ELISA) and animal culture (Kumada *et al*., 2010). Both polymers are liquids at room temperature and are therefore ideal candidates for the entrapment of SOD using the dip coating approach to enzyme loading. This approach has been used previously in our research group (Bolger, 2007) (Baker, 2013).

Extensive studies were carried out by other research groups in relation to the optimal unit of activity to incorporate in the O_2^- biosensor (Mesároš *et al.*, 1998). They found that the amount of SOD incorporated into the polypyrole was proportional to the concentration in the electropolymerisation solution. The optimal SOD concentration was determined to be between 200-350 U/mL SOD. This literature study was used as the starting point for the O_2^- biosensor. Initial experiments were carried out to investigate styrene as an immobiliser when incorporating various dips of 200 U of SOD. One, two, five and ten layers of SOD were investigated.

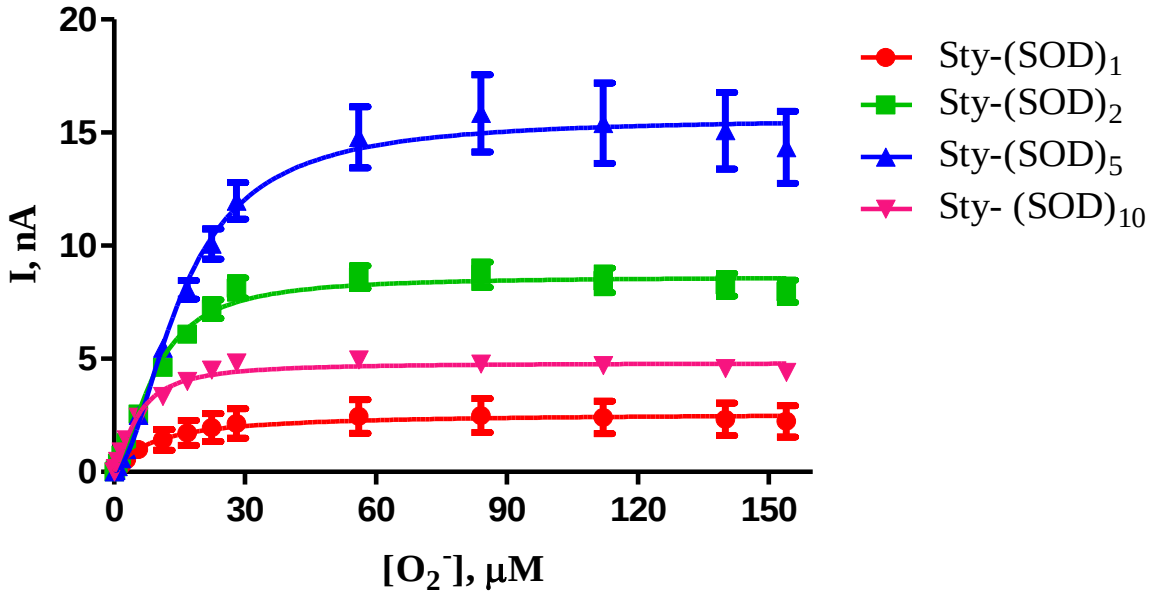

	Sty-(SOD)$_1$			Sty-(SOD)$_2$			Sty-(SOD)$_5$			Sty(SOD)$_{10}$		
	Mean	S.E.M	n	Mean	S.E.M	n	Mean	S.E.M	n	Mean	S.E.M	*n*
V_{max}, nA	2.43	0.13	4	8.56	0.12	4	15.65	0.24	8	4.77	0.07	4
K_m, µM	7.57	1.51	4	9.08	0.42	4	15.47	0.54	8	5.08	0.30	4
α	1.39	0.32	4	1.80	0.12	4	1.82	0.11	8	1.51	0.11	4
Sensitivity, nA/µM	0.13	0.004	4	0.41	0.02	4	0.52	0.02	8	0.30	0.03	4
R^2	0.96	-	4	0.99	-	4	0.99	-	8	0.94	-	4

Figure 4.1: The mean current-concentration profiles for O_2^- calibrations (*Top*) and comparison table (*Bottom*) in PBS (pH 7.4) buffer solution containing XOD at 21°C using designs Sty-(SOD)$_1$, Sty-(SOD)$_2$, Sty-(SOD)$_5$ and Sty-(SOD)$_{10}$. CPA carried out at +700 mV *vs.* SCE.

Upon examining the data in Figure 4.1, an increase in V_{max} and sensitivity is apparent as the number of layers of enzyme is increased. Sty-$(SOD)_1$ recorded a very small V_{max} value of 2.43 ± 0.13 nA (n = 4) and a very poor sensitivity of 0.13 ± 0.004 nA/µM. This result is mainly due to insufficient loading of the enzyme onto the Pt surface resulting in poor analyte detection. A similar trend is observed for the Sty-$(SOD)_2$ design, however, there is a significant increase ($P < 0.0001$) in V_{max} from 2.43 ± 0.13 nA (n = 4, Sty$(SOD)_1$) to 8.56 ± 0.12 nA (n = 4, Sty$(SOD)_2$). There is also a considerable improvement in sensitivity to 0.41 ± 0.02 nA/µM. Five layers of enzyme produced the highest substrate detection and this dip coating process proved advantageous over the other designs. Five individual layers of enzyme with drying time (4 minutes) allowed the enzyme to be fixed in place prior to the subsequent dip coating layer resulting in a high sensitivity being recorded. This design gave an improved V_{max} of 15.65 ± 0.24 nA, and a sensitivity of 0.52 ± 0.02 nA/µM. This suggests that there is good enzyme loading on the Pt surface resulting in high analyte detection. However, increasing the number of layers of enzyme to ten resulted in a decrease in enzyme loading and a significantly lower ($P < 0.0001$) V_{max} of 4.77 ± 0.07 nA being recorded. The incorporation of 10 layers of enzyme also had a detrimental effect on the sensitivity reducing it significantly ($P < 0.0001$) to 0.30 ± 0.03 nA/µM when compared to the Sty-$(SOD)_5$ design. An explanation for this trend could be that incorporating ten layers of enzyme results in the enzyme binding sites becoming constricted or blocked due to enzyme overload on the sensor surface.

Interestingly, the K_m concentrations remain very similar for all biosensor designs except for the Sty-$(SOD)_5$ design. The K_m concentrations recorded were 7.57 ± 1.51 µM (n= 4, Sty-$(SOD)_1$), 9.08 ± 0.42 µM (n = 4, Sty-$(SOD)_2$) and 5.08 ± 0.30 µM (n = 4, Sty-$(SOD)_{10}$). This low concentration could potentially be as a result of low enzyme loading on the sensor surface therefore, a reduction in diffusional constraints. A K_m value of 15.47 ± 0.54 µM (n = 8) is observed for the design Sty-$(SOD)_5$. This suggests a higher diffusional barrier perhaps as a result of higher enzyme loading. Further evidence for this high enzyme loading is the high sensitivity achieved of 0.52 ± 0.24 nA/µM (n = 8), the largest sensitivity recorded for this set of experiments. All designs show α values greater than 1 indicating sigmoidal enzyme kinetics. The designs Sty-$(SOD)_2$ and Sty-$(SOD)_5$ gave almost identical α values of 1.80 and 1.82 respectively.

In summary, the dip adsorption method using five layers of enzyme produced the highest V_{max} and sensitivity and was continued within the next section. One layer of enzyme resulted in insufficient enzyme loading with a low sensitivity being recorded. This method was eliminated in future designs.

4.3.2. Enzyme Unit of Activity Study

This section investigates the effect of changing the concentration of the enzyme solution. The unit of activity was increased to 400 U/mL and lowered to 100 U/mL in order to determine the optimal unit activity of the enzyme. From Section 4.3.1, five layers of enzyme demonstrated the highest sensitivity so this result was utilised. However, as the final goal is to develop a biosensor sensitive and selective for the *in-vivo* environment, experiments were performed in order to further increase the sensitivity and to improve the kinetic parameters by changing the concentration of the enzyme. Initial experiments were performed using styrene as the immobiliser and then five layers of enzyme with different concentrations (100 U/mL, 200 U/mL, 400 U/mL).

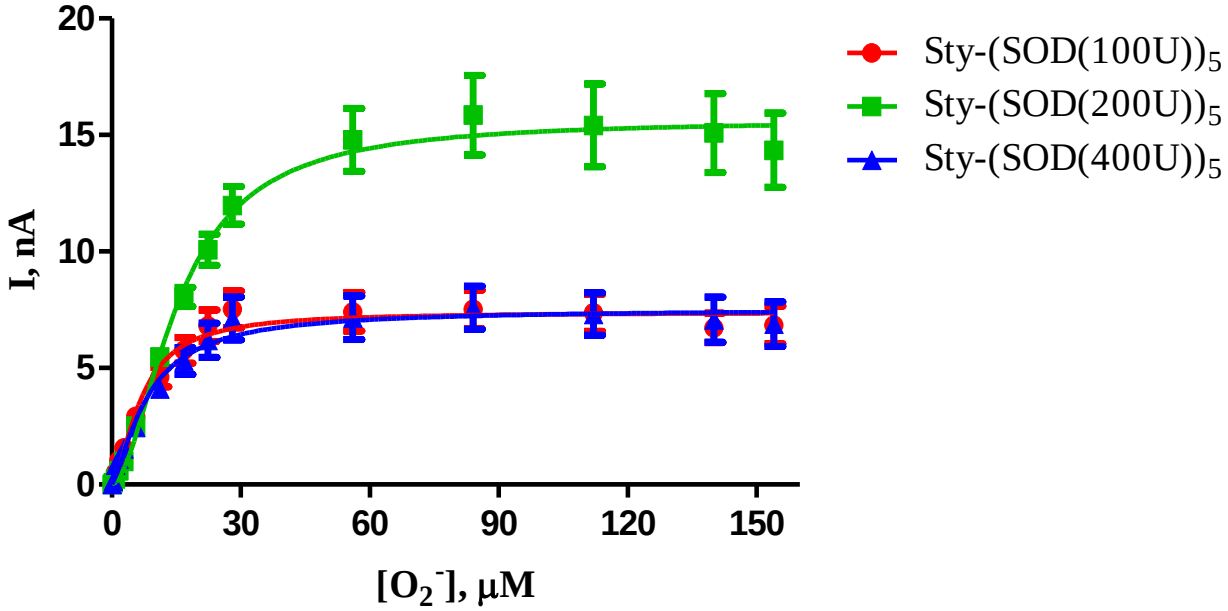

	Sty-(SOD(100U))$_5$			Sty-(SOD(200U))$_5$			Sty-(SOD(400U))$_5$		
	Mean	S.E.M	n	Mean	S.E.M	n	Mean	S.E.M	n
V_{max}, nA	7.40	0.10	12	15.65	0.24	8	7.53	0.13	12
K_m, µM	6.86	0.31	12	15.47	0.54	8	8.28	0.46	12
α	1.60	0.09	12	1.82	0.11	8	1.38	0.10	12
Sensitivity, nA/µM	0.41	0.03	12	0.52	0.02	8	0.35	0.03	12
R^2	0.96	0.01	12	0.99	0.003	8	0.94	0.03	12

Figure 4.2: The mean current-concentration profiles for O_2^- calibrations *(Top)* and comparison table *(Bottom)* in PBS (pH 7.4) buffer solution containing XOD at 21°C using designs Sty-(SOD(100U))$_5$, Sty-(SOD(200U))$_5$ and Sty-(SOD(400U))$_5$. CPA carried out at +700 mV *vs.* SCE.

Figure 4.2 above shows the mean current-concentration profile and the kinetic parameters associated with varying the unit activity of the enzyme. These biosensor designs were calibrated in an attempt to validate literature reports where the optimal enzyme concentration was determined to be between 200-350 U/mL (Mesároš *et al.*, 1998). The data in Figure 4.2 demonstrates that 200 U/mL of enzyme is optimal giving a V_{max} of 15.65 ± 0.54 nA and a sensitivity of 0.52 ± 0.02 nA/µM (n = 8, Sty(SOD(200U)$_5$). The V_{max} current produced by 200 U/mL (15.65 ± 0.24 nA) is significantly increased ($P < 0.0001$) compared to the 100 U/mL (7.40 ± 0.10 nA), and 400 U/mL (7.53 ± 0.13 nA) respectively. Interestingly, the V_{max} for 100 U/mL (7.40 ± 0.10 nA) is almost identical to the V_{max} when incorporating 400 U/mL (7.53 ± 0.13 nA). This suggests that utilising 5 layers of the higher enzyme concentration (400 U/mL) results in similar kinetic parameters being recorded as those observed previously when incorporating 10 layers of 200 U/mL of enzyme suggesting similar enzyme loading for the two designs.

A comparison of the K_m concentrations shows that incorporating either 100/400 U/mL has significantly lowered ($P < 0.0001$) the K_m concentration in both cases compared to using 200 U/mL (15.79 ± 0.56 µM). This reduction is potentially as a result of a low enzyme loading resulting in a reduction in the diffusional constraints. 100 U/mL

concentration of enzyme produced the lowest K_m concentration of 6.86 ± 0.31 µM. A low K_m concentration is desirable for this sensor due to the nanomolar concentration of O_2^- in the *in-vivo* environment.

The sensitivities of the three different biosensor designs were compared. The highest sensitivity was achieved when incorporating 200 U/mL of enzyme (0.52 ± 0.02 nA/µM), in both cases changing the concentration of the enzyme resulted in a significant decrease in sensitivity ($P < 0.0001$) being recorded from 0.41 ± 0.03 nA/µM (n = 12, Sty-(SOD(100U))$_5$) and 0.35 ± 0.03 nA/µM (n = 12, Sty-(SOD(400U))$_5$). All three designs, Sty-(SOD(100U))$_5$, Sty-(SOD(200U))$_5$ and Sty-(SOD(400U))$_5$, produced sigmoidal Michaelis-Menten kinetics. The α values recorded were 1.60, 1.82 and 1.38 respectively

In summary, the dip adsorption method incorporating five layers of 200 U/mL SOD, produced the highest sensitivity and the most ideal Michaelis-Menten enzyme kinetics, therefore this enzyme concentration was used in all of the biosensor designs in the following experiments.

4.3.3 The Addition of Glutaraldehyde

GA has been used widely for the immobilisation of enzymes in the construction of biosensors. GA is a linear 5-carbon dialdehyde which reacts with several functional groups on proteins including amines, thiols, phenols and imidazole groups. Usually GA cross-links to the ε-amino groups of the lysine residues on the enzyme. Lysine residues are usually located on the protein surface rather than at the catalytic site. This is advantageous as the enzyme structure and biological conformation usually remains preserved. The stability of the enzyme can typically be increased by cross-linking because intra and intermolecular cross-links lead to a more rigid molecule that can resist conformational changes (Migneault *et al.*, 2004). It has been reported that the concentration of GA used affects the degree or extent of cross-linking with low concentrations not being able to form sufficient cross-linkages to effect the precipitation of the enzyme (Broun, 1976). Another research group found that enzymatic activity was directly proportional to the concentration of GA used with high concentrations of GA leading to extensive cross-linking resulting in loss of enzyme

activity due to distortion of the active site (Chui and Wan, 1997). GA exists in multiple forms in aqueous solutions so it is still unclear as to the exact mechanism of the cross-linking process. It is generally accepted that reactions between the carbonyl group of the GA and the amino groups of the protein takes place yielding a Schiff base and at pH 8 and higher the GA forms an insoluble polymer which causes the immobilisation of the enzyme (de Melo *et al*., 1999).

Initial experiments were performed using a GA concentration (0.5%) that was previously used in the development of a choline biosensor (Baker, 2013). This concentration was investigated using the dip adsorption method. Biosensor designs were manufactured using various dips; two, five and ten layers of enzyme and GA were investigated.

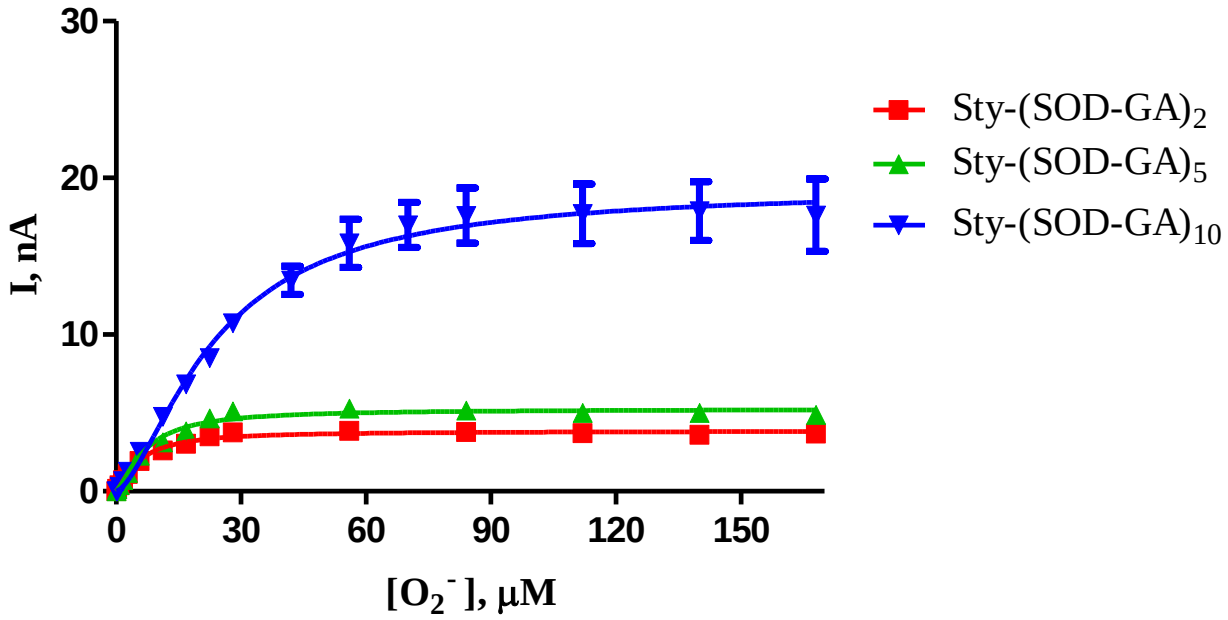

	Sty-$(SOD-GA)_2$			Sty-$(SOD-GA)_5$			Sty-$(SOD-GA)_{10}$		
	Mean	S.E.M	n	Mean	S.E.M	n	Mean	S.E.M	*n*
V_{max}, nA	3.85	0.06	8	5.42	0.06	12	18.87	0.41	6
K_m, µM	5.42	0.33	8	6.87	0.25	12	22.90	1.09	6
α	1.38	0.09	8	1.42	0.06	12	1.55	0.10	6
Sensitivity, nA/µM	0.39	0.01	8	0.42	0.01	12	0.43	0.01	6
R^2	0.99	-	8	0.99	-	12	0.99	-	6

Figure 4.3: The mean current-concentration profiles for O_2^- calibrations *(Top)* and comparison table *(Bottom)* in PBS (pH 7.4) buffer solution containing XOD at 21°C using designs Sty-$(SOD-GA)_2$, Sty-$(SOD-GA)_5$ and Sty-$(SOD-GA)_{10}$. CPA carried out at +700 mV *vs.* SCE.

The data presented in Figure 4.3 shows the effect the addition of a GA layer has on the biosensor's sensitivity and kinetic parameters. The GA layer was added in an attempt to secure the enzyme layer in place before the addition of subsequent layers of enzyme by dip coating. The results above show that the addition of GA has resulted in a significant decrease ($P < 0.0001$) in the V_{max} from 8.56 ± 0.12 nA Sty-$(SOD)_2$ to 3.85 ± 0.06 nA Sty-$(SOD-GA)_2$). A similar trend was observed for the sensitivity, a decrease ($P = 0.8247$) was observed from 0.41 ± 0.02 nA/µM Sty-$(SOD)_2$ to 0.39 ± 0.06 nA/µM (Sty-$(SOD-GA)_2$). Similarly, a significant decrease ($P < 0.0001$) in V_{max} was also recorded for 5 layers of enzyme and GA (5.42 ± 0.06 nA) Sty-$(SOD-GA)_5$ when compared to the same design just incorporating enzyme (15.65 ± 0.24 nA) Sty–$(SOD)_5$. The sensitivity was also significantly reduced ($P = 0.0005$) from 0.52 ± 0.02 nA/µM (Sty-(SOD_5) to 0.42 ± 0.01 nA/µM (Sty-$(SOD-GA)_5$). These results show that the addition of GA seems to have a detrimental effect. An explanation for this trend may be that the GA is cross-linking the enzyme too tightly, restricting access of the substrate to the active sites of the enzyme. The addition of GA into the biosensor design may result in some degree of enzyme denaturation as demonstrated by the decreased sensitivity and V_{max}.

However, a different trend is observed when incorporating 10 layers of enzyme and GA. An increase in V_{max} and K_m is observed in this design, however, there is no change in the sensitivity: 0.42 ± 0.01 nA/µM (Sty-(SOD-GA)$_{5)}$ and 0.43 ± 0.01 nA/µM (Sty-(SOD-GA)$_{10}$). This trend may be explained by an increase in enzyme loading on the sensor surface, therefore the detrimental effects of GA being reversed as more enzyme is available for the substrate to access.

From the data in Figure 4.3, it is apparent that there is a stepwise increase in the K_m concentrations on addition of more layers of enzyme and GA. The K_m value increased from 5.42 ± 0.33 µM (Sty- (SOD-GA)$_2$) to 6.87 ± 0.25 µM (Sty-(SOD-GA)$_5$), and then increased further to 22.90 ± 1.06 µM (Sty-(SOD-GA)$_{10}$). This trend may potentially be due to increased enzyme loading resulting in higher diffusional constraints. All biosensor designs produced sigmoidal Michaelis-Menten kinetics with α values of 1.38 (Sty-(SOD-GA)$_2$), 1.42 (Sty-(SOD-GA)$_5$) and 1.55 (Sty-(SOD-GA)$_{10}$).

4.3.4 Introduction of Bovine Serum Albumin

The use of BSA has been extensively documented in the development of biosensors. BSA is an inert lysine rich protein which has been employed in biosensor designs for both enzyme protection and stabilisation. BSA has been reported to be utilised in biosensor designs in conjunction with GA (Wilson and Thévenot, 1989) (Sassolas *et al.*, 2012). The GA cross-links the BSA in addition to the enzyme thus limiting the direct enzyme cross-linking, resulting in higher enzyme activity and stability. Cross-linked enzyme aggregates prepared with BSA were better overall catalysts and showed higher operational stability in organic solvents and higher thermal stability. This is an ideal strategy when the starting protein concentration is low and when the protein is vulnerable to loss of activity due to extensive cross-linking (Shah *et al.*, 2006). BSA could potentially protect the enzyme coated on the Pt surface during the harsh cross-linking process or hinder access of the substrate to the active sites of the enzyme layers below, due to its comparatively larger size. Ryan *et al.* developed a biosensor for L-Glutamic acid by co-polymerisation of the enzyme within the PPD polymer. The addition of BSA into the biosensor design protected the enzyme from inactivation

during the polymerisation process (Ryan *et al.*, 1997). The incorporation of additives for enzyme stabilisation has also been widely investigated. Studies focusing on the stability of the enzyme has been reported by Costa *et al*. They found that the introduction of BSA increased the half-life of catalase, even seeing a three-fold increase from 11 to 43 when utilising BSA with GA at 30°C (Costa *et al.*, 2002).

Initial experiments investigated using 1 % BSA, a concentration that was previously found to be optimum in the development of a choline sensor while incorporating a GA concentration of 0.5 % (Baker, 2013). The BSA was positioned after the enzyme in the dip coating process in order to protect the enzyme. Also, the BSA could provide lysine residues for the GA to cross-link with instead of direct enzyme cross-linking. Various layers of enzyme, BSA and GA were investigated.

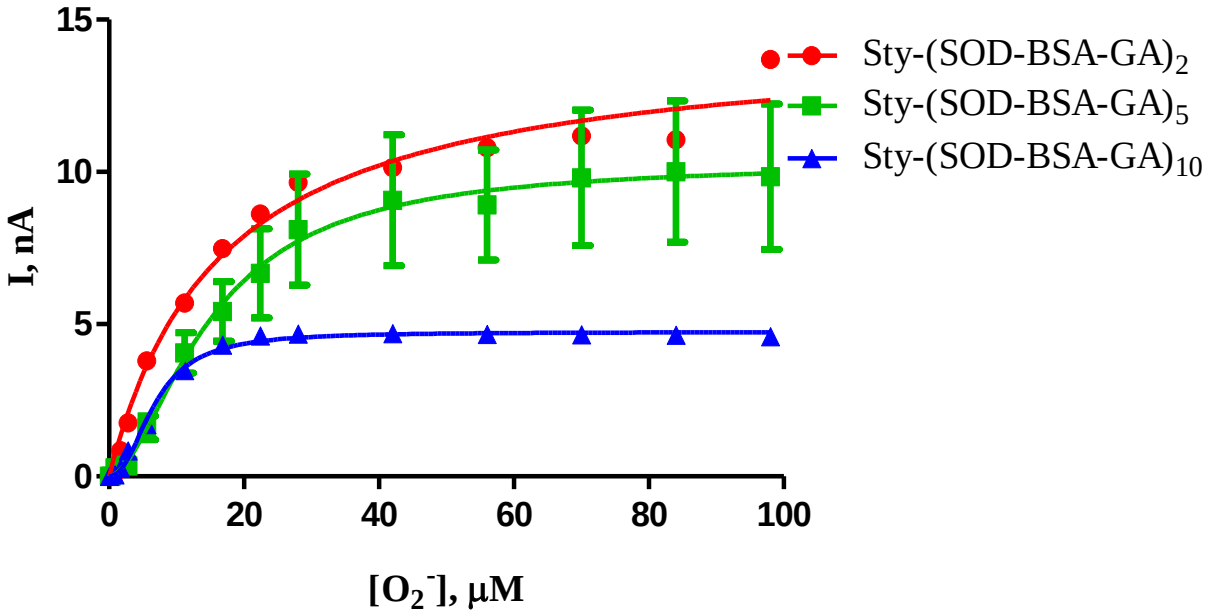

	Sty-(SOD-BSA-GA)$_2$			Sty-(SOD-BSA-GA)$_5$			Sty-(SOD-BSA-GA)$_{10}$		
	Mean	S.E.M	n	Mean	S.E.M	n	Mean	S.E.M	n
V_{max}, nA	13.49	0.48	3	10.33	0.50	6	4.74	0.4	4
K_m, µM	14.15	1.27	3	15.02	1.46	6	6.76	0.19	4
α	1.15	0.08	3	1.74	0.27	6	2.23	0.11	4
Sensitivity, nA/µM	0.47	0.03	3	0.34	0.02	6	0.32	0.01	4
R^2	0.97	-	3	0.98	-	6	0.99	-	4

Figure 4.4: The mean current-concentration profiles for O_2^- calibrations *(Top)* and comparison table *(Bottom)* in PBS (pH 7.4) buffer solution containing XOD at 21°C using designs Sty-(SOD-BSA-GA)$_2$, Sty-(SOD-BSA-GA)$_5$ and Sty-(SOD-BSA-GA)$_{10}$. CPA carried out at +700 mV *vs.* SCE.

The data presented in Figure 4.4 demonstrates the changes in kinetic parameters on addition of BSA into the biosensor design. On examination of the results it is clear, that there is a stepwise decrease in V_{max} from 13.49 ± 0.48 nA (Sty-(SOD-BSA-GA)$_2$) to 10.33 ± 0.50 nA (Sty-(SOD-BSA-GA)$_5$), and then a further decrease to 4.74 ± 0.40 nA is observed when incorporating 10 layers of BSA (Sty-(SOD-BSA-GA)$_{10}$). A similar trend is observed with sensitivity with the highest value (0.47 ± 0.03 nA/µM) achieved for Sty-(SOD-BSA-GA)$_2$ and then a decrease observed on incorporation of additional layers of BSA. These trends suggest that two layers of BSA is efficient in providing sufficient enzyme stability and protection with additional layers having detrimental effects on the kinetic parameters. This trend may be attributed to restricted access of the substrate to the active site of the enzyme, or, alternatively the comparatively larger size of the BSA may decrease the amount of enzyme successfully immobilised onto the sensor surface.

The K_m concentration has increased for both the Sty-(SOD-BSA-GA)$_2$ and the Sty-(SOD-BSA-GA)$_5$ when compared to the same designs without BSA. The K_m concentration recorded was 14.15 ± 1.27 µM (n = 3, Sty-(SOD-BSA-GA)$_2$) compared to 5.42 ± 0.28 µM (n = 6, Sty-(SOD-GA)$_2$). The same trend is observed when

incorporating 5 layers of enzyme, BSA and GA. There is a significant increase ($P < 0.0001$) in K_m from 6.87 ± 0.25 µM (n = 8, Sty-$(SOD\text{-}GA)_5$) to 15.02 ± 1.46 µM (n = 6, Sty-$(SOD\text{-}BSA\text{-}GA)_5$). An explanation for this trend is that the addition of the large BSA protein has resulted in higher diffusional constraints for the substrate to reach the active sites of the enzyme. A different trend is observed when comparing 10 layers of enzyme, BSA and GA. In this instance, the K_m concentration is significantly decreased ($P < 0.0001$) from 22.90 ± 1.09 µM (n = 6, Sty-$(SOD\text{-}GA)_{10}$) to 6.76 ± 0.19 µM (n = 4, Sty-$(SOD\text{-}BSA\text{-}GA)_{10}$).

Sigmoidal Michaelis-Menten behaviour is observed for all designs Sty-$(SOD\text{-}BSA\text{-}GA)_2$, Sty-$(SOD\text{-}BSA\text{-}GA)_5$ and Sty$(SOD\text{-}BSA\text{-}GA)_{10}$ resulting in α values of 1.15, 1.74 and 2.23 respectively. In summary, this section has determined that the sensor design Sty-$(SOD\text{-}BSA\text{-}GA)_2$ improved the sensitivity, increased the V_{max} and increased the K_m concentration when compared to the same sensor design incorporating just GA.

4.3.5 Addition of Polyethyleneimine

PEI has been used in the fabrication of biosensors for both immobilisation (McMahon *et al*., 2006) and stabilisation (Patel *et al*., 2000) (Brena and Batista-Viera, 2006). PEI has proven beneficial in the development of biosensors for its ability to increase sensitivity (McMahon *et al.*, 2006), reduce the Michaelis constant K_m and increase the linear region slope (McMahon *et al.*, 2007). PEI is a polybasic positively charged polyelectrolyte (pKa 9.7) aliphatic amine with the highest concentration of amino groups per unit of all synthetic polymers (Jezkova *et al.*, 1997) (Gupta *et al.*, 2000). It is believed that the beneficial effect which PEI has on the biosensor performance is attributed to the formation of polyanionic/polycationic complexes between the polycationic PEI and the polyanionic enzyme which reduces enzyme deactivation (Jezkova *et al.*, 1997). This in turn, decreases the electrostatic repulsion between the enzyme substrate and biosensor components (McMahon *et al.*, 2007). The negative charges on the enzyme are assumed to electrostatically react with the positive charges of the polycation resulting in a stable configuration for long term stability of the biosensor. The development of this stable configuration with enhancement of the

positive charges facilitated the electron transfer yielding higher signals (Belay *et al*., 1999).

Experiments were undertaken to investigate the effect 2% PEI has on the dip coating process. This concentration was chosen as a starting point as this was found to be ideal in a previously developed biosensor in the research group (Baker, 2013). Initial experiments were carried out using two, five and ten layers of 200 U/mL SOD, 0.5% GA and 2% PEI in an attempt to improve the biosensor's kinetic parameters and sensitivity. The PEI was positioned directly after the GA layer and before the subsequent enzyme layer.

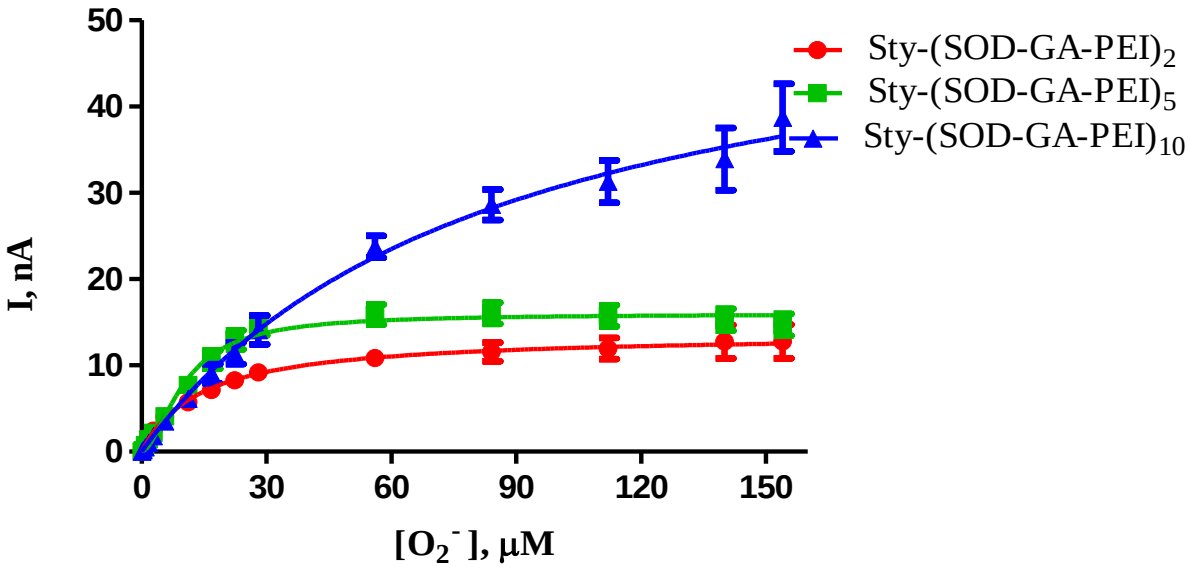

	Sty-(SOD-GA-PEI)$_2$			Sty(SOD-GA-PEI)$_5$			Sty(SOD-GA-PEI)$_{10}$		
	Mean	S.E.M	n	Mean	S.E.M	n	Mean	S.E.M	n
V_{max}, nA	14.32	0.43	11	15.98	0.15	17	51.65	3.13	12
K_m, µM	16.22	1.45	11	10.33	0.27	17	69.46	8.90	12
α	0.90	0.05	11	1.73	0.07	17	1.08	0.05	12
Sensitivity, nA/µM	0.86	0.04	11	0.91	0.02	17	0.65	0.02	12
R^2	0.99	-	11	0.99	-	17	0.97	-	12

Figure 4.5: The mean current-concentration profiles for O_2^- calibrations *(Top)* and comparison table *(Bottom)* in PBS (pH 7.4) buffer solution containing XOD at 21°C using designs Sty-(SOD-GA-PEI)$_2$, Sty-(SOD-GA-PEI)$_5$ and Sty-(SOD-GA-PEI)$_{10}$. CPA carried out at +700 mV *vs.* SCE.

The results in Figure 4.5 show the effect the introduction of PEI has on the dip coating process. There is a marked improvement in sensitivity when compared to previous biosensor designs. The introduction of PEI into the biosensor designs results in good enzyme kinetics, low K_m concentrations and high sensitivities being achieved for both Sty-(SOD-GA-PEI)$_2$ and Sty-(SOD-GA-PEI)$_5$ designs. Comparing these optimum designs shows an increase ($P = 0.0002$) in sensitivity from 0.86 ± 0.04 nA/µM ($n = 11$, Sty-(SOD-GA-PEI)$_2$) to 0.91 ± 0.02 nA/µM ($n = 17$, Sty-(SOD-GA-PEI)$_5$) and shows a significant increase ($P = 0.0034$) in V_{max} from 14.32 ± 0.43 nA (Sty-(SOD-GA-PEI)$_2$ to 15.98 ± 0.15 nA (Sty-(SOD-GA-PEI)$_5$). This trend suggests that higher enzyme loading is achieved and the substrate has unrestricted access to the active sites of the enzyme when incorporating 5 layers of SOD, GA and PEI. PEI is assumed to promote the electron transfer between the active site of the immobilised SOD and the electrode and/or increase the enzyme turnover rate resulting in a higher sensitivity being observed for the biosensor designs.

A significant decrease ($P < 0.0001$) in the K_m concentration is observed from 16.22 ± 1.45 µM ($n = 11$, Sty-(SOD-GA-PEI)$_2$) to 10.33 ± 0.27 µM ($n = 17$, Sty-(SOD-GA-PEI)$_5$). The reduction in the K_m concentration demonstrates advantageous kinetics for

the currents at the lower concentrations which are closer to the physiological range. An explanation for this is that the addition of PEI helps reduce the electrostatic barrier between neighbouring enzymes and the anionic substrate rather that a reduction in diffusional constraints. This explanation is also valid for the increase in sensitivity in the analytically important linear region slope. A large K_m value (69.46 ± 8.90 μM) is observed for Sty-(SOD-GA-PEI)$_{10}$, which indicates a large diffusional barrier for the analyte. This suggests that the PEI is hindering the access of the substrate to the active sites of the enzyme.

Michaelis-Menten behaviour is observed for both designs Sty-(SOD-GA-PEI)$_2$ and Sty-(SOD-GA-PEI)$_{10}$ with α values of 0.90 and 1.08 respectively. These values are very close to the ideal value of 1. Sigmoidal kinetics are observed for the design Sty-(SOD-GA-PEI)$_5$ with an α value of 1.73 indicating positive cooperativity.

In summary, the introduction of this stabiliser has shown beneficial characteristics for further studies with the potential to secure more enzyme and biosensor components onto the electrode surface. The design Sty-(SOD-GA-PEI)$_5$ obtained the best sensitivity achieved so far in the manufacture process. This design also showed a low K_m concentration and a high V_{max} value.

4.3.6. Concentration Studies

4.3.6.1. Polyethyleneimine Concentration

The introduction of PEI into the biosensor design resulted in a marked improvement in the kinetic parameters as shown in Section 4.3.5. Different concentrations of PEI could potentially improve the sensitivity of the biosensor. This section investigates the effect of three different PEI concentrations - 1%, 2% (as presented previously in Section 4.3.5.) and 3%. This study was undertaken to investigate the effect of changing the concentration of PEI has on the kinetic parameters observed for the different biosensor designs.

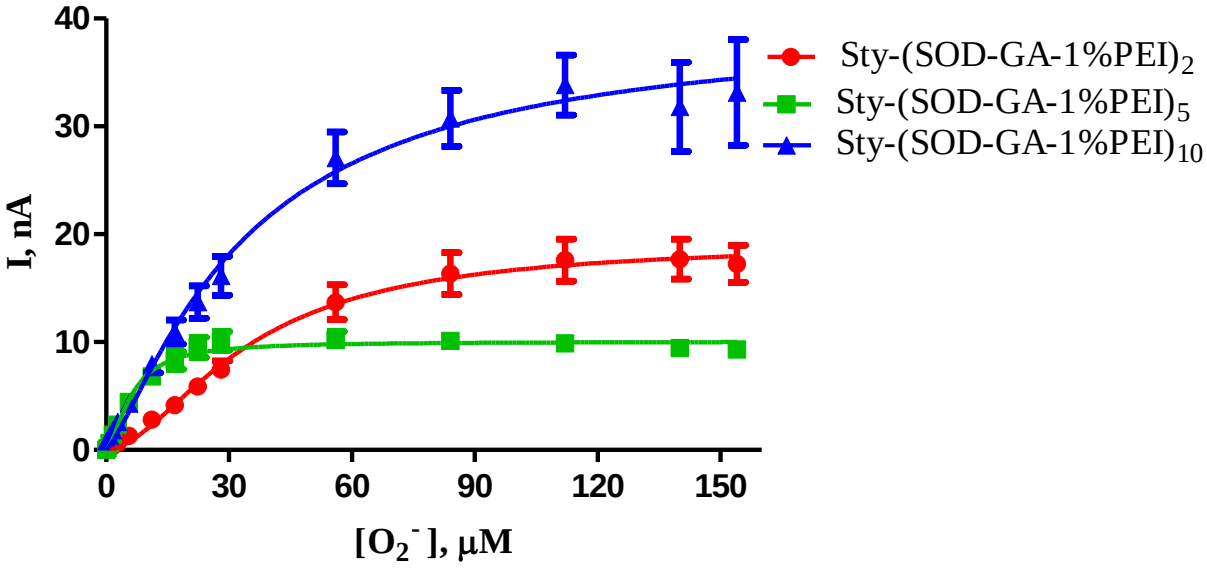

	Sty-(SOD-GA-1%PEI)$_2$			Sty-(SOD-GA-1%PEI)$_5$			Sty(SOD-GA-1%PEI)$_{10}$		
	Mean	S.E.M	n	Mean	S.E.M	n	Mean	S.E.M	n
V_{max}, nA	19.25	0.53	8	10.05	0.10	12	39.50	0.485	11
K_m, µM	34.42	1.86	8	6.09	0.22	12	34.11	2.78	11
α	1.76	0.12	8	1.64	0.08	12	1.276	0.08	11
Sensitivity, nA/µM	0.25	0.004	8	0.85	0.04	12	0.64	0.003	11
R^2	0.9989	-	8	0.99	-	12	0.999	-	11

Figure 4.7: The mean current-concentration profiles for O_2^- calibrations *(Top)* and comparison table *(Bottom)* in PBS (pH 7.4) buffer solution containing XOD at 21°C using designs Sty-(SOD-GA-1%PEI)$_2$, Sty-(SOD-GA-1%PEI)$_5$ and Sty-(SOD-GA-1%PEI)$_{10}$. CPA carried out at +700 mV *vs.* SCE.

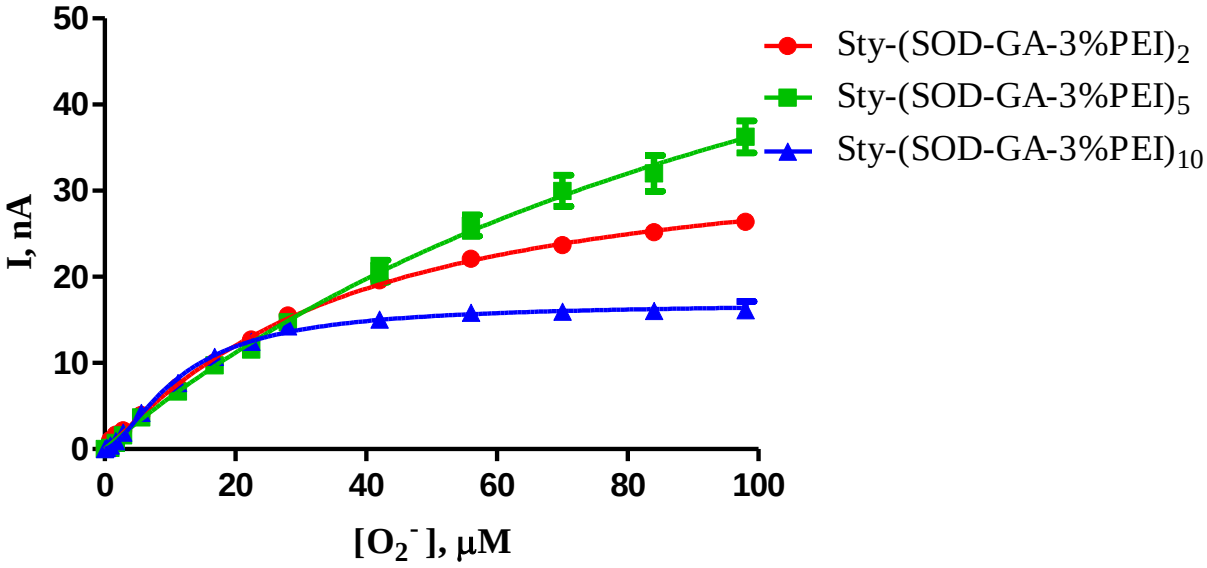

	Sty-(SOD-GA-3%PEI)$_2$			Sty-(SOD-GA-3%PEI)$_5$			Sty-(SOD-GA-3%PEI)$_{10}$		
	Mean	S.E.M	n	Mean	S.E.M	n	Mean	S.E.M	n
V_{max}, nA	35.15	0.95	4	72.76	6.25	11	16.98	0.19	8
K_m, µM	35.89	2.05	4	100.30	15.26	11	11.63	0.31	8
α	1.117	0.032	4	1.063	0.040	11	1.576	0.057	8
Sensitivity, nA/µM	0.63	0.03	4	0.63	0.03	11	0.70	0.02	8
R^2	0.98	0.012	4	0.98	0.004	11	0.99	0.002	8

Figure 4.8: The mean current-concentration profiles for O_2^- calibrations *(Top)* and comparison table *(Bottom)* in PBS (pH 7.4) buffer solution containing XOD at 21°C using designs Sty-(SOD-GA-3%PEI)$_2$, Sty-(SOD-GA-3%PEI)$_5$ and Sty-(SOD-GA-3%PEI)$_{10}$. CPA carried out at +700 mV *vs.* SCE.

The results above show the mean current-concentration profiles and kinetic parameters for both 1% and 3% PEI. The results incorporating 2% PEI are shown in Figure 4.5. The graphs show the effect of changing the concentration of PEI on the kinetic parameters.

Decreasing the PEI concentration to 1% resulted in a similar trend to incorporating 2% PEI. The best design was Sty-(SOD-GA-1%PEI)$_5$. This design showed a good sensitivity of 0.85 ± 0.04 nA/µM (n = 12), a low K_m value 6.09 ± 0.22 µM and good enzyme kinetics demonstrated by an α value close to 1. The same result was achieved when incorporating 2% PEI concentration with the best results being observed for the Sty-(SOD-GA-2%PEI)$_5$ design.

Both Sty-(SOD-GA-1%PEI)$_2$ and Sty-(SOD-GA-1%PEI)$_{10}$ designs resulted in a lower sensitivity and higher K_m concentrations being achieved when compared to the Sty-(SOD-GA-1%PEI)$_5$. There is a significant decrease in sensitivity ($P < 0.0001$) from 0.85 ± 0.04 nA/µM (n = 12, Sty-(SOD-GA-1%PEI)$_5$) to 0.25 ± 0.004 nA/µM (n = 8, Sty-(SOD-GA-1%PEI)$_2$). There is a significant decrease ($P < 0.0001$) in V_{max} from 19.25 ± 0.53 nA (Sty-(SOD-GA-1%PEI)$_2$) to 10.05 ± 0.10 nA (Sty-(SOD-GA-1%PEI)$_5$). However, there is a significant increase ($P < 0.0001$) in the K_m value from 6.09 ± 0.22 µM (Sty-(SOD-GA-1%PEI)$_5$) to 34.42 ± 1.86 µM (Sty-(SOD-GA-1%PEI)$_2$). This increase in K_m is not ideal as the *in-vivo* concentration is in the low nanomolar region. An explanation for these trends is that the Sty-(SOD-GA-1%PEI)$_2$ biosensor design results in low enzyme loading, or the PEI smothers the enzyme resulting in higher diffusional constraints for the substrate. A similar trend is observed for the Sty-(SOD-GA-1%PEI)$_{10}$ design. In this instance, the V_{max} is significantly ($P < 0.0001$) increased from 10.05 ± 0.10 nA (n = 12, Sty-(SOD-GA-1%PEI)$_5$) to 39.50 ± 0.49 nA (n = 11, Sty-(SOD-GA-1%PEI)$_{10}$) and the K_m concentration is significantly increased ($P < 0.0001$) from 6.09 ± 0.22 µM (n = 12, Sty-(SOD-GA-1%PEI)$_5$) to 34.11 ± 2.78 µM (n= 11, Sty-(SOD-GA-1%PEI)$_{10}$). A detrimental effect on sensitivity is observed with the value decreasing significantly ($P < 0.0001$) from 0.85 ± 0.04 nA/µM (n =12, Sty-(SOD-GA-1%PEI)$_5$) to 0.64 ± 0.003 nA/µM (n = 11, Sty-(SOD-GA-1%PEI)$_{10}$). This trend suggests hindered access of the substrate to the active sites of the enzyme due to diffusional constraints. In summary the design Sty-(SOD-GA-

1%PEI)$_5$ gave the best results when incorporating 1% PEI similarly to when incorporating 2% PEI, where Sty-(SOD-GA-2%PEI)$_5$ gave the optimum results.

Increasing the concentration of PEI to 3% had a detrimental effect on the sensitivity and the K_m concentration. Both Sty-(SOD-GA-3%PEI)$_2$ and Sty-(SOD-GA-3%PEI)$_5$ showed the same sensitivity of 0.63 ± 0.04 nA/µM and high K_m concentrations of 35.89 ± 2.05 µM and 100.30 ± 15.26 µM respectively. This suggests that access of the active site to the substrate is restricted due to diffusional constraints. This can be justified as there is a 2:1 ratio of biosensor components to enzyme, therefore this may be causing the active sites to be hindered due to the presence of excess GA and PEI. However, a different trend is observed for the Sty-(SOD-GA-3%PEI)$_{10}$ design. This design gave the best sensitivity of 0.70 ± 0.02 nA/µM, a low K_m concentration of 11.63 ± 0.31 µM and a V_{max} of 16.98 ± 0.19 nA. This design also shows sigmoidal enzyme kinetics with an α value of 1.58.

The results below (Figure 4.9) show a comparison of the best designs incorporating the various PEI concentrations (1%, 2% and 3%).

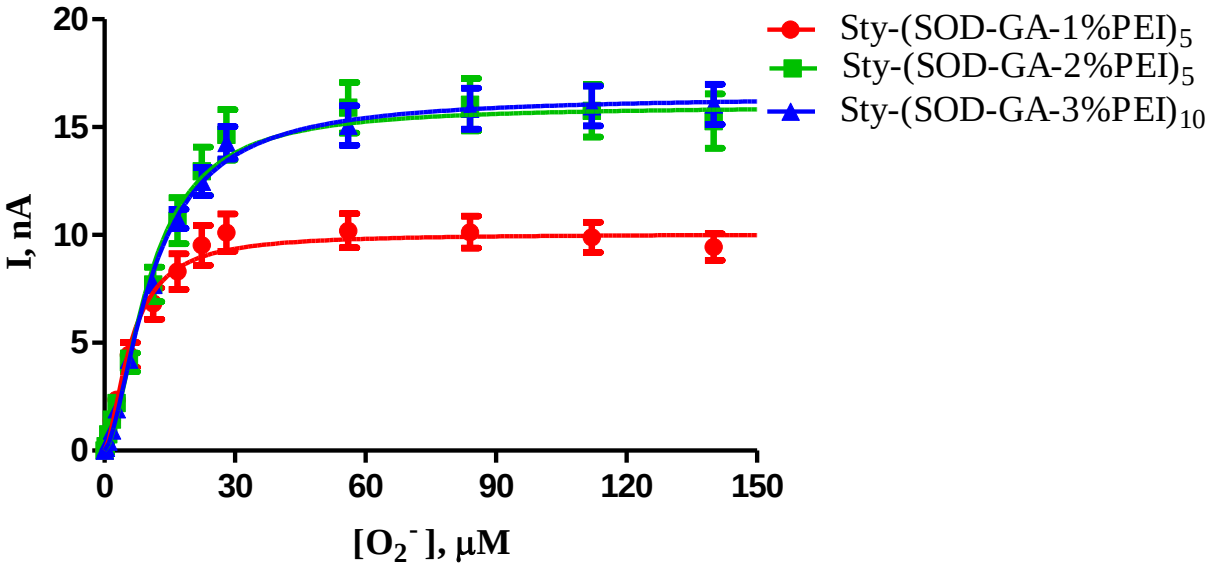

	Sty-(SOD-GA-1%PEI)$_5$			Sty-(SOD-GA-2%PEI)$_5$			Sty-(SOD-GA-3%PEI)$_{10}$		
	Mean	S.E.M	n	Mean	S.E.M	n	Mean	S.E.M	n
V_{max}, nA	10.05	0.10	12	15.98	0.15	17	16.98	0.19	8
K_m, µM	6.09	0.22	12	10.33	0.27	17	11.63	0.31	8
α	1.64	0.08	12	1.73	0.07	17	1.58	0.06	8
Sensitivity, nA/µM	0.85	0.04	12	0.91	0.02	17	0.70	0.02	8
R^2	0.99	-	12	0.99	-	17	0.99	-	8

Figure 4.9: The mean current-concentration profiles for O_2^- calibrations *(Top)* and comparison table *(Bottom)* in PBS (pH 7.4) buffer solution containing XOD at 21°C using designs Sty-(SOD-GA-1%PEI)$_5$, Sty-(SOD-GA-2%PEI)$_5$ and Sty-(SOD-GA-3%PEI)$_{10}$. CPA carried out at +700 mV *vs.* SCE.

The graph and table above show the kinetic and performance parameters for the best biosensor designs incorporating various concentrations of PEI. All designs show high sensitivities, low K_m concentrations and sigmoidal kinetics with α values greater than 1.

There is a significant increase in V_{max} ($P < 0.0001$) observed from 10.05 ± 0.10 nA (Sty-(SOD-GA-1%PEI)$_5$) to 15.98 ± 0.15 nA (Sty-(SOD-GA-2%PEI)$_5$). A significant increase in sensitivity ($P < 0.0001$) is also demonstrated from 0.85 ± 0.04 nA/µM (Sty-(SOD-GA-1%PEI)$_5$) to 0.91 ± 0.02 nA/µM (Sty-(SOD-GA-2%PEI)$_5$). These results indicate that the biosensor design Sty-(SOD-GA-2%PEI)$_5$ has optimum characteristics with high enzyme loading yielding a higher sensitivity and V_{max}.

Unlike 1% and 2% PEI, 3% PEI shows different results where the best design is Sty-(SOD-GA-3%PEI)$_{10}$. This design resulted in a significant decrease in sensitivity ($P < 0.0001$) from 0.91 ± 0.02 nA/µM (Sty-(SOD-GA-2%PEI)$_5$) to 0.70 ± 0.02 nA/µM (Sty-(SOD-GA-3%PEI)$_{10}$. A significant increase ($P < 0.0001$) in the K_m concentration from 10.33 ± 0.27 µM (n = 17, Sty-(SOD-GA-2%PEI)$_5$) to 11.63 ± 0.31 µM (n = 8, Sty-(SOD-GA-3%PEI)$_{10}$) is observed.

In summary, the results obtained in this section suggest that the best sensor design incorporating PEI is Sty-(SOD-GA-2%PEI)$_5$. This design showed the best kinetic parameters and a sensitivity of 0.91 ± 0.02 nA/µM (n = 17) the best achieved by any sensor design so far.

The next section investigates the effect of changing the GA concentration (0.05%, 0.5% and 1%) using various concentrations of PEI (1%, 2% and 3%). As shown in the previous sections 5 layers of enzyme and biosensor components seems to be optimum so this was used to investigate the effects of changing the GA concentration. It seems that 5 layers provides sufficient enzyme loading and accessibility for the substrate to the active sites resulting in ideal enzymatic parameters being observed.

4.3.6.2. Glutaraldehyde Concentration

In the beginning, the GA concentration chosen was 0.5% GA as this was demonstrated to be optimum in a choline biosensor that was previously fabricated in the research group (Baker, 2013). However, research had proven that the cross-linking process can sometimes be too harsh resulting in poor enzyme kinetics and loss of activity so a lower concentration of GA (0.05%) was utilised (Chui and Wan, 1997). A O_2^- biosensor developed by another research group utilised very low concentrations of GA (0.005%). They tested a variety of different concentrations and showed that higher concentrations of GA had detrimental effects on the enzyme activity (Emregül, 2005). On the other hand, 0.5% GA could be too low of a concentration to provide sufficient enzyme cross-linking so a higher concentration (1% GA) was tested to test its effects. Research shows that the amount of cross-linking agent used affects the degree or extent of cross-linking with low concentrations of GA unable to form sufficient cross-linkages to effect precipitation of the enzyme (Broun, 1976) .

In this section, different concentrations of GA were utilised (0.05% and 1% GA) with varying concentrations (1%, 2%, 3%) of PEI in an effort to improve the sensitivity of the biosensor. From the previous section (4.3.6.1) 5 layers was shown to be optimum giving a high sensitivity and a low K_m concentration which is desirable for the low O_2^- concentration *in-vivo* so this was used in this section.

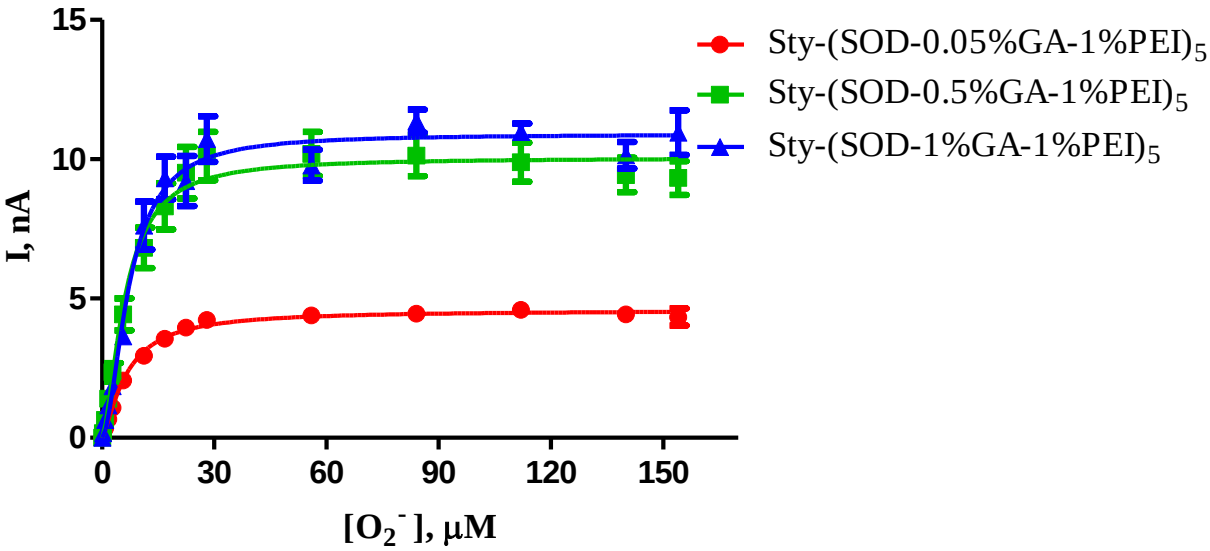

	Sty-(SOD-0.05%GA-1%PEI)$_5$			Sty-(SOD-0.5%GA-1%PEI)$_5$			Sty-(SOD-1%GA-1%PEI)$_5$		
	Mean	S.E.M	n	Mean	S.E.M	n	Mean	S.E.M	n
V_{max}, nA	4.58	0.04	6	10.05	0.15	12	10.90	0.13	7
K_m, µM	6.52	0.21	6	6.09	0.22	12	7.32	0.28	7
α	1.37	0.05	6	1.64	0.08	12	1.81	0.10	7
Sensitivity, nA/µM	0.36	0.006	6	0.85	0.01	12	0.65	0.01	7
R^2	0.99	-	6	0.99	-	12	0.99	-	7

Figure 4.10: The mean current-concentration profiles for O_2^- calibrations (Top) and comparison table (Bottom) in PBS (pH 7.4) buffer solution containing XOD at 21°C using designs Sty-(SOD-0.05%GA-1%PEI)$_5$, Sty-(SOD-0.5%GA-1%PEI)$_5$ and Sty-(SOD-1%GA-1%PEI)$_{10}$. CPA carried out at +700 mV vs. SCE.

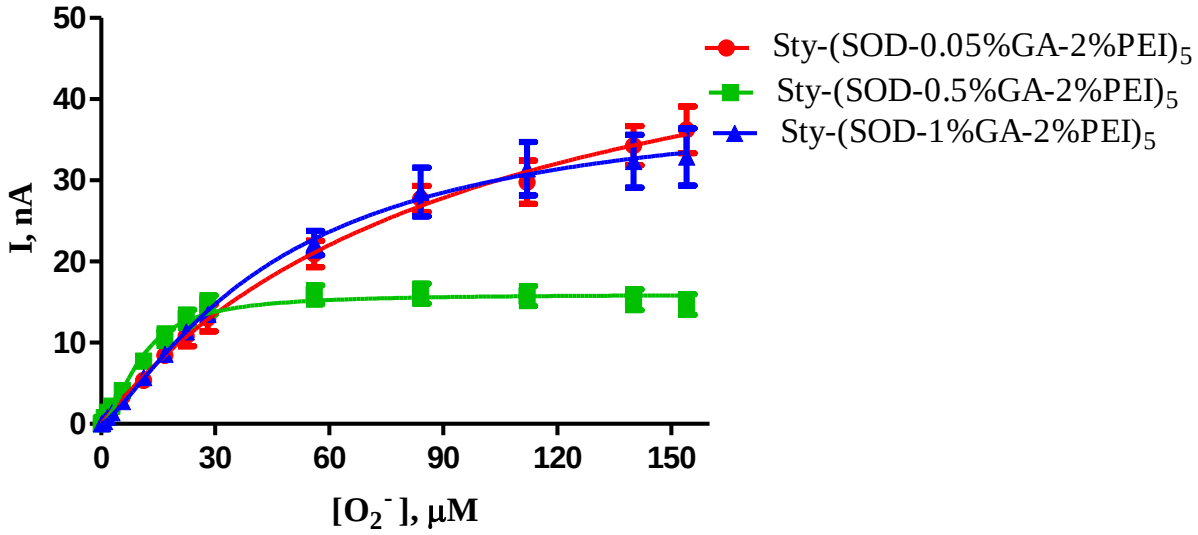

	Sty-(SOD-0.05%GA-2%PEI)$_5$			Sty-(SOD-0.5%GA-2%PEI)$_5$			Sty-(SOD-1%GA-2%PEI)$_5$		
	Mean	S.E.M	n	Mean	S.E.M	n	Mean	S.E.M	n
V_{max}, nA	60.08	5.56	8	15.98	0.15	17	40.38	1.90	7
K_m, µM	104.70	20.34	8	10.33	0.27	17	45.90	4.50	7
Sensitivity, nA/µM	0.63	0.01	8	0.91	0.06	17	0.51	0.01	7
α	0.99	0.05	8	1.73	0.07	17	1.30	0.08	7
R^2	0.99	-	8	0.99	-	17	0.99	-	7

Figure 4.11: The mean current-concentration profiles for O_2^- calibrations *(Top)* and comparison table *(Bottom)* in PBS (pH 7.4) buffer solution containing XOD at 21°C using designs Sty-(SOD-0.05%GA-2%PEI)$_5$, Sty-(SOD-0.5%GA-2%PEI)$_5$ and Sty-(SOD-1%GA-2%PEI)$_5$. CPA carried out at +700 mV *vs.* SCE.

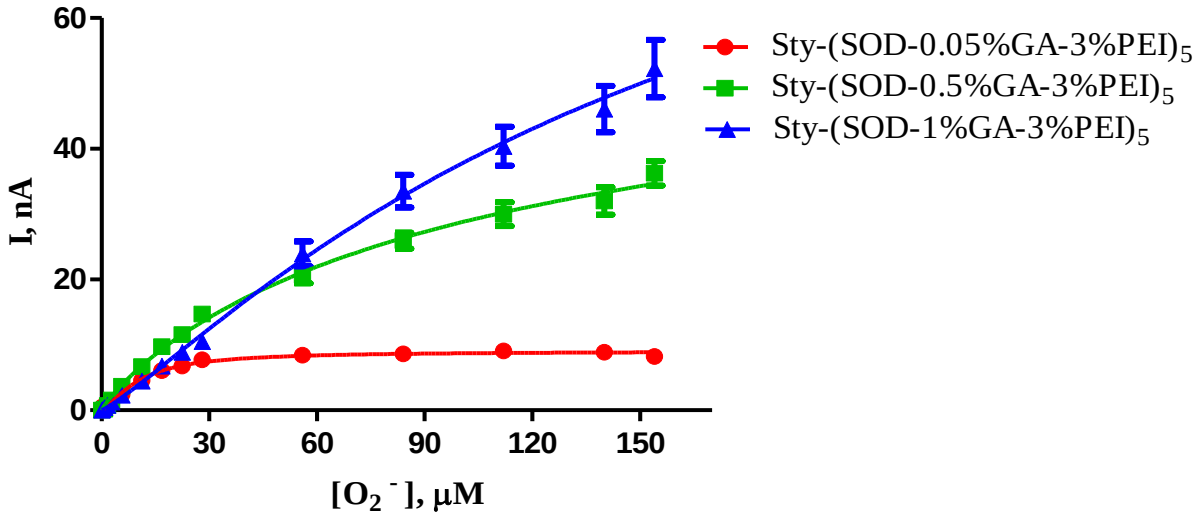

	Sty-(0.05%GA-3%PEI)$_5$			Sty-(SOD-0.5%GA-3%PEI)$_5$			Sty-(SOD-1%GA-3%PEI)$_5$		
	Mean	S.E.M	n	Mean	S.E.M	n	Mean	S.E.M	n
V_{max}, nA	9.03	0.16	8	61.60	4.71	11	108.20	14.85	8
K_m, µM	10.27	0.54	8	116.40	20.13	11	171.10	37.03	8
α	1.45	0.10	8	0.89	0.04	11	1.17	0.06	8
Sensitivity, nA/µM	0.36	0.01	8	0.68	0.04	11	0.47	0.02	8
R^2	0.99	-	8	0.99	-	11	0.99	-	8

Figure 4.12: The mean current-concentration profiles for O_2^- calibrations *(Top)* and comparison table *(Bottom)* in PBS (pH 7.4) buffer solution containing XOD at 21°C using designs Sty-(SOD-0.05%GA-3%PEI)$_5$, Sty-(SOD-0.5%GA-3%PEI)$_5$ and Sty-(SOD-1%GA-3%PEI)$_5$. CPA carried out at +700 mV *vs.* SCE.

The results above show that when incorporating 1% PEI, Sty-(SOD-0.5%GA-1%PEI)$_5$ was optimum giving the best sensitivity of 0.85 ± 0.01 nA/µM and a low K_m concentration of 6.09 ± 0.22 µM (n = 12). A low V_{max} (4.58 ± 0.04 nA, n = 6) was achieved using the lower concentration of GA (0.05%) suggesting that this concentration is too low in order to sufficiently secure the enzyme layers on the Pt surface. In comparison, the design Sty-(SOD-1%GA-1%PEI)$_5$ achieved a very similar K_m and V_{max} to Sty-(SOD-0.5%GA-1%PEI)$_5$, however a significant decrease ($P < 0.0001$) from 0.85 ± 0.01 nA/µM (n = 12, Sty-(SOD-0.5%GA-1%PEI)$_5$) to 0.65 ± 0.01 nA/µM (n = 7, Sty(SOD-1%GA-1%PEI)$_5$) in sensitivity was observed. This trend suggests that the enzyme turnover is more efficient for the design incorporating 0.5% GA, however, the diffusional constraints for both Sty-(SOD-0.5%GA-1%PEI)$_5$ and Sty-(SOD-1%GA-1%PEI)$_5$ are similar as demonstrated by their small K_m concentrations.

The trend differs when incorporating 2% PEI. Sty-(SOD-0.5%GA-2%PEI)$_5$, again similar to 1% PEI, gave the best results with a sensitivity of 0.91 ± 0.06 nA/µM (n = 17). However, for the design utilising the lower concentration of GA (Sty-(SOD-0.05%GA-2%PEI)$_5$) poor enzyme kinetics are observed with a K_m concentration of 104.70 ± 20.34 µM (n = 8). This suggests a high diffusional barrier for the substrate or restricted access to the active sites of the enzyme. The biosensor design utilising the higher concentration of GA (Sty-(SOD-1%GA-2%PEI)$_5$) results in a high K_m value of 45.90 ± 4.50 µM and a low sensitivity of 0.51 ± 0.01 nA/µM (n = 7). These results suggest that the cross-linking process is too harsh resulting in distortion of the enzyme structure. With this distortion the accessibility and accommodation of the substrate may be reduced, affecting the retention of biological activity.

An opposite trend is observed when incorporating 3% PEI. In this case, the design utilising the lower concentration of GA (Sty-(SOD-0.05%GA-3%PEI)$_5$) gave the best results in terms of enzyme kinetics, however, a low sensitivity of 0.36 ± 0.01 nA/µM (n = 8) was observed. This suggests that the diffusional constraints were greatly reduced. This trend, however, is more likely to be as a result of a decrease in the number of layers obstructing the enzyme as the GA was unable to secure the enzyme layers, rather than an effect of the GA itself, as the sensitivity was severely affected. The introduction of higher concentrations of GA results in a significant increase ($P <$

0.0001) in V_{max} from 61.60 ± 4.71 nA (n = 11, Sty-(SOD-0.5%GA-3%PEI)$_5$) to 108.20 ± 14.85 nA (n = 8, Sty-(SOD-1%GA-3%PEI)$_5$). A similar trend is observed for the K_m concentration, increasing the GA concentration results in a significant increase (P = 0.0007) from 116.40 ± 20.13 µM (n = 11, Sty-(SOD-0.5%GA-3%PEI)$_5$) to 171.10 ± 37.03 µM (n = 8, Sty-(SOD-1%GA-3%PEI)$_5$). These poor enzyme kinetics may be explained by the enzyme becoming 'smothered' due to the high concentrations of the biosensor components. However, the best sensitivity of 0.68 ± 0.04 nA/µM (n = 11) was achieved for the design Sty-(SOD-0.5%GA-3%PEI)$_5$.

This section illustrates the effects of changing the GA concentration. It is clear that low concentrations of GA (0.05%) are insufficient in securing the enzyme layers on the Pt surface. On the other hand, the higher concentration of GA (1%) usually results in lower sensitivities being achieved. An explanation for this trend is that the cross-linking process is too harsh resulting in distortion of the enzyme structure. It can be concluded that the optimum GA concentration is 0.5%. This concentration will be used in each biosensor design in future studies.

4.3.6.3. Bovine Serum Albumin Concentration

The previous section illustrated the effect the GA concentration has on sensitivity. BSA has also been shown to have an effect on sensitivity (see Section 4.3.4). However, BSA has never been incorporated into a design utilising both PEI and GA so this section looks at the introduction of BSA into these designs. 0.5% GA was found to be optimum with 1% and 2% PEI giving the best results. In this section various concentrations of BSA (1%, 0.1% and 0.01%) were investigated to examine their effects on the sensitivity and kinetic parameters.

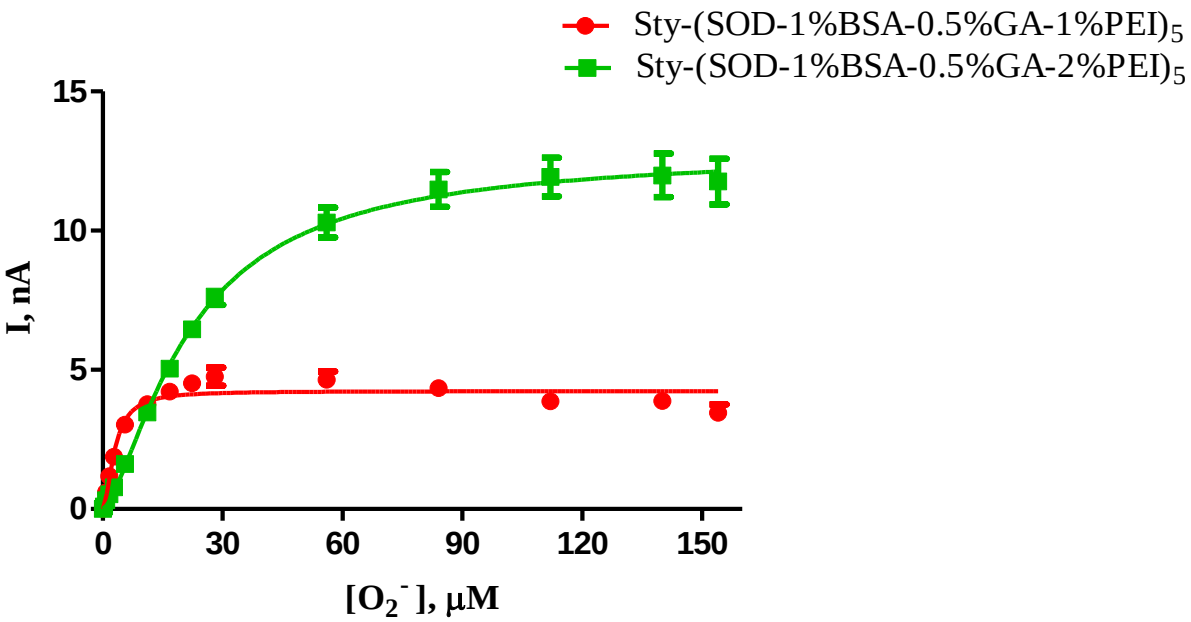

	Sty-(SOD-1%BSA-0.5%GA-1%PEI)$_5$			Sty-(SOD-1%BSA-0.5%GA-2%PEI)$_5$		
	Mean	S.E.M	n	Mean	S.E.M	n
V_{max}, nA	4.24	0.06	8	12.82	0.14	12
K_m, µM	3.00	0.16	8	21.82	0.53	12
α	1.78	0.16	8	1.46	0.05	12
Sensitivity, nA/µM	0.70	0.001	8	0.28	0.008	12
R^2	0.99	-	8	0.99	-	12

Figure 4.13: The mean current-concentration profiles for O_2^- calibrations *(Top)* and comparison table *(Bottom)* in PBS (pH 7.4) buffer solution containing XOD at 21°C using designs Sty-(SOD-1%BSA-0.5%GA-1%PEI)$_5$ and Sty-(SOD-1%BSA-0.5%GA-2%PEI)$_5$. CPA carried out at +700 mV *vs.* SCE.

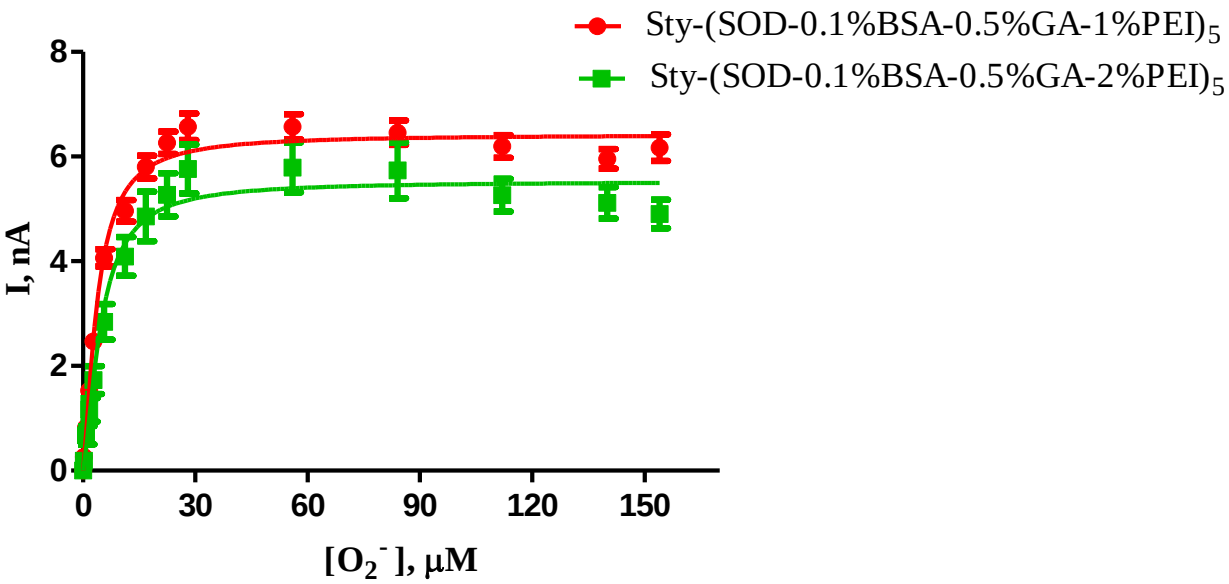

	Sty-(SOD-0.1%BSA-0.5%GA-1%PEI)$_5$			Sty-(SOD-0.1%BSA-0.5%GA-2%PEI)$_5$		
	Mean	S.E.M	n	Mean	S.E.M	n
V_{max}, nA	6.42	0.05	7	5.53	0.06	12
K_m, µM	3.78	0.13	7	4.71	0.21	12
α	1.45	0.06	7	1.50	0.08	12
Sensitivity, nA/µM	0.91	0.03	7	0.70	0.04	12
R^2	0.99	-	7	0.99	-	12

Figure 4.14: The mean current-concentration profiles for O_2^- calibrations *(Top)* and comparison table *(Bottom)* in PBS (pH 7.4) buffer solution containing XOD at 21°C using designs Sty-(SOD-0.1%BSA-0.5%GA-1%PEI)$_5$ and Sty-(SOD-0.1%BSA-0.5%GA-2%PEI)$_5$. CPA carried out at +700 mV *vs.* SCE.

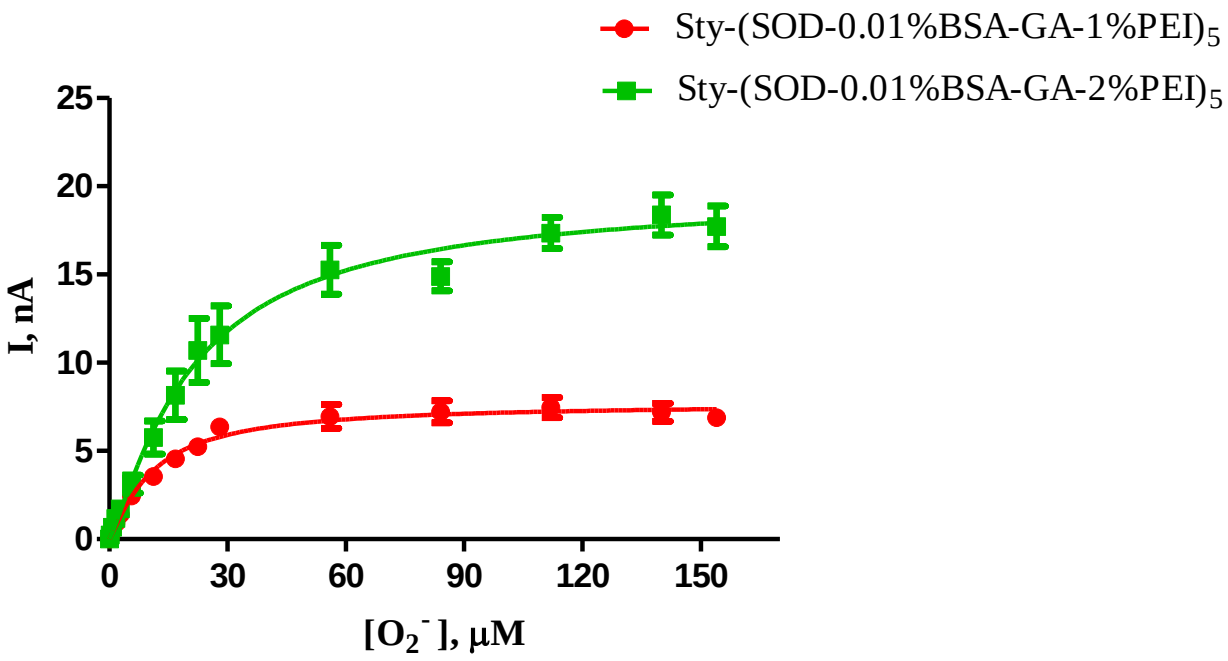

	Sty-(SOD-0.01%BSA-0.5%GA-1%PEI)$_5$			Sty-(SOD-0.01%BSA-0.5%GA-2%PEI)$_5$		
	Mean	S.E.M	n	Mean	S.E.M	n
V_{max}, nA	7.68	0.11	11	19.56	0.49	9
K_m, µM	10.91	0.48	11	21.17	1.30	9
α	1.19	0.05	11	1.21	0.07	9
Sensitivity, nA/µM	0.54	0.02	11	0.61	0.04	9
R^2	0.99	-	11	0.99	-	9

Figure 4.15: The mean current-concentration profiles for O_2^- calibrations *(Top)* and comparison table *(Bottom)* in PBS (pH 7.4) buffer solution containing XOD at 21°C using designs Sty-(SOD-0.01%BSA-0.5%GA-1%PEI)$_5$ and Sty-(SOD-0.01%BSA-0.5%GA-2%PEI)$_5$. CPA carried out at +700 mV *vs.* SCE.

The preceding results illustrate the effects that changing the concentration of BSA has on the sensitivity. It is clear, that the introduction of BSA into the biosensor design results in a decrease in the K_m concentration, particularly when incorporating 0.1% BSA, without compromising the sensitivity. However, there is a significant decrease ($P < 0.0001$) in V_{max} from 10.05 ± 0.10 nA (n = 12, Sty-(SOD-0.5%GA-1%PEI)$_5$) to 6.42 ± 0.05 nA (n = 7, Sty-(SOD-0.1%BSA-0.5%GA-1%PEI)$_5$) resulting from the introduction of BSA into the biosensor design. The K_m concentration observed was 3.78 ± 0.13 µM (n = 7), the lowest concentration achieved thus far. The sensitivity increased ($P = 0.2476$) from 0.85 ± 0.04 nA/µM (n = 12, Sty-(SOD-0.5%GA-1%PEI)$_5$) to 0.91 ± 0.03 nA/µM (n = 7, Sty-(SOD-0.1%BSA-0.5%GA-1%PEI)$_5$) on inclusion of BSA. This suggests that the inclusion of 1% BSA is beneficial when incorporating 0.5% GA and 1% PEI improving the sensitivity and K_m concentration. A similar trend is observed when incorporating 2% PEI, however, in this instance the K_m concentration is reduced significantly ($P < 0.0001$) from 10.33 ± 0.27 µM (n = 17, Sty-(SOD-0.5%GA-2%PEI)$_5$) to 4.71 ± 0.21 µM (n = 12, Sty-(SOD-0.1%BSA-0.5%GA-2%PEI)$_5$) on the inclusion of BSA into the design process. The sensitivity has also been compromised with a significant decrease ($P < 0.0001$) observed from 0.91 ± 0.02 nA/µM (n = 17, Sty-(SOD-0.5%GA-2%PEI)$_5$) to 0.70 ± 0.04 nA/µM (n = 12, Sty-(SOD-0.1%BSA-0.5%GA-2%PEI)$_5$). This trend suggests that the BSA may hinder access of the substrate to some of the active sites of the enzyme due to its particularly large size.

This is supported further by the higher concentration of BSA (1%) appearing to block access of the substrate to the active sites as a small V_{max} (4.24 ± 0.06 nA, n = 8) is achieved with a K_m concentration of just 3.00 ± 0.16 µM (n = 8) when incorporating 1% PEI. The sensitivity is significantly reduced ($P < 0.0001$) from 0.85 ± 0.04 nA/µM (n = 12, Sty-(SOD-0.5%GA-1%PEI)$_5$) to 0.70 ± 0.0009 nA/µM (n = 8, Sty-(SOD-1%BSA-0.5%GA-1%PEI)$_5$). However, the same trend is not demonstrated when incorporating 2% PEI. This biosensor design demonstrates a higher V_{max} and K_m concentration when compared to 1% PEI. Conversely, a significant decrease ($P < 0.0001$) in V_{max} is observed from 15.98 ± 0.15 nA (n = 17, Sty-(SOD-0.5%GA-2%PEI)$_5$) to 12.82 ± 0.14 nA (n = 12, Sty-(SOD-1%BSA-0.5%GA-2%PEI)$_5$), a significant increase ($P < 0.0001$) in K_m concentration is observed from 10.33 ± 0.27 µM (n = 17, Sty-(SOD-0.5%GA-2%PEI)$_5$) to 21.82 ± 0.53 µM (n = 12, Sty-(SOD-

1%BSA-0.5%GA-2%PEI)$_5$) on addition of 1% BSA into the biosensor design. The sensitivity is significantly compromised ($P < 0.0001$) from 0.91 ± 0.02 nA/µM (n = 17, Sty-(SOD-0.5%GA-2%PEI)$_5$) to 0.28 ± 0.008 nA/µM (n = 12, Sty-(SOD-1%BSA-0.5%GA-2%PEI)$_5$. This result suggests further that the incorporation of 1% BSA hinders access of the substrate to the active site of the enzyme resulting in a reduced V_{max} and sensitivity.

The lower concentration of BSA (0.01%) seems to add no benefit to the design, only adding extra layers and perhaps compromising the access of the substrate to the active site and creating a diffusional barrier. The design Sty-(SOD-0.01%BSA-0.5%GA-1%PEI)$_5$ produced the highest V_{max} of 7.68 ± 0.11 nA and the highest K_m concentration of 10.91 ± 0.48 µM. However, the sensitivity of 0.54 ± 0.02 nA/µM is the lowest obtained when compared to using 1% and 0.1% BSA and incorporating 1% PEI. The design incorporating 2% PEI (Sty-(SOD-0.01%BSA-0.5%GA-2%PEI)$_5$) with a V_{max} of 19.56 ± 0.49 nA and K_m concentration of 21.17 ± 1.30 µM is almost identical to the design Sty-(SOD-1%BSA-0.5%GA-2%PEI)$_5$ which produced a lower V_{max} of 12.82 ± 0.14 nA and a K_m concentration of 21.82 ± 0.53 µM (n = 12).

For 1% PEI there is a stepwise increase in V_{max} following reduction of the BSA concentration from 4.24 ± 0.05 nA (n = 8, Sty-(SOD-0.5%GA-1%BSA-1%PEI)$_5$) to 6.42 ± 0.05 nA (n = 7, Sty-(SOD-0.5%GA-0.1%BSA-1%PEI)$_5$) and then the highest value of 7.68 ± 0.11 nA (n = 11, Sty-(SOD-0.5%GA-0.01%BSA-1%PEI)$_5$) is observed when incorporating the lowest concentration of BSA. A similar trend is observed for the K_m concentration where the lowest concentration of BSA gave the highest value of 10.91 ± 0.48 µM (n = 11, Sty-(SOD-0.01%BSA-0.5%GA-1%PEI)$_5$) and the highest concentration of BSA recording the lowest K_m value of 3.00 ± 0.16 µM (n = 8, Sty-(SOD-1%BSA-0.5%GA-1%PEI)$_5$). However, the sensitivity is compromised with the lowest sensitivity of 0.54 ± 0.02 nA/µM (n = 11, Sty-(SOD-0.01%BSA-0.5%GA-1%PEI)$_5$) being recorded when incorporating 0.01% BSA. A similar trend is not observed when utilising 2% PEI. In this instance, 0.01% BSA gave an almost identical ($P = 0.6160$) K_m concentration (21.82 ± 0.53 µM, n = 12, Sty-(SOD-1%BSA-0.5%GA-2%PEI)$_5$) to the design utilising 1% BSA Sty-(SOD-0.01%BSA-0.5%GA-2%PEI)$_5$ (21.17 ± 1.30 µM, n = 9). However, there is a significant increase ($P < 0.0001$) in sensitivity from 0.28 ± 0.008 nA/µM (n = 8, Sty-(SOD-1%BSA-0.5%GA-

2%PEI)$_5$) to 0.61 ± 0.04 nA/µM (n = 9, Sty-(SOD-0.01%BSA-0.5%GA-2%PEI)$_5$) when incorporating the lower concentration of BSA. All biosensor designs illustrated sigmoidal enzyme kinetics giving α values close to 2.

This section has illustrated the effects of changing the concentration of BSA in the dipping series. Previously 0.5% GA proved optimum, however, both 1% and 2% PEI proved beneficial so these concentrations were compared when changing the concentration of BSA. In this set of experiments 1% PEI gave the best results when incorporating 1%, 0.1% and 0.01% BSA in terms of kinetic parameters and sensitivities. Since both 1% BSA and 0.1% BSA gave optimum results these concentrations were used in the next section where the BSA was mixed with GA.

4.3.7. Bovine Serum Albumin:Glutaraldehyde (BSA:GA)

In this section, an investigation was undertaken to evaluate the contribution the BSA (1%) and (0.1%) solutions are having on enzyme protection, when used in conjunction with GA cross-linking. Research suggests that the incorporation of GA with BSA is beneficial (Migneault *et al.*, 2004) (Payne, 1973). As alluded to previously, GA is thought to exert its effect through its involvement with the lysine amino groups. BSA is an inert lysine rich protein therefore, incorporating BSA can potentially increase the amount of lysine residues with which GA can cross-link, therefore increasing enzyme immobilisation. Furthermore, the addition of BSA can aid in protecting the enzyme as the GA will preferentially cross-link with the BSA rather than the enzyme itself *(*Li *et al*., 1999), due to its larger size and increased lysine residues.

This section investigates the effects of mixing 0.1%/1% BSA with 0.5% GA and then incorporating 1%/2% PEI as the final layer after the BSA:GA mixture and preceding the subsequent layer of enzyme. This investigation was undertaken to try and optimise the kinetic parameters. The introduction of BSA proved beneficial (see Section 4.3.6.3) in reducing the K_m without compromising the sensitivity, however, the low V_{max} achieved is not ideal. The mixing of BSA with GA could potentially increase the sensitivity and V_{max} as a result of the GA cross-linking with the lysine rich BSA rather than directly to the enzyme.

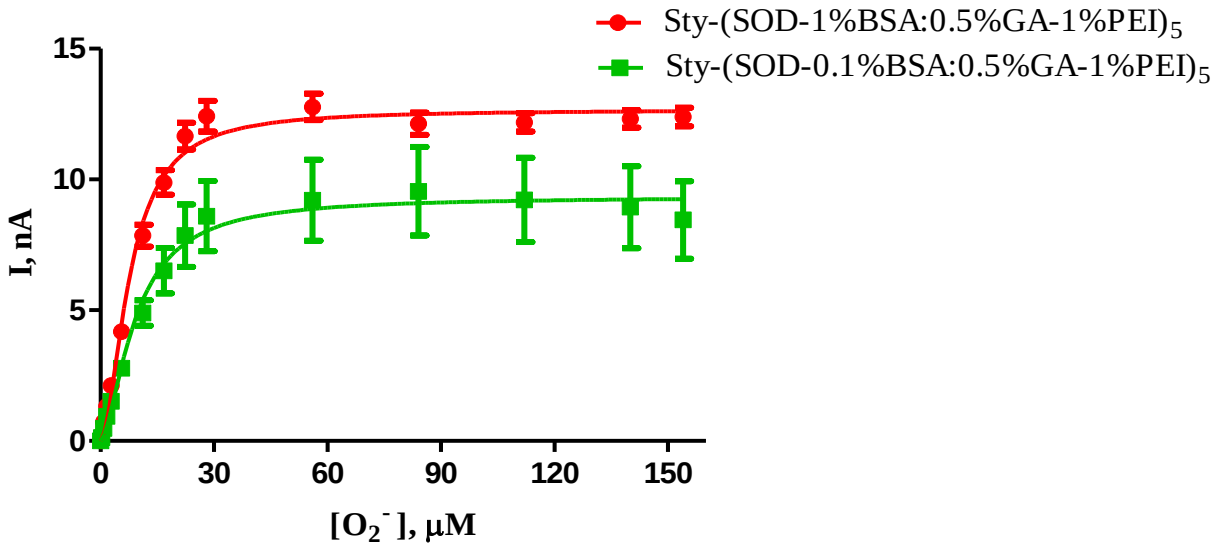

	Sty-(SOD-1%BSA:0.5%GA-1%PEI)$_5$			Sty-(SOD-0.1%BSA:0.5%GA-1%PEI)$_5$		
	Mean	S.E.M	n	Mean	S.E.M	n
V_{max}, nA	12.67	0.10	8	9.34	0.22	8
K_m, µM	7.76	0.20	8	9.23	0.64	8
α	1.80	0.07	8	1.63	0.16	8
Sensitivity, nA/µM	0.70	0.01	8	0.44	0.02	8
R^2	0.99	-	8	0.99	-	8

Figure 4.16: The mean current-concentration profiles for O_2^- calibrations *(Top)* and comparison table *(Bottom)* in PBS (pH 7.4) buffer solution containing XOD at 21°C using designs Sty-(SOD-1%BSA:0.5%GA-1%PEI)$_5$ and Sty-(SOD-0.1%BSA:0.5%GA-1%PEI)$_5$. CPA carried out at +700 mV *vs.* SCE.

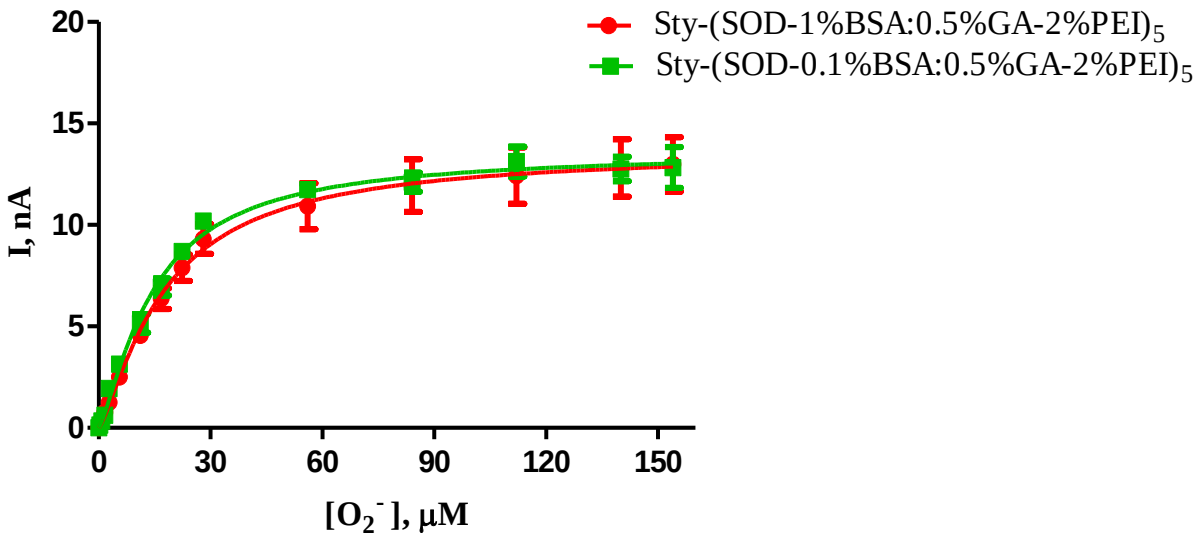

	Sty-(SOD-1%BSA:0.5%GA-2%PEI)$_5$			Sty-(SOD-0.1%BSA:0.5%GA-2%PEI)$_5$		
	Mean	S.E.M	n	Mean	S.E.M	n
V_{max}, nA	13.67	0.25	12	13.62	0.17	8
K_m, µM	17.83	0.81	12	14.73	0.47	8
α	1.29	0.06	12	1.32	0.05	8
Sensitivity, nA/µM	0.41	0.008	12	0.47	0.03	8
R^2	0.99	-	12	0.97	-	8

Figure 4.17: The mean current-concentration profiles for O_2^- calibrations *(Top)* and comparison table *(Bottom)* in PBS (pH 7.4) buffer solution containing XOD at 21°C using designs Sty-(SOD-1%BSA:0.5%GA-2%PEI)$_5$ and Sty-(SOD-0.1%BSA:0.5%GA-2%PEI)$_5$. CPA carried out at +700 mV *vs.* SCE.

A comparison graph and data table of kinetic parameters are presented in Figure 4.16 and Figure 4.17. The graph illustrates the comparison of BSA concentrations mixed with 0.5% GA, the table presents the kinetic parameter comparisons for each design. Following incorporation of 1% PEI, a significant decrease ($P < 0.0001$) in V_{max} from 12.67 ± 0.10 nA (n = 8, Sty-(SOD-1%BSA:0.5%GA-1%PEI)$_5$) to 9.34 ± 0.22 nA (n = 8, Sty-(SOD-0.1%BSA:0.5%GA-1%PEI)$_5$) is observed. A similar trend occurs with sensitivity. There is a significant decrease ($P < 0.0001$) in sensitivity from 0.70 ± 0.01 nA/µM (n = 8, Sty-(SOD-1%BSA: 0.5%GA-1%PEI)$_5$) to 0.44 ± 0.02 nA/µM (n = 8, Sty-(SOD-0.1%BSA:0.5%GA-1%PEI)$_5$) when utilising the lower concentration of BSA in the dipping series. Both designs show sigmoidal enzyme kinetics with α values of 1.80 ± 0.07 (Sty-(SOD-1%BSA:0.5%GA-1%PEI)$_5$) and 1.63 ± 0.16 (Sty-(SOD-0.1%BSA:0.5%GA-1%PEI)$_5$). An explanation for this trend could be that the lysine rich BSA is binding to the GA rather than the BSA 'smothering' the enzyme and blocking access of the substrate to the active sites. However, as a decrease in sensitivity is observed the cross-linking process is less efficient than previous designs, predominantly as a result of the GA cross-linking with the BSA rather than the enzyme, resulting in a weaker cross-linking process.

The same results were not observed when incorporating 2% PEI. Interestingly, almost identical ($P = 0.8840$) V_{max} values were recorded for both designs 13.67 ± 0.25 nA (Sty-(SOD-1%BSA:0.5%GA-2%PEI)$_5$) and 13.62 ± 0.17 nA (Sty-(SOD-0.1%BSA:0.5%GA-2%PEI)$_5$). An increase in sensitivity ($P = 0.0894$) is observed from 0.41 ± 0.008 nA/µM (n = 12, Sty-(SOD-1%BSA:0.5%GA-2%PEI)$_5$) to 0.47 ± 0.03 nA/µM (n = 8, Sty-(SOD-0.1%BSA:0.5%GA-2%PEI)$_5$). A significant decrease ($P = 0.0044$) in the K_m concentration is demonstrated from 17.83 ± 0.81 µM (n = 12, Sty-(SOD-1%BSA:0.5%GA-2%PEI)$_5$) to 14.73 ± 0.47 µM (n = 8, Sty-(SOD-0.1%BSA:0.5%GA-2%PEI)$_5$). These results suggest that utilising a higher concentration of BSA (1%) adds no additional protective or stabilising effects when compared to the lower concentration.

In summary, this section has demonstrated the effect of mixing 1%/0.1% BSA with 0.5% GA. The results illustrate that incorporating both BSA and GA separately in the dip coating process results in lower K_m concentrations and higher sensitivities being achieved when compared to mixing the two components.

4.3.8. Methyl Methacrylate Modifications

There have been previous reports of enzyme immobilisation based on methacrylate derivatives. Enzyme electrodes based on methacrylate's have received significant attention in the development of biosensors (Pérez *et al.*, 2006). Methacrylate monomers consisting of an alkyl group, an acrylate ester group and a functional carboxyl group can react with a wide range of monomers and functionalised molecules providing flexible polymer chains. A glucose biosensor has been developed by simultaneously immobilising both GOx and ferrocene in a copolymer film based on poly(2-hydroxyethyl methacrylate) and methyl methacrylate (MMA)(Bean *et al.*, 2005). Poly (MMA) is a clear colourless polymer used regularly in optical applications. The optical properties of pMMA such as colorimetric changes, luminescence effects and light refractions are used in fibre optic sensors and optical waveguides or cladding (Kim, 2005) (Pérez *et al.*, 2006). Dai *et al*, utilised poly(MMA) in the development of a graphite sensor for vitamin C as the monomer possesses certain characteristics that were important in the biosensor design such as low cost and mechanical stability (Dai *et al.*, 2008).

This section investigates the effect of changing the immobilisation matrix of the biosensor from styrene to MMA to investigate its effects on sensitivity and kinetic parameters. The best design incorporating Sty (Sty-(SOD-0.5%GA-2%PEI)$_5$) was utilised in this set of experiments.

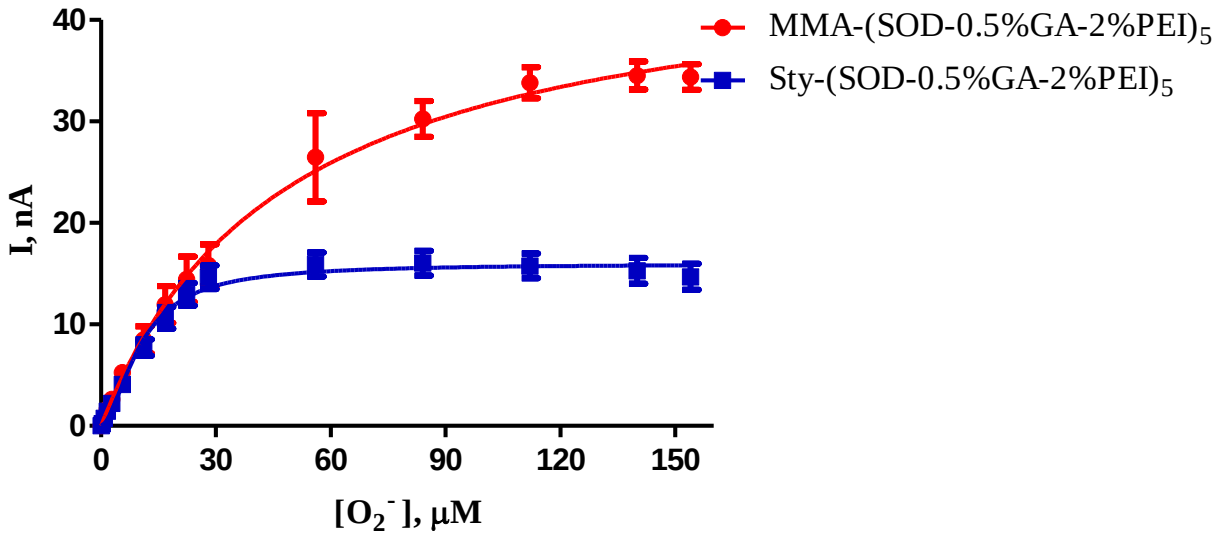

	MMA-(SOD-0.5%GA-2%PEI)$_5$			Sty-(SOD-0.5%GA-2%PEI)$_5$		
	Mean	S.E.M	n	Mean	S.E.M	n
V_{max}, nA	44.23	1.67	12	15.95	0.15	17
K_m, µM	42.30	3.78	12	10.33	0.27	17
α	1.08	0.05	12	1.73	0.07	17
Sensitivity, nA/µM	0.96	0.03	12	0.91	0.06	17
R^2	0.99	-	12	0.99	-	17

Figure 4.18: The mean current-concentration profiles for O_2^- calibrations *(Top)* and comparison table *(Bottom)* in PBS (pH 7.4) buffer solution containing XOD at 21°C using designs MMA-(SOD-0.5%GA-2%PEI)$_5$ and Sty-(SOD-0.5%GA-2%PEI)$_5$. CPA carried out at +700 mV *vs.* SCE.

A comparison graph and the data table of kinetic parameters are shown in Figure 4.18. It is clear that the introduction of MMA has significantly increased ($P < 0.0001$) the V_{max} from 15.95 ± 0.15 nA (n = 17, Sty-(SOD-0.5%GA-2%PEI)$_5$) to 44.23 ± 1.67 nA (n = 12, MMA-(SOD-0.5%GA-2%PEI)$_5$). However, there is a significant increase ($P < 0.0001$) in the K_m concentration from 10.33 ± 0.27 µM (n =17, Sty-(SOD-0.5%GA-2%PEI)$_5$) to 42.30 ± 3.78 µM (n = 12, MMA-(SOD-0.5%GA-2%PEI)$_5$). This increase in the K_m concentration is not ideal as the O_2^- concentration is so low in the *in-vivo* environment. This trend suggests that the MMA design produces poorer enzyme kinetics with a higher V_{max} and K_m concentration. Sigmoidal enzyme kinetics are produced by the Sty-(SOD-0.5%GA-2%PEI)$_5$ with an α value of 1.76 ± 0.07 being recorded while the MMA-(SOD-0.5%GA-2%PEI)$_5$) design demonstrates ideal enzyme kinetics with an α value of 1.08 ± 0.05 being obtained. The Sty-(SOD-0.5%GA-2%PEI)$_5$ design shows a co-operative effect where the binding of the substrate to one active site on the enzyme increases the affinity of other sites on the enzyme to bind more molecules of substrate therefore sigmoidal kinetics are observed.

The MMA-(SOD-0.5%GA-2%PEI)$_5$ design demonstrates a significant increase ($P = 0.0132$) in sensitivity to 0.96 ± 0.03 nA/µM (n = 12) when compared to the Sty-(SOD-0.5%GA-2%PEI)$_5$ with a sensitivity of 0.91 ± 0.06 nA/µM (n = 17). However, as the MMA-(SOD-0.5%GA-2%PEI)$_5$ illustrates poorer enzyme kinetics with a higher K_m concentration and a higher V_{max} being recorded this design is not ideal and the Sty-(SOD-0.5%GA-2%PEI)$_5$ is favourable. Furthermore, another important factor in biosensor development is the sensor's reproducibility. The Sty-(SOD-0.5%GA-2%PEI)$_5$ is more reproducible than the MMA-(SOD-0.5%GA-2%PEI)$_5$ design, with the latter showing higher errors for all its kinetic parameters when compared to the styrene design.

4.3.9 Best Design

Throughout this chapter experiments were performed to investigate the effect the immobilisation matrix, unit of activity, BSA, GA and PEI had on the O_2^- biosensor. The goal was to obtain a biosensor with a high sensitivity and a low K_m concentration representative of good Michaelis-Menten kinetics. The best design was determined to be Sty-(SOD-0.5%GA-2%PEI)$_5$.. However, another design Sty-(SOD-0.1%BSA-0.5%GA-1%PEI)$_5$ also showed good enzyme kinetics and an identical sensitivity was recorded.

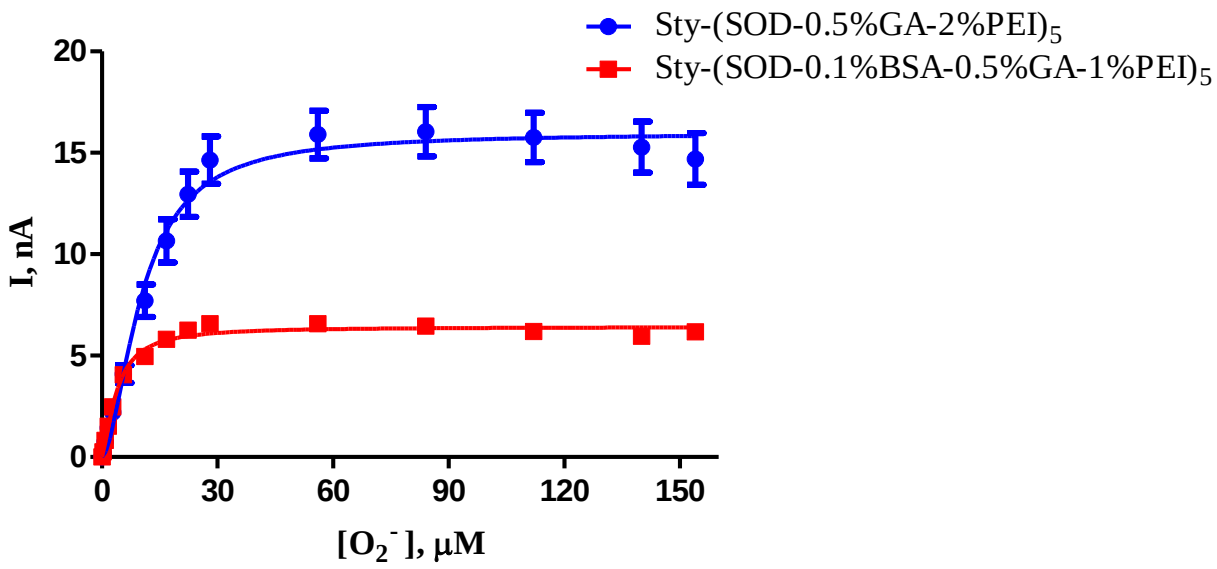

	Sty-(SOD-0.1%BSA-0.5%GA-1%PEI)$_5$			Sty-(SOD-0.5%GA-2%PEI)$_5$		
	Mean	S.E.M	n	Mean	S.E.M	n
V_{max}, nA	6.42	0.05	7	15.95	0.15	17
K_m, µM	3.78	0.13	7	10.33	0.27	17
α	1.45	0.06	7	1.73	0.07	17
Sensitivity, nA/µM	0.91	0.03	7	0.91	0.06	17
R^2	0.99	-	7	0.99	-	17

Figure 4.19: The mean current-concentration profiles for O_2^- calibrations *(Top)* and comparison table *(Bottom)* in PBS (pH 7.4) buffer solution containing XOD at 21°C using designs Sty-(SOD-0.1%BSA-0.5%GA-1%PEI)$_5$ and Sty-(SOD-0.5%GA-2%PEI)$_5$. CPA carried out at +700 mV *vs.* SCE.

A comparison graph and data table of kinetic parameters are presented in Figure 4.18. This section represents the best combination of kinetic parameters for the detection of O_2^- using different biosensor components.

The designs illustrate differences for each of the kinetic parameters. The Sty-(SOD-0.1%BSA-0.5%GA-1%PEI)$_5$ shows a significant decrease ($P < 0.0001$) in V_{max} (6.42 ± 0.05 nA, n = 7) compared to the Sty-(SOD-0.5%GA-2%PEI)$_5$ (15.98 ± 0.15 nA, n = 17). A significant increase ($P < 0.0001$) in the K_m concentration is observed from 3.78 ± 0.13 µM (n = 7, Sty-(SOD-0.1%BSA-0.5%GA-1%PEI)$_5$) to 10.33 ± 0.27 µM (n = 17, Sty-(SOD-0.5%GA-2%PEI)$_5$). Both designs showed sigmoidal enzyme kinetics with α values of 1.45 (Sty-(SOD-0.1%BSA-0.5%GA-1%PEI)$_5$) and 1.73 (Sty-(SOD-0.5%GA-2%PEI)$_5$). Overall, the Sty-(SOD-0.5%GA-2%PEI)$_5$ gave the best results and this design will be used for future studies.

4.4 Conclusion

This chapter details the modifications undertaken in the development of a O_2^- biosensor. The immobilisation matrices utilised were both styrene and MMA. It was determined that 5 layers of enzyme immobilised within these matrices was optimal for the biosensor design. The optimal enzyme unit of activity was determined to be a 200 U/mL enzyme solution. The incorporation of a cross-linker GA, alongside PEI proved advantageous, however, the inclusion of the stabiliser BSA resulted in a significant decrease in the V_{max} and K_m concentration. These three components were extensively characterised in terms of their effect on the immobilisation of the enzyme until the optimal arrangement was determined for maximising O_2^- detection. The best design is Sty-(SOD-0.5%GA-2%PEI)$_5$ which has a sensitivity of 0.91 ± 0.06 nA/µM, V_{max} of 15.98 ± 0.15 nA and a K_m concentration of 10.33 ± 0.27 µM (n = 17). Therefore, this chapter concludes the successful development of a biosensor with a satisfactory sensitivity to detect O_2^- *in-vivo*.

4.5 References

Baker KL. (2013) *The Development of Microelectrochemical Choline and Acetycholine Biosensors for Real-Time Neurochemical Monitoring.* Ph.D. Thesis, National University of Ireland, Maynooth.

Bean LS, Heng LY, Yamin BM, *et al.* (2005) The electrochemical behaviour of ferrocene in a photocurable poly(methyl methacrylate-co-2-hydroxylethyl methacrylate) film for a glucose biosensor. *Bioelectrochemistry* 65: 157-162.

Belay A, Collins A, Ruzgas T, *et al.* (1999) Redox hydrogel based bienzyme electrode for l-glutamate monitoring. *Journal of Pharmaceutical and Biomedical Analysis* 19: 93-105.

Bolger FB. (2007) *The In-Vitro and In-Vivo Characterisation and Application of Real-Time Sensors and Biosensors for Neurochemical Studies of Brain Energy Metabolism*. Ph.D. Thesis, National University of Ireland, Maynooth.

Brena BM and Batista-Viera F. (2006) Immobilization of enzymes. *Immobilization of Enzymes and Cells*: 15-30.

Broun GB. (1976) Chemically aggregated enzymes. *Methods in Enzymology*. Academic Press, 263-280.

Campanella L, Favero G, Persi L, *et al.* (2000) New biosensor for superoxide radical used to evidence molecules of biomedical and pharmaceutical interest having radical scavenging properties. *Journal of Pharmaceutical and Biomedical Analysis* 23: 69-76.

Chui WK and Wan LSC. (1997) Prolonged retention of cross-linked trypsin in calcium alginate microspheres. *Journal of Microencapsulation* 14: 51-61.

Costa SA, Tzanov T, Filipa Carneiro A, *et al*. (2002) Studies of stabilization of native catalase using additives. *Enzyme and Microbial Technology* 30: 387-391.

Dai H, Wu X, Wang Y, *et al.* (2008) An electrochemiluminescent biosensor for vitamin C based on inhibition of luminol electrochemiluminescence on graphite/poly(methylmethacrylate) composite electrode. *Electrochimica Acta* 53: 5113-5117.

de Melo JV, Bello ME, de Azevêdo WM, *et al.* (1999) The effect of glutaraldehyde on the electrochemical behavior of polyaniline. *Electrochimica Acta* 44: 2405-2412.

Emregül E. (2005) Development of a new biosensor for superoxide radicals. *Analytical and Bioanalytical Chemistry* 383: 947-954.

Fabian RH, DeWitt DS and Kent TA. (1995) *In vivo* Detection of Superoxide Anion Production by the Brain Using a Cytochrome c Electrode. *Journal of Cerebral Blood Flow & Metabolism* 15: 242-247.

Ganesana M, Erlichman JS and Andreescu S. (2012) Real-time monitoring of superoxide accumulation and antioxidant activity in a brain slice model using an electrochemical cytochrome c biosensor. *Free Radical Biology and Medicine* 53: 2240-2249.

Gupta V, Nath S and Chand S. (2000) Estimation of proteins in the presence of polyethylenimine. *Biotechnology Letters* 22: 927-929.

Hu S, Xu C, Luo J, *et al.* (2000) Biosensor for detection of hypoxanthine based on xanthine oxidase immobilized on chemically modified carbon paste electrode. *Analytica Chimica Acta* 412: 55-61.

Jezkova J, Iwuoha EI, Smyth MR, *et al.* (1997) Stabilisation of an osmium bis-bipyridyl polymer-modified carbon paste amperometric glucose biosensor using polyethyleneimine. *ElectroAnalysis* 9: 978-984.

Kim G. (2005) A PMMA composite as an optical diffuser in a liquid crystal display backlighting unit (BLU). *European Polymer Journal* 41: 1729-1737.

Kumada Y, Kuroki D, Yasui H, *et al*. (2010) Characterisation of polystyrene-binding peptides (PS-tags) for site-specific immobilization of proteins. *Journal of Bioscience and Bioengineering* 109: 583-587.

Li Y-G, Zhou Y-X, Feng J-L, *et al*. (1999) Immobilisation of enzyme on screen-printed electrode by exposure to glutaraldehyde vapour for the construction of amperometric acetylcholinesterase electrodes. *Analytica Chimica Acta* 382: 277-282.

Lowry JP, McAteer K, El Atrash SS, *et al*. (1994) Characterisation of Glucose Oxidase-Modified Poly(phenylenediamine)-Coated Electrodes *in vitro* and *in vivo*: Homogeneous Interference by Ascorbic Acid in Hydrogen Peroxide Detection. *Analytical Chemistry* 66: 1754-1761.

Maier CM and Chan PH. (2002) Book review: role of superoxide dismutases in oxidative damage and neurodegenerative disorders. *The Neuroscientist* 8: 323-334.

Manning P and McNeil CJ. (2011) Electrochemical and optical sensing of reactive oxygen species: pathway to an integrated intracellular and extracellular measurement platform. *Biochemical Society Transactions* 39: 1288-1292.

Manning P, McNeil CJ, Cooper JM, *et al*. (1998) Direct, Real-Time Sensing of Free Radical Production by Activated Human Glioblastoma Cells. *Free Radical Biology and Medicine* 24: 1304-1309.

Mateo C, Palomo JM, Fernandez-Lorente G, *et al*. (2007) Improvement of enzyme activity, stability and selectivity via immobilization techniques. *Enzyme and Microbial Technology* 40: 1451-1463.

McMahon CP, Rocchitta G, Kirwan SM, *et al.* (2007) Oxygen tolerance of an implantable polymer/enzyme composite glutamate biosensor displaying polycation-enhanced substrate sensitivity. *Biosensors and Bioelectronics* 22: 1466-1473.

McMahon CP, Rocchitta G, Serra PA, *et al.* (2006) The efficiency of immobilised glutamate oxidase decreases with surface enzyme loading: an electrostatic effect, and reversal by a polycation significantly enhances biosensor sensitivity. *Analyst* 131: 68-72.

McNeil CJ and Manning P. (2002) Sensor-based measurements of the role and interactions of free radicals in cellular systems. *Reviews in Molecular Biotechnology* 82: 443-455.

Mesároš Š, Vaňková Ž, Grunfeld S, *et al*. (1998) Preparation and optimisation of superoxide microbiosensor. *Analytica Chimica Acta* 358: 27-33.

Migneault I, Dartiguenave C, Bertrand MJ, *et al.* (2004) Glutaraldehyde: behavior in aqueous solution, reaction with proteins, and application to enzyme crosslinking. *Biotechniques* 37: 790-806.

Patel NG, Erlenkötter A, Cammann K, *et al*. (2000) Fabrication and characterisation of disposable type lactate oxidase sensors for dairy products and clinical analysis. *Sensors and Actuators B: Chemical* 67: 134-141.

Payne JW. (1973) Polymerisation of proteins with glutaraldehyde. Soluble molecular-weight markers. *Biochemical Journal* 135: 867-873.

Pérez JPH, López-Cabarcos E and López-Ruiz B. (2006) The application of methacrylate-based polymers to enzyme biosensors. *Biomolecular Engineering* 23: 233-245.

Ryan MR, Lowry JP and O'Neill RD. (1997) Biosensor for Neurotransmitter L-Glutamic Acid Designed for Efficient Use of L-Glutamate Oxidase and Effective Rejection of Interference. *Analyst* 122: 1419-1424.

Sassolas A, Blum LJ and Leca-Bouvier BD. (2012) Immobilisation strategies to develop enzymatic biosensors. *Biotechnology Advances* 30: 489-511.

Shah S, Sharma A and Gupta MN. (2006) Preparation of cross-linked enzyme aggregates by using bovine serum albumin as a proteic feeder. *Analytical Biochemistry* 351: 207-213.

Thévenot DR, Toth K, Durst RA, *et al*. (2001) Electrochemical biosensors: recommended definitions and classification1. *Biosensors and Bioelectronics* 16: 121-131.

Tian Y, Mao L and Ohsaka T. (2006) Electrochemical biosensors for superoxide anion. *Current Analytical Chemistry* 2: 51-58.

Wang Z, Liu D, Gu H, *et al.* (2013) NTA-modified carbon electrode as a general relaying substrate to facilitate electron transfer of SOD: Application to *in vivo* monitoring of O_2^- in a rat brain. *Biosensors and Bioelectronics* 43: 101-107.

Wang Z, Zhang L-M and Tian Y. (2014) Progress on Electrochemical Determination of Superoxide Anion. *Chinese Journal of Analytical Chemistry* 42: 1-9.

Wilson GS and Thévenot DR. (1989) Unmediated amperometric enzyme electrodes. *Biosensors: Pratical Approach*: 1-17.

Chapter 5: Interferences

5.1. Introduction

It is well documented that reactive oxygen species (ROS) can be formed under many different conditions and in many different cellular compartments however, the number of enzymes that generate superoxide (O_2^-) is relatively low. O_2^- can be produced by nicotinamide adenine dinucleotide phosphase (NADPH) oxidases (Lambeth, 2004), xanthine oxidase (XOD) (McCord and Fridovich, 1969), aldehyde oxidase (Kundu *et al*., 2007), cytochrome P450 (Sligar et al., 1974) and the mitochondrial electron-transport chain (Loschen *et al.*, 1974). It is documented that the most important source of O_2^- *in-vivo* in aerobic eukaryotic cells is the mitochondrial electron-transport chain. Mitochondria consume oxygen (O_2) associated with the process of oxidative phosphorylation. Under normal metabolic conditions approximately 95-97% of the O_2 is reduced to H_2O; a small fraction of the O_2 consumed (1-3%) may form O_2^-. Leakage of electrons to O_2 to form O_2^- can take place in components of complexes I and complex III of the electron-transport chain and under certain conditions from complex II (Halliwell and Gutteridge, 2015).

XOD has been established to be an important source of biological free radical generation. XOD catalyses the univalent and divalent reduction of molecular O_2 generating O_2^- and hydrogen peroxide (H_2O_2) and results in the oxidation of xanthine to uric acid (UA) (Eqn 5.1) (Kuppusamy and Zweier, 1989) (Aitken *et al.*, 1993).

$$\text{Xanthine} + H_2O + O_2 \xrightarrow{\text{XOD}} \text{UA} + O_2^- + 2H^+ \qquad \textbf{Eqn. 5.1}$$

In addition to the generation of O_2^- and H_2O_2 other toxic secondary radicals such as the hydroxyl radical ($^{\bullet}OH$) maybe formed through Haber Weiss or Fenton-type reactions with transition metals especially iron (Link and Riley, 1988) (Rowley and Halliwell, 1983) (Fong *et al*., 1973) (Kellogg and Fridovich, 1975). Cytochrome c is also shown to be reduced by XOD under aerobic conditions and in the absence of exogenous electron carriers, is caused by the O_2^- anion (Fridovich, 1970).

The steps involved in the development of a first generation O_2^- biosensor were presented in the previous chapter. The superoxide dismutase (SOD) functionalised

biosensor is based on the electrooxidation of H_2O_2 generated during the O_2^- catalytic dismutation. Mesaros *et al.* developed a O_2^- biosensor with the enzyme immobilised in a polypyrole film during electropolymerisation on a Pt surface. The biosensor was held at +700 mV *vs.* SCE and had a detection limit of 15 nM (Mesároš *et al.*, 1998). Campanella and co-workers developed a O_2^- biosensor with SOD physically entrapped in a kappa-carrageenan gel membrane sandwiched between a Pt disc electrode and a dialysis membrane (Campanella *et al.*, 2000). However, these biosensors do not apply any technique to distinguish the H_2O_2 produced by the SOD catalysed dismutation of O_2^- from that endogenously produced in the biological systems (Wang *et al.*, 2014). They also suffered from low selectivity due to the high over potential required for the oxidation of H_2O_2 (Calas-Blanchard *et al.*, 2014).

Second generation O_2^- biosensors based on redox mediators have been developed to overcome the interference problems from UA and H_2O_2. These redox mediators facilitate the electron transfer between SOD and the electrode. Endo *et al.* developed a second generation biosensor based on a ferrocene derivative mediator (Endo *et al.*, 2002). The ferrocene-carboxaldehyde and SOD were co-immobilised on a Pt surface using glutaraldehyde (GA) and then protected by a polyurethane membrane. Kintzios *et al.* developed a second generation biosensor based on a similar design to Endo and co-workers (Kintzios *et al.*, 2006). This biosensor was composed of SOD, the mediator ferrocene-carboxaldehyde, cyananide, bovine serum albumin (BSA) and GA were immoblised on a gold working electrode and then coated with polyurethane for protection. These biosensors were held at +500 mV, however, this applied potential still suffers drawbacks due to interferences in biological systems therefore limiting the practical uses of these biosensors *in-vivo.* Lvovich and Sheeline developed a two channel sensor capable of detecting the O_2^- radical and H_2O_2 (Lvovich and Scheeline, 1997). A glassy carbon working microelectrode covered by an electrodeposited polypyrrole/horseradish peroxidase layer was developed as a H_2O_2 sensor. The O_2^- sensor was developed from another glassy carbon microelectrode covered by a composite membrane of an inside layer of polypyrrole/horseradish peroxidase and an outside layer of SOD. The two working electrodes with a Pt auxiliary electrode and a tungsten oxide (WO_3) reference electrode were contained in a 6 mm diameter Teflon cylinder and the two electrodes were held at +60 mV *vs.* WO_3 at pH 5.1. Although second generation biosensors prove advantageous as O_2^- biosensors, they too also

suffer from drawbacks in the *in-vivo* environment, including leaching of the untethered mediator from the enzyme layer, toxicity in biological tissues and redox interferences (oxidized ferrocenes can be reduced by ascorbic acid (AA) present in most biological media) (McMahon *et al.*, 2007).

Third generation biosensors are based on the direct electron transfer between the active centre of redox enzymes and the electrode. These biosensors are very attractive due to the simple procedure required for their design, as well as their high sensitivity and selectivity. Ohsaka *et al.* developed a biosensor based on direct electron transfer between SOD and the electrode surface (Ohsaka *et al.*, 2002). SOD was immobilised on a gold electrode via a self-assembled monolayer of cysteine. This monolayer was found to be an effective promoter for direct electron transfer of SOD and allowed the detection of O_2^- by measuring the steady-state current at +300 mV and/or -200 mV *vs.* Ag/AgCl. Tian *et al.* developed a SOD based biosensor utilising a carbon fibre microelectrode (Tian *et al.*, 2005). Au nanoparticles were electrodeposited on the carbon fibre which was sequentially modified by a self-assembled monolayer of cysteine for the immobilisation of SOD. Amperometric detection of O_2^- was performed by polarising the electrode at +250 mV or −150 mV *vs.* Ag/AgCl. Rajesh and co-workers developed a biosensor for the direct and simultaneous determination of O_2^- and nitrite ion by immobilising SOD on a polypyrrole polymer enhanced by carbon nanotubes to increase the biosensor's sensitivity (Rajesh *et al.*, 2010). Cyclic voltammetry was used to measure the electrochemical behaviour of the biosensor, where in the presence of O_2^- the quasi-reversible peaks of SOD became reversible. The anodic and cathodic peak currents also increased in the presence of O_2^-.

This chapter considers the products produced in the xanthine/XOD system, investigates whether these products are electroactive at +700 mV and explains techniques which can be incorporated in order to reduce their contribution from the biosensor's signal. Few reports exist of first generation biosensors incorporating SOD that address these interference reports particularly when utilising a potential of +700 mV.

5.2 Experimental

All instrumentation and experimental software used in this chapter are described in Chapter 3, Section 3.2. All chemicals and solutions used are detailed in Section 3.3.2.1.

The electrodes were constructed from a 1 mm Pt cylinder as depicted in Section 3.4.2. The sensor designs and the manufacturing process is explained in detail in Section 3.5.2.

All experimental data was collected using the cell set-up described in Section 3.6.1. All data was recorded in PBS containing 0.002 U XOD. Constant potential amperometry (CPA) was performed where the sensor was held at +700 mV *vs* SCE. Different aliquots of 1 mM xanthine were injected into the electrochemical cell as described in Section 3.6.3.

The data is reported as mean ± SEM where n denotes the number of electrodes used. The significance of difference observed was estimated using two-tailed t-tests. Paired t-tests were used when comparing data collected from the same electrode, unpaired t-tests were used for comparing data from different electrodes.

5.3. Results

This chapter identifies the potential electroactive interferences produced in the xanthine/XOD system. Possible strategies are proposed to eliminate the signal attributed to these interferent molecules from the biosensor current. The aim of this chapter is to determine an accurate and selective representation of current generated by the enzymatic dismutation of O_2^- at the Pt surface.

5.3.1. Xanthine Calibration on Pt Electrodes.

This section investigates the current generated on bare Pt electrodes using the electrochemical set-up for the generation of $O_2^{\cdot-}$. Bare Pt electrodes were calibrated in PBS containing 0.002 U of XOD and various aliquots of xanthine were added to the electrochemical cell. As per Equation 5.1, it is important to demonstrate that UA is produced as a by-product of the xanthine/XOD system. UA is electroactive at +700 mV therefore, a UA signal should be observed on the Pt 1 mm electrodes held at +700 mV *vs.* SCE.

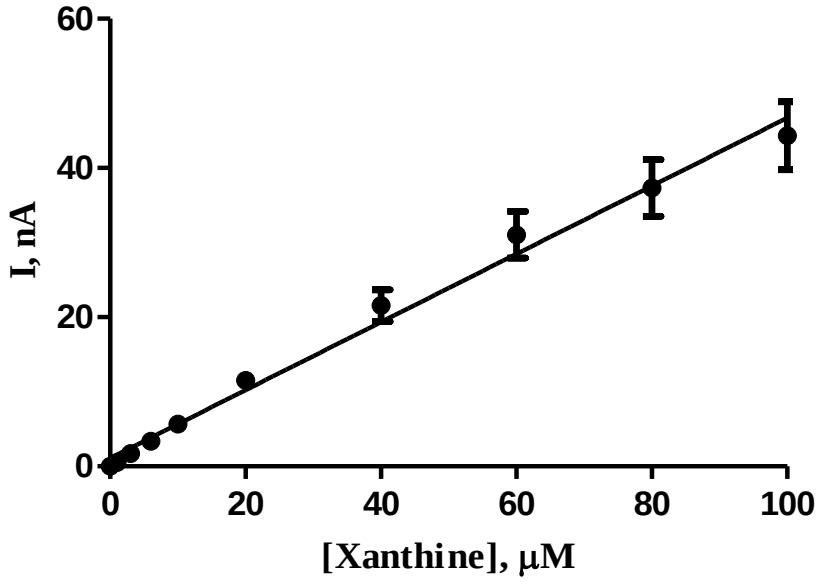

	Bare Pt-1mm Cylinder		
[Xanthine], µM	Mean	S.E.M	n
0	0.00	0.00	22
1	0.54	0.09	22
3	1.75	0.23	22
6	3.35	0.41	22
10	5.65	0.54	22
20	11.50	1.07	22
40	21.56	2.13	22
60	31.05	3.14	22
80	37.33	3.79	22
100	44.32	4.56	22
$I_{100\mu M}$, nA	44.32	4.56	22
Sensitivity, nA/µM	0.45	0.02	22
R^2	0.99	-	22

Figure 5.1: A current-concentration profile *(Top)* and comparison table *(Bottom)* for a xanthine calibration in PBS containing 0.002 U XOD using bare Pt 1 mm cylinders. CPA carried out at +700 mV *vs.* SCE. All currents are background subtracted (1.26 ± 0.08 nA).

Figure 5.1 above shows the mean current-concentration profile and the mean current values for a xanthine calibration performed in PBS containing 0.002 U XOD. The O_2^- radical is produced by the oxidation of xanthine to UA in the presence of XOD (George and Struthers, 2008) (Aitken *et al.*, 1993). UA is an electroactive species at +700 mV (O'Neill and Lowry, 2006).

It is clear, that a large proportion of the current generated by the xanthine-XOD calibration is UA. The current generated on addition of 100 µM xanthine is 44.32 ± 4.56 nA (n = 22). A linear response $r^2 = 0.99$ (n = 22) is observed for the first time. The enzyme kinetics observed in the previous chapter (Chapter 4 - Development) are

masked in this section, by the huge contribution UA has on the signal. The contribution of UA can be made negligible by the incorporation of an *o*-phenylenediamine (*o*-PD) layer onto the sensor surface. The electropolymerisation of *o*-PD for the rejection of interferences has been utilised regularly in biosensor designs (O'Neill, 1996) (Rothwell *et al.*, 2010) (Wilson and Gifford, 2005). PPD is permeable to H_2O_2 but efficient elimination of UA is demonstrated due to a 'self-blocking' phenomenon where at high concentrations the polymer becomes blocked, decreasing the sensitivity of large interfering species such as UA (Rothwell *et al.*, 2008) (O'Brien *et al*., 2007) (Craig and O'Neill, 2003).

In summary, this section demonstrated that the current generated on addition of 100 µM xanthine is 44.32 ± 4.56 nA (n = 22, bare Pt Electrode). This contribution must be eliminated from the biosensor signal otherwise the large UA signal will mask the enzyme kinetics.

5.3.2 Uric Acid Calibration on Pt Electrodes

This section investigates the current generated during a UA calibration over the physiological range of 0-60 µM. This will provide a comparison for the current generated during the O_2^- calibration which generates UA as a by-product. Bare Pt 1 mm electrodes were calibrated over the UA range of 0-60 µM in PBS (pH 7.4) at +700 mV *vs* SCE.

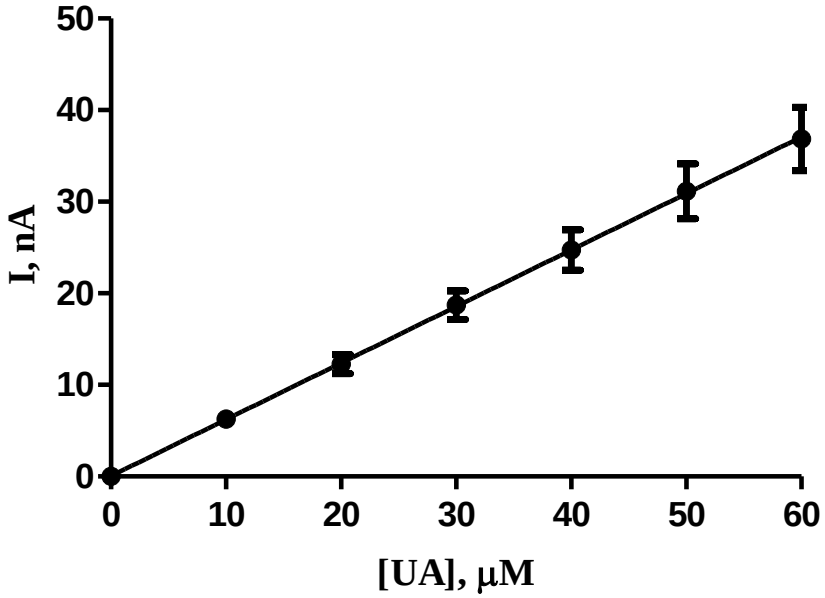

	Bare Pt-1mm Cylinder		
[UA], µM	Mean	S.E.M	n
0	0.00	0.00	18
10	6.26	0.68	18
20	12.27	1.03	18
30	18.72	1.56	18
40	24.73	2.22	18
50	31.14	2.99	18
60	36.84	3.46	18
$I_{60\mu M}$, nA	36.84	3.46	18
Sensitivity, nA/µM	0.617	0.003	18
R^2	0.99	-	18

Figure 5.2: A current-concentration profile *(Top)* and comparison table *(Bottom)* for a UA calibration in PBS using bare Pt 1 mm cylinders. CPA carried out at +700 mV *vs.* SCE. All currents are background subtracted (0.88 ± 0.04 nA)

Figure 5.2 shows the current generated on addition of various aliquots of UA into the electrochemical cell. This data shows a linear response ($r^2 = 0.99$) and a sensitivity of 0.617 ± 0.003 nA/µM. Interestingly, comparing the current generated on addition of 60 µM xanthine and 60 µM UA there is no significant difference (P = 0.2230) in the current recorded of 31.05 ± 3.14 nA (n = 22) and 36.84 ± 3.46 nA (n = 18) respectively. This result suggests that a similar quantity of UA is produced in the PBS solution on addition of 60 µM xanthine as the addition of 60 µM of a standard solution of UA. This suggests that the current generated during the xanthine calibration is attributed to the production of UA and this contribution must be negated.

As alluded to previously, the electropolymerisation of *o*-PD for the rejection of interferences has been utilised in the development of biosensors. The next section investigates what impact the introduction of this size exclusion polymer has on the current generated in the xanthine calibration.

5.3.3 Xanthine Calibration on Pt-PPD Electrodes

As discussed in Section 5.3.1, PPD is used regularly in the development of biosensors and has widely been reported to have excellent permselective properties being permeable to H_2O_2 and being an efficient blocker of interference analytes. The O_2^- biosensor developed in Chapter 4 is a first generation biosensor where the current generated by the oxidation of H_2O_2 at the working electrode held at +700 mV relative to the SCE is proportional to the concentration of the O_2^- radical in solution. Therefore, the addition of PPD does not affect the biosensor's signal due to the permeability of H_2O_2 to the PPD layer. This section investigates the effect introducing this permselective layer has on the current generated in the xanthine calibration. The method utilised for electropolymeristion of *o*-PD onto the Pt surface is described in detail in Chapter 3, Section 3.5.1

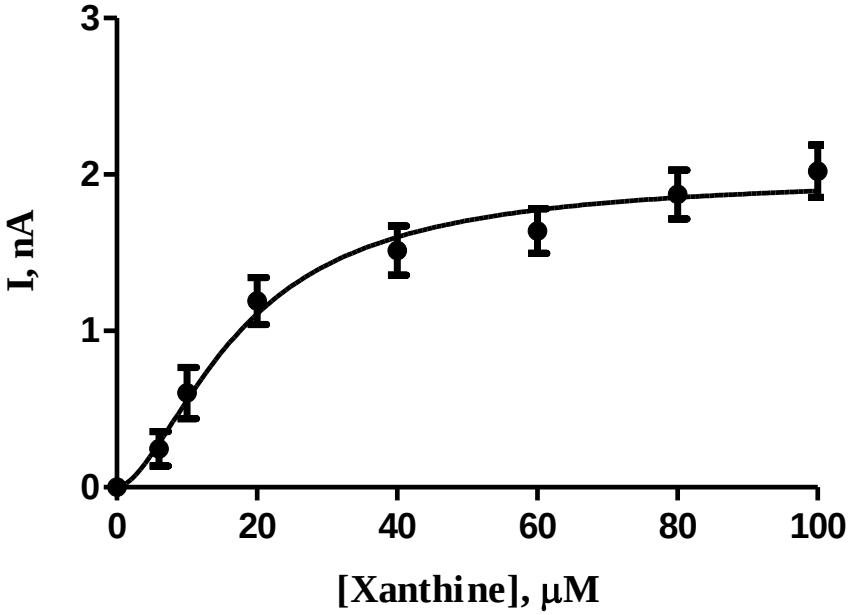

	Pt-PPD Electrode		
[Xanthine], µM	Mean	S.E.M	n
1	-0.11	0.06	16
3	-0.04	0.07	16
6	0.25	0.11	16
10	0.60	0.16	16
20	1.19	0.15	16
40	1.52	0.16	16
60	1.64	0.14	16
80	1.87	0.16	16
100	2.02	0.17	16
Sensitivity, nA/µM	0.07	0.01	16
R^2	0.97	-	16

Figure 5.3: A current-concentration profile *(Top)* and comparison table *(Bottom)* for a xanthine calibration in PBS containing 0.002 U XOD using Pt-PPD sensors. CPA carried out at +700 mV *vs.* SCE. All currents are background subtracted (0.93 ± 0.09 nA).

The results above show a significant decrease ($P < 0.0001$) in the sensitivity from 0.45 ± 0.02 nA/µM (n = 22, bare Pt electrode) to 0.07 ± 0.01 nA/µM (n = 16, Pt-PPD). A significant decrease ($P < 0.0001$) in the $I_{100\mu M}$ from 44.32 ± 4.56 nA (n = 22, bare Pt electrode) to 2.02 ± 0.17 nA (n = 16, Pt-PPD) is observed when PPD is included in the sensor design. Both these trends suggest that the incorporation of PPD has made the contribution from UA negligible. In the previous chapter (Chapter 4, Development) all the biosensor designs incorporate a PPD layer before modification with the various biosensor components (Styrene, SOD, BSA, GA and PEI). This eliminates any contribution attributed to the production of UA in the electrochemical cell.

Interestingly, the bare Pt electrodes gave a linear calibration response ($r^2 = 0.99$, n = 22) to xanthine, however, the electrodes incorporating the size exclusion polymer show hyperbolic kinetics typical of an enzyme reaction. This was previously masked by the huge contribution UA had on the current generated in the xanthine/XOD system resulting in a linear response over the calibration range. However, the current generated on addition of 100 µM xanthine into the electrochemical cell is 2.02 ± 0.17 nA for the Pt-PPD electrodes and this signal is higher than expected.

The next section will investigate the current generated at physiological levels of UA using Pt-PPD electrodes. This will provide a comparison for the results obtained here. In summary, this section investigated the current generated at a Pt-PPD electrode calibrated using the xanthine/XOD system. There is a significant reduction ($P < 0.0001$) in the sensitivity and $I_{100\mu M}$ recorded on addition of the PPD layer. The PPD layer has eliminated the current attributed to UA from the sensor's signal.

5.3.4. Uric Acid Calibration on Pt-PPD Electrodes

This section investigates the current generated over the physiological range (0 – 60 µM) for UA on Pt-PPD electrodes (O'Neill and Lowry, 2006) (O'Neill and Lowry, 1995). The previous section (Section 5.3.3) demonstrated that the current generated on addition of 100 µM xanthine is 2.12 ± 0.17 nA (n = 16, Pt-PPD). This set of experiments were performed in N_2 saturated PBS (pH 7.4) at +700 mV *vs.* SCE over a N_2 cloud. The calibration comprises of six 10 µL aliquots of UA each corresponding to a 10 µM concentration of UA. This section will provide a comparison for the results observed in the previous section (Section 5.3.3.)

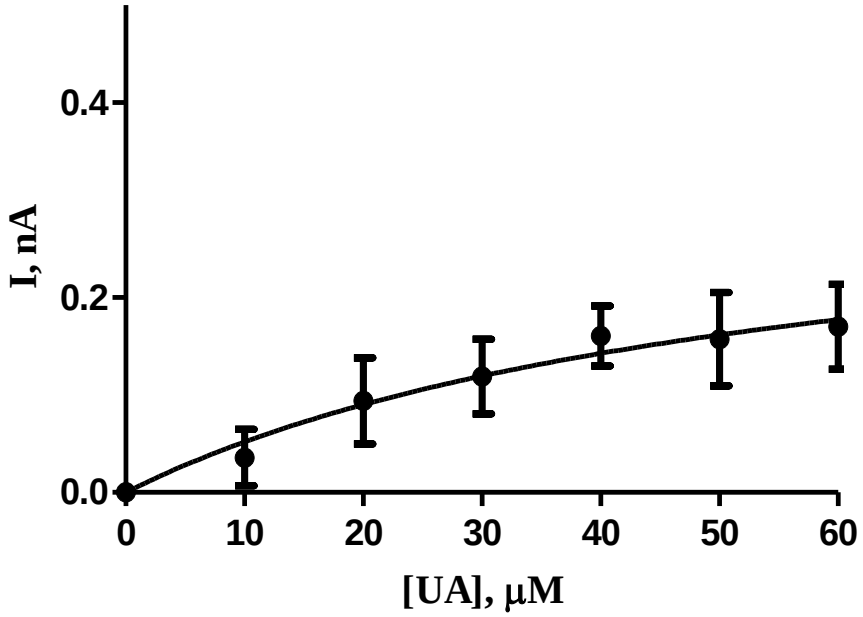

	Pt-PPD Electrode		
[UA], µM	Mean	S.E.M	n
10	0.04	0.03	9
20	0.09	0.04	9
30	0.12	0.04	9
40	0.16	0.03	9
50	0.16	0.05	9
60	0.17	0.04	9
$I_{60\mu M}$, nA	0.17	0.04	9
Sensitivity, nA/µM	0.0042	0.0004	9
R^2	0.97	-	9

Figure 5.4. : A current-concentration profile *(Top)* and comparison table *(Bottom)* for a UA calibration on Pt-PPD electrodes in PBS (pH 7.4). CPA carried out at +700 mV *vs* SCE. All currents are background subtracted (0.65 ± 0.11 nA).

It is clear from the results above, that there is principally a flat plateau response for the major part of the concentration range up to 60 µM. This shape can be explained in terms of saturation of the PPD with UA, leading to a 'self blocking' phenomenon. The same results were observed for the interferent AA where the geometry of the electrodes was found to influence the growth of the PPD (Rothwell *et al.*, 2009) (McMahon *et al.*, 2004).

The $I_{60\mu M}$ recorded for the UA calibration is 0.17 ± 0.04 nA (n = 9, Pt-PPD) which is significantly lower ($P < 0.0001$) than the $I_{60\mu M}$ of 1.64 ± 0.14 nA (n = 16, Pt-PPD) observed for the xanthine calibration. This result suggests that another interferent molecule is contributing to the current produced in the xanthine calibration. O_2^- spontaneously dismutates to H_2O_2, with a pH dependent second order rate of ~ 10^5 $M^{-1}s^{-1}$ at pH 7.0 (Miwa *et al.*, 2008) (Bielski *et al.*, 1985). This H_2O_2 is electroactive at +700 mV so this may be contributing to the $I_{60\mu M}$ of 1.64± 0.14 nA (n = 16, Pt-PPD) for the xanthine calibration. Link and Riley determined the concentration of O_2^-, H_2O_2 and UA formed in the xanthine/XOD system (Link and Riley, 1988). The total

amounts of each analyte formed during 1 h incubation of the reaction system were determined. In the uncompartmentalised system, where XOD (150 mU) was added directly to the xanthine (0.3 mM) solution resulted in the generation of 167 µM H_2O_2, 66 µM O_2^- and 150 µM UA. In the compartmentalised system the concentration of the products measured was one order of magnitude lower than that found in the uncompartmentalised system when utilising 1.5 U XOD. The ratios of UA to H_2O_2 were comparable in the two systems and were approximately 0.35 and 1.00 respectively. This suggests that UA and H_2O_2 are produced in the xanthine/XOD system in large quantities. Both these species are electroactive at +700 mV so there contribution must be accounted for in the biosensor's signal.

This section investigates the signal recorded on Pt-PPD electrodes after the addition of various aliquots of UA (0 – 60 µM). These results were used as a comparison for the results obtained in Section 5.3.3. It was determined that another interferent molecule is contributing to the 1.64 ± 0.14 nA, (n = 16, Pt-PPD) generated during the xanthine/XOD calibration. This result was determined by comparing the small current of 0.17 ± 0.04 nA (n = 9, Pt-PPD) observed during a UA calibration with the 2.02 ± 0.17 nA (n =16, Pt-PPD) generated on the addition of 100 µM xanthine. The hypothesis drawn for the generation of the 2.02 ± 0.17 nA is that the spontaneous dismutation of O_2^- is taking place in the electrochemical cell generating H_2O_2 which is electroactive at +700 mV and this is contributing to the signal generated on the Pt-PPD electrodes in the xanthine/XOD system.

.

5.3.5. Determination of other Interferents in the Xanthine/Xanthine Oxidase System

This section investigates whether the spontaneous dismutation of O_2^- is contributing to the overall biosensor current. In Section 5.3.3 we found that the current generated on addition of 100 µM xanthine on Pt-PPD electrodes was 2.02 ± 0.17 nA (n = 16). However, as seen in Section 5.3.4 the Pt-PPD electrodes only recorded a current of 0.17 ± 0.04 nA (n = 9) at physiological levels of UA. The hypothesis drawn from these results is that the current generated in the xanthine/XOD system should be lower than 0.5 nA if the interferent in the system is just UA. This section determines some

potential causes of the 2.02 ± 0.17 nA current generated in the xanthine/XOD system for the Pt-PPD electrodes. Reverting back to the original equation involving xanthine and XOD (Eqn 5.1)

$$\text{Xanthine} + H_2O + O_2 \xrightarrow{\text{XOD}} UA + O_2^- + 2H^+ \qquad \textbf{Eqn. 5.1}$$

By assessment of this equation, a hypothesis is that the spontaneous dismutation of O_2^- is taking place in the electrochemical cell generating H_2O_2 from the free H^+ ions available in the electrolyte. This could lead to the 'unwanted' production of H_2O_2 and this may contribute to the biosensor's signal. This theoretical 'unwanted' H_2O_2 production is verified by the incorporation of catalase into the experimental protocol.

Catalase is a tetrameric enzyme with a molecular weight of 240 kDA. The active site is characterised by a tyrosine as the proximal heme ligand and by a conserved histidine and asparagine on the distal side of the heme. The restricted access of the long narrow channel leading from the surface of the protein to the distal face of the heme may contribute to the fact that this enzyme is selective to the small H_2O_2 molecule (Pakhomova *et al.*, 2009). Mueller *et al* studied the decomposition of H_2O_2 at physiological levels in human erythrocytes using a sensitive H_2O_2 assay *(*Mueller *et al.*, 1997). This research group found that the exponential decay of H_2O_2 observed in the presence of purified erythrocyte catalase was followed down to 10^{-9} mol/L H_2O_2 at pH 7.4. H_2O_2 decomposition by catalase depended linearly on H_2O_2 concentration and even at very low H_2O_2 concentrations glutathione peroxidase another enzyme responsible for controlling H_2O_2 levels reaches only approximately 8% of the rate at which catalase simultaneously degrades H_2O_2. This research shows how effective catalase is at degrading H_2O_2 and suggests an almost exclusive role of catalase in eliminating H_2O_2 in normal human red blood cells. The primary function of catalase is the catalytic removal of the potentially toxic H_2O_2 by decomposing it to H_2O and O_2 (Eqn 5.2).

$$2H_2O_2 \xrightarrow{\text{Catalase}} O_2 + 2H_2O \qquad \textbf{Eqn. 5.2}$$

This section investigates the effect the administration of a single 200 µL injection of catalase has on the current generated at Pt-PPD sensors on addition of 100 µM xanthine.

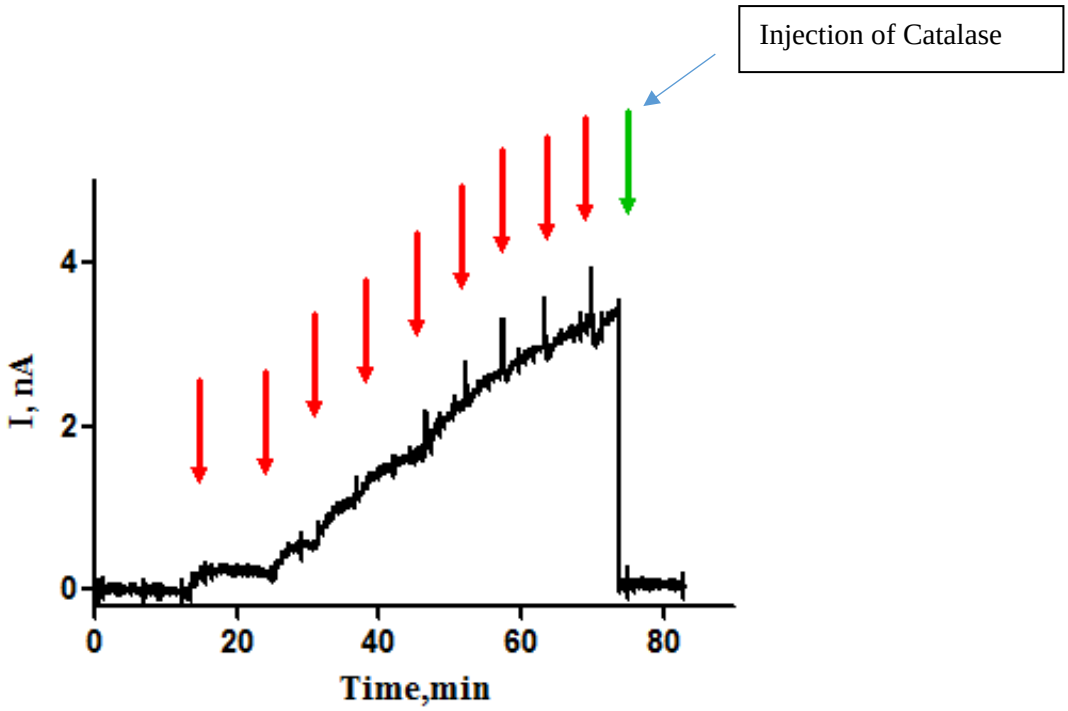

Figure 5.5: Typical raw data trace for a xanthine-XOD calibration on Pt-PPD sensors. The red arrows indicate sequential addition of 1, 3, 6, 10, 20, 40, 60, 80 and 100 µM xanthine injections. The green arrow indicates a 200 µL injection of catalase where we see a decrease in current to baseline.

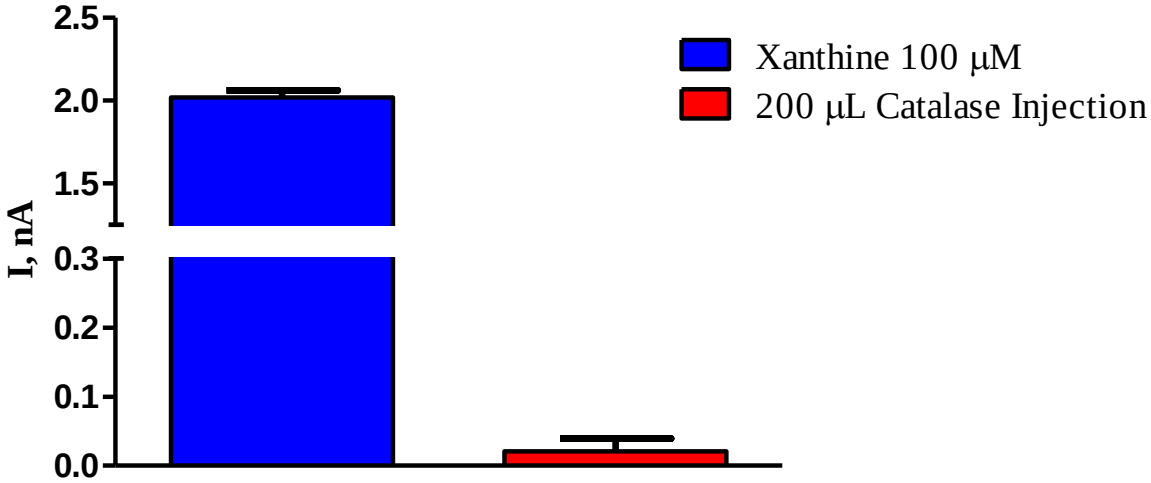

Xanthine (100 µM)			200 µL Catalase Injection		
Mean	S.E.M	n	Mean	S.E.M	n
2.02	0.17	16	0.02	0.06	11

Figure 5.6: Bar chart showing the current comparison between $I_{100\mu M}$ xanthine prior to a 200 µL injection of catalase on Pt–PPD sensors. The introduction of catalase shows an instantaneous decrease in current to baseline with a mean current value of 0.02 ± 0.06 nA (n = 11).

Figure 5.5 above shows a typical raw data trace for a xanthine/XOD calibration on Pt-PPD electrodes. The green arrow represents the administration of a 200 µL injection of catalase. Figure 5.6 shows a bar chart comparing the current generated on addition of 100 µM xanthine and then the signal detected on administration of a single 200 µL injection of catalase. Both these results support the hypothesis that the spontaneous dismutation of O_2^- is taking place in the bulk solution therefore, generating this spontaneously produced H_2O_2.

The introduction of catalase degrades the spontaneously produced H_2O_2 to H_2O and molecular O_2 (O'Brien *et al*., 2007). These by-products are not electroactive at +700 mV therefore, an instantaneous decrease in current to baseline is observed. This agrees with the hypothesis that the spontaneous dismutation of O_2^- generating H_2O_2 is taking place in the electrochemical cell resulting in the generation of 2.02 ± 0.17 nA (n = 16, Pt-PPD) on addition of 100 µM xanthine .

Another investigation carried out to verify that the spontaneous dismutation of O_2^- is taking place in the bulk solution was to perform a xanthine/XOD calibration on a Pt-Catalase biosensor. The Pt-Catalase biosensor used has previously been developed in the research group (O'Brien *et al.*, 2007). This biosensor has catalase immobilised on the Pt surface which degrades the H_2O_2 to H_2O and O_2, therefore the H_2O_2 response should be lower at the Pt-Catalase biosensor than at the Pt-PPD sensor.

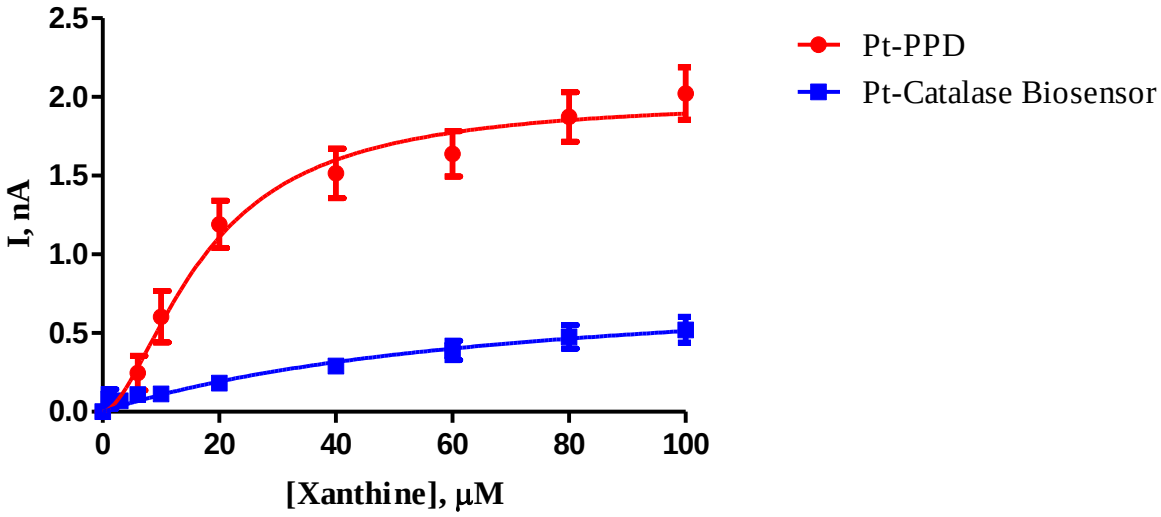

Kinetic Parameters	Pt-PPD			Pt-Catalase Biosensor		
	Mean	S.E.M	n	Mean	S.E.M	n
$I_{100\mu M}$, nA	2.022	0.167	16	0.521	0.082	8
Sensitivity, nA/µM	0.066	0.005	16	0.0050	0.0003	8
R^2	0.97	-	16	0.97	-	8

Figure 5.7: The mean current-concentration profile *(Top)* and comparison table *(Bottom)* for xanthine/XOD calibrations for Pt-PPD and Pt-Catalase biosensor in PBS (pH 7.4). CPA carried out at +700 mV *vs* SCE. All currents are background subtracted.

Figure 5.7 above illustrates the difference in current and sensitivity of the Pt-PPD sensor and Pt-Catalase biosensor calibrated in the xanthine-XOD system. This figure suggests that the spontaneous dismutation of O_2^- is taking place in the electrolyte.

A significant decrease ($P < 0.0001$) in $I_{100\mu M}$ is observed from 2.02 ± 0.17 nA (n = 16, Pt-PPD) to 0.52 ± 0.08 nA (n = 8, Pt–Catalase biosensor). The catalase biosensor has catalase immobilised on the Pt surface which degrades the H_2O_2 into H_2O and O_2 resulting in a lower signal being detected. This result suggests that spontaneously produced H_2O_2 is produced in the bulk solution. This catalase biosensor incorporates

a permselective layer (PPD) on the sensor surface, however a small detection of UA is observed similar to Section 5.3.4. A H_2O_2 calibration was performed on the Pt-Catalase biosensors prior to the xanthine calibration to examine the biosensor's sensitivity to H_2O_2. The exposure of the Pt-Catalase biosensor to high concentrations of H_2O_2 is postulated to degrade the PPD layer explaining the slight increase in response when compared to the UA calibration performed on Pt-PPD electrodes (Section 5.3.4).

The decrease in current for the Pt-Catalase biosensor compared to the Pt-PPD sensor is expected as the catalase is immobilised on the sensor surface and decomposes the generated H_2O_2. The current generated (2.02 ± 0.17 nA) is difficult to eliminate from the biosensor's signal unlike UA where the addition of an interference layer (PPD) can eliminate its contribution, small molecules like H_2O_2 can permeate this ultrathin layer (Lowry and O'Neill, 1994) (Murphy, 1998) (Hamdi *et al.*, 2005). The current generated due to the spontaneous dismutation of O_2^- will have to be eliminated or accounted for in order to find the true O_2^- current detected at the sensor surface. A dual sensor design could be incorporated where one sensor would have immobilised SOD on the Pt surface detecting the spontaneously produced H_2O_2 and the O_2^- and the other sensor would have no SOD immobilised and so would just detect the spontaneously produced H_2O_2. A subtraction method would result in a true indication of the O_2^- detected at the sensor surface.

In summary, this section determined that the spontaneous dismutation of O_2^- is taking place in the bulk solution resulting in the generation of H_2O_2. This result was verified using catalase and performing a xanthine/XOD on a Pt-Catalase biosensor. A dual sensor design is suggested in order to eliminate the signal attributed to the spontaneous dismutation of O_2^- from the biosensor's signal.

5.3.6 Effect of Xanthine Calibration on Different Biosensor Components

This section focuses on determining whether any of the biosensor components i.e. stabiliser, cross-linker or immobiliser at the concentrations found to be optimum (Chapter 4, Section 4.3.10) influence the current generated during a xanthine/XOD calibration. This set of experiments involved modifying the Pt-PPD electrodes with styrene, GA and PEI and then calibrating these sensors in the xanthine/XOD system at +700 mV *vs.* SCE. This set of experiments were performed prior to determining the optimum biosensor design particularly the number of layers of each component so for these experiments 1 layer of styrene, 2 layers of PEI and GA and then the whole design (Sty-(0.5%GA-2%PEI)$_2$) were investigated. For this in order to find the true representation of current attributed to the spontaneously produced H_2O_2, the calibration was extended to match the O_2^- calibration. As mentioned previously, (Chapter 3, Section 3.5.3) the addition of 600 µM xanthine corresponds to 154 µM O_2^- which is the calibration range observed in Chapter 4 so in this section xanthine aliquots (0 – 600 µM) were added to the electrochemical cell.

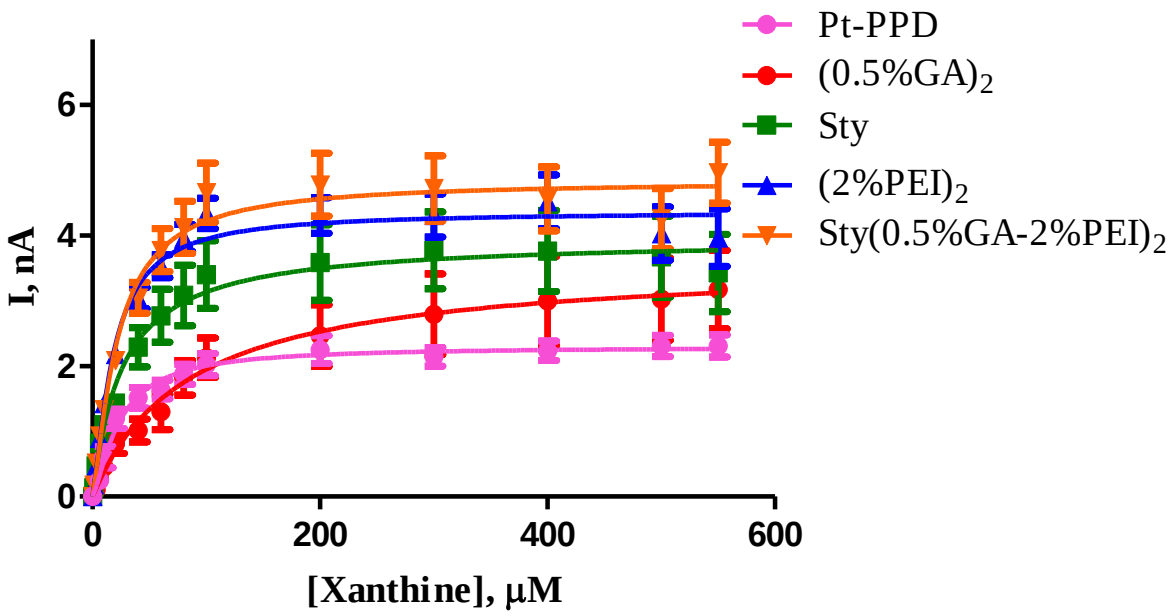

	Sty(0.5%GA-2%PEI)$_2$			Pt-PPD			Sty		
	Mean	S.E.M	n	Mean	S.E.M	n	Mean	S.E.M	n
$I_{600\mu M}$, nA	4.96	0.46	28	2.31	0.17	16	3.42	0.59	15
Sensitivity, nA/µM	0.14	0.004	28	0.07	0.006	16	0.14	0.01	15
R^2	0.99	-	28	0.97	-	16	0.99	-	15

	(0.5%GA)$_2$			(2%PEI)$_2$		
	Mean	S.E.M	n	Mean	S.E.M	n
$I_{600\mu M}$, nA	3.17	0.60	8	3.97	0.44	12
Sensitivity, nA/µM	0.04	0.002	8	0.15	0.005	12
R^2	0.99	-	8	0.99	-	12

Figure 5.8: The mean current-concentration profile *(Top)* and comparison table *(bottom)* in PBS (pH 7.4) buffer solution containing 0.002 U XOD at 21°C using sensors Pt-PPD, Pt-Sty, Pt-(0.5%GA)$_2$, Pt-(2%PEI)$_2$ and Pt-Sty-(0.5%GA-2%PEI)$_2$. CPA carried out at +700 mV *vs* SCE.

The results above show that the introduction of PEI and Sty into the sensor design results in a significant increase ($P < 0.0001$) in sensitivity from 0.07 ± 0.006 nA/µM (n = 16, Pt-PPD) to 0.15 ± 0.005 nA/µM (n = 12, (2%PEI)$_2$) and 0.14 ± 0.01 nA/µM (n = 15, Sty) respectively. Interestingly, (2%PEI)$_2$, Sty-(0.5%GA-2%PEI)$_2$ and Sty designs give almost identical sensitivities of 0.15 ± 0.005 nA/µM (n = 12), 0.14 ± 0.004 nA/µM (n = 28) and 0.14 ± 0.01 nA/µM (n = 15) respectively. This suggests that the biosensor components PEI and styrene have an affinity for the H_2O_2 produced in the electrochemical cell resulting in a one fold increase in sensitivity when compared to the Pt-PPD design with a sensitivity of 0.07 ± 0.006 nA/µM (n = 16).

All designs show an increase in the $I_{600\mu M}$ when compared to the Pt-PPD design. The $I_{600\mu M}$ recorded for the Pt-PPD design was 2.31 ± 0.17 nA. This is significantly lower ($P < 0.0001$) than the $I_{600\mu M}$ current of 3.42 ± 0.59 nA (n = 15, Sty) and significantly

lower ($P < 0.0001$) than the 3.17 ± 0.60 nA (n = 8, Sty-$(0.5\%GA)_2$). A similar trend is observed for the $I_{600\mu M}$ generated by the $(2\%PEI)_2$ and Sty-$(0.5\%GA\text{-}2\%PEI)_2$ designs where a significant increase ($P < 0.0001$) in both cases is observed when compared to the Pt-PPD design. The highest $I_{600\mu M}$ of 4.96 ± 0.46 nA (n = 28) is observed for Sty-$(0.5\%GA\text{-}2\%PEI)_2$. These results suggest that the introduction of the various immobilisers, stabilisers and cross-linkers into the sensor manufacture process results in an increase in the $I_{600\mu M}$ and sensitivity suggesting that styrene, PEI and GA have a small affinity for the H_2O_2 generated in the electrochemical cell.

All designs show enzyme kinetics reaching a plateau on addition of approximately 100 µM xanthine into the electrochemical cell. These enzyme kinetics were previously masked by the high UA contribution (see Section 5.3.2.) but the addition of the PPD layer into all sensor designs has resulted in enzyme kinetics being observed. These enzyme kinetics are observed as the PBS contains 0.002 U of the enzyme XOD which is used to produce the O_2^- radical on addition of various aliquots of xanthine.

In summary, this section has investigated the contribution the various biosensor components has on the signal produced in the xanthine/XOD system. All designs show an increase in the $I_{600\mu M}$ when compared to the Pt-PPD design. Some designs demonstrated a one fold increase in sensitivity.

5.3.7 Superoxide Biosensors with/without the PPD layer

This chapter outlines the experiments carried out to examine the potential interferences in the xanthine-XOD calibration and illustrates techniques to minimise their contribution to the biosensor's signal. This section investigates the effect the size exclusion polymer PPD has on the sensitivity of O_2^- biosensors. A xanthine calibration was performed on biosensors that contain a PPD layer and biosensors that have no *o*-PD electropolymerised onto the Pt surface before modification with the various biosensor components. These experiments were performed in order to confirm the significant contribution UA has on the biosensor's signal unless eliminated successfully. It is expected that the biosensor without the inclusion of a PPD layer prior to modification with the various biosensor components would demonstrate a higher response as a result of the contribution from UA, the enzymatic dismutation of

O_2^- and the spontaneous dismutation of O_2^- both generating H_2O_2. However, the biosensor incorporating the PPD layer prior to the additional biosensor modifications will be expected to have a lower response as a result of the elimination of the UA contribution from the electrochemical signal (See Section 5.3.3).

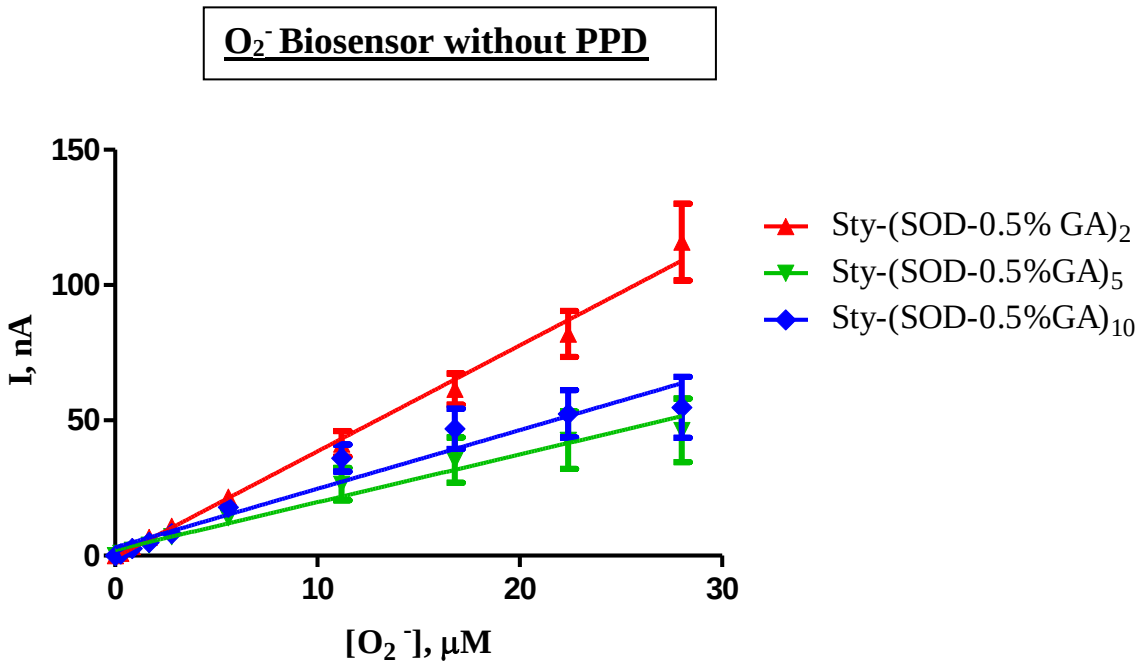

	Sty-(SOD-0.5%GA)$_2$			Sty-(SOD-0.5%GA)$_5$			Sty-(SOD-0.5%GA)$_{10}$		
	Mean	S.E.M	n	Mean	S.E.M	n	Mean	S.E.M	n
$I_{28\mu M}$, nA	115.88	14.15	4	46.33	11.74	8	54.82	11.30	8
Sensitivity, nA/µM	3.96	0.12	4	2.15	0.07	8	2.90	0.11	8
R^2	0.99	-	4	0.99	-	8	0.99	-	8

Figure 5.9: A mean current-concentration profile for O_2^- calibration *(Top)* and comparison table *(bottom)* in PBS (pH 7.4) buffer solution containing 0.002 U XOD at 21°C using designs Sty-(SOD-0.5%GA)$_2$, Sty-(SOD-0.5%GA)$_5$ and Sty-(SOD-0.5%GA)$_{10}$. CPA carried out at +700 mV *vs.* SCE.

O_2^- Biosensor with PPD

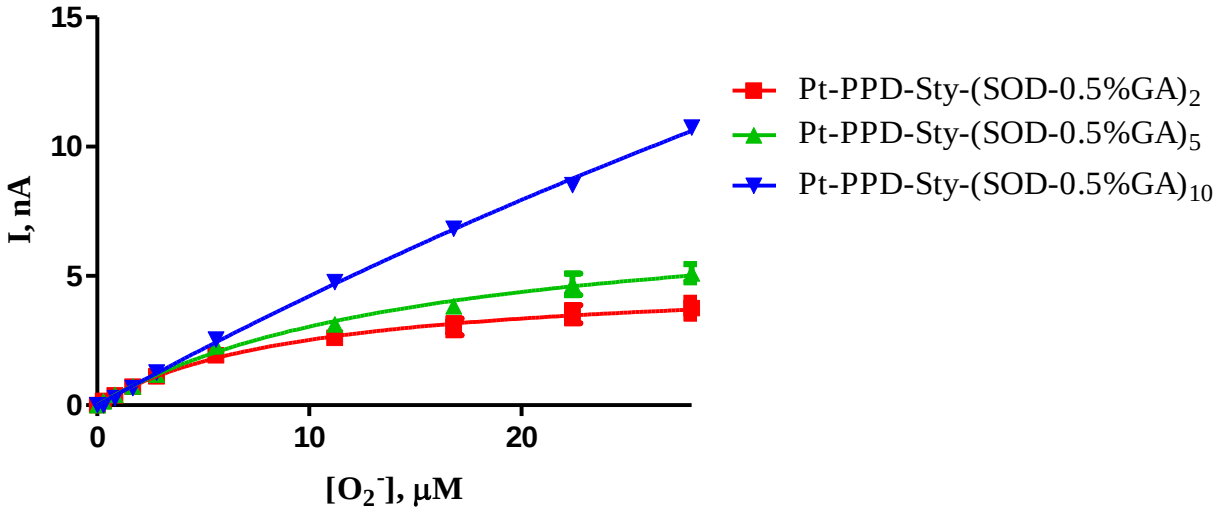

	Pt-PPD-Sty-(SOD-0.5%GA)$_2$			Pt-PPD-Sty-(SOD-0.5%GA)$_5$			Pt-PPD-Sty-(SOD-0.5%GA)$_{10}$		
	Mean	S.E.M	n	Mean	S.E.M	n	Mean	S.E.M	n
$I_{28\mu M}$, nA	3.76	0.40	8	5.10	0.35	8	10.74	0.21	6
Sensitivity, nA/µM	0.39	0.01	8	0.42	0.01	8	0.43	0.01	6
R^2	0.99	-	8	0.99	-	8	0.99	-	6

Figure 5.10: The mean current-concentration profiles for O_2^- calibrations *(Top)* and comparison table *(Bottom)* in PBS (pH 7.4) buffer solution containing 0.002 U XOD at 21°C using designs Pt-PPD-Sty-(SOD-0.5%GA)$_2$, Pt-PPD-Sty-(SOD-0.5%GA)$_5$ and Pt-PPD-Sty-(SOD-0.5%GA)$_{10}$. CPA carried out at +700 mV vs. SCE.

Figure 5.9 and Figure 5.10 above depicts the changes in current and sensitivity on addition of the permselective layer PPD into the biosensor designs. On examination of the results it is clear, that there is a decrease in the current and sensitivity recorded following incorporation of PPD into the biosensor designs.

The biosensor designs without a PPD layer gave higher currents of 115 ± 14.15 nA (n = 4, Sty-(SOD-0.5%GA)$_2$) , 46.33 ± 11.74 nA (n = 8, Sty-(SOD-0.5%GA)$_5$) and 54.82 ± 11.30 nA (n = 8, Sty-(SOD-0.5%GA)$_{10}$) when compared to the same designs incorporating PPD on addition of 100 µM corresponding to 28 µM O_2^- (see Section 3.6.3). These results demonstrate a stepwise decrease in the current on introduction of additional layers of enzyme and GA except an increase is observed for the design Sty-(SOD-0.5%GA)$_{10}$ when compared to the Sty-(SOD-0.5%GA)$_5$ design. The same trend is observed when comparing the sensitivities of the different designs. The highest sensitivity of 3.96 ± 0.12 nA/µM (n = 4) is achieved for the design Sty-(SOD-0.5%GA)$_2$. A significant decrease ($P < 0.0001$) is observed in sensitivity from 3.96 ± 0.12 nA/µM (n = 4, Sty-(SOD-0.5%GA)$_2$) to 2.15 ± 0.07 nA/µM (n = 8, Sty-(SOD-0.5%GA)$_5$) . Similarly, there is a significant decrease ($P < 0.0001$) in sensitivity from 3.96 ± 0.12 nA/µM (n = 4, Sty-(SOD-0.5%GA)$_2$) to 2.90 ± 0.11 nA/µM (n = 8, Sty-(SOD-0.5%GA)$_{10}$). Conversely, a significant increase in sensitivity ($P < 0.0001$) is observed from 2.15 ± 0.07 nA/µM (n =8, Sty-(SOD-0.5%GA)$_5$) to 2.90 ± 0.11 nA/µM (n = 8, Sty-(SOD-0.5%GA)$_{10}$). All the biosensor designs Sty-(SOD-0.5%GA)$_2$, Sty-(SOD-0.5%GA)$_5$ and Sty-(SOD-0.5%GA)$_{10}$ showed a linear response on addition of 100 µM xanthine.

In comparison, the biosensor designs incorporating the PPD layer prior to modification with the various biosensor components demonstrated lower currents and sensitivities. On examining the results, it is noticed, that a stepwise increase is observed in the current on the introduction of additional layers of enzyme and GA. The current recorded was 3.76 ± 0.40 nA (n = 8, Pt-PPD-Sty-(SOD-0.5%GA)$_2$) , this value is significantly increased ($P < 0.0001$) to 5.10 ± 0.35 nA (n = 8, Pt-PPD-Sty-(SOD-0.5%GA)$_5$) and significantly increased ($P < 0.0001$) to 10.74 ± 0.21 nA (n = 6) for the Pt-PPD-Sty-(SOD-0.5%GA)$_{10}$ design. Interestingly, both Pt-PPD-Sty-(SOD-0.5%GA)$_5$ and Pt-PPD-Sty-(SOD-0.5%GA)$_{10}$ recorded almost identical sensitivities ($P = 0.0653$) of 0.42 ± 0.01 nA/µM (n = 8) and 0.43 ± 0.01 nA/µM (n = 6) respectively.

A significant decrease ($P < 0.0001$) in sensitivity is recorded from 0.42 ± 0.01 nA/µM (n = 8, Pt-PPD-Sty-(SOD-0.5%GA)$_5$) and 0.43 ± 0.01 nA/µM (n = 6, Pt-PPD-Sty-(SOD-0.5%GA)$_{10}$) to 0.39 ± 0.01 nA/µM (n = 8, Pt-PPD-Sty-(SOD-0.5%GA)$_2$). This low sensitivity can be explained due to insufficient enzyme loading on the sensor due to the presence of just two coats of enzyme on the Pt surface compared to five or ten layers. Both Pt-PPD-Sty-(SOD-0.5%GA)$_2$ and Pt-PPD-Sty-(SOD-0.5%GA)$_5$ demonstrate enzyme kinetics over the calibration range, however, a linear response is observed for the Pt-PPD-Sty-(SOD-0.5%GA)$_{10}$.

A significant decrease ($P < 0.0001$) in current is observed from 115.88 ± 14.15 nA (n = 4, Sty-(SOD-0.5%GA)$_2$) to 3.76 ± 0.40 nA (n = 8, Pt-PPD-Sty-(SOD-0.5%GA)$_2$). A similar trend is observed for the sensitivity where a significant decrease ($P < 0.0001$) is recorded from 3.96 ± 0.12 nA/µM (n = 4, Sty-(SOD-0.5%GA)$_2$) to 0.39 ± 0.01 nA/µM (n = 8, Pt-PPD-Sty-(SOD-0.5%GA)$_2$). The same result is determined for the designs incorporating two and five layers where a significant decrease ($P < 0.0001$) in current is recorded from 46.33 ± 11.74 nA (n = 8, Sty-(SOD-0.5%GA)$_5$) to 5.10 ± 0.35 nA (n = 8, Pt-PPD-Sty-(SOD-0.5%GA)$_5$), similarly for the sensitivity where a significant decrease ($P < 0.0001$) is observed from 2.15 ± 0.07 nA/µM (n = 8, Sty-(SOD-0.5%GA)$_5$) to 0.42 ± 0.01 nA/µM (n = 8, Pt-PPD-Sty-(SOD-0.5%GA)$_5$). A significant decrease ($P < 0.0001$) in current at 28 µM O_2^- is recorded from 54.82 ± 11.30 nA (n = 8, Sty-(SOD-0.5%GA)$_{10}$) to 10.71 ± 0.21 nA (n = 6, Pt-PPD-Sty-(SOD-0.5%GA)$_{10}$). Similarly, a significant decrease ($P < 0.0001$) in sensitivity is demonstrated from 2.90 ± 0.11 nA/µM (n = 8, Sty-(SOD-0.5%GA)$_{10}$) to 0.43 ± 0.01 nA/µM (n = 6, Pt-PPD-Sty-(SOD-0.5%GA)$_{10}$).

In conclusion, all sensor designs incorporating the PPD layer showed a significant decrease ($P < 0.0001$) in current and sensitivity when compared to the same biosensor design without the inclusion of the PPD layer calibrated in the xanthine-XOD system. The incorporation of PPD into the biosensor designs resulted in Michaelis-Menten kinetics over the calibration range. These enzyme kinetics can be attributed to the enzyme SOD immobilised on the Pt surface and the presence of XOD in the PBS solution. An explanation for these results is that the inclusion of a PPD layer in the biosensor designs has resulted in the elimination of the current attributed to UA from the biosensor's signal, therefore, reducing the current and sensitivities recorded. All

biosensor designs previously demonstrated in Chapter 4 incorporate a PPD layer in their design reducing interferent signals which includes the UA contribution.

5.3.8 Blank Sensor

This section investigates the current generated from the blank sensor. This blank sensor is composed of the biosensor components found to be optimum (Chapter 4, Section 4.3.10.) except without the SOD enzyme. A dual sensor design will be employed in order to find the true value of O_2^- detected at the sensor surface. This technique is employed as we determined that O_2^- undergoes spontaneous dismutation to H_2O_2 due to the presence of excess H^+ ions in the electrolyte (Section 5.3.5.). The dual sensor system incorporates one biosensor which is modified with SOD to detect the spontaneously produced H_2O_2 and the O_2^-. The other sensor incorporates no SOD, therefore this sensor would detect just the spontaneously produced H_2O_2. A subtraction method would give a true indication of the concentration of O_2^- detected at the Pt surface. A similar method is incorporated for a catalase based biosensor for H_2O_2 monitoring. The catalase-based H_2O_2 biosensor consists of a pair of Pt electrodes, one with catalase immobilised on the electrode (CAT electrode) and one without catalase (blank electrode)(O'Brien *et al.*, 2007). The H_2O_2 response is thus the difference in signal between the blank electrode (without enzyme) and the corresponding CAT electrode.

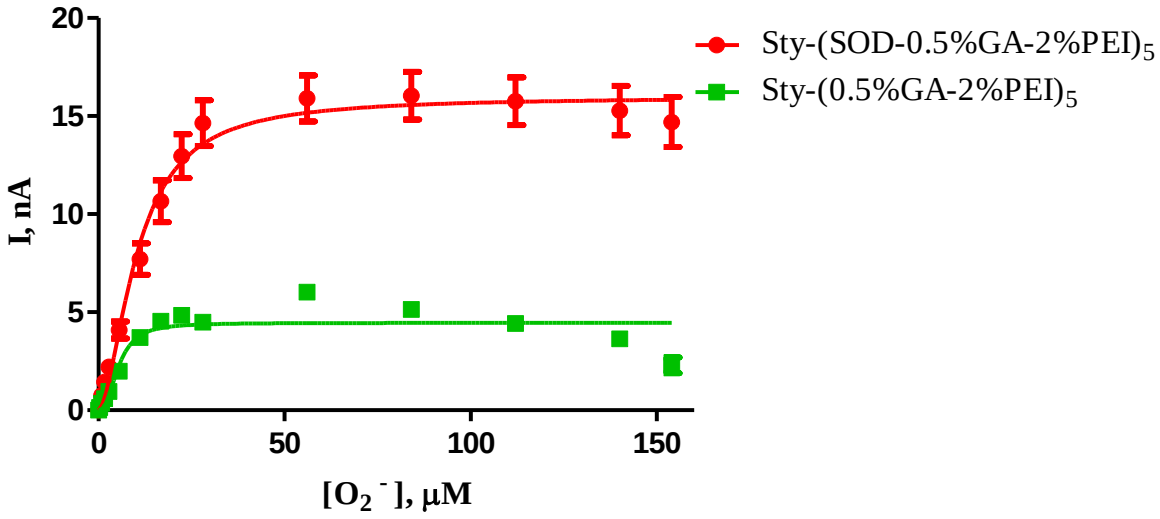

	Sty-(0.5%GA-2%PEI)$_5$			Sty-(SOD-0.5%GA-2%PEI)$_5$		
	Mean	S.E.M	n	Mean	S.E.M.	n
$I_{154\mu M}$, nA	2.29	0.40	16	15.98	0.15	17
Sensitivity, nA/µM	0.33	0.005	16	0.91	0.06	17
R^2	0.99	-	16	0.99	-	17

Figure 5.11: The mean current-concentration profiles for O_2^- calibrations *(Top)* and comparison table *(Bottom)* in PBS (pH 7.4) buffer solution containing 0.002 U XOD at 21°C using designs Sty-(SOD-0.5%GA-2%PEI)$_5$ and Sty-(0.5%GA-2%PEI)$_5$. CPA carried out at +700 mV *vs*. SCE.

The graph above illustrates the dual sensor design in operation which utilises a subtraction method to eliminate the current attributed to the spontaneous dismutation of O_2^- from the biosensor's signal. There is a significant decrease ($P < 0.0001$) observed in the current from 15.98 ± 0.15 nA (n = 17, Sty-(SOD-0.5%GA-2%PEI)$_5$) to 2.29 ± 0.40 nA (n = 16, Sty-(0.5%GA-2%PEI)$_5$) at 158 µM O_2^-. This indicates that the generation of H_2O_2 produced by the spontaneous dismutation of O_2^- accounts for ~ 2.30 nA of current generated at the O_2^- biosensor at 158 µM O_2^-. Similarly, a significant decrease ($P < 0.0001$) in sensitivity is observed from 0.91 ± 0.06 nA/µM

(n = 17, Sty-(SOD-0.5%GA-2%PEI)$_5$) to 0.33 ± 0.005 nA/µM (n = 16, Sty-(0.5%GA-2%PEI)$_5$). These results show that the production of H_2O_2 from the spontaneous dismutation of O_2^- accounts for only a small signal compared to the signal attributed to the enzymatic dismutation of O_2^- by SOD. This suggests that the enzymatic dismutation of O_2^- by SOD is more favourable than the spontaneous dismutation.

Both sensors incorporate a PPD layer before modification with the various biosensor components to eliminate the UA contribution, therefore, both designs demonstrate Michaelis-Menten kinetics over the calibration range. The table below illustrates the current generated using the O_2^- biosensor and the blank sensor on addition of various aliquots of xanthine into the electrochemical cell.

Table 5.1: Comparison table of mean current values for the O_2^- biosensor and the blank sensor. O_2^- calibration carried out in PBS buffer solution containing 0.002 U XOD at 21°C. CPA carried out at +700 mV *vs.* SCE. All currents are background subtracted.

	Sty(SOD-0.5%GA-2%PEI)$_5$			Sty(0.5%GA-2%PEI)$_5$			Difference		
[O_2^-], µM	Mean	S.E.M	n	Mean	S.E.M	n	Mean	S.E.M	n
0.00	0.00	0.00	17	0.00	0.00	16	0.00	0.00	17
0.28	0.20	0.04	17	0.14	0.02	16	0.06	0.02	17
0.84	0.75	0.09	17	0.37	0.04	16	0.38	0.05	17
1.68	1.43	0.19	17	0.59	0.05	16	0.84	0.05	17
2.80	2.21	0.22	17	0.96	0.07	16	1.25	0.15	17
5.60	4.09	0.43	17	1.99	0.16	16	2.10	0.27	17
11.20	7.71	0.80	17	3.70	0.27	16	4.01	0.53	17
16.80	10.66	1.07	17	4.54	0.34	16	6.12	0.73	17
22.40	12.96	1.12	17	4.84	0.37	16	8.12	0.75	17
28.00	14.65	1.17	17	4.49	0.39	16	10.16	0.78	7
56.00	15.90	1.17	17	6.03	0.30	16	9.87	0.87	17
84.00	16.04	1.22	17	5.13	0.22	16	10.91	1.0	17
112.00	15.76	1.22	17	4.42	0.34	16	11.34	0.88	17
140.00	15.28	1.26	17	3.63	0.35	16	11.65	0.91	17
154.00	14.70	1.27	17	2.29	0.40	16	12.41	0.87	17

The table above illustrates the difference in current between the sensor incorporating the SOD and the blank electrode. This difference is important as the O_2^- biosensor will utilise a dual sensor design. The O_2^- biosensor containing the SOD enzyme will be subtracted from the blank sensor (Sty-(0.5%GA-2%PEI)$_5$) which will give a true indication of the concentration of O_2^- detected at the Pt surface. Only a small number of research groups have constructed first generation O_2^- biosensors for the detection of H_2O_2 produced from the O_2^- dismutation catalysed by SOD that employ techniques to differentiate the H_2O_2 produced by the SOD-catalysed dismutation of O_2^- from that endogenously produced in biological systems. McNeil and co-workers developed a O_2^- biosensor based on SOD-coated platinised activated carbon electrodes (PACE) (Pontie and Bedioui, 1999). The SOD-coated biosensor was polarised at +320 mV to estimate the H_2O_2 produced by the enzymatic disproportionation of O_2^- through its oxidation current. This group mentions using a subtraction method to eliminate the current generated due to the natural disproportionation of O_2^- and this was subtracted from the combined current. This was measured and eliminated by using a second electrode consisting of BSA coated PACE in conjunction with the bipotentiostat poised at + 320 mV *vs.* Ag/AgCl.

O_2^- dismutation by SOD is first order with regard to O_2^- concentration whereas the spontaneous dismutation is second order. O_2^- spontaneously dismutates to H_2O_2, with a pH-dependent second order rate of ~10^5 $M^{-1}s^{-1}$ at pH 7.0 (Miwa *et al*., 2008). The equilibrium constant for the O_2^- dismutation to H_2O_2 is K ~ 10^{18} at pH 7.0, therefore this reaction is considered irreversible except in cases of very high levels of SOD and very low concentrations of O_2^- (Liochev and Fridovich, 2003). SOD accelerates the destruction of O_2^- by increasing the rate constant for spontaneous dismutation by < 1,000 fold and making the rate of O_2^- decay first order compared to the second order reaction with respect to O_2^- concentration. This means that SOD is more efficient at accelerating the decomposition of O_2^- compared with the spontaneous dismutation, at low O_2^- concentrations (Miwa *et al.*, 2008). This suggests that the enzymatic dismutation of O_2^- is more favourable than the spontaneous dismutation of O_2^- in the electrolyte.

In summary, this section demonstrates the dual sensor design in operation. The O_2^- biosensor described in this section consists of a pair of Pt electrodes, one with SOD

immobilised on the electrode (O_2^- biosensor) and one without SOD (blank electrode). If this sensor is used *in-vivo*, the two electrodes will be implanted in close proximity and the current from each will be simultaneously recorded. The H_2O_2 response of the blank sensor is lower than the SOD biosensor as this biosensor has SOD immobilised on the Pt surface which facilitates the enzymatic dismutation of O_2^- with the production of H_2O_2. Both sensors observe a signal from the spontaneous dismutation of H_2O_2 in the electrochemical cell, however, this response can be subtracted from the O_2^- biosensor to find the true response from the enzymatic dismutation of O_2^-.

5.3.9. Limit of Detection

The O_2^- radical has a very low *in-vivo* concentration of between 50-200 nM in biological samples (Mesároš *et al.*, 1998). The limit of detection (LOD) is an important parameter to consider when designing biosensors to monitor fast transients in brain analytes whose extracellular fluid (ECF) levels are invariable low such as O_2^-. This value is the minimum concentration of a particular substrate that the sensor can be said to reliably detect. The LOD is usually determined using the widely applied criterion of three times the standard deviation of the baseline (O'Neill *et al*., 2008). Below this calculated value the signal is compromised due to noise constraints in the electrochemical set-up therefore any changes smaller than the LOD are unreliable and cannot be attributed to a change in the O_2^- level.

The combined baseline current of eight O_2^- biosensors was 0.886 ± 0.0095 nA (n = 8). The O_2^- biosensor design (Sty-(SOD-0.5%GA-2%PEI)$_5$) demonstrated a sensitivity of 0.91 ± 0.07 nA/µM (n = 17). The LOD was determined to be 0.026 ± 0.002 µM which is within the physiological range thus potentially suitable for *in-vivo* monitoring.

5.3.10. Response Time

During *in-vitro* calibrations measurements are performed under quiescent conditions. Once a stock concentration aliquot is injected into the electrochemical cell the time taken to reach steady-state (equilibrium) is dependent on both the amount of material being removed from the bulk and the rate at which it is transferred, i.e. mass transfer as dictated by diffusion and thermodynamic considerations. However, in order to

facilitate a quick and even distribution of the analyte a small amount of convection (i.e. the solution is stirred at *ca.* 1 Hz for *ca.* 5 s) is introduced following injection. As such, the response time, which is defined as the time for the response to rise from 10% to 90% of the maximum amplitude for the concentration step (i.e. $t_{10-90\%}$), is difficult to separate from the mixing time. Typical data for the O_2^- biosensor is shown below in Figure 5.12, and we can see from this data that $t_{10-90\%}$ is less than the mixing time and of the order of *ca.* 1-2 s.

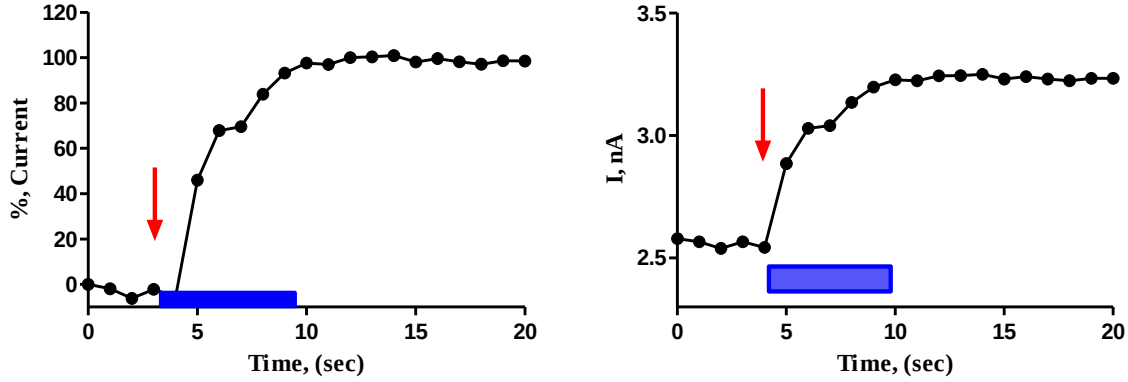

Figure 5.12: A typical example of a response time for a xanthine injection of 40 µM in PBS (pH 7.4) buffer solution at 21°C for the O_2^- biosensor. CPA carried out at +700 mV *vs.* SCE. Arrow indicates the point of injection and blue rectangle symbolises the stirring time.

This is similar to the $t_{10-90\%}$ values reported for other Pt-based biosensors (Hu and Wilson, 1997) (Tian *et al.*, 2009), and is *ca.* 5 times faster than values reported for carbon-based biosensors (Kulagina *et al.*, 1999). A more accurate picture is given by flow stream analysis which typically gives values of *ca.* 1 s for Pt-based microelectrode arrays (MEAs)(Bruno *et al.*, 2004). While such determinations *in-vitro* give an indication/estimation of the response time it is difficult to translate this directly to the *in-vivo* environment (von Woedtke *et al.*, 1991) (Versmold *et al.*, 1978). Generally, where we have observed $t_{10-90\%}$ values of less than the mixing time *in-vitro* we have found response times *in-vivo* in the millisecond range (Lowry *et al.*, 1994) (Lowry *et al.*, 1998) (Bolger *et al.*, 2011(b)). This has also been observed for Pt-based MEAs (Burmeister *et al.*, 2008).

5.3.11: Extensive Interference Study

This chapter highlights the interferences in the xanthine/XOD system. These interferent molecules include UA and the H_2O_2 produced by the spontaneous dismutation of O_2^- in the electrolyte. The application of this biosensor *in-vivo* is much more complicated than a straightforward transfer from the practice *in-vitro*. The brain is anatomically complicated and contains a wide range of electroactive substances, brain tissue presenting a complex environment that includes surfactants, electrode poisons, electrocatalysts and a tissue matrix that both restricts mass transport to the electrode and reacts physiologically to the presence of the probe (O'Neill and Lowry, 2006). The selectivity of the sensor to a range of potential interferents in the brain ECF must be examined. The compounds tested were monoamine neurotransmitters dopamine (DA) and 5-hydroxytryptomine (5-HT), their metabolites 3,4-dihydroxyphenylacetic acid (DOPAC), homovanillic acid (HV) and 5-hydroxyindoleacetic acid (5-HIAA), AA and its oxidised form dehydroascorbic acid (DHAA), the amino acids L-tyrosine, L-cysteine, L-tryptophan, the purine metabolite UA and another anti-oxidant glutathione (Bolger et al., 2011(b)) (O'Brien et al., 2007).

This experiment was conducted under an atmosphere of N_2 and all PBS solutions were N_2 saturated prior to commencement of the experiment. CPA was performed at +700 mV *vs.* SCE. The various substances were added as a standard aliquot of 50 µL, which corresponded to the relevant ECF concentration of the particular substance if known. The concentration of each of the interferent molecules used were at least the *in-vivo* concentration, however, in the case of L-cysteine, L-tyrosine, L-tryptophan and glutathione the *in-vivo* concentrations are not known so a relatively high µM concentration was chosen. As AA is the main interferent in the brain with the highest concentration in the ECF a full AA calibration (0-1000 µM) was performed in N_2 saturated PBS at + 700 mV *vs.* SCE to ensure the O_2^- biosensor was sufficiently selective to this interferent before potential usage in the *in-vivo* environment

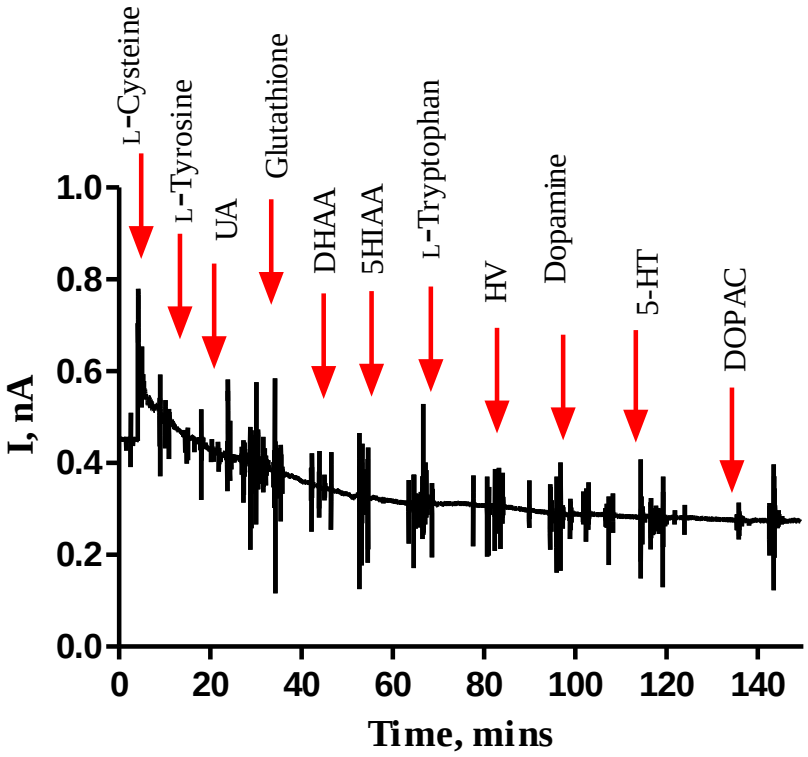

Figure 5.13: A typical raw data trace for an interference calibration performed in PBS (pH 7.4) at 21°C at +700 mV vs. SCE. The eleven red arrows indicate the addition of a 50 µL injection of an interferent solution into the electrochemical cell.

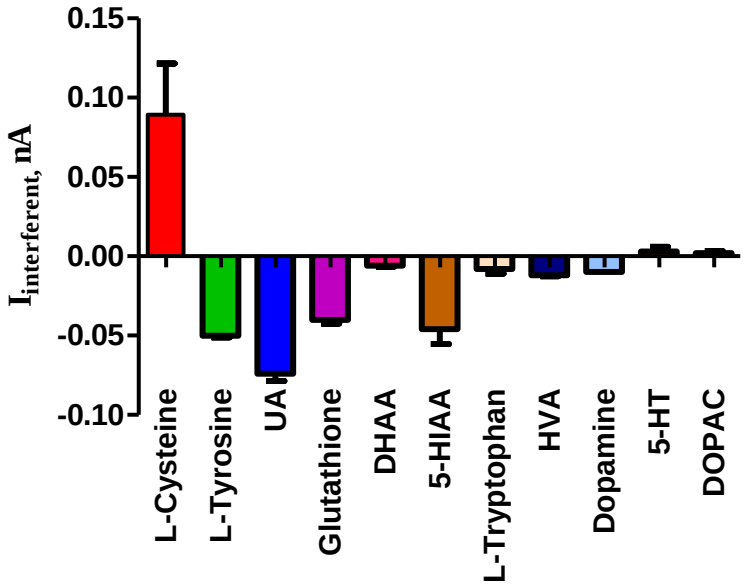

	Response from Baseline			Response from Interferent		
Interferent	**Mean**	**S.E.M**	**n**	**Mean**	**S.E.M.**	**n**
L-Cysteine (50 µM)	**0.089**	**0.056**	**3**	**0.089**	**0.056**	**3**
L-Tyrosine (100 µM)	**0.039**	**0.054**	**3**	**-0.050**	**0.002**	**3**
UA (50 µM)	**-0.035**	**0.046**	**3**	**-0.074**	**0.008**	**3**
Glutathione (50 µM)	**-0.075**	**0.042**	**3**	**-0.040**	**0.004**	**3**
DHAA (100 µM)	**-0.081**	**0.043**	**3**	**-0.006**	**0.001**	**3**
5-HIAA (50 µM)	**-0.127**	**0.027**	**3**	**-0.046**	**0.016**	**3**
L-Tryptophan (100 µM)	**-0.135**	**0.022**	**3**	**-0.008**	**0.005**	**3**
HVA (10 µM)	**-0.147**	**0.023**	**3**	**-0.012**	**0.001**	**3**
Dopamine (0.05 µM)	**-0.158**	**0.023**	**3**	**-0.010**	**0.000**	**3**
5-HT (0.01 µM)	**-0.155**	**0.018**	**3**	**0.003**	**0.005**	**3**
DOPAC (20 µM)	**-0.157**	**0.016**	**3**	**0.002**	**0.002**	**3**

Figure 5.14: A bar chart showing the sensitivity of the O_2^- biosensor to a range of interferent molecules *(Top)* and a results table *(Bottom)* for an interferent calibration in N_2 saturated PBS (pH 7.4) buffer solution using the Sty-(SOD-0.5%GA-2%PEI)$_5$ design. CPA carried out at +700 mV *vs.* SCE.

The results obtained from this investigation into the rejection of a range of interferents present in the brain ECF are presented in Figure 5.14. The results table illustrates the cumulative current obtained from the addition of interferent aliquots and also the individual current change from each interferent aliquot addition.

A small increase in current of 0.089 ± 0.056 nA (n = 3) is observed on addition of a 50 µM aliquot of L-Cysteine into the electrochemical cell, however, this contribution is negligible. Negative values were obtained suggesting no detection of the specific interferent, however, the negative response can be attributed to baseline drift. The overall current detected after addition of the eleven interferent molecules is - 0.157 ± 0.016 nA (n = 3). This result suggests that the O_2^- biosensor (Sty-(SOD-0.5%GA-2%PEI)$_5$) is selective towards O_2^- detection in the *in-vivo* environment. The figure below shows an AA calibration performed on the O_2^- biosensor

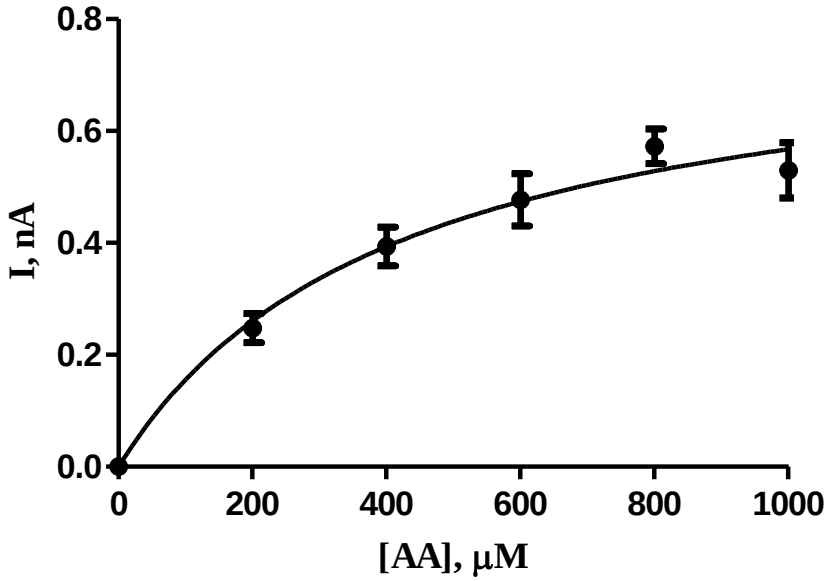

	Pt-PPD Electrode		
[AA], µM	Mean	S.E.M	n
200	0.25	0.03	7
400	0.39	0.03	7
600	0.48	0.05	7
800	0.57	0.03	7
1000	0.53	0.05	7

Figure 5.15: The mean current-concentration profile for an AA calibration *(Top)* and comparison table *(Bottom)* in PBS (pH 7.4) buffer solution at 21°C using the O_2^- biosensor. CPA carried out at +700 mV *vs.* SCE.

It is clear from the results above, that there is principally a flat plateau response for the major part of the concentration range up to 1000 µM. This shape can be explained in terms of saturation of the PPD layer with AA, leading to a 'self- blocking' phenomenon. The current detected at physiological levels of AA was 0.48 ± 0.05 nA (n = 7) which indicates that the O_2^- biosensor is sufficient in negating the AA response in the *in-vivo* environment.

In summary, this section has determined that the O_2^- biosensor is selective to the target analyte with only a small contribution detected at the sensor surface from twelve interferent species in the brain. These results suggests that the O_2^- biosensor can potentially be used in the *in-vivo* environment for the detection of O_2^-.

5.4: Conclusion

The aim of this chapter was to investigate the interferences in the xanthine/XOD system and to examine what influence these interferents might have on the biosensor's signal. This chapter demonstrated that UA is produced as a by-product of the xanthine/XOD system. This interferent molecule was successfully eliminated with the addition of the size exclusion polymer PPD. PPD blocks access of larger interferent molecules such as AA and UA but allows access of smaller molecules such as H_2O_2, therefore the biosensor's signal is not compromised.

This chapter also indicated that the spontaneous dismutation of O_2^- is taking place in the electrochemical cell generating H_2O_2. The production of H_2O_2 by the spontaneous dismutation of O_2^- was determined using catalase, a single 200 µL injection resulted in an instantaneous reduction in the electrochemical signal back to baseline. This was also verified using a Pt-Catalase biosensor, where the signal was significantly reduced ($P < 0.0001$) when compared to the Pt-PPD sensor. However, this contribution is harder to eliminate from the biosensor's signal as H_2O_2 is permeable to the thin PPD layer. A dual sensor design can be employed and Section 5.3.8 shows this design in operation. The O_2^- biosensor described in this section consists of a pair of Pt electrodes, one with SOD immobilised on the electrode (O_2^- biosensor) and one without SOD (blank electrode). The H_2O_2 response of the blank sensor is lower than the SOD biosensor as this biosensor has SOD immobilised on the Pt surface which facilitates the enzymatic dismutation of O_2^- with the production of H_2O_2. Both sensors observe a signal from the spontaneous dismutation of O_2^- in the electrochemical cell, however, this response can be subtracted from the SOD biosensor to give the true response from the enzymatic dismutation of O_2^-.

This chapter also determined the response time and the LOD of the O_2^- biosensor. Both these parameters are useful and both are related to the biosensor's response to the

substrate. These parameters are crucial when developing biosensors to monitor fast transients in brain analytes where the ECF concentration is very low. The LOD of the biosensor was determined to be 0.026 ± 0.002 µM with a sub second response time. The interference by endogenous electroactive species was also determined by carrying out an extensive interference study on the O_2^- biosensor. This study demonstrated that the O_2^- biosensor is selective to the detection of O_2^- in the *in-vivo* environment.

5.5 References

Aitken R, Buckingham D and Harkiss D. (1993) Use of a xanthine oxidase free radical generating system to investigate the cytotoxic effects of reactive oxygen species on human spermatozoa. *Journal of Reproduction and Fertility* 97: 441-450.

Bielski BHJ, Cabelli DE, Arudi RL, *et al.* (1985) Reactivity of HO2/O−2 Radicals in Aqueous Solution. *Journal of Physical and Chemical Reference Data* 14: 1041-1100.

Bolger FB, McHugh SB, Bennett R, *et al.* (2011(b)) Characterisation of carbon paste electrodes for real-time amperometric monitoring of brain tissue oxygen. *Journal of Neuroscience Methods* 195: 135-142.

Bruno JP, Sarter M, Gash C, *et al.* (2004) Choline-and acetylcholine-sensitive microelectrodes. *Eur. J. Neurosci* 20: 1545.

Burmeister JJ, Pomerleau F, Huettl P, *et al.* (2008) Ceramic-based multisite microelectrode arrays for simultaneous measures of choline and acetylcholine in CNS. *Biosensors and Bioelectronics* 23: 1382-1389.

Calas-Blanchard C, Catanante G and Noguer T. (2014) Electrochemical Sensor and Biosensor Strategies for ROS/RNS Detection in Biological Systems. *ElectroAnalysis* 26: 1277-1286.

Campanella L, Favero G, Persi L, *et al.* (2000) New biosensor for superoxide radical used to evidence molecules of biomedical and pharmaceutical interest having radical scavenging properties. *Journal of Pharmaceutical and Biomedical Analysis* 23: 69-76.

Craig JD and O'Neill RD. (2003) Comparison of simple aromatic amines for electrosynthesis of permselective polymers in biosensor fabrication. *Analyst* 128: 905-911.

Endo K, Miyasaka T, Mochizuki S, *et al.* (2002) Development of a superoxide sensor by immobilization of superoxide dismutase. *Sensors and Actuators B: Chemical* 83: 30-34.

Fong KL, McCay PB, Poyer JL, *et al.* (1973) Evidence that peroxidation of lysosomal membranes is initiated by hydroxyl free radicals produced during flavin enzyme activity. *Journal of Biological Chemistry* 248: 7792-7797.

Fridovich I. (1970) Quantitative aspects of the production of superoxide anion radical by milk xanthine oxidase. *Journal of Biological Chemistry* 245: 4053-4057.

George J and Struthers AD. (2008) The Role of Urate and Xanthine Oxidase Inhibitors in Cardiovascular Disease. *Cardiovascular Drug Reviews* 26: 59-64.

Halliwell B and Gutteridge JM. (2015) *Free Radicals in Biology and Medicine*: Oxford University Press, USA.

Hamdi N, Wang J and Monbouquette HG. (2005) Polymer films as permselective coatings for H_2O_2-sensing electrodes. *Journal of Electroanalytical Chemistry* 581: 258-264.

Hu Y and Wilson GS. (1997) Rapid Changes in Local Extracellular Rat Brain Glucose Observed with an *In Vivo* Glucose Sensor. *Journal of Neurochemistry* 68: 1745-1752.

Kellogg EW and Fridovich I. (1975) Superoxide, hydrogen peroxide, and singlet oxygen in lipid peroxidation by a xanthine oxidase system. *Journal of Biological Chemistry* 250: 8812-8817.

Kintzios S, Marinopoulou I, Moschopoulou G, *et al.* (2006) Development of a novel, multi-analyte biosensor system for assaying cell division: Identification of cell proliferation/death precursor events. *Biosensors and Bioelectronics* 21: 1365-1373.

Kulagina NV, Shankar L and Michael AC. (1999) Monitoring glutamate and ascorbate in the extracellular space of brain tissue with electrochemical microsensors. *Analytical Chemistry* 71: 5093-5100.

Kundu TK, Hille R, Velayutham M, *et al.* (2007) Characterisation of superoxide production from aldehyde oxidase: An important source of oxidants in biological tissues. *Archives of Biochemistry and Biophysics* 460: 113-121.

Kuppusamy P and Zweier JL. (1989) Characterisation of free radical generation by xanthine oxidase. Evidence for hydroxyl radical generation. *Journal of Biological Chemistry* 264: 9880-9884.

Lambeth JD. (2004) NOX enzymes and the biology of reactive oxygen. *Nat Rev Immunol* 4: 181-189.

Link EM and Riley PA. (1988) Role of hydrogen peroxide in the cytotoxicity of the xanthine/xanthine oxidase system. *Biochemical Journal* 249: 391-399.

Liochev SI and Fridovich I. (2003) Reversal of the superoxide dismutase reaction revisited. *Free Radical Biology and Medicine* 34: 908-910.

Loschen G, Azzi A, Richter C, *et al.* (1974) Superoxide radicals as precursors of mitochondrial hydrogen peroxide. *FEBS Letters* 42: 68-72.

Lowry JP, McAteer K, El Atrash SS, *et al.* (1994) Characterization of Glucose Oxidase-Modified Poly(phenylenediamine)-Coated Electrodes *in vitro* and *in vivo*: Homogeneous Interference by Ascorbic Acid in Hydrogen Peroxide Detection. *Analytical Chemistry* 66: 1754-1761.

Lowry JP, Miele M, O'Neill RD, *et al.* (1998) An amperometric glucose-oxidase/poly(o-phenylenediamine) biosensor for monitoring brain extracellular glucose: *in vivo* characterisation in the striatum of freely-moving rats. *Journal of Neuroscience Methods* 79: 65-74.

Lowry JP and O'Neill RD. (1994) Partial characterisation *in vitro* of glucose oxidase-modified poly (phenylenediamine)-coated electrodes for neurochemical analysis *in vivo*. *ElectroAnalysis* 6: 369-379.

Lvovich V and Scheeline A. (1997) Amperometric Sensors for Simultaneous Superoxide and Hydrogen Peroxide Detection. *Analytical Chemistry* 69: 454-462.

McCord JM and Fridovich I. (1969) Superoxide dismutase an enzymic function for erythrocuprein (hemocuprein). *Journal of Biological Chemistry* 244: 6049-6055.

McMahon CP, Killoran SJ, Kirwan SM, *et al.* (2004) The selectivity of electrosynthesised polymer membranes depends on the electrode dimensions: implications for biosensor applications. *Chemical Communications*: 2128-2130.

McMahon CP, Rocchitta G, Kirwan SM, *et al.* (2007) Oxygen tolerance of an implantable polymer/enzyme composite glutamate biosensor displaying polycation-enhanced substrate sensitivity. *Biosensors and Bioelectronics* 22: 1466-1473.

Mesároš Š, Vaňková Ž, Grunfeld S, *et al.* (1998) Preparation and optimisation of superoxide microbiosensor. *Analytica Chimica Acta* 358: 27-33.

Miwa S, Muller FL and Beckman KB. (2008) The Basics of Oxidative Biochemistry. In: Miwa S, Beckman KB and Muller FL (eds) *Oxidative Stress in Aging: From Model Systems to Human Diseases.* Totowa, NJ: Humana Press, 11-35.

Mueller S, Riedel HD and Stremmel W. (1997) Direct evidence for catalase as the predominant H_2O_2-removing enzyme in human erythrocytes. *Blood* 90: 4973-4978.

Murphy LJ. (1998) Reduction of Interference Response at a Hydrogen Peroxide Detecting Electrode Using Electropolymerized Films of Substituted Naphthalenes. *Analytical Chemistry* 70: 2928-2935.

O'Neill RD. (1996) Strategies for decreasing ascorbate interference at glucose oxidase-modified poly(o-phenylenediamine)-coated electrodes. *Analyst* 121: 773-777.

O'Neill RD and Lowry JP. (1995) On the significance of brain extracellular uric acid detected with *in-vivo* monitoring techniques: a review. *Behavioural Brain Research* 71: 33-49.

O'Neill RD and Lowry JP. (2006) Voltammetry *In Vivo* for Chemical Analysis of the Living Brain. *Encyclopedia of Analytical Chemistry*. John Wiley & Sons, Ltd.

O'Brien K, Killoran S, O'Neill R, *et al.* (2007) Development and characterisation *in vitro* of a catalase-based biosensor for hydrogen peroxide monitoring. *Biosensors and Bioelectronics* 22: 2994-3000.

O'Neill RD, Rocchitta G, McMahon CP, *et al.* (2008) Designing sensitive and selective polymer/enzyme composite biosensors for brain monitoring *in vivo*. *TrAC Trends in Analytical Chemistry* 27: 78-88.

Ohsaka T, Tian Y, Shioda M, *et al.* (2002) A superoxide dismutase-modified electrode that detects superoxide ion. *Chemical Communications*: 990-991.

Pakhomova S, Gao B, Boeglin WE, *et al*. (2009) The structure and peroxidase activity of a 33-kDa catalase-related protein from Mycobacterium avium ssp. paratuberculosis. *Protein Science* 18: 2559-2568.

Pontie M and Bedioui F. (1999) Selective and sensitive electrochemical biosensing of superoxide anion production by biological systems: a short overview of recent trends. *Analusis* 27: 564-569.

Rajesh S, Kanugula AK, Bhargava K, *et al.* (2010) Simultaneous electrochemical determination of superoxide anion radical and nitrite using Cu,ZnSOD immobilised on carbon nanotube in polypyrrole matrix. *Biosensors and Bioelectronics* 26: 689-695.

Rothwell SA, Killoran SJ, Neville EM, *et al.* (2008) Poly (o-phenylenediamine) electrosynthesized in the absence of added background electrolyte provides a new permselectivity benchmark for biosensor applications. *Electrochemistry Communications* 10: 1078-1081.

Rothwell SA, Killoran SJ and O'Neill RD. (2010) Enzyme immobilisation strategies and electropolymerisation conditions to control sensitivity and selectivity parameters of a polymer-enzyme composite glucose biosensor. *Sensors* 10: 6439-6462.

Rothwell SA, Kinsella ME, Zain ZM, *et al.* (2009) Contributions by a Novel Edge Effect to the Permselectivity of an Electrosynthesized Polymer for Microbiosensor Applications. *Analytical Chemistry* 81: 3911-3918.

Rowley DA and Halliwell B. (1983) Formation of Hydroxyl Radicals from Hydrogen Peroxide and Iron Salts by Superoxide- and Ascorbate-Dependent Mechanisms: Relevance to the Pathology of Rheumatoid Disease. *Clinical Science* 64: 649-653.

Sligar SG, Lipscomb JD, Debrunner PG, *et al.* (1974) Superoxide anion production by the autoxidation of cytochrome P450cam. *Biochemical and Biophysical Research Communications* 61: 290-296.

Tian F, Gourine AV, Huckstepp RTR, *et al*. (2009) A microelectrode biosensor for real time monitoring of l-glutamate release. *Analytica Chimica Acta* 645: 86-91.

Tian Y, Mao L, Okajima T, *et al.* (2005) A carbon fiber microelectrode-based third-generation biosensor for superoxide anion. *Biosensors and Bioelectronics* 21: 557-564.

Versmold H, Linderkamp O, Stuffer K, *et al.* (1978) *In Vivo* vs. *In Vitro* Response Time of Trancutaneous Po2 Electrodes A comparison of four devices in newborn infants. *Acta Anaesthesiologica Scandinavica* 22: 40-48.

von Woedtke T, Fischer U, Brunstein E, *et al*. (1991) Implantable glucose sensors: comparison between *in vitro* and *in vivo* kinetics. *The International Journal of Artificial Organs* 14: 473-481.

Wang Z, Zhang LM and Tian Y. (2014) Progress on Electrochemical Determination of Superoxide Anion. *Chinese Journal of Analytical Chemistry* 42: 1-9.

Wilson GS and Gifford R. (2005) Biosensors for real-time *in vivo* measurements. *Biosensors and Bioelectronics* 20: 2388-2403.

Chapter 6: NO and O_2 Monitoring in PD Model

6.1: Introduction

Parkinson's disease (PD) is the second most common neurodegenerative disease (GandhiDauer and Przedborski, 2003) (von Bohlen und Halbach, 2005) (Sharma *et al.*, 2013), characterised by resting tremors, rigidity, bradykinesia and postural instability (Duty and Jenner, 2011) (Betarbet *et al.*, 2002) (Martin and Teismann, 2009). Epidemiologic studies indicate that several factors increase the risk of developing PD; these include exposure to pesticides, herbicides, industrial chemicals, wood pulp mills and farming. Other exogenous toxins have been associated with the disease; trace metals, cyanide, organic solvents, carbon monoxide and carbon disulphide (Olanow and Tatton, 1999). The neuropathological feature of PD is dopamine cell degeneration in the substantia nigra pars compacta (SNpc) which leads to an insufficient availability of striatal dopamine and the presence of intraneuronal proteinaceous cytoplasmic inclusions termed Lewy bodies (Dauer and Przedborski, 2003) (Schapira and Jenner, 2011).

Animal models have been used extensively to study neuronal and behavioural alterations caused by PD. The administration of reserpine to rodents has been suggested as a pharmacological model of PD based on the effects of this monoamine-depleting agent on motor activity. The reserpine-treated model was one of the earliest animal models employed in PD research. Carlsson *et al.* in 1957 demonstrated the therapeutic effects of L -3,4-dihydroxyphenylalaine (L-DOPA) in the treatment of the 'tranquillizing' effects of reserpine treatment in mice (Carlsson *et al.*, 1957) (Duty and Jenner, 2011). Therefore, the reserpine model has been utilised as a potential screen for symptomatic efficiency of new treatments for PD and has aided in the understanding of the link between monoamine depletion and Parkinsonism symptoms.

Reserpine administered peripherally in the dose range of 1-10 mg/kg interferes with the storage of monoamines in intracellular vesicles causing monoamine depletion in nerve terminals (Leão *et al.*, 2015) (Arora and Chopra, 2013) (Dluzen *et al.*, 2008) (Gołembiowska and Dziubina, 2012). The administration of an acute dose of reserpine (1-10 mg/kg) induces irreversible deficits in motor function including catalepsy, tremor, muscular rigidity and hypolocomotion (Fernandes *et al.*, 2012) (Santos *et al.*, 2013) (Antkiewicz-Michaluk *et al*., 2015). Reserpine works by inhibiting the vesicular monoamine transporter 2 (VMAT-2). The blockage of dopamine vesicular uptake

results in the accumulation of neurotoxic dopamine oxidation by-products. It is well documented that reserpine produces ~85% loss of dopamine in the SNpc and >95% dopamine depletion in the striatum within 2 hrs of injection (Heeringa and Abercrombie, 1995). Dopamine reacts with molecular O_2 to form dopamine-quinones which can deplete the antioxidant glutathione, generating reactive oxygen species (ROS) such as hydrogen peroxide (H_2O_2) and superoxide (O_2^-) during this process (Fernandes *et al.*, 2012). When the production of ROS exceeds the ability of the antioxidant system to eliminate these cytotoxic species, oxidative damage occurs. Therefore each of these dopamine derived reactive molecules is potentially detrimental to the normal functioning of the dopamine neuron (See Chapter 1, Section 1.7). The reserpine model can induce oxidative stress. Reserpine in the dose range of 1-10 mg/kg induces decreases in catalase, superoxide dismutase (SOD) and the total content of reduced glutathione and ATP. Similarly, reserpine increases glutathione peroxidase activity, oxidised glutathione, lipid peroxidation, nitric oxide (NO) and iron levels (Leão *et al*., 2015).

Research conducted has shown that a single administration of reserpine in low doses (0.1-0.5 mg/kg) induces deficits in emotional memory without causing any motor alterations (Fernandes *et al.*, 2008) (Carvalho *et al.*, 2006). These findings corroborate studies with PD patients where deficits in emotional memory precede the appearance of motor deficits (Bowers et al., 2006). Fernandes *et al.* proposed a possible progressive pharmacological model of PD involving the repeated administration of 0.1 mg/kg reserpine to rodents, and evaluated motor behaviour and memory performance. They also investigated oxidative damage by measuring lipid peroxidation in the striatum and hippocampus (Fernandes *et al.*, 2012).

This chapter investigates the role of oxidative stress in the manifestation of PD using the reserpine animal model. For this research, NO and O_2 electrodes were implanted in the striatum and the animals were administered with either one single dose (5 mg/kg) or a repeated lose dose (0.1 mg/kg) of reserpine. As alluded to previously and shown below in Figure 6.1, the reserpine model induces oxidative stress so therefore, using these amperometric sensors the changes in NO and O_2 levels can be monitored continuously in real-time. NO is proposed as a marker of oxidative stress and recently the research group used the *in-vivo* measurement of NO to infer corresponding

changes in oxidative stress levels in a paraquat animal model of PD (Finnerty *et al.*, 2013(b)).

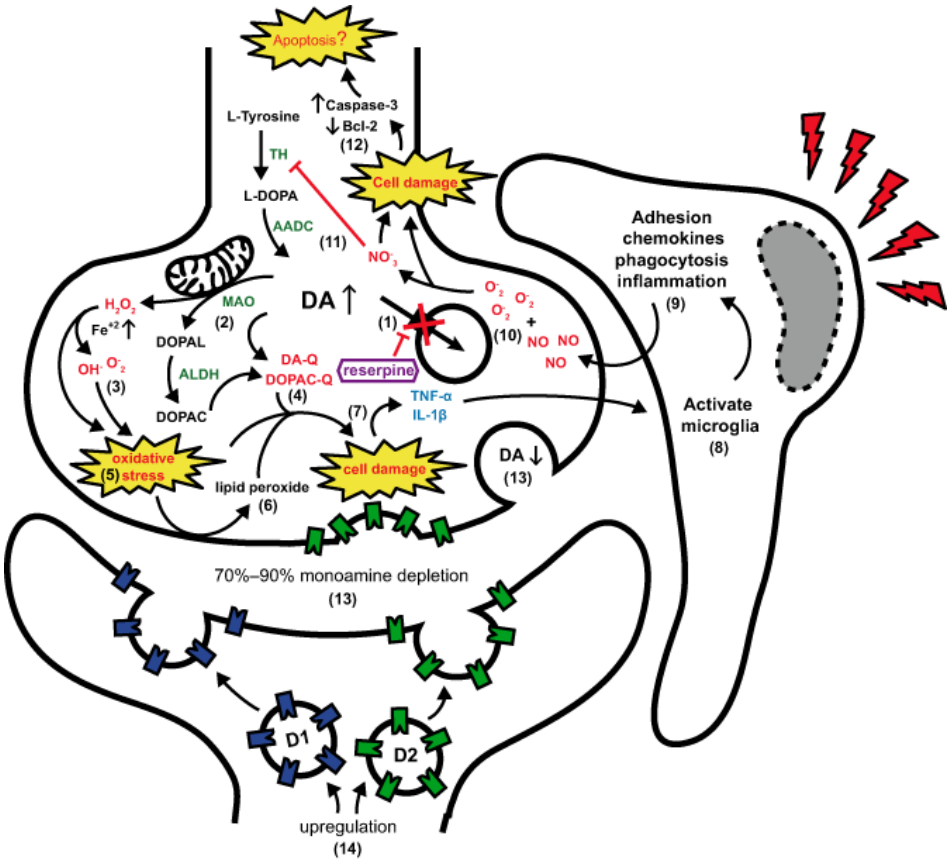

Figure 6.1: Neurochemical and molecular events after reserpine treatment. (1) Reserpine precludes dopamine (DA) storage. (2) Increased DA is metabolised in the cytoplasm (3) generating reactive oxygen species (ROS) and (4) highly reactive quinones (DA-Q and DOPAC-Q) (5) resulting in oxidative stress and (6) lipid peroxidation. (7) Accumulation of ROS and reactive quinones leads to cell damage and proinflammatory signalisation. (8) Activation of microglia by tumor necrosis factor (TNF)-α and interleukin (IL)-1β (9) amplify proinflammatory signalisation resulting in (10) nitric oxide (NO) increase and peroxynitrite (NO_3^-) formation with free superoxide (O_2^-). (11) NO_3^- inhibits tyrosine hydroxylase (TH) activity and (12) reinforces cell damage committing cell fate in proapoptotic signalisation. At the same time, (13) monoamine depletion in the synaptic cleft results in (14) upregulation of D1 and D2 receptors on the postsynaptic and presynaptic membrane. AADC, aromatic L-amino acid decarboxylase; ALDH, aldehyde dehydrogenases; MAO, monoamine oxidase. Figure reproduced from (Leão *et al.*, 2015).

6.2 Experimental

The instrumentation and software for all experiments carried out in this chapter are described in Section 3.2. All chemicals and solutions utilised are presented in Section 3.3. The surgical procedure for the implantation of the relevant sensors is described in Section 3.8.2.

The sensors used for these experiments were the Pt-based NO sensor (see Section 3.5.3) and the carbon paste O_2 sensors (see Section 3.4.1). A potential of +900 mV and -650 mV *vs.* SCE was applied to the NO and O_2 sensors respectively. An increase in the reduction current is indicative of an increase in O_2 while an increase in the oxidation current is indicative of an increase in NO. All experiments were carried out in freely-moving Wistar rats. Two doses of reserpine were administered during these experiments; a single 5 mg/kg injection and then a lower 0.1 mg/kg dose every second day with a total of ten injections. Each injection was administered subcutaneously at ~ 12:00 hr.

All data is reported as mean ± SEM and n = number of electrodes unless otherwise stated. All statistical analysis was carried out using GraphPad prism and yielded a P value result, which is the probability value that specifies if the results observed are significantly different. Area under the Curve (AUC) was performed using GraphPad prism to quantify any changes observed in the sensor signal for statistical analysis. The baseline value was taken as the first 30 mins to allow for baseline drift and all data was baseline subtracted prior to performing AUC analysis. The net area subtracts the area of the peaks below the baseline from the area of peaks above the baseline. The total area value calculated includes the positive peaks, negative peaks, peaks that are not high or too narrow to count.

6.3 Results

The results section comprises of data from the manufacture of the NO and O_2 sensors *in-vitro* prior to the implantation in the striatum. All the data shown is obtained from NO/O_2 electrodes that have been implanted bilaterally in the left/right striatum of the rat brain following the surgical procedure detailed in Section 3.8.2. These sensor types have been fully characterised *in-vivo* (Finnerty *et al.*, 2012) (Brown *et al.*, 2009) (Bolger *et al.*, 2011(b)) (Bolger and Lowry, 2005) so this chapter utilises these sensors in an animal model of PD to monitor the changes in striatal NO and O_2 levels.

6.3.1 *In-Vitro* Nitric Oxide Sensors

A Pt-based NO sensor extensively characterised *in-vitro* and *in-vivo* is utilised throughout this research. The operational characteristics of this sensor such as sensitivity, selectivity, response time and limit of detection (LOD) are well characterised (Brown *et al.*, 2009). This sensor has also been utilised in different application studies including an animal model of schizophrenia (Pålsson *et al.*, 2009). For this study the effect of phencyclidine (PCP) alone or in conjunction with the NOS inhibitor L-NAME, on NO levels was investigated in the medial prefrontal cortex of freely moving rats. Research has also recently been performed using this NO sensor in a model of PD (Finnerty *et al.*, 2013(b)). This research monitored the changes in NO levels after the exposure of animals to various quantities of the external toxin paraquat. In this study the observation of a characteristic change in NO levels supports the theoretical prediction of a bi-stable neurochemical switching mechanism for the exposure to PD risk factors above a certain magnitude. *In-vivo* measurements in rats show a switching phenomenon for repeated toxic insults of 30 mg/kg paraquat while low levels 5 mg/kg do not.

All NO calibrations were performed at +900 mV *vs.* SCE over the concentration range of 0-1 µM. Details of the experimental procedure is provided in Chapter 3, Section 3.6.7. Average results obtained for these calibrations are shown below in Figure 6.2.

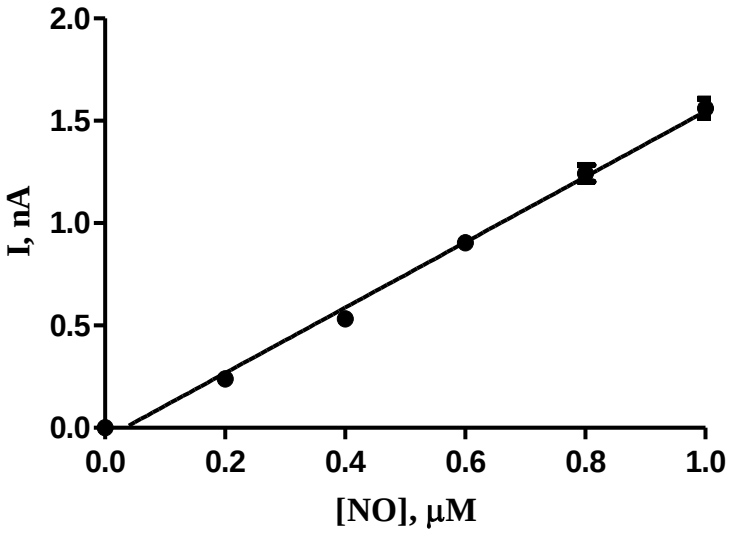

	NO Sensor		
[NO], µM	Mean	S.E.M	n
0.2	0.24	0.01	36
0.4	0.53	0.02	36
0.6	0.90	0.03	36
0.8	1.24	0.04	36
1	1.56	0.05	36
Sensitivity, nA/µM	1.60	0.05	36
R^2	0.99	-	36

Figure 6.2: The mean current-concentration profiles for NO calibrations *(Top)* and comparison table *(Bottom)* performed on NO sensors in PBS (pH 7.4) at 21°C using NO sensors. CPA carried out at +900 mV *vs.* SCE. All currents are background subtracted (0.11 ± 0.01 nA)

The figure above shows the current generated on addition of various aliquots of NO (0.2 – 1 µM). A linear response is observed over the calibration range with a current of 1.56 ± 0.05 nA (n = 36) recorded on addition of 1 µM NO. The NO was synthesised in-house and the relevant concentration was determined using UV spectrometry and

the Beer-Lambert Law. This procedure is detailed in Section 3.7. The sensitivity achieved of 1.60 ± 0.05 nA/µM (n = 36) is almost identical (P = 0.46) to the published sensitivity of 1.67 ± 0.08 nA/µM (n = 14) (Brown *et al.*, 2009). In addition, the selectivity of the NO sensors were investigated prior to implantation. As AA is the main interferent in the brain, AA calibrations (0 – 1000 µM) were performed at + 900 mV *vs.* SCE on the NO sensors to ensure their selectivity before implantation. Average results obtained are shown below in Figure 6.3.

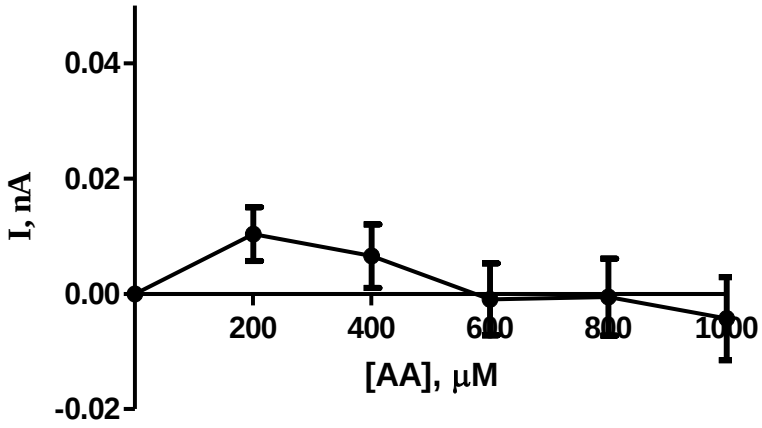

	NO Sensor		
[AA], µM	Mean	S.E.M	n
200	0.010	0.005	33
400	0.007	0.006	33
600	-0.001	0.006	33
800	-0.001	0.006	33
1000	-0.004	0.007	33

Figure 6.3: The mean current-concentration profiles for AA calibrations *(Top)* and comparison table *(Bottom)* calibrated on NO sensors in PBS (pH 7.4) at 21°C. CPA carried out at +900 mV *vs.* SCE.

The figure above demonstrates the efficiency of the NO sensors in rejecting AA. A small change in current is observed (-0.004 ± 0.007 nA, (n = 33)) on addition of 1000 µM AA with a negligible non-linear response observed over the calibration range. The small negative current recorded can be attributed to no AA detection at the electrode but a slight deviation in baseline over the time scale of the calibration. This compares to similar data published by the research group using variations of the NO sensor (Wynne *et al*., 2014).

Direct contact of electrochemical sensors with biological samples *in-vivo* can result in a decrease in sensitivity. The figure below shows a typical comparison between NO calibrations pre- and post-implantation and determines the impact the implantation of the sensors in the *in-vivo* environment exerts on the sensor's sensitivity.

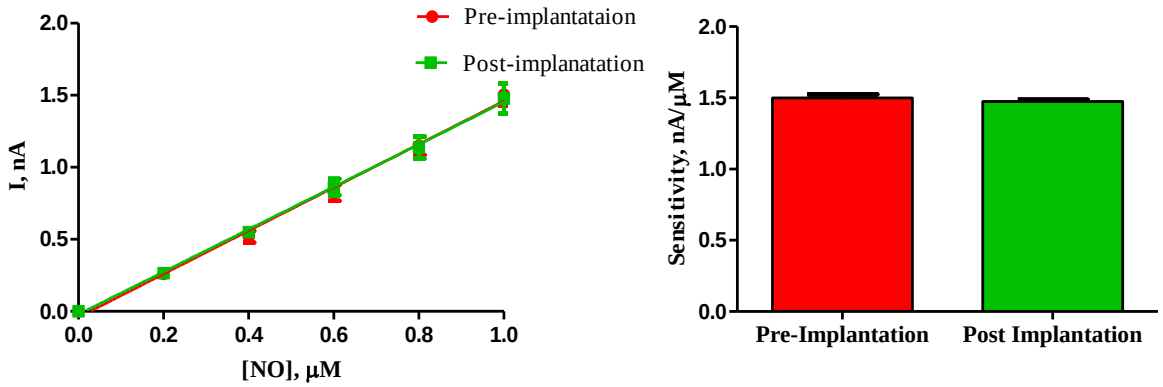

	Pre-Implantation			Post-Implantation		
[NO], µM	Mean	S.E.M	n	Mean	S.E.M	n
0.2	0.26	0.02	4	0.26	0.02	4
0.4	0.52	0.41	4	0.55	0.04	4
0.6	0.82	0.05	4	0.86	0.06	4
0.8	1.15	0.06	4	1.14	0.08	4
1	1.50	0.08	4	1.48	0.10	4
Sensitivity, nA/µM	1.50	0.05	4	1.47	0.03	4
R^2	0.99	-	4	0.99	-	4

Figure 6.4: The mean current-concentration profiles for pre/post-implantation NO calibrations *(Top Left)*, bar chart comparing the sensitivities pre- and post-implantation *(Top, Right)* and comparison table *(Bottom)*. NO sensors calibrated in PBS (pH 7.4) at 21°C. CPA carried out at +900 mV *vs.* SCE.

The figure above demonstrates that NO sensors calibrated pre- and post-implantation gave almost identical currents on addition of various aliquots of NO into the PBS buffer solution. Similarly, the sensitivity observed pre-implantation (1.50 ± 0.05 nA/µM, n = 4)) remains uncompromised post implantation with a sensitivity of 1.47 ± 0.03 nA/µM (n = 4) being recorded. This result suggests that direct contact of the NO sensors with biological samples *in-vivo* does not degrade the Nafion® layer and therefore the sensitivity of the sensor remains similar pre- and post-implantation.

In summary, this section demonstrates that similar sensitivities to NO were recorded for NO sensors when compared to published work by the research group. The sensor is selective to NO and retains its sensitivity after implantation for ~20 days. This sensor is used throughout this chapter to monitor the changes in NO levels after reserpine administration

6.3.2 *In-Vitro* Oxygen Sensors

A wide variety of sensors have been employed for the direct monitoring of O_2, some incorporating noble metal electrodes including gold (El-Deab and Ohsaka, 2003) (Holmström *et al*., 1998) and Pt (Bolger *et al.*, 2011(a)), however, the use of carbon-based electrodes has been reported by several research groups (Lowry *et al.*, 1996) (Bazzu *et al*., 2009) (Venton *et al.*, 2003). These carbon electrodes are advantageous because of their *in-vivo* stability and minimal surface poisoning (Bolger and Lowry, 2005). O_2 calibrations were performed at -650 mV *vs.* SCE and involved the addition of various aliquots of an O_2 saturated PBS solution into the electrochemical cell. This experimental procedure is detailed in Chapter 3, Section 3.6.6. The concentration range utilised was between 0 and 125 µM which is within the brain tissue concentration range of between 40 µM to 80 µM (Bolger *et al*., 2011(a)). Average data obtained from these calibrations is shown below in Figure 6.5.

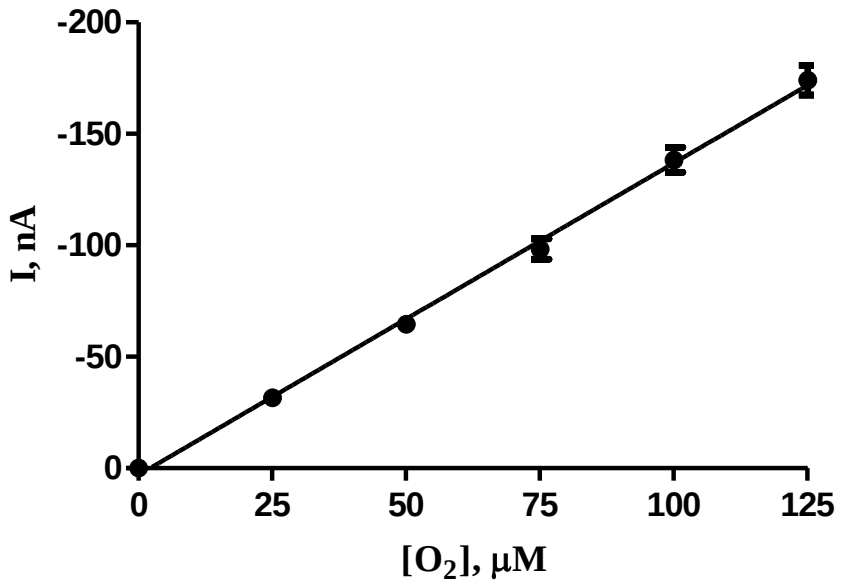

	Carbon Paste Electrode		
$[O_2]$, µM	Mean	S.E.M	n
25	-31.35	1.84	19
50	-64.37	3.46	19
75	-98.16	4.60	19
100	-138.15	5.63	19
125	-173.89	6.69	19
Sensitivity, nA/µM	-1.40	0.03	19
R^2	0.99	-	19

Figure 6.5: The mean current-concentration profiles for O_2 calibrations *(Top)* and comparison table *(Bottom)* performed with carbon paste electrodes in PBS (pH 7.4) at 21°C. CPA carried out at -650 mV *vs.* SCE. All currents are background subtracted (-3.27 ± 0.56 nA).

The results above show the current generated on addition of various aliquots of O_2 saturated PBS into the electrochemical cell. The calibration shows a linear response with a current of -173.89 ± 6.69 nA (n = 19) obtained on addition of 125 µM O_2. The sensitivity recorded of -1.40 ± 0.03 nA/µM is significantly increased (P = 0.002) compared to the published sensitivity of -1.09 ± 0.03 nA/µM (Bolger *et al.*, 2011(a)). An explanation for this is the electrodes are packed more loosely giving an increased surface area. These carbon paste electrodes have been extensively characterised and found to be highly selective with a subsecond response time and a LOD calculated at 0.09 µM (Bolger *et al.*, 2011(b)). Therefore, this sensor is ideal for the *in-vivo* monitoring of O_2 in an animal model of PD.

The mammalian brain is a hostile environment for implanted sensors as it contains several electrode poisons such as lipids and proteins, however, carbon paste electrodes are less prone to surface poisoning and are very stable even after weeks of continuous recording in the brain (Fillenz and O'Neill, 1986) (Bolger *et al.*, 2011(b)). Post *in-vivo* calibrations were performed after euthanasia to investigate the effects the *in-vivo* environment had on the sensitivity of the carbon paste electrodes. Average post calibration data is shown below in Figure 6.6.

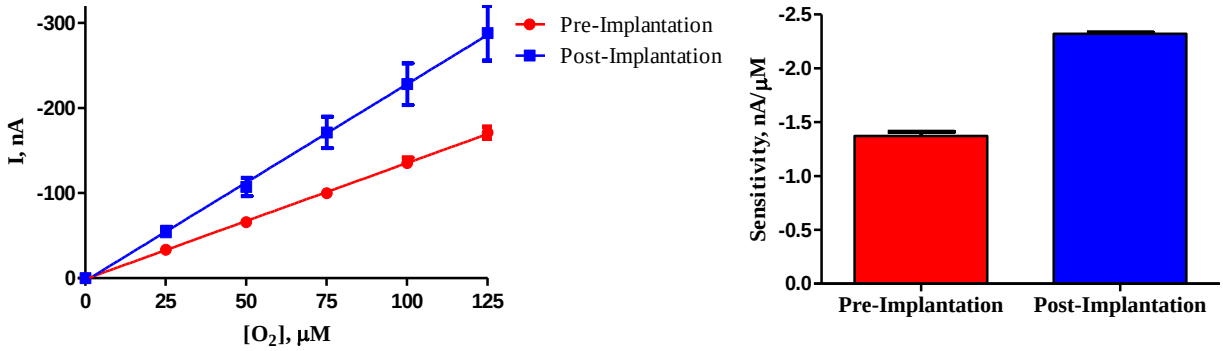

	Pre-Implantation			Post- Implantation		
$[O_2]$, µM	Mean	S.E.M	n	Mean	S.E.M	n
25	- 33.14	2.34	12	-53.76	6.28	10
50	- 65.42	3.97	12	-106.94	10.80	10
75	- 99.50	4.83	12	-171.12	18.41	10
100	- 135.19	6.22	12	-227.92	24.55	10
125	- 170.77	7.31	12	-287.74	32.26	10
Sensitivity, nA/µM	-1.37	0.01	12	-2.32	0.03	10
R^2	0.99	-	12	0.99	-	10

Figure 6.6: The mean current-concentration profiles for pre/post-implantation O_2 calibrations *(Top Left)*, bar chart comparing the sensitivities pre- and post-implantation *(Top, Right)* and comparison table *(Bottom)*. O_2 sensors calibrated in PBS (pH 7.4) at 21°C. CPA carried out at -650 mV *vs.* SCE.

The results above provide a comparison between the current generated during an O_2 calibration pre- and post-implantation in the striatum. It is clear, that the sensitivity is not compromised on exposure to surface poisons, however, a significant increase ($P < 0.0001$) in sensitivity is observed from -1.37 ± 0.01 nA/µM (pre-implantation, n = 12) to -2.32 ± 0.03 nA/µM (post-implantation, n = 10). This novel resistance to poisoning appears to be, the presence of the pasting silicon oil. Conversely, the variability is higher in the carbon paste electrodes post implantation postulating that the *in-vivo*

environment may have a small effect on the electrode conformation. Ormonde and O'Neill found that carbon paste electrodes exposed to brain tissue resulted in the removal of the pasting oil from the active surface of the electrode. The electron transfer was faster at the resulting powder-type surface which lead to a shift in the oxidation wave for AA (Ormonde and O'Neill, 1990). These results suggests that the conformation of the electrode to a powder like surface has resulted in an increase in O_2 sensitivity as seen above in Figure 6.6.

6.3.3 Nitric Oxide Single Dose Reserpine

6.3.3.1 Baseline Nitric Oxide Recording

NO has been implicated in the regulation of sleep (Obal Jr and Krueger, 2003) (Wisor *et al*., 2011) (Calabrese *et al.*, 2007). NO levels *in-vivo* are highly labile, as the half-life of NO is less than one second (Barbosa *et al.*, 2008), therefore changes in NO need to be monitored continuously. Wisor and co-wokers stated 'that individual effects of nNOS deficiency in the suprachiasmatic nucleus, basal forebrain, sleep active neurons and other nNOS–positive sites have distinct effects, some of which are wake promoting and others are sleep promoting' (Wisor *et al.*, 2011). The baseline recorded data in this section (which represents the control data set) was analysed using 13 sensors in 4 animals and the data was analysed over 12 hr periods to monitor the diurnal changes in NO levels recorded during the light and dark phases. This analysis was carried out to provide the control data for the reserpine experiments, however, this can be compared to results published by Kostin and co-workers. Kostin *et al.* used the Nafion® modified NO sensor developed in our research group for real-time detection of NO levels in the perifornical-lateral hypothalamic area (PF-LHA) across sleep-wake cycles, dark-light phases, and during prolonged waking. The use of these sensors by Kostin as an independent research group validates the use of this NO sensor. This study demonstrated that NO levels in the PF-LHA exhibit sleep-wake as well as diurnal modulation (Kostin *et al*., 2013). Average baseline data over 72 hours is shown below in Figure 6.7.

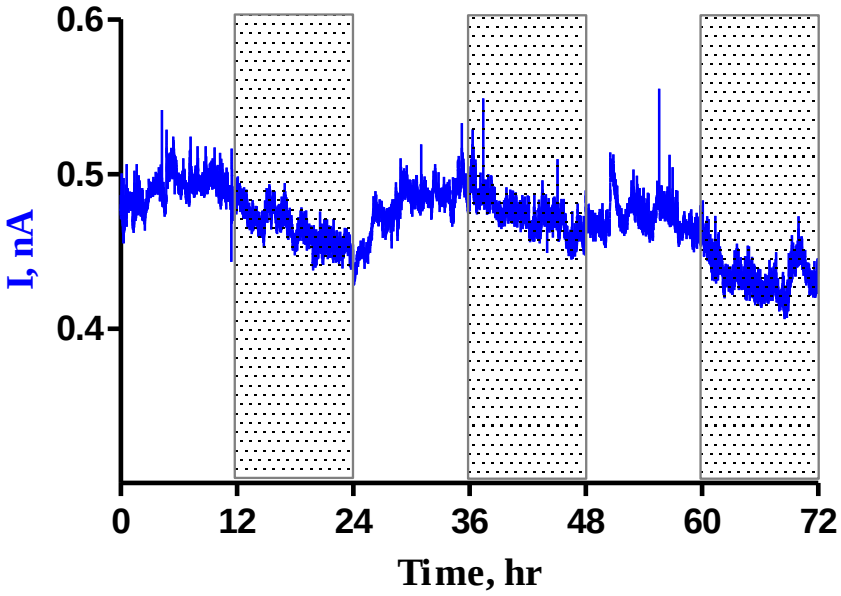

Figure 6.7: A time *vs.* current change graph of baseline NO currents monitored by NO sensors (13 sensors in 4 animals) implanted in the striatum over 72 hrs. The shaded region corresponds to the dark phase. Average SEM recorded for the NO signal was 0.051 nA (n = 13).

It is clear, from this real-time continuous trace that NO levels change depending on the time of day when implanted in the striatum. It is evident, that NO levels increase during the light phase when the animals tend to sleep while a decrease in NO levels is observed during the dark phase when the animals are more active. Kostin *et al* also showed similar analysis for NO sensors implanted in the PF-LHA showing a continuous real-time trace over 72 hrs. This research showed an opposing trend here the electrode generated currents were higher during the dark phase (Kostin *et al*., 2013). Conversely, Cespuglio and co-workers demonstrated the changes in the NO signal recorded over a 24 hr period in the frontal cortex (Cx) and the nucleus raphe dorsalis (nRD). In the Cx the NO signal was higher during the dark phase and lower during the light phase, however, similar to the results shown in Figure 6.7, the NO levels recorded in the nRD were lower during the dark phase and higher during the light phase (Cespuglio *et al*., 2012). This work utilised a carbon fiber sensor first pretreated with a triangular current in PBS and then coated with porphyrin-nickel and Nafion®. Differential pulsed voltammetry allowed for the detection of NO at +650 mV (Burlet and Cespuglio, 1997). Therefore, NO recordings show diurnal changes,

however, the nychthemeral changes throughout both the light and dark phases are region specific.

AUC analysis was performed to quantify any observed changes in the NO levels recorded during the light and dark phases. The baseline was taken as the first 30 minutes and each 12 hr time period was analysed individually and the mean of the three day and night periods were calculated. Figure 6.8 below depicts the results achieved by this analysis.

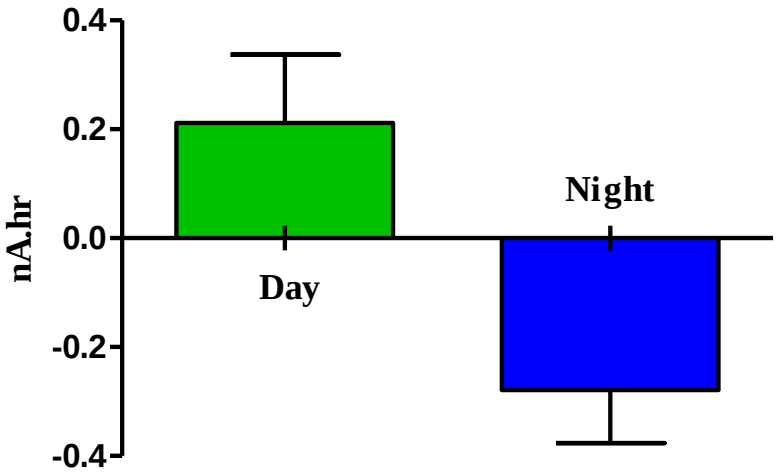

Figure 6.8: A bar chart demonstrating the changes in AUC for NO levels over a 72 hr period (3 day periods and 3 night periods) in 4 animals (n = 13). All data was background subtracted and the net area calculated was plotted.

The figure above demonstrates the changes in the NO levels over a 72 hr time period. It is clear, that this represents the trend observed previously in Figure 6.7. The day period shows an increase in NO levels when compared to baseline symbolised by the recorded positive net area of 0.212 ± 0.125 nA.hr (n = 9). However, the night period shows a different trend, the NO levels decrease demonstrated by the recorded negative net area of -0.279 ± 0.097 nA.hr (n = 13). No significant difference (P = 0.6724) is observed between the net total AUC for the day and night period. These results emphasis the significance of the diurnal changes observed in the NO levels recorded over any 24 hr time period. These NO diurnal changes will be considered throughout the remainder of this chapter when analysing any long-terms effects of reserpine on NO levels.

Another essential factor to consider is the baseline stability of this NO sensor in the *in-vivo* environment. Finnerty *et al*. demonstrated that this particular NO sensor shows baseline stability over a successive 8-day period for sensors implanted in the striatum with no significant difference in sensitivity being recorded (Finnerty *et al.*, 2012).

This continuous real-time baseline data will be used to provide a comparison for the effect the administration of a single 5 mg/kg injection of reserpine has on striatal NO levels. As reserpine has a long lasting effect it is very important to have baseline data corresponding to the differences in the NO levels during the light and dark phases to provide a comparison for the diurnal changes observed after administration of the drug. It is also clear, that over the 72 hr time period the baseline remains very stable, therefore any deviation from the baseline signal can be attributed to the administration of a control or drug particularly the short term effect of these stimuli.

6.3.3.2 Saline Administration

A typical example of the effect a saline administration (NaCl, 0.9%, s.c.) has on the NO current is shown in Figure 6.9(a) and Figure 6.9(b). Figure 6.9(a) shows the average response a subcutaneous saline injection has on NO levels monitored with 8 NO sensors implanted in the striatum of 2 animals. Figure 6.9(b) shows a typical example of a saline injection highlighting the initial effects of the injection on the NO levels. The systemic administration of reserpine on the NO sensor response may be compared against the control experiments shown in this section.

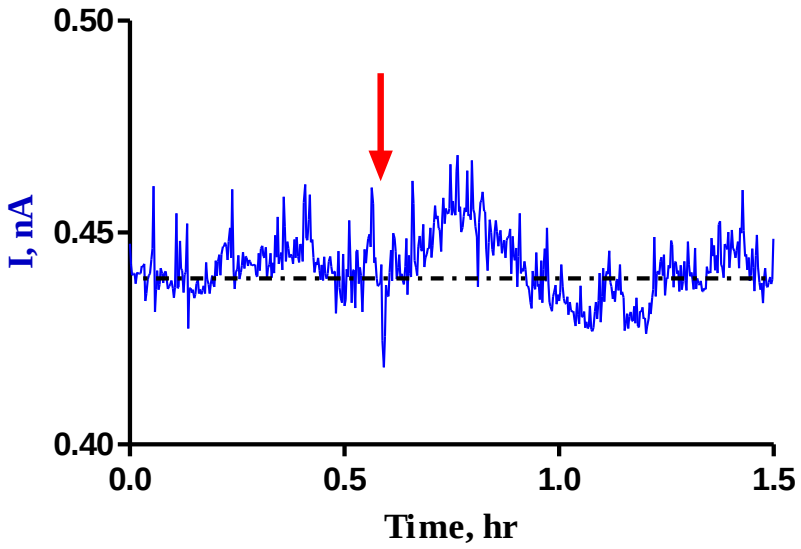

Figure 6.9(a): Mean current *vs.* time response of NO levels on the administration of a 1 mL saline injection subcutaneously for NO sensors (n = 8) implanted in the striatum. The red arrow represents the administration of the injection. The average SEM current recorded was 0.056 nA (n = 8).

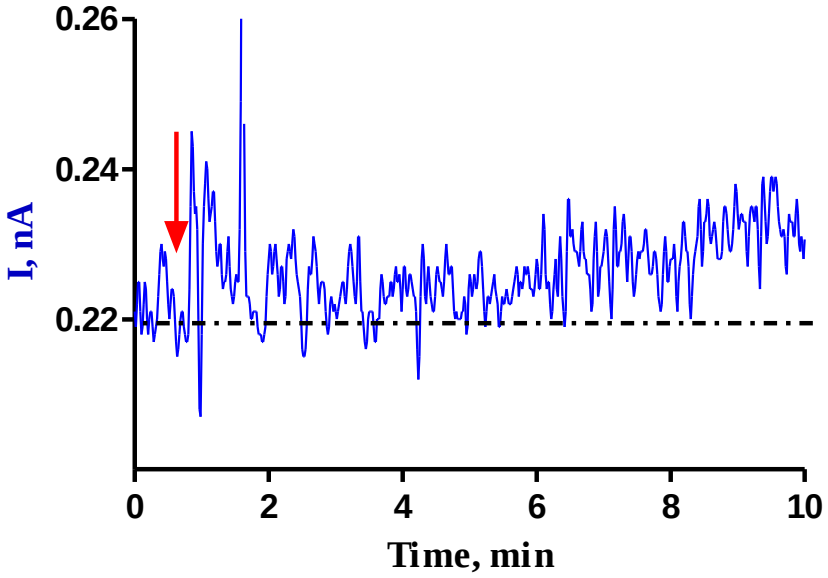

Figure 6.9(b): A typical example of a 1 mL saline injection monitored by a NO sensor implanted in the striatum of a freely moving animal. The arrow is indicative of the point of injection.

The results above show the effect an s.c. saline injection has on the NO levels. Upon the administration of saline a brief fluctuation in NO is observed which is due to the physical manipulation of the animal and post injection activity, however, this increase in NO is short-lived (see Figure 6.9(b)). Figure 6.9(a) shows the mean current *vs.* time profile for the administration of a saline injection subcutaneously. It is clear, that an increase (22 pA) in NO (0.463 ± 0.058 nA (n = 8)) is observed after the injection, however this is not significantly different (P = 0.7834) from the pre-injection baseline of 0.441 ± 0.055 nA, (n = 8). The NO signal returns to baseline levels (0.441 ± 0.055 nA) after *ca.* 30 minutes. This result demonstrates that an initial increase in the oxidation current is recorded, due to injection stress which causes an increase in NO directly after the administration of the injection. This compares to published work by the research group where the systemic administration of saline (i.p. injection) resulted in a transient increase in NO signal (22 ± 3 pA, n = 9) from baseline for NO sensors implanted in the striatum (Finnerty *et al.*, 2012). The NO levels returned to baseline levels after 13 ± 4 min similar to the results shown in Figure 6.9(a) and Figure 6.9(b).

In summary, this section demonstrated that the NO response which is attributable to the injection itself is minimal. No significant difference (P > 0.05) was observed between pre- and post-injection baseline levels. No lasting effect on the response of the NO sensor was observed following the systemic administration of saline with the NO signal returning to the same pre-injection baseline signal after *ca.* 30 minutes.

6.3.3.3 Single 5 mg/kg Reserpine

Reserpine is the most clinically useful of the Rauwolfia alkaloids and was first isolated by Muller *et al.* in 1952. Reserpine is a di-ester compound containing six methoxyl groups, one basic N atom which can be quaternised and a second N which is weakly basic and is present as an NH group (see Figure 6.10) and is an indole base. Reserpine is a colourless, crystalline powder which is absorbed rapidly, and is readily soluble in aqueous solutions up to a concentration of 0.5% reserpine (Stitzel, 1976).

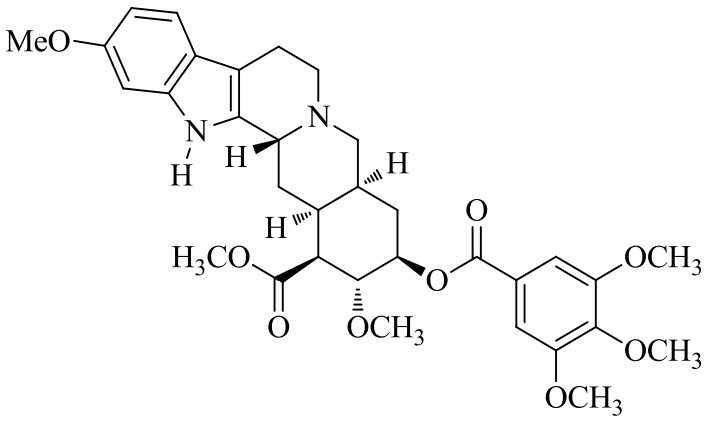

Figure 6.10: Chemical structure of reserpine (Guo *et al.*, 2015)

The administration of reserpine to rodents has been suggested as a pharmacological model of PD. Reserpine interferes with the storage of monoamines in intracellular vesicles causing monoamine depletion in nerve terminals and after the administration of high doses hypolocomotion and muscular rigidity is observed. Few reports exist in the literature that monitor the changes in NO *in-vivo* after administration of the drug, however, several research groups have used tissue samples to monitor the levels of lipid peroxidation in the striatum and hippocampus. This set of experiments investigates the effect a single 5 mg/kg reserpine injection subcutaneously has on the NO levels in the striatum recorded for several days to determine the long-term effects of the drug. The short-term effects of reserpine on the NO levels monitored by NO sensors (n = 12) implanted in the striatum is shown in Figure 6.11(a).

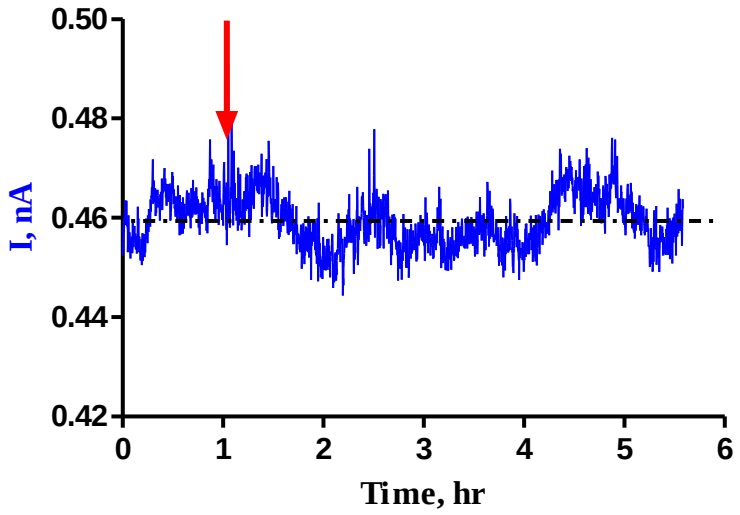

Figure 6.11(a): Mean time *vs.* current profile of the short-term effect of a single 5 mg/kg s.c. injection of reserpine on NO levels recorded by NO sensors implanted in the striatum of freely-moving animals (n = 12). The red arrow is indicative of the point of injection. The average SEM current recorded was 0.069 nA (n = 12).

Figure 6.11(a) demonstrates the NO response monitored for a period of 6 hrs immediately following the systemic administration of reserpine (5 mg/kg). Similar to the saline injection a slight increase is observed after the injection which is attributed to injection stress, however, this increase is short-lived and the NO signal returns to baseline levels after about 30 minutes.

This NO sensor has been extensively characterised *in-vivo* and has been used in animal models of PD and schizophrenia. To emphasis this, a typical example demonstrating the effect an interperitoneal injection of the NO precursor L–arginine has on the NO levels is shown below in Figure 6.11 (b). This example highlights the effectiveness of the NO sensor in monitoring real-time changes in the NO levels upon administration of a drug and this data has been previously published by the research group (Brown *et al.*, 2009*)*.

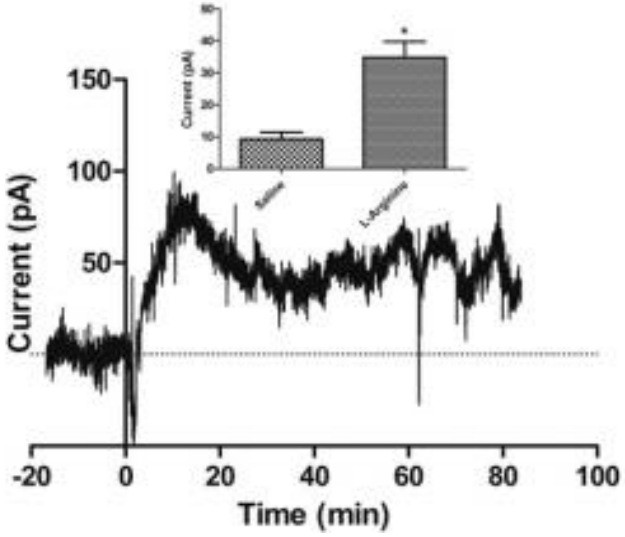

Figure 6.11(b): An example of the systemic administration of L-arginine on the NO response of a NO sensor implanted in the striatum of a freely-moving animal. The inset shows a comparison between the effect of saline *vs.* L-arginine injection (Brown *et al*., 2009).

The data above highlights the effectiveness of the NO sensor in monitoring any immediate changes in the NO levels upon administration of a drug. This can be used to compare the NO levels recorded after the systemic administration of reserpine (5 mg/kg). Research performed by Heeringa and Abercrombie demonstrated that reserpine produces ~ 85% loss of dopamine in the SNpc and > 95% dopamine depletion in the striatum within 2 hrs of the initial injection (Heeringa and Abercrombie, 1995) (Duty and Jenner, 2011). On examination of the results in Figure 6.11(a) 2 hrs after the initial administration of the injection the NO current recorded (0.456 ± 0.053 nA, (n =12)) is almost identical (P = 0.9375) to the pre-injection baseline current of 0.462 ± 0.054 nA, (n = 12) suggesting no change in the NO levels in the striatum.

Bilska *et al.* demonstrated that the levels of NO increased in the striatum and prefrontal cortex in response to reserpine induced oxidative stress. The level of nitrites was determined using Roche's test which is a "nitric oxide colorimetric assay". The results were calculated according to standard curves obtained for a solution of sodium nitrite (6 – 600 µM) using the change in absorbance measured before and after incubation with sulphanilamide and N-(1-naphthyl)-ethylenediamine dihydrochloride (Bilska *et al*., 2007). Cunha and co-workers used the Griess assay where the metabolites were

determined using nitrogen oxides (NO = nitrite plus nitrate). The nitrate was converted into nitrite by nitrate reduction and measured using the Griess reaction at 540 nm. The values obtained from the assay represent the amount of nitrite and nitrate derived from NO contained in the cerebral cortex. This research determined that two s.c. injections of 1 mg/kg reserpine with an interval of 48 hrs showed no significant difference in NOx levels when compared to the control group in the striatum of male Swiss mice (Cunha *et al.*, 2016). Chen *et al*. used Roche's test to determine the level of nitrites and the concentration of nitrite was used as an index for the NO level in the tested tissue. This research utilised a 1 mg/kg reserpine dose and showed a significant increase in NO production in the hippocampus of the Wistar rat on administration of the drug when compared to the control group (Chen *et al.*, 2016).

Okano *et al.* submitted male Wistar-Kyoto rats to reserpine (5 mg/kg) intraperitoneally three times a week for 12 weeks. After 5 weeks a range of vasoactive substances related to blood pressure were monitored including the NOx concentration and dopamine levels in the plasma. The NOx concentrations were determined using the Griess reaction. They found no significant difference in the NOx concentration or dopamine levels in the plasma after this experimental treatment with reserpine (Okano *et al.*, 2005). This research also concluded that reserpine induced sedation, a behavioural depression manifested by bradykinesia and hunched posture. However, no signs of convulsions or tremor were observed. The literature results above emphasises the inconsistency in the results obtained in relation to the effect the administration of reserpine has on NO levels in the *in-vivo* environment.

It is clear from Figure 6.11(a), that only a slight deviation from the baseline value is observed after 5 hrs of reserpine administration, thus it was necessary to analysis the NO signal over an extended period (120 hr) to see the long-term effects of the drug. This is shown in Figure 6.11 (c).

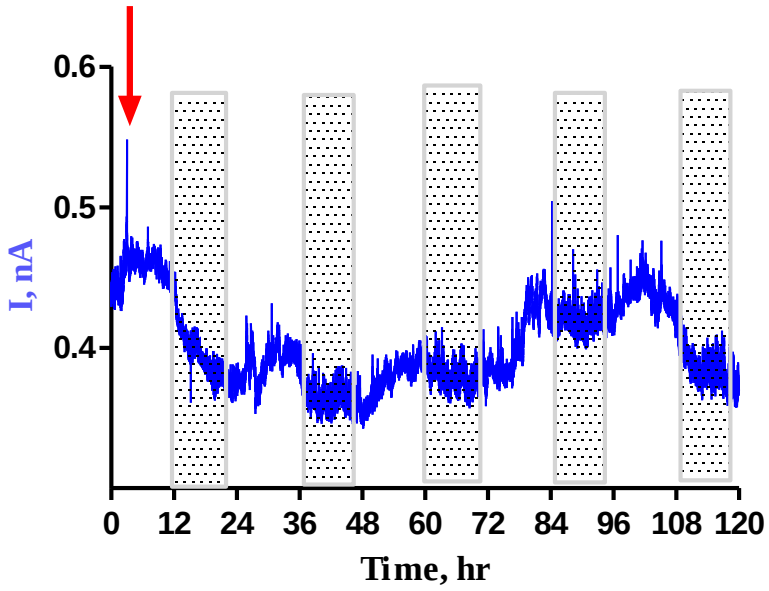

Figure 6.11(c): The average NO signal (n = 12) recorded in the striatum over a continuous 120 hr period after the systemic administration of reserpine (5 mg/kg). The red arrow indicates the administration of the drug. The shaded region represents the dark phase. Average SEM current recorded by the sensors was 0.051 nA (n = 12).

Similar to the baseline NO data (see Figure 6.7) diurnal changes are observed; an increase in the NO signal is observed during the light phase while a decrease in the NO signal is recorded during the dark phase when the animals are more active. This is the same result as observed in the baseline data postulating that reserpine does not interfere with the sleep-wake cycle of the animals, at least in terms of diurnal cycle. Reserpine however, depletes various biogenic amines including serotonin and catecholamines such as dopamine and norepinephrine, therefore it would be expected to cause profound changes in the sleep cycle. Hoffman & Domino demonstrated the comparative effects of reserpine (0.01, 0.04 and 0.14 mg/kg) on the sleep cycle of man and cat. This research found that reserpine depressed slow wave or non-rapid eye movement (NREM) sleep in man and cats. This effect was seen on the night of reserpine administration as well as two or three subsequent nights after administration in man, however in cats the duration of this dose dependent effect was 24 -36 hr. Rapid eye movement (REM) sleep was greatly depressed for 48 hr in the cat, while in man REM sleep was sharply decreased on the night of reserpine administration, with a subsequent large increase in REM sleep (35-66% of total sleep time) on the second

night after reserpine which exceeded the deficit observed the night after administration of the drug (Hoffman and Domino, 1969).

AUC analysis was performed in order to quantify any changes in the NO signal observed as a result of the systemic administration of reserpine. A 72 hr time period (3 days and 3 nights) was utilised and this was compared to the baseline data shown in Figure 6.7. The baseline was taken *ca.* 30 minutes (11:30-12:00) before the administration of the drug and each 12 hr time period was analysed individually and the mean calculated. All data was background subtracted before the AUC analysis was performed. Figure 6.12 compares the results of the AUC analysis on the baseline and reserpine data sets.

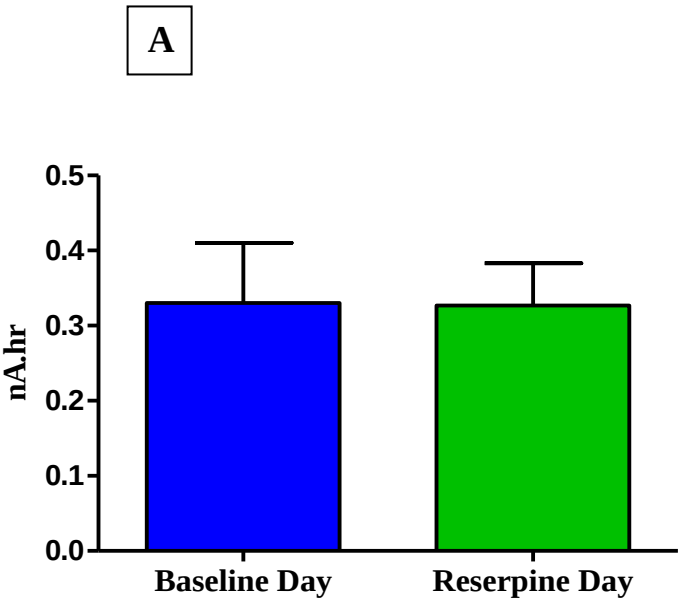

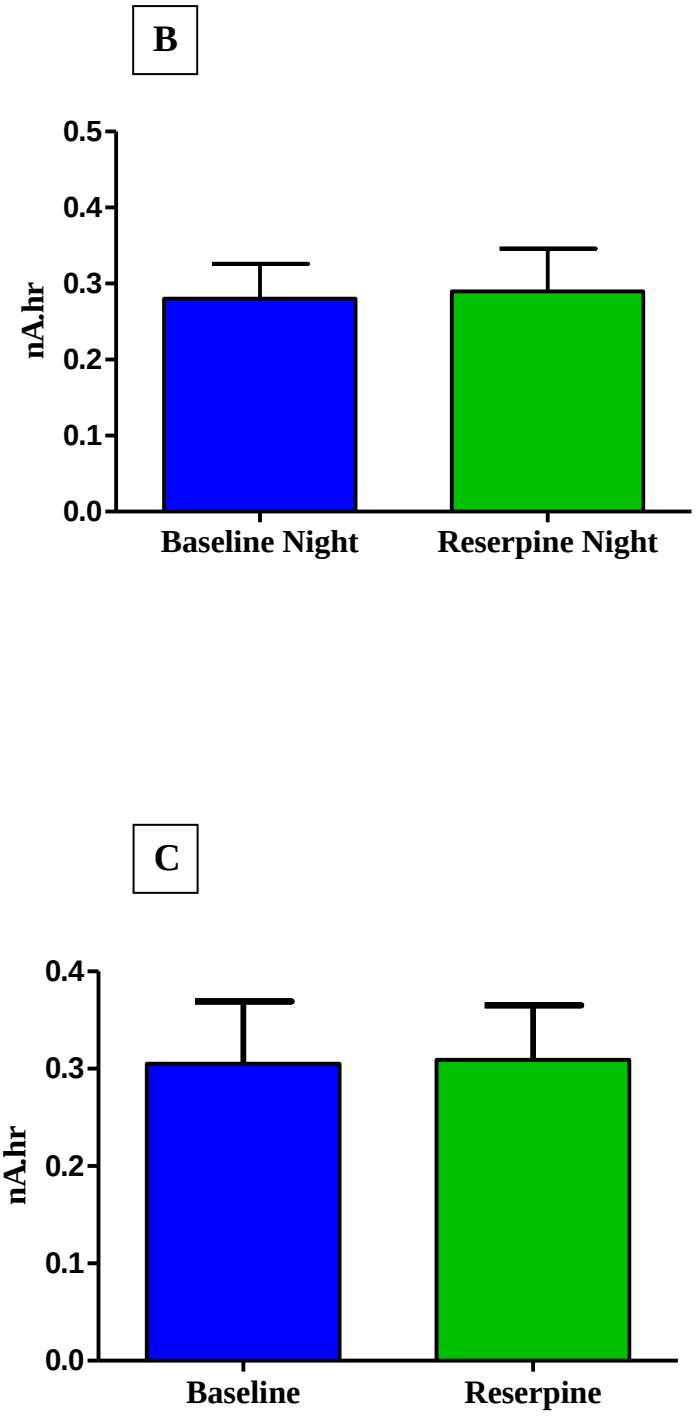

Figure 6.12: A bar chart displaying the changes in AUC for baseline NO levels and NO levels after a single systemic administration of reserpine (5 mg/kg) for NO sensors implanted in the striatum. This bar chart displays the changes over the course of 3 day periods (A) three night periods (B) and the total over the 72 hr (C) with the total area plotted.

It is clear, from the results displayed above that the AUC differs depending on the time of day. Similar to the results shown in Figure 6.8 the NO levels increase during the light phase highlighted by the larger AUC value recorded of 0.33 ± 0.08 nA.hr (n = 9) when compared to the night period where an AUC value of 0.28 ± 0.05 nA.hr, (n = 13) was recorded for the baseline data over a 72 hr time period. Comparing the AUC value for striatal NO levels recorded during the day shows no significant difference (P = 0.9750) between the value recorded after the administration of reserpine (0.327 ± 0.056, n = 12) and the baseline value of 0.33 ± 0.08, (n = 9). The AUC values recorded during the night period show similar results to the day period. Interestingly, almost identical AUC values (P = 0.8632) were recorded for the baseline NO levels (0.28 ± 0.046, n = 13) and the NO levels after reserpine administration where an AUC value of 0.29 ± 0.056 nA.hr was calculated. Similarly, analysing the data over a 72 hr period observed almost identical (P = 0.9632) AUC values of 0.305 ± 0.064 nA.hr (n = 13) for the baseline and a value of 0.309 ± 0.056 nA.hr (n = 12) after reserpine administration. These results suggest that reserpine does not alter the NO levels in the striatum.

Throughout these experiments the animals were accessed for good health and any changes in their natural behaviour were documented. This administered dose of reserpine is reported to cause hypolocomotion, muscle rigidity catalepsy, limb rigidity, and oral tremor. Reserpine can also induce aversive and recognition memory deficits, anxiety like behaviour and depressive and anhedonic–like behaviour (Leão *et al*., 2015). After the administration of reserpine, the animals maintained their weight, showed minor changes in their natural behaviour (front feet raised) and although more subdued/ less active during the day, they behaved normally when provoked.

In summary, this section highlights the influence a single (5 mg/kg) dose of reserpine has on striatal NO levels and also demonstrates the diurnal changes observed during the light and dark cycles. AUC analysis was performed to quantify the changes in NO levels, however, it was demonstrated that no significant difference was recorded after reserpine administration when compared to baseline levels.

6.3.4. Oxygen Sensors Single Dose Reserpine

6.3.4.1: Baseline Oxygen Recording

All O_2 sensors utilised during the *in-vivo* experiments were carbon paste electrodes and were calibrated prior to implantation to ensure sufficient sensitivity was achieved. These carbon paste electrodes are favourable for *in-vivo* use, with the research group demonstrating no significant variation in the baseline O_2 current observed over a 21 day period. This research also demonstrated a stable baseline when recording from these electrodes for up to 84 days (Bolger *et al.*, 2011(b)). However, the O_2 baseline can undergo spontaneous fluctuation attributed to physiological phenomena such as feeding, grooming and activity (Lowry *et al.*, 1997) several times during a 24 hr period.

Research has demonstrated that changes in tissue O_2 levels measured by carbon paste electrodes are related to changes in cerebral blood flow (Lowry *et al.*, 1997) which are then comparable to the BOLD signal from fMRI studies (Lowry *et al*., 2010) (Francois *et al.*, 2012). Therefore, tissue O_2 levels measured using these electrodes can be used to evaluate neural activity in localised brain regions in freely moving animals (Li *et al*., 2011) (Russell *et al.*, 2012). These carbon paste electrodes have been utilised in an animal model of schizophrenia (Finnerty *et al.*, 2013(a)) where the changes in O_2, NO and glucose levels were monitored after administration of various quantities of PCP. Kealy *et al.* also used these sensors for the simultaneous recording of O_2 and glucose in the hippocampus (Kealy *et al.*, 2013). Therefore, these carbon paste electrodes are ideal for *in-vivo* monitoring of O_2 levels in this PD animal model. Different tissues have different O_2 demands depending on their metabolic needs. The consumption of O_2 also results in the generation of free radicals that have damaging effects on cells and are implicated in neurodegeneration. The brain is particularly vulnerable to the effects of these ROS due to its high demand for O_2 and its abundance of highly peroxidisable substrates (Gandhi and Abramov, 2012). Reserpine has been used as a treatment for hypertension (see Section 6.3.4.3) and as mentioned above tissue O_2 measured by carbon paste electrodes are related to changes in cerebral blood

flow. Average baseline data for carbon paste electrodes implanted in the striatum over 84 hr period is shown below in Figure 6.13.

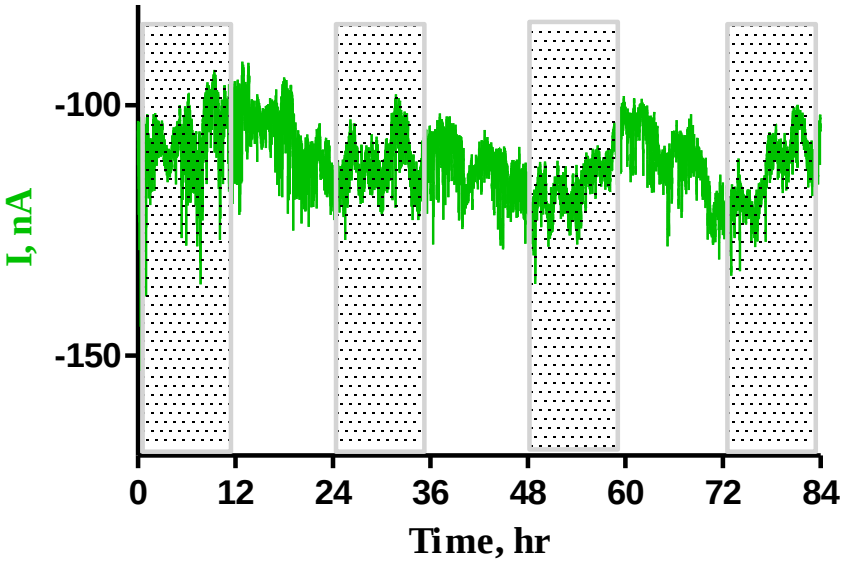

Figure 6.13: A time *vs.* current change graph of baseline O_2 currents monitored using carbon paste electrodes (6 sensors in 3 animals) implanted in the striatum over 84 hr. The shaded region corresponds to the dark phase. The average SEM current recorded for the O_2 sensors was 15.28 nA (n = 6)

It is clear, from this real-time continuous trace that striatal O_2 levels change depending on the time of day. It is evident that O_2 levels increase during the light phase (when the animals tend to sleep) symbolised by an increase in the reduction current and there is a decrease in O_2 levels during the dark phase marked by a decrease in the reduction current. As this measured real-time O_2 change is the dynamic balance between supply and utilisation, utilisation is higher during the dark cycle when the animals are more active. Literature has reported that physiological phenomena influence the O_2 signal, for example a 22 nA increase in measured O_2 is observed for grooming and a 26 nA increase for feeding/drinking (Bolger *et al.*, 2011(b)). Kealy *et al.* determined the basal O_2 concentration in the hippocampus by matching the baseline current to the post-implantation sensitivity, these results found that the concentration was higher during the day (100.26 ± 5.76 µM) and decreases slightly during the night (99.37 ± 5.51 µM) (Kealy *et al.*, 2013) which is similar for carbon paste electrodes implanted in the striatum as shown in Figure 6.13 above. McHugh *et al.* used CPA and carbon paste

electrodes to monitor changes in tissue O_2 and demonstrated that tissue O_2 signals were typically highest during REM sleep, active waking period, then quiet sleep and NREM sleep. This research revealed significantly higher O_2 signals during REM sleep compared with NREM and quiet waking but not active waking (McHugh *et al*., 2011).

AUC analysis was performed to quantify the changes in striatal O_2 levels over a normal 72 hr time frame. The data was analysed during the light (07:00-19:00) and during the night (19:00-07:00) period over a 72 hr period (3 day periods, 3 night periods). All data was background subtracted (first 30 minutes of each time period was taken as the baseline) and each 12 hr time period was analysed individually and the average was calculated. The net area for each time period was plotted in a bar chart as presented below in Figure 6.14

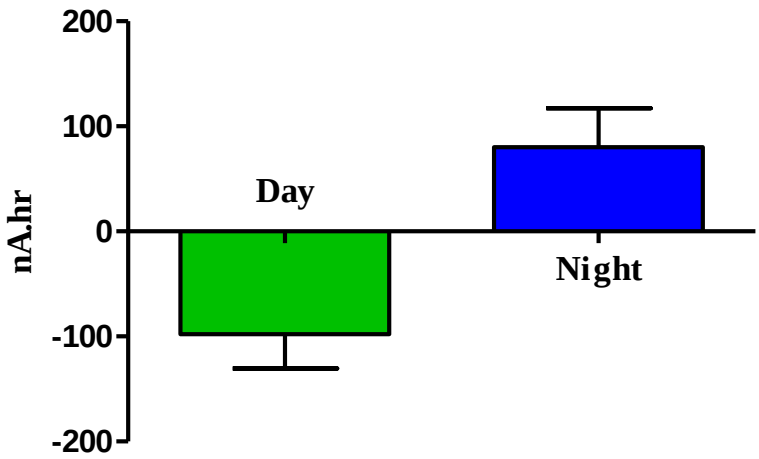

Figure 6.14: A bar chart demonstrating the changes in AUC for O_2 levels over a 72 hr period (3 day periods and 3 night periods) in 3 animals (n = 6). All data was background subtracted and the net area calculated was plotted.

It is clear from the results above that striatal O_2 levels change depending on the time of day. As observed previously in Figure 6.13 O_2 levels increase during the day when the animals tend to sleep and decrease during the night period when the animals are more active. An increase in O_2 levels during the day period is further supported by the negative net total AUC value of -97.8 ± 32.57 nA.hr (n = 6) recorded. A positive net area total of 80.02 ± 37.12 nA.hr (n = 6) was calculated during the night period symbolising a decrease in the O_2 levels which was observed previously in Figure 6.13. O_2 levels are very variable over a 24 hr time period therefore, a more targeted test was

performed. AUC analysis was performed taking the last 4 hr of both the day and night periods. Similarly, this result recorded a negative net area of -15.03 ± 5.12 nA.hr (n = 6) for the last 4 hrs of the day period and a positive value of 15.15 ± 9.76 nA.hr (n = 6) for the last 4 hrs of the night period. This AUC analysis is used to quantify the changes observed in the O_2 levels over a 24 hr time period. No significant difference (P = 0.7262) in the net area is observed when comparing the day and night period striatal O_2 levels which highlights the importance of considering the diurnal O_2 changes when analysing data over long periods of time.

Another important factor is baseline stability, especially as these carbon paste electrodes could be implanted for at least 20 days. Bolger and Lowry demonstrated the stability of the carbon paste electrodes over long periods of time in the *in-vivo* environment. This work observed no significant variation in the O_2 baseline over a 21 day period which was monitored by carbon paste electrodes implanted in the striatum, hippocampus, prefrontal cortex and nucleus accumbens of Wistar/Sprague-Dawley rats. This research also demonstrated a stable baseline when recording from these electrodes for up to 84 days (Bolger *et al*., 2011(b)).

This continuous real-time baseline trace will be used to provide a comparison to determine the impact a single 5 mg/kg dose of reserpine has on striatal O_2 levels. It is imperative to have baseline data corresponding to the differences in the O_2 levels recorded during the light and dark phases to provide a comparison for the diurnal changes observed after administration of the drug. In summary, this section demonstrates the diurnal O_2 changes observed over a 24 hr time period and these changes were quantified using AUC analysis where a significant difference was determined for the O_2 levels monitored during the light and dark cycles.

6.3.4.2 Saline Administration

A typical example of the effect a saline administration (NaCl, 0.9%, s.c.) has on the O_2 current is shown in Figure 6.15(a) and Figure 6.15(b). The systemic administration of 1 mL saline subcutaneously is used as a control for the reserpine injection – thus the initial effects of the injection can be eliminated. Figure 6.15(a) shows the average O_2 response of 5 O_2 sensors implanted in the striatum of 2 animals upon the

administration of a saline injection subcutaneously over a 90 minute period, while Figure 6.15(b) shows a typical example of a saline injection highlighting the initial effects of the injection on the O_2 levels in the striatum.

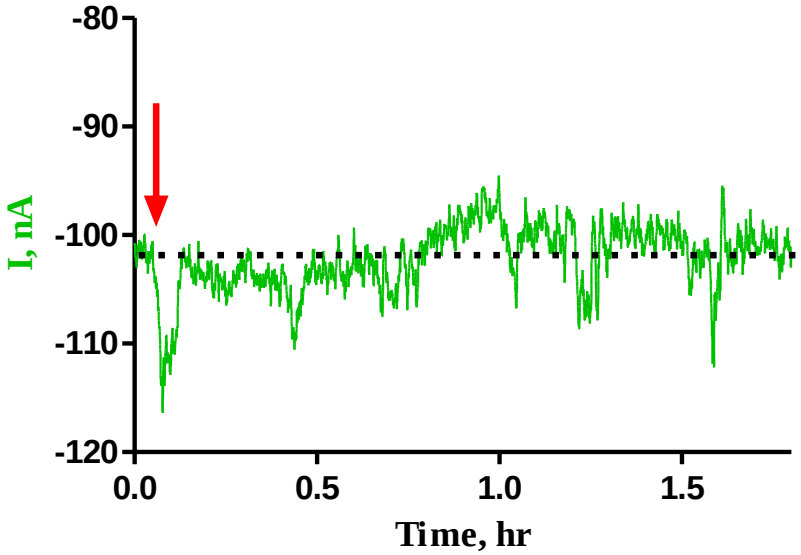

Figure 6.15(a): Mean current *vs.* time response for striatal O_2 levels following the administration of a 1 mL saline injection subcutaneously (n = 5). The red arrow indicates the point of injection. Average SEM recorded for the O_2 sensors was 14.63 nA (n = 5).

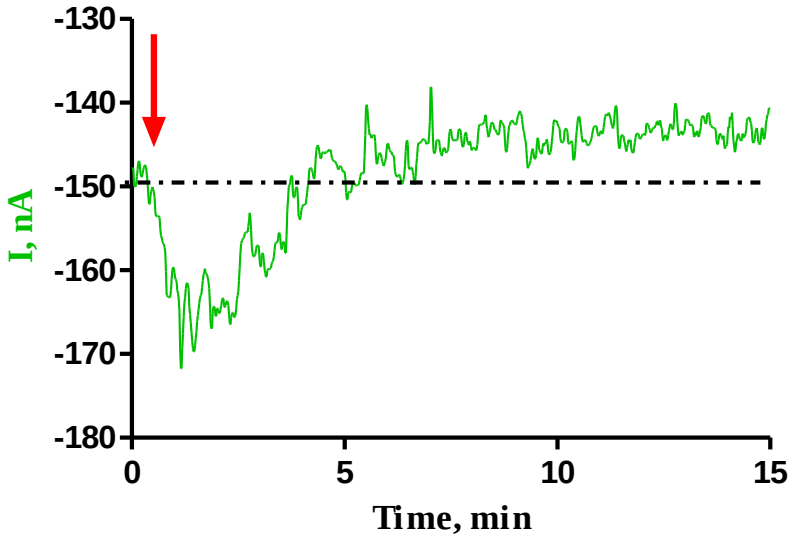

Figure 6.15(b): A typical example of a 1 mL saline injection monitored using an O_2 sensor implanted in the striatum of a freely-moving animal. The arrow indicates the point of injection.

Analysis of the data in Figure 6.15(a) and Figure 6.15(b) indicates an increase in the observed O_2 current upon injection of saline. The current changed (P = 0.6423) from a baseline current of -103.9 ± 16.1 nA (n = 5) to -116.4 ± 20.2 nA (n = 5) after saline administration. This ~ 13 nA change was observed *ca.* 1 minute after the initial injection. This O_2 response is short lived and the signal returned to a post injection baseline of (-104.4 ± 16.2 nA, n = 5) within *ca.* 5 minutes.

This initial response is attributed to physical manipulation of the animal which resulted in the observed stress response. Bolger *et al.* showed a similar transient response on administration of a saline injection i.p. observing an increase of 13.5 ± 3.7 nA (n = 4) (Bolger and Lowry, 2005). This is similar to the results obtained in this section with an increase of 12.46 ± 6.2 nA (n = 5) being obtained after the administration of a saline injection subcutaneously.

In summary, this section demonstrated the effect the administration of a 1 mL saline injection subcutaneously has on O_2 levels. No significant difference in the current (P = 0.6423) was observed after the administration of the injection and the O_2 levels returned to baseline levels after *ca.* 5 minutes. These results will be used as a control for the reserpine injection to account for the initial change in O_2 levels attributed to a stress response.

6.3.4.3 Single (5 mg/kg) Reserpine Administration

Reserpine has been used in the treatment of high blood pressure for centuries, however in westernised countries its use has fallen precipitously due to several adverse side effects caused in the 1950's and 60's. These side effects include depression, gastric bleeding and breast cancer. However, these side effects were observed when the daily dose of reserpine was 0.25 mg three times daily to as much as 10 mg per day. This dose is considerable higher than the dose recommended now of between 0.05–0.25 mg/day, which is well tolerated with many of these adverse side effects no longer evident (Barzilay *et al.*, 2007). A daily dose of 0.5 mg/day of reserpine provides modest antihypertensive action and blood pressure is reduced by 3/5 mm Hg. In combination with a thiazide a more pronounced decrease in blood pressure is observed reaching 14/11 mm Hg. A single daily dose of 0.25 to 0.5 mg produces the

antihypertensive effect as its pharmacological action develops slowly and continues for a long time - its effectiveness is attested to its worldwide use (Rosenthal and Page, 2012).

Carbon paste electrodes have been demonstrated to serve as an index of increases in regional cerebral blood flow when the supply of O_2 from the blood stream shows a substantial increase over utilisation. In this instance the measurement of O_2 in brain tissue monitored by a carbon paste electrode can be used as a reliable index of increases in cerebral blood flow (Lowry *et al*., 1997). The short-term effect of the administration of reserpine is shown in Figure 6.16(a). This demonstrates the effect the administration of a single 5 mg/kg reserpine injection has on the O_2 signal monitored by carbon paste electrodes over an 8 hr period after the administration of the drug subcutaneously.

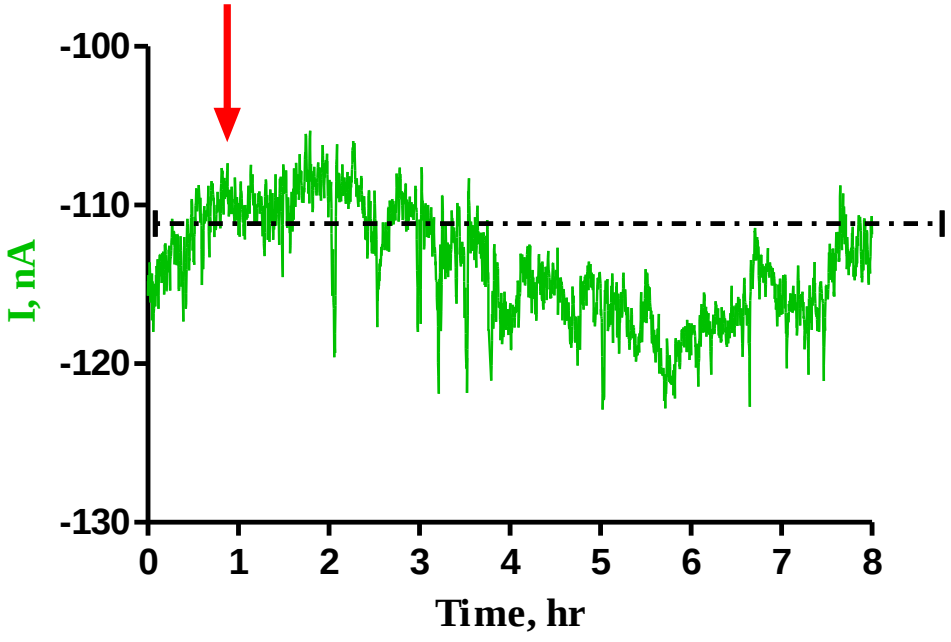

Figure 6.16(a): Mean time *vs.* current profile of the short-term effect of a single 5 mg/kg s.c. injection of reserpine on O_2 levels recorded using carbon paste electrodes implanted in the striatum of freely moving animals (n = 6). The red arrow is indicative of the point of injection. Average SEM recorded for the carbon paste electrodes was 13.16 nA (n = 6)

Figure 6.16(a) shows the O_2 response monitored for a period of 8 hrs immediately following the systemic administration of reserpine (5 mg/kg). It is evident, that the O_2 levels remain stable, however, the levels increased after ~ 3 hrs and remain increased for the remainder of the 6 hr time period observed. AUC analysis was performed and no significant difference (P = 0.8460) was demonstrated between the value calculated 6 hr after the saline administration (37.76 ± 7.82 nA.hr, (n = 3)) to the value obtained after the reserpine administration (40.54 ± 8.75 nA.hr, (n = 6)). These spontaneous fluctuations in the baseline can be attributed to physiological stimuli such as grooming and feeding as naturally occurring deviations in the O_2 baseline occur several times during a 24 hr period. This is reflective of the real-time measurement of O_2 as the dynamic balance between supply and utilisation (Bolger *et al.*, 2011(b)). However, the effectiveness of the carbon paste electrodes ability to monitor real-time O_2 changes has been previously published and is observed below in Figure 6.16(b). This figure shows a typical example of the effect an intraperitoneal injection of chloral hydrate (350 mg/kg) has on O_2 levels monitored in the rat striatum.

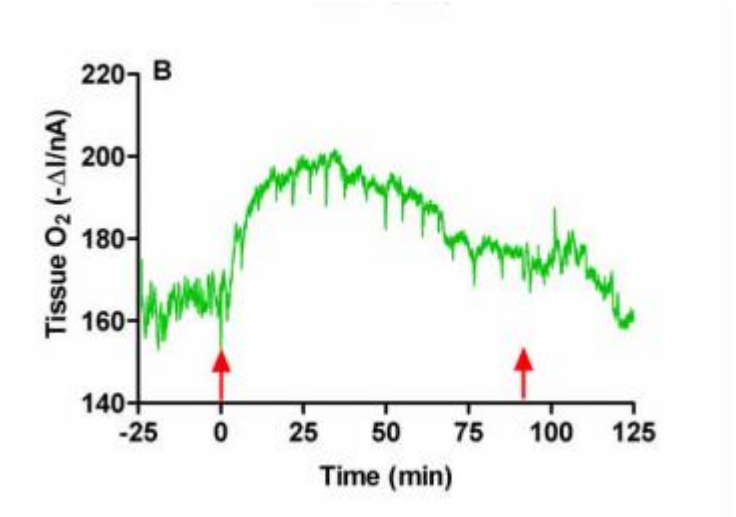

Figure 6.16(b): A typical example of the effects of an intraperitoneal injection of chloral hydrate (350 mg/kg) on tissue O_2 monitored in the rat striatum with a carbon paste electrode. The arrows indicate the point of injection and also recovery from the anaesthetic. Figure from (Bolger and Lowry, 2005)

This figure shows the effect that the administration of chloral hydrate has on O_2 levels. This demonstrates the effectiveness of the carbon paste electrodes in monitoring changes in O_2 levels following pharmacological intervention. However, comparing the above figure where an instantaneous increase in the O_2 levels is recorded following the administration of chloral hydrate, there seems to be no change in the O_2 levels over an 8 hr period after the administration of reserpine. This trend suggests that reserpine administration induces no effect in changing tissue O_2 levels monitored by carbon paste electrodes implanted in the striatum.

Hafkenschiel *et al.* showed preliminary observations detailing the effects of reserpine (a total dose varying between 2.5 and 5.5 mg) on cerebral blood flow, O_2 and glucose metabolism in five hypertensive patients one hour after administration of the injection. This research demonstrated that cerebral blood flow, glucose and O_2 consumption remained constant (Hafkenschiel *et al.*, 1955). Analysing the data shown above in Figure 6.16(a) showed no significant change ($P = 0.8455$) in the O_2 levels two hrs after administration of the drug (-113.78 ± 11.69 nA, $n = 6$) when compared to the pre-injection baseline of -110 ± 11.69 nA, $n = 6$). Similarly, five hrs after the administration of the drug there is a slight change ($P = 0.6383$) in O_2 levels recorded to -119.46 ± 13.99 nA ($n = 6$) compared to the pre-injection baseline of -110.35 ± 11.69 nA ($n = 6$). Reserpine is known to exhibit long-term effects therefore the O_2 levels were monitored and analysed over a 120 hr time period (see Figure 6.16(c)) in order to investigate the effects of the drug over such periods.

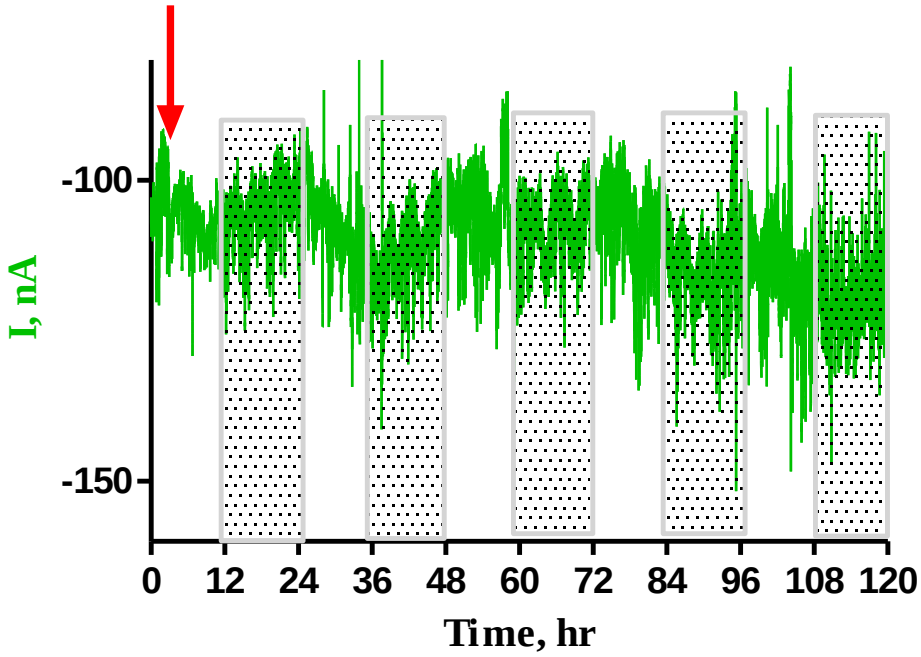

Figure 6.16(c): The average O_2 signal (n = 5) recorded in the striatum over a continuous 120 hr period after the systemic administration of reserpine (5 mg/kg). The red arrow indicates the administration of the reserpine. The shaded region represents the dark phase. Average SEM recorded for the carbon paste electrodes was 18.56 nA (n = 5).

It is clear, from the results above that diurnal changes are observed very similar to those demonstrated in the continuous O_2 baseline graph (see Figure 6.13). Similar to the baseline data the O_2 levels increase during the light cycle and decrease during the dark phase when the animals are more active. However, the O_2 levels are relatively stable over the 120 hr time period except for small spontaneous fluctuations in the O_2 signal which are expected. AUC analysis was performed on the reserpine and the baseline O_2 data recorded by carbon paste electrodes in order to quantify any changes in the O_2 levels observed following the drug administration. This analysis was performed over a 72 hr time period starting at 11:30 and each 12 hr period was analysed individually and the average of the 3 values calculated. All data was background subtracted with the first 30 minutes of each day and night period used as the baseline before AUC analysis was performed and the results are shown below in Figure 6.17.

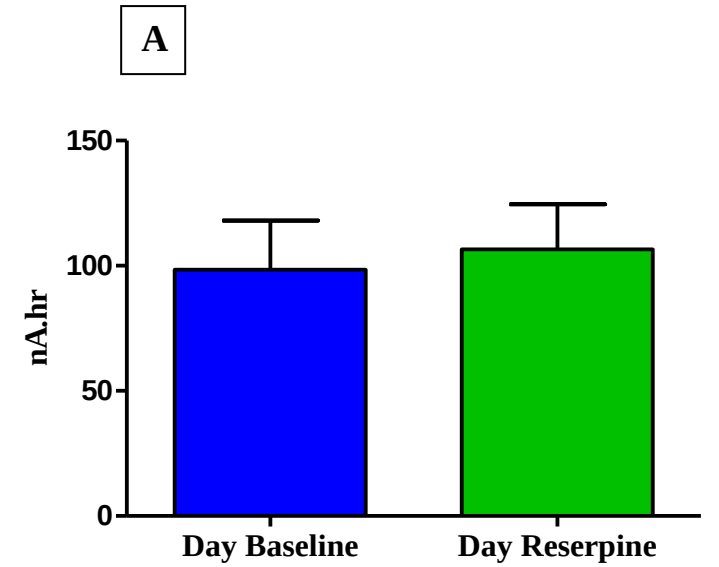
A
150
100
50
0
nA.hr
Day Baseline
Day Reserpine

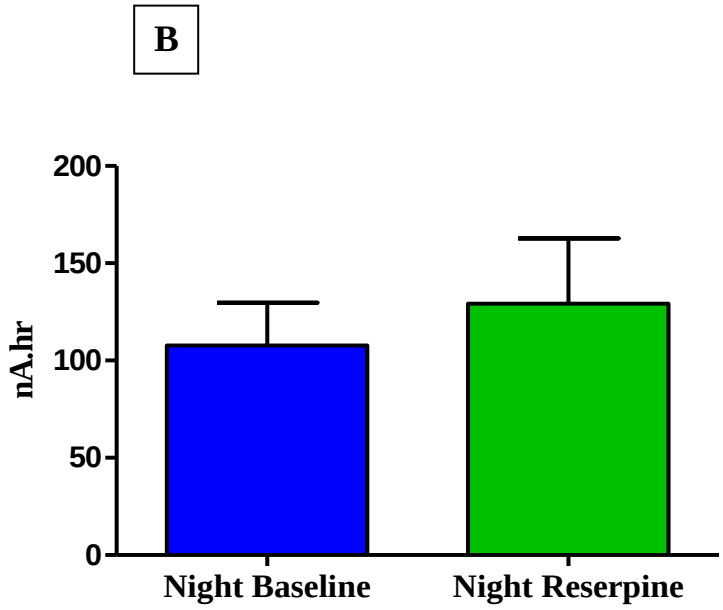
B
200
150
100
50
0
nA.hr
Night Baseline
Night Reserpine

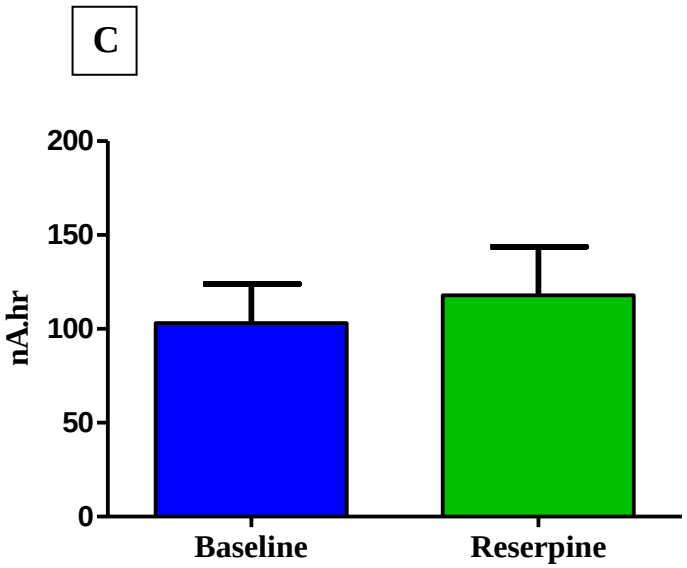

Figure 6.17: A bar chart displaying the changes in AUC for baseline O_2 levels and O_2 levels after a single systemic administration of reserpine (5 mg/kg) for carbon paste electrodes implanted in the striatum. This bar chart displays the changes over the course of 3 day periods (A) 3 night periods (B) and then over 72 hr (C) with the average total area plotted.

It is clear, from the results above that only small variations in the O_2 levels are observed during the dark and light periods after the administration of reserpine. Analysing the data shows an increase in the total area recorded from 98.43 ± 19.60 nA.hr (n = 6) during the light period to 129.26 ± 33.49 nA.hr obtained during the night period. This is indicative of the diurnal O_2 changes where an increase is observed during the light period, i.e. smaller value as higher number of negative peaks recorded and a decrease is observed during the dark period highlighted by the higher total area value calculated. Comparing the baseline and the long-term reserpine effects on striatal O_2 levels using the AUC analysis shows no significance difference (P = 0.7711) between the baseline value of 98.43 ± 19.60 nA.hr (n = 6) and the reserpine treated value of 106.56 ± 18.06 nA.hr (n = 5) during the 3 day periods recorded over the 72 hr time period. Similarly, no significant difference (P = 0.5921) is observed between the baseline value of 129.26 ± 33.49 nA.hr (n = 6) compared to the reserpine treated value of 107.67 ± 22.10 nA.hr (n = 5) calculated over 3 night periods. These results suggest that the O_2 levels remain stable and unchanged from baseline after the administration of a single 5 mg/kg reserpine injection when comparing 72 hr time periods using AUC analysis. Analysing the data over the 72 hr period shows almost

identical (P = 0.6608) AUC values of 113 ± 26.54 nA.hr (n = 6) for the baseline and 107.11 ± 20.08 nA.hr (n = 5) after reserpine administration.

Again, similar to the NO experiments no signs of motor impairment were observed in the animals. The animals appeared to behave naturally and reacted normally when provoked, however they appeared more subdued after administration of reserpine. Similarly, some animals showed a front paws raised affect and appeared to be less active than the previous days. Some animals showed an increase in weight after the administration of reserpine with animals gaining up to 10 g overnight. Weight gain is a common side effect of this drug.

6.3.5 Effect of Multiple Dose Reserpine on Nitric Oxide Levels

6.3.5.1 Baseline Nitric Oxide Recording

All NO levels were monitored continuously over several days using NO sensors (see Section 3.5.3) implanted in the striatum. As mentioned previously, these electrodes are ideal for *in-vivo* use demonstrating a high sensitivity to NO, good selectivity, fast response time and long-term stability in the *in-vivo* environment. Average baseline data for NO sensors implanted in the striatum over 72 hrs is shown below in Figure 6.18.

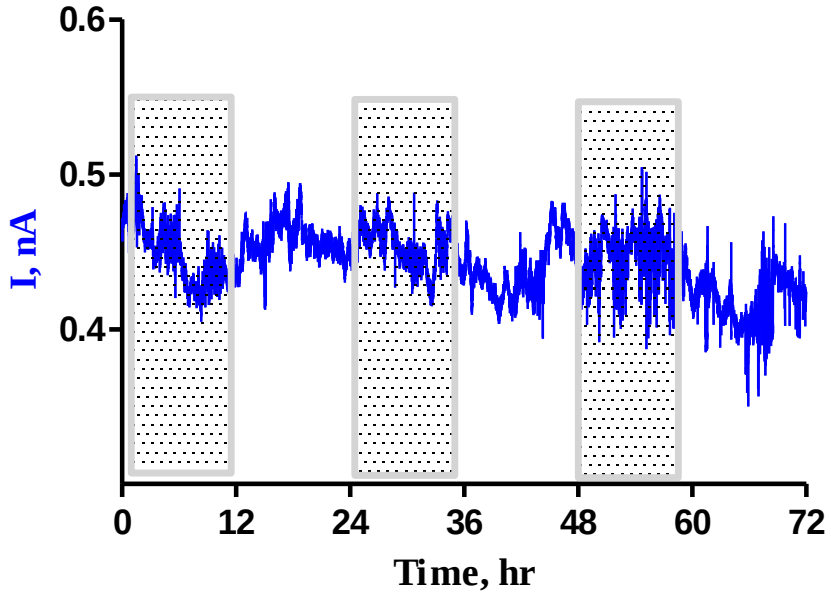

Figure 6.18: A time *vs.* current change graph of baseline NO levels monitored by NO sensors (n = 4) implanted in the striatum over 72 hrs. The shaded region corresponds to the dark phase. Average SEM recorded for the NO signal was 0.046 nA (n = 4)

It is clear, that the same diurnal changes are observed similar to Figure 6.7. During the light phase (07:00-19:00) NO levels increase while during the dark phase (19:00-07:00) NO levels decrease. The baseline current remains stable over the 72 hrs with only small fluctuations observed and no significant difference (P = 0.3503) observed between the current recorded after the first hour (0.476 ± 0.057 nA) when compared to that at 72 hrs (0.383 ± 0.072 nA). This is imperative as the next section investigates the use of these NO sensors in a chronic PD model for up to 30 days. The animals were submitted to repeated administration (10 injections in total) of a sub-effective dose of reserpine (0.1 mg/kg) every second day. This baseline data will provide a comparison for the reserpine experiments where any deviation in the NO signal is attributable to a drug response.

6.3.5.2. Repeated Administration of Reserpine on Nitric Oxide Levels

Apart from the motor disturbance, other symptoms are presented by parkinsonian patients including expressive cognitive deficits which are related to dysfunction in working memory and also problem and planning solving. Furthermore, PD sufferers present alterations in stimulus response associations, implicit learning, feed-back based learning, reversal learning and spatial memory (Fernandes *et al.*, 2008). Cooper *et al.* demonstrated the indication of dissociation of cognition and motor control in early PD suggesting that cognitive dysfunction is independent of frontostriatal dopamine deficiency which underlies motor disability (Cooper *et al.*, 1991).

Recently, research has demonstrated that utilising reserpine at low doses modifies cognitive function without causing motor deficits. Carvalho *et al.* investigated several doses (0.1, 0.25 and 0.5 mg/kg) with all doses impairing memory, however, only the largest dose induced hypolocomotion (Carvalho *et al.*, 2006). Fernandes and co-workers also used various low doses of reserpine (0.1, 0.25 and 0.5 mg/kg) and then submitted the animals to various behavioural tasks including novel object recognition, contextual fear conditioning and a spatial working memory task 24 hrs after the administration of reserpine. Both the novel object recognition task and the spontaneous alternation task, which evaluates spatial working memory and recognition memory, showed no effects after administration of reserpine (i.e. exploring new objects and the amount of alternation) when compared to the control group. However, the contextual fear conditioning task showed a significant decrease in freezing duration found for the reserpine treated animals when compared to the controls (Fernandes *et al.*, 2008).

Another study by Fernandes and co-workers evaluated the repeated administration of reserpine as a possible pharmacological model of PD with progressive features. In this research, the animals were submitted to a repeated treatment of reserpine (0.1 mg/kg) and then motor behaviour, memory performance and the levels of lipid peroxidation were measured (Fernandes *et al.*, 2012). This research was used as a reference for the *in-vivo* experiments discussed in this section. Average NO levels monitored using NO sensors implanted in the striatum following the administration of ten reserpine (0.1 mg/kg) injections subcutaneously is shown below in Figure 6.19.

1

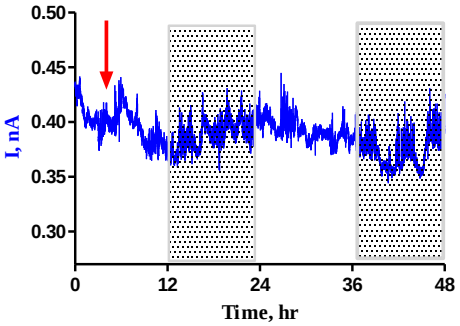
0.50
0.45
0.40
0.35
0.30
I, nA
0
12
24
36
48
Time, hr

2

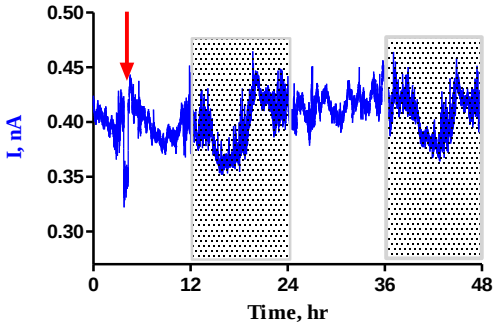
0.50
0.45
0.40
0.35
0.30
I, nA
0
12
24
36
48
Time, hr

3

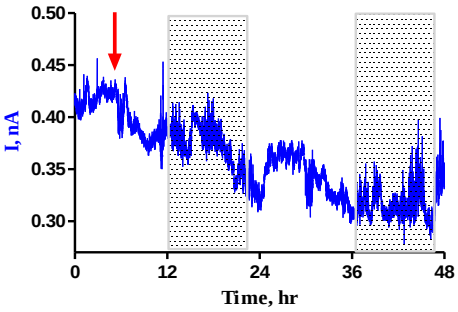
0.50
0.45
0.40
0.35
0.30
I, nA
0
12
24
36
48
Time, hr

4

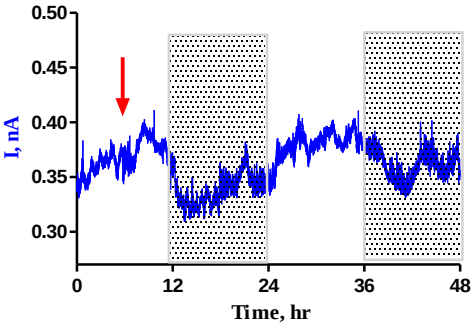
0.50
0.45
0.40
0.35
0.30
I, nA
0
12
24
36
48
Time, hr

5

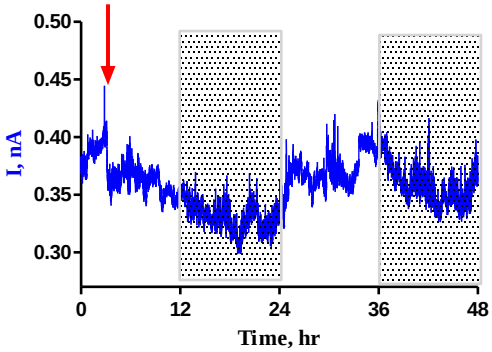
0.50
0.45
0.40
0.35
0.30
I, nA
0
12
24
36
48
Time, hr

6

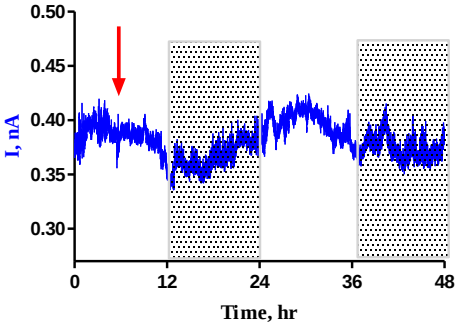
0.50
0.45
0.40
0.35
0.30
I, nA
0
12
24
36
48
Time, hr

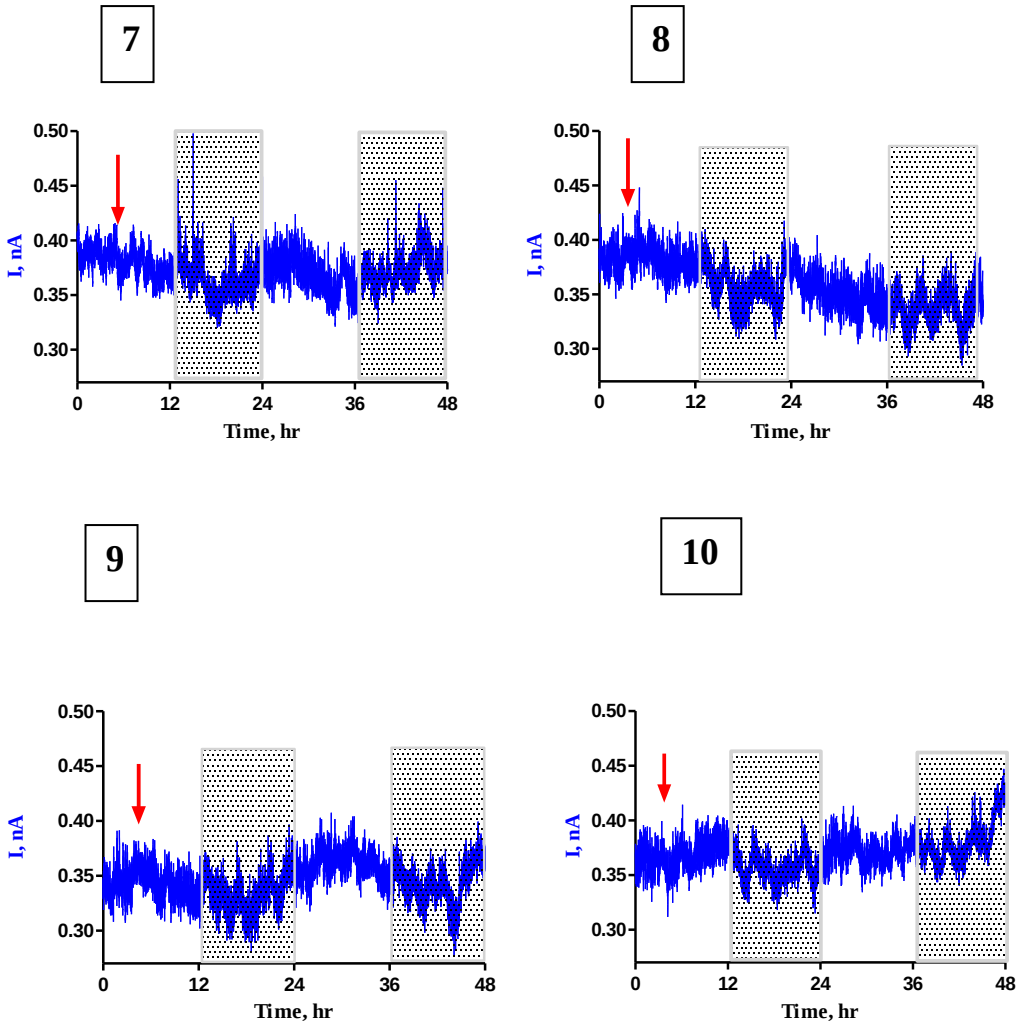

Figure 6.19: The average NO signal (n = 3 - 7) recorded in the striatum over a continuous 48 hr period after the systemic administration of reserpine (0.1 mg/kg). This figure depicts the repeated administration of reserpine (0.1 mg/kg). Each number corresponds to the relevant injection (1-10), the red arrow indicates the administration of the reserpine. The shaded region represents the dark phase.

The figure above illustrates the impact the repeated administration of reserpine induces on NO levels monitored by NO sensors implanted in the striatum. The diurnal changes are still evident with the same trend observed; an increase in the NO signal during the light phase when the animals are less active and a decrease in the NO signal during the dark phase when the animals are active. The administration of saline subcutaneously is used as a control for this set of experiments (see Section 6.3.3.2). There is an initial increase in NO levels after the administration of the reserpine

injection subcutaneously, however, the signal returns to baseline levels within 30 minutes.

Abílio and co-workers demonstrated a significant increase in striatal lipid peroxidation when compared to the control group when treated with alternate day reserpine (0.1 mg/kg) injections subcutaneously for 19 days (Abílio *et al.*, 2002). Similarly, Fernandes *et al.* demonstrated a significant increase in striatal lipid peroxidation after the treatment of Wistar rats with 10 (0.1 mg/kg) reserpine injections subcutaneously, however no significant difference was observed after the 7^{th} injection. This result shows the progressive nature of this animal model of PD. Conversely, no significant difference in the hippocampal lipid peroxidation was demonstrated 48 hrs after the administration of the 7^{th} or 10^{th} reserpine (0.1 mg/kg) injections (Fernandes *et al.*, 2012). Both these research publications measured lipid peroxidation by the quantification of malondialdehyde (MDA). Duplicates of each sample were used to determine the MDA by measurement of a fluorescent product formed from the reaction of this aldehyde with thiobarbituric acid. However, neither publications measured the NO levels directly but speculated that the treatment with reserpine can result in the accumulation of neurotoxic dopamine oxidants that can induce the production of ROS exceeding the ability of the antioxidant system to eliminate them resulting in oxidative damage (Caudle *et al.*, 2008) (Cadenas and Davies, 2000), therefore, an increase in NO is expected.

AUC analysis was performed in order to quantify any changes in striatal NO levels as a result of the administration of reserpine (0.1 mg/kg). Each 48 hr period corresponding to each reserpine injection (1-10) were analysed separately. The day and night periods AUC analysis were calculated individually in order to factor in the diurnal NO changes shown previously in Figure 6.7. All data was background subtracted prior to performing AUC analysis and then the total area was plotted as shown below in Figure 6.20.

A

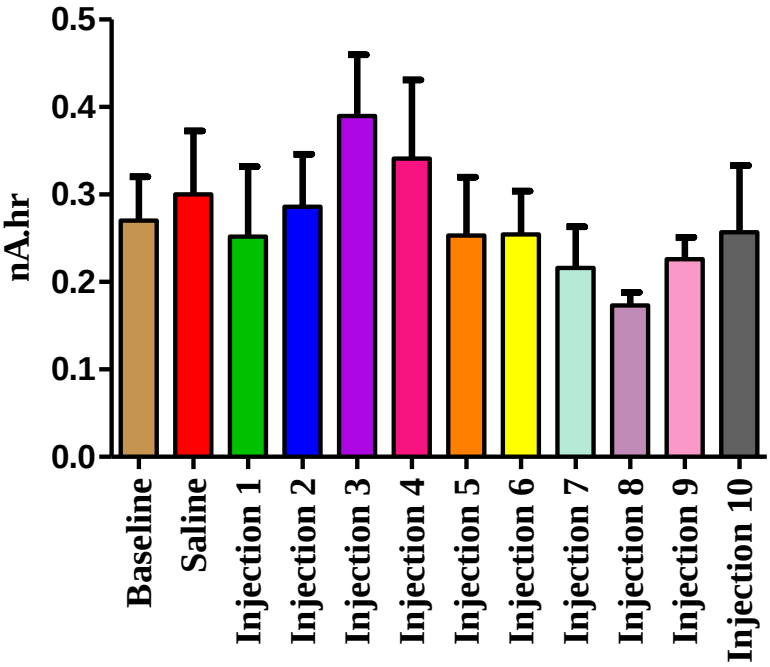
0.5
0.4
0.3
0.2
0.1
0.0
nA.hr
Baseline
Saline
Injection 1
Injection 2
Injection 3
Injection 4
Injection 5
Injection 6
Injection 7
Injection 8
Injection 9
Injection 10

B

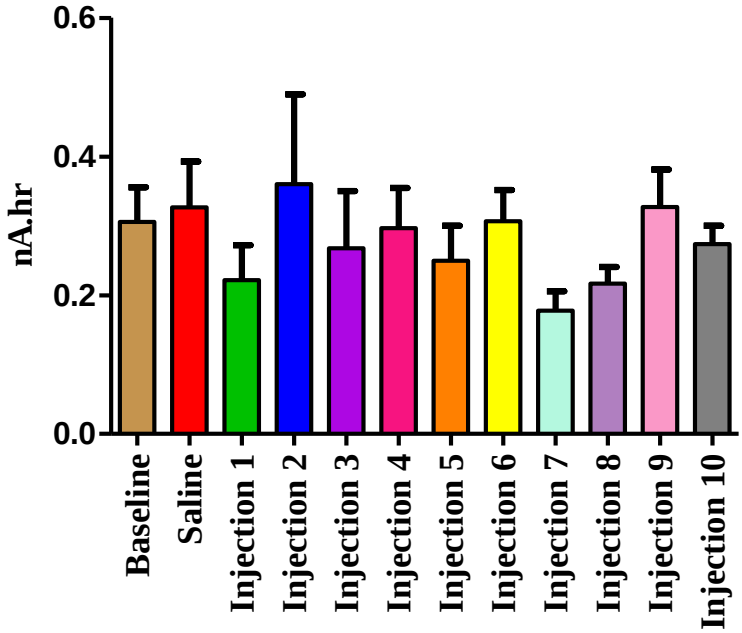
0.6
0.4
0.2
0.0
nA.hr
Baseline
Saline
Injection 1
Injection 2
Injection 3
Injection 4
Injection 5
Injection 6
Injection 7
Injection 8
Injection 9
Injection 10

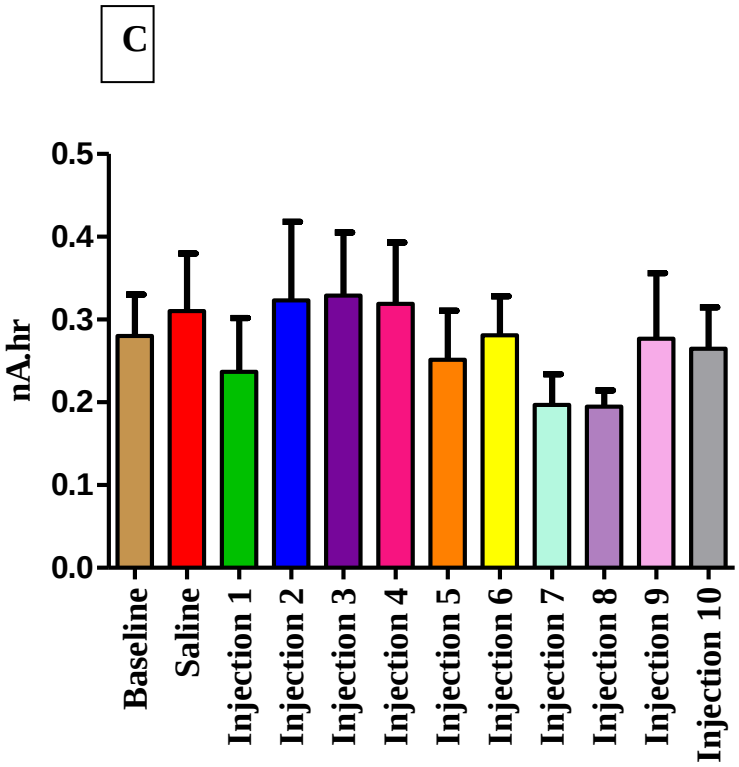

Figure 6.20: A bar chart displaying the changes in AUC for baseline NO levels, saline NO levels and NO levels during multiple injections of reserpine (0.1 mg/kg) monitored by NO sensors implanted in the striatum. This bar chart displays the changes over the course of 2 day periods starting at 11:30 (A) 2 night periods beginning at 23:30 (B) and then over the 48 hr period (C) with the average total area plotted.

The figure above displays the differences in the AUC values calculated for the NO levels in the striatum over two day periods (A), two night periods (B) and over the 48 hr period (C). However, these results are preliminary, the experiments need to be repeated to provide conclusive results as the last 4 injections show data corresponding to one animal with 4 NO sensors implanted. Over a 48 hr period there is no significant difference ($P = 0.7504$) observed between the AUC calculated for the baseline (0.288 ± 0.05 nA.hr, $n = 6$) and the saline injection (0.31 ± 0.07 nA.hr, $n = 7$). This indicates that the initial injection stress does not influence the AUC analysis, therefore any noticeable differences in the AUC calculated can be attributed to a reserpine affect.

Analysing the data over 48 hrs, it is noticed that a decrease ($P = 0.6115$) is observed after injection 1 (0.237 ± 0.075 nA.hr, $n = 6$) when compared to the baseline value of 0.288 ± 0.05 nA.hr ($n = 7$), however injections 2, 3 and 4 show almost identical values of 0.323 ± 0.095 nA.hr ($n = 3$), 0.329 ± 0.076 nA.hr, ($n = 3$) and 0.319 ± 0.074 nA.hr

(n = 7) respectively and are not significantly different (P = 0.6679, P = 0.5970 and P = 0.6819) to the baseline of 0.288 ± 0.05 nA.hr (n = 6). Injection 5 shows a decrease (P = 0.7248) in the AUC calculated to 0.2515 ± 0.059 nA.hr (n = 7) and a similar result is observed for the 6th injection where an AUC value of 0.281 ± 0.047 nA.hr (n = 7) is observed which is not significantly different (P = 0.9886) to the baseline value of 0.288 ± 0.07 nA.hr (n = 6). No significant decrease (P = 0.2634) is observed during the 48 hr period after the administration of the 7th reserpine injection when compared to the baseline value (0.288 ± 0.05 nA.hr, n = 6). In this instance an AUC value of 0.197 ± 0.0375 nA.hr (n = 4) was calculated. Similarly, a decrease (P = 0.2232) is recorded for the AUC value calculated for the 8th injection, however, an almost identical value to injection 7 was recorded, with a value of 0.195 ± 0.0195 nA.hr (n = 4) being achieved. Injection 9 and 10 shows no significance difference (P = 0.9737 and P = 0.8443) in the total area calculated compared to the baseline with values of 0.277 ± 0.079 nA.hr (n = 4) and 0.265 ± 0.05 nA.hr being recorded respectively.

It is important to emphasise that these results are preliminary and further investigations using this progressive model are needed to verify these findings as the last 4 injections have n = 4 in one animal. However, the animals submitted to this sub-effective reserpine dose every second day appeared to show all signs of natural behaviour, maintained their weight throughout the course of the 20 days and reacted normally when provoked. However, ocular discharge was observed in the animals - again this is hypothesised to be a drug effect with nasal congestion known to be the main side effect of the drug when administered to treat hypertension. Fernandes and co-workers speculate a correlation between the striatal lipid peroxidation observed after injection 10 with the motor impairment observed during the catalepsy behaviour (Fernandes *et al*., 2012). However, no motor impairments appeared in any of the animals used in this research.

6.3.6. Effect of Multiple Dose Reserpine on O_2 levels

6.3.6.1. Baseline Oxygen Recording

All O_2 levels were monitored using carbon paste electrodes implanted in the striatum. As mentioned previously, these electrodes are ideal for *in-vivo* use demonstrating a high sensitivity to O_2, good selectivity, fast response time and long-term stability in the *in-vivo* environment. Average baseline data for carbon paste electrodes implanted in the striatum over an 84 hr period is displayed below in Figure 6.21.

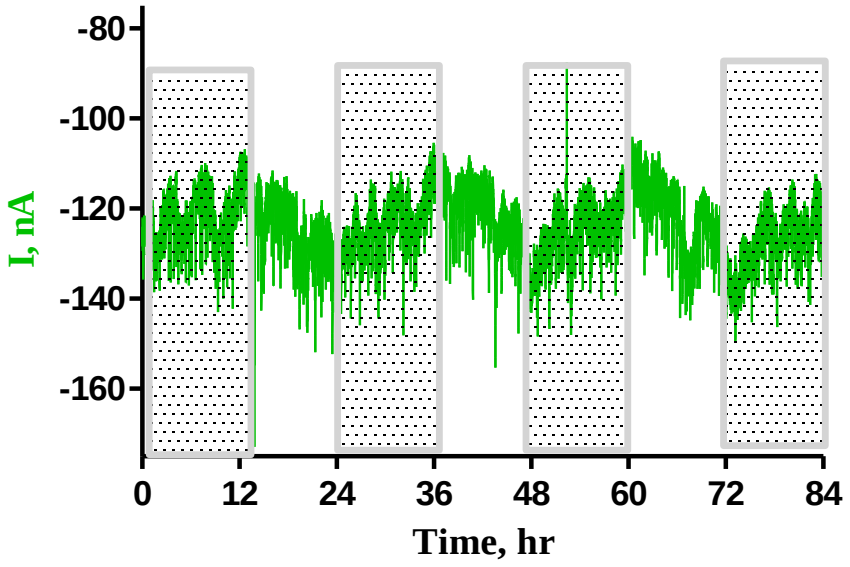

Figure 6.21: A time *vs.* current change graph of baseline O_2 currents monitored using carbon paste electrodes (8 sensors in 2 animals) implanted in the striatum over 84 hrs. The shaded region corresponds to the dark phase. The average SEM current recorded for these sensors was 6.62 nA (n = 8)

The results above show the same trend as observed in Figure 6.13. The O_2 levels were monitored using carbon paste electrodes implanted in the striatum and display characteristic diurnal changes. The O_2 levels increase during the light phase when the animals usually sleep and decrease during the dark phase when the animals are more active. This suggests that O_2 utilisation is slightly higher during the dark phase when compared to the light phase. This continuous baseline recording over an 84 hr time

period is stable with only small fluctuations observed related to O_2 utilisation during various physiological phenomenon i.e. feeding, grooming and movement.

In summary, the data displays a stable baseline current with slight fluctuations observed indicative of the real-time monitoring of O_2. This baseline will provide a comparison for the repeated administration of reserpine (0.1 mg/kg) data, with any observed changes in the O_2 levels attributable to a drug effect.

6.3.6.2 Effect of Multiple Administration of Reserpine on Oxygen Levels

As mentioned previously, the repeated administration of a sub-effective dose (0.1 mg/kg) of reserpine is utilised as a pharmacological model of the progressive nature of PD. The administration of a single low dose of reserpine can induce deficits in emotional memory without causing motor alterations. This section investigates the effect the repeated administration of reserpine has on O_2 levels to determine the role of O_2 in the manifestation of oxidative stress in the striatum. Average O_2 levels monitored using carbon paste electrodes implanted in the striatum after administration of ten reserpine (0.1 mg/kg) injections subcutaneously is shown below in Figure 6.22

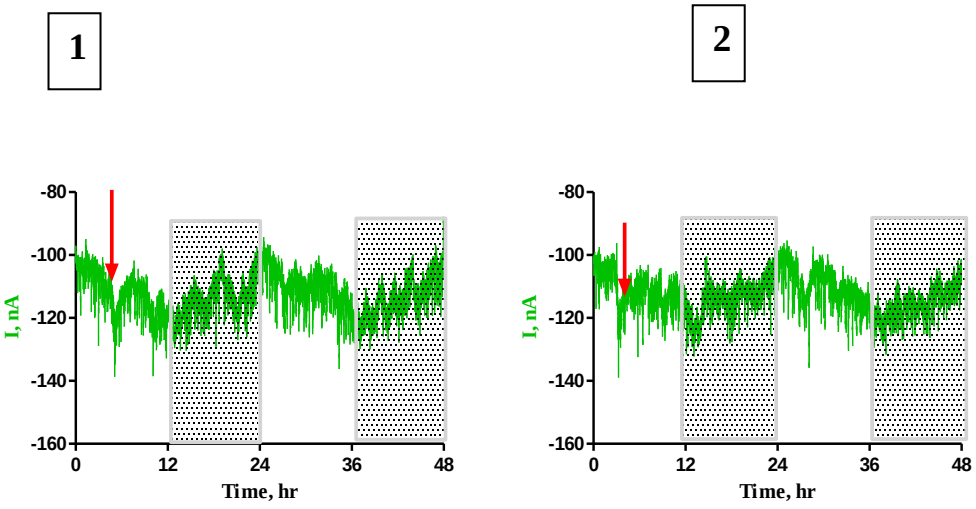

3

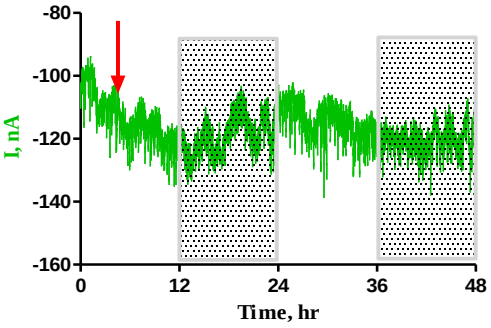
-80
-100
-120
-140
-160
I, nA
0
12
24
36
48
Time, hr

4

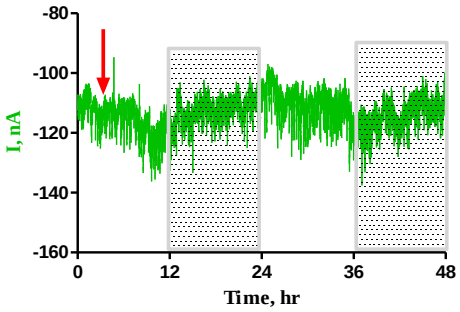
-80
-100
-120
-140
-160
I, nA
0
12
24
36
48
Time, hr

5

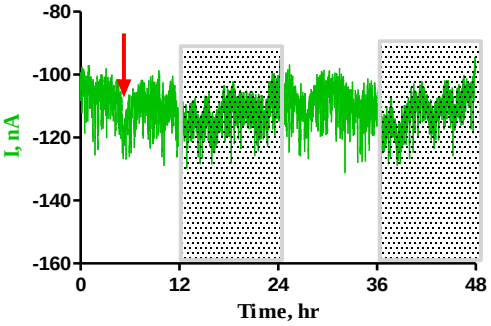
-80
-100
-120
-140
-160
I, nA
0
12
24
36
48
Time, hr

6

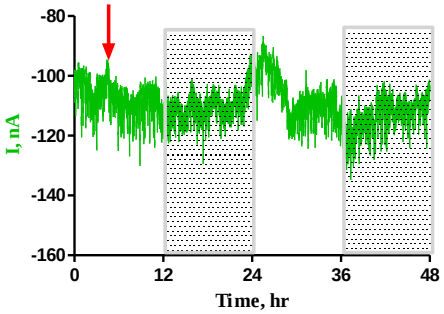
-80
-100
-120
-140
-160
I, nA
0
12
24
36
48
Time, hr

7

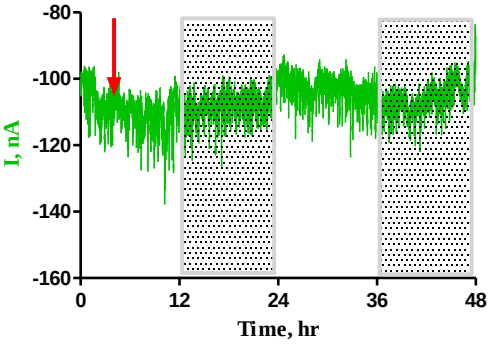
-80
-100
-120
-140
-160
I, nA
0
12
24
36
48
Time, hr

8

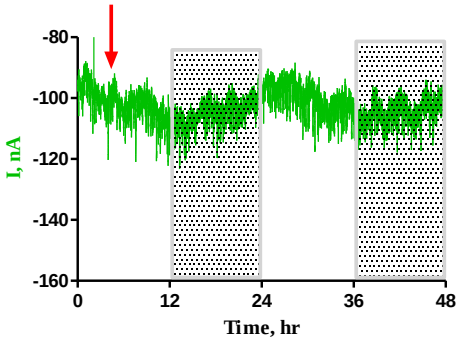
-80
-100
-120
-140
-160
I, nA
0
12
24
36
48
Time, hr

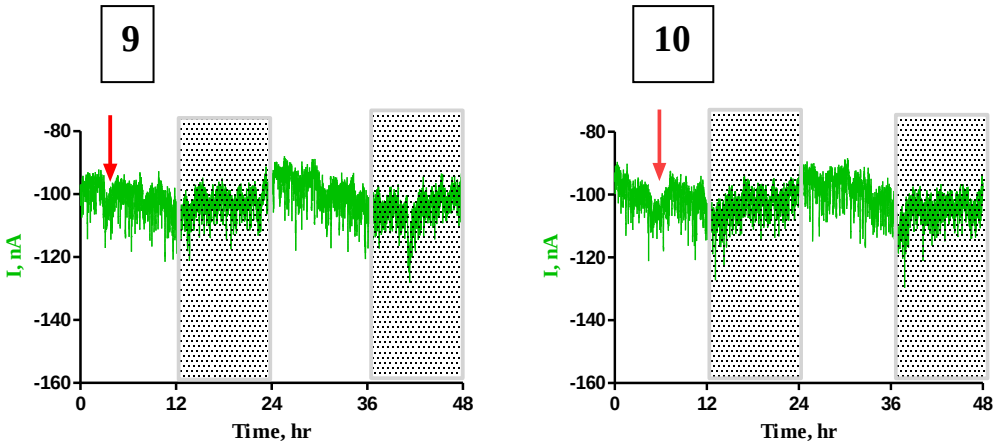

Figure 6.22: The average O_2 signal (n = 8) recorded in the striatum over a continuous 48 hr period following the repeated systemic administration of reserpine (0.1 mg/kg). Each number corresponds to the relevant injection (1-10), the red arrow indicates the administration of the reserpine injection. The shaded region represents the dark phase. The average SEM current for the O_2 sensors over the 10 reserpine injections was 5.12 ± 0.26 nA (n = 8).

The results above display the effect the repeated administration of reserpine has on the O_2 levels monitored by carbon paste electrodes implanted in the striatum. It is clear that similar to the baseline trace (see Figure 6.21) the O_2 levels change depending on the time of day. The O_2 levels increase during the light cycle (07:00-19:00) and decrease during the dark phase (19:00-07:00) when the animals are active. This trend is observed for all 48 hr time periods after the administration of the various reserpine injections (1-10).

Analysing the data over a 48 hr period, AUC analysis was performed in order to quantify any changes in striatal O_2 levels as a result of the drug administration. As mentioned previously for the NO sensors, each 12 hr data set was analysed individually and the mean was calculated. All data was background subtracted and the results are shown below in Figure 6.23

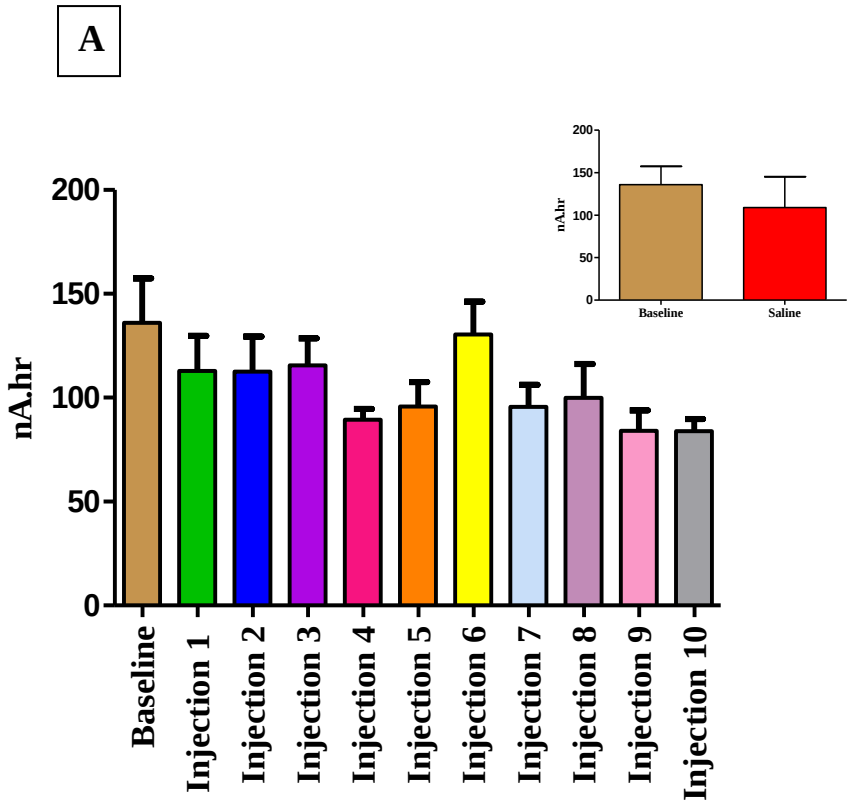
A
nA.hr
200
150
100
50
0
Baseline
Injection 1
Injection 2
Injection 3
Injection 4
Injection 5
Injection 6
Injection 7
Injection 8
Injection 9
Injection 10
nA.hr
200
150
100
50
0
Baseline
Saline

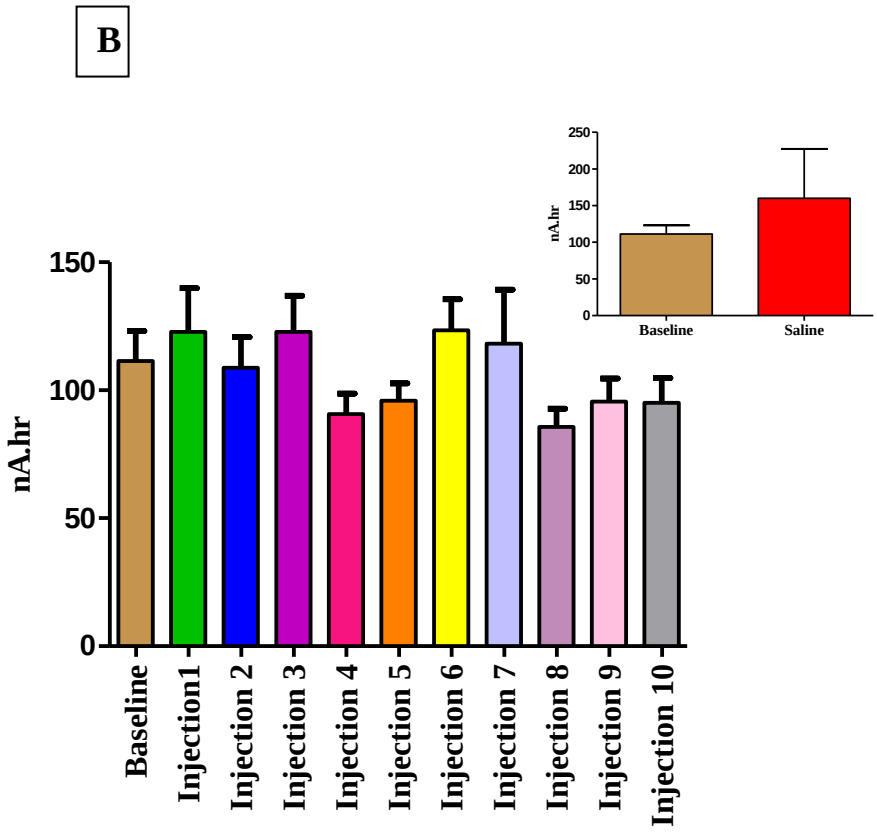
B
nA.hr
150
100
50
0
Baseline
Injection1
Injection 2
Injection 3
Injection 4
Injection 5
Injection 6
Injection 7
Injection 8
Injection 9
Injection 10
nA.hr
250
200
150
100
50
0
Baseline
Saline

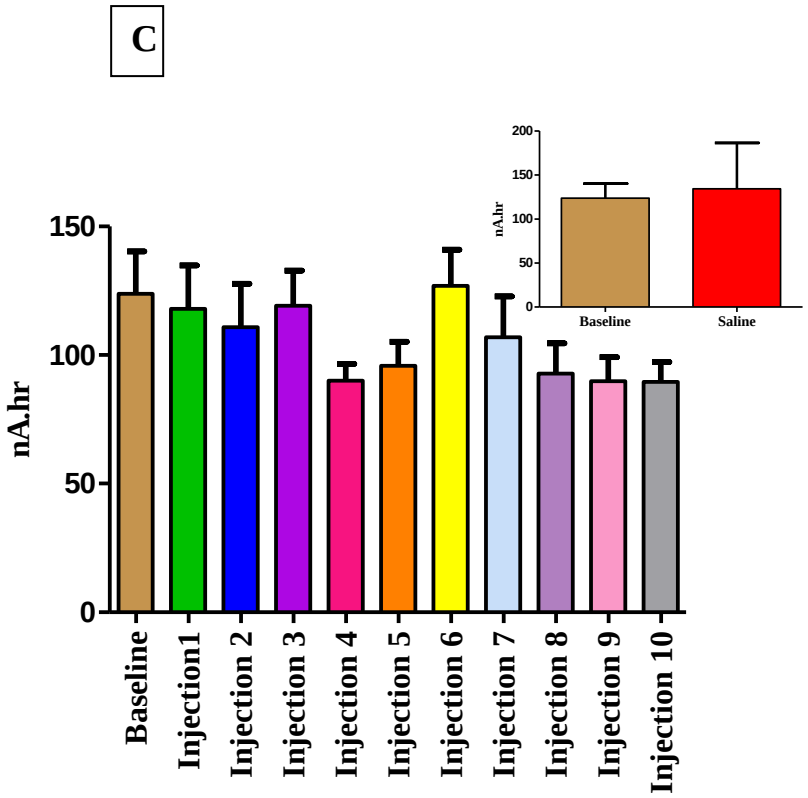

Figure 6.23: A bar chart displaying the changes in AUC for baseline O_2 levels and O_2 levels during multiple injections of reserpine (0.1 mg/kg) monitored by carbon paste electrodes implanted in the striatum. Inset displays a comparison between the AUC calculated for O_2 levels recorded during a baseline period and after a saline injection. This bar chart displays the changes over the course of 2 day periods starting at 11:30 (A) 2 night periods beginning at 23:30 (B) and over the 48 hr period (C) with the average total area plotted.

The figure above displays the differences in the AUC values calculated during a baseline period and after the administration of 10 reserpine injections. The inset displays the difference between the AUC value calculated for the O_2 levels recorded during a baseline period and after the administration of saline. The saline injection, however, needs to be repeated as this shows a n = 2 in one animal so the error calculated is very large.

Analysing the data over a 48 hr period gives a baseline AUC value of 123.76 ± 16.55 nA.hr (n = 8) and this value will be used to compare the effect of the drug on the striatal O_2 levels. A change (P = 0.8083 and P = 0.5918) in the AUC value is recorded

48 hrs after the 1st and 2nd injection when compared to the baseline levels, with values of 117.90 ± 16.97 nA.hr (n = 8) and 110.75 ± 14.42 nA.hr being obtained respectively. Injection 3 shows a similar result (P = 0.8345) to the baseline with a value of 119.20 ± 13.60 nA.hr calculated. However, a small change (P = 0.0791 and P = 0.1634) in the AUC is recorded for injections 4 and 5 respectively, however, both values 90.04 ± 6.57 nA.hr (n = 8) and 95.82 ± 9.32 nA.hr are not significantly different to the baseline value of 123.76 ± 16.55 nA.hr (n = 8). Injection 6 shows an almost identical AUC value (P = 0.8850) of 126.95 ± 13.97 nA.hr (n = 8) when compared to the baseline value which suggests no variation in O_2 levels in the striatum after the administration of the 6th injection. However, similarly to the NO levels the O_2 levels change between the 7th and 10th injections. A difference (P = 0.4578) in the AUC value (106.92 ± 15.87 nA.hr, n = 8) is observed after the 7th injection when compared to the baseline value of 123.76 ± 16.55 nA.hr. Similarly, injection 8 demonstrates a further change in the AUC value recorded to 92.87 ± 11.72 nA.hr which is not significantly different (P = 0.1489) to the baseline value of 123.76 ± 16.55 nA.hr (n = 8). Injections 9 and 10 show almost identical values of 89.77 ± 9.45 nA.hr and 89.50 ± 7.81 nA.hr, respectively, with neither significantly different (P = 0.0962 and P = 0.0822) to the baseline value of 123.76 ± 16.55 nA.hr (n = 8).

The animals submitted to the repeated dose of reserpine every second day showed no visible difference in their appearance, however, they developed ocular discharge after the 3/4th injection of reserpine. Nasal congestion is the main side effect of reserpine. The animals maintained their weight over the 30 days and reacted normally when provoked. Again, as mentioned previously, no signs of motor impairment were observed in the animals particularly between injections 7-10 which has been previously reported (Fernandes *et al.*, 2012). However, in the absence of detailed behavioural testing (novel object recognition, fear conditioning etc) it is difficult to replicate these results in this research. However, no signs of motor impairment were observed in any of the animals submitted to the reserpine treatment.

In summary, this section provides a detailed account of the effect the repeated administration of reserpine (0.1 mg/kg) has on striatal O_2 levels. The change in these O_2 levels were quantified using AUC analysis, however, no significant difference was observed in any of the values.

6.3.7: Light Reversal

This section investigates the impact light reversal; lights on (19:00-07:00) and lights off (07:00-19:00) induces on NO and O_2 levels monitored using NO sensors and carbon paste electrodes respectively implanted in the striatum. A baseline period of 48 hrs was given to allow the sensors to settle before the animals started the light reversal experiments. As shown previously in Figure 6.7, NO shows diurnal changes, NO levels in the striatum increase during the day and decrease at night when the animals are more active. Similarly, striatal O_2 levels show diurnal changes as demonstrated previously in Figure 6.12. This shows a similar result to NO with O_2 levels increasing during the day and decreasing at night when O_2 utilisation is higher. The animals used in this set of experiments were used previously in the repeated administration of reserpine experiments, however, they were given a rest period of 2 weeks before the commencement of the light reversal experiment to eliminate/minimise any effect of the drug. Figure 6.24 shows the influence light reversal induces on striatal O_2 and NO levels over a week, monitored using NO sensors and carbon paste electrodes.

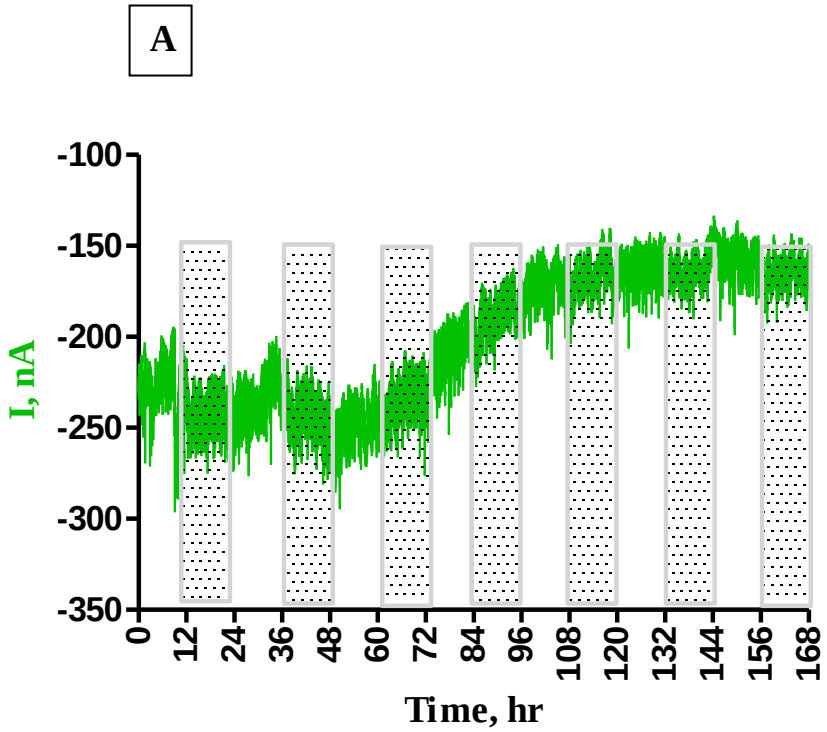

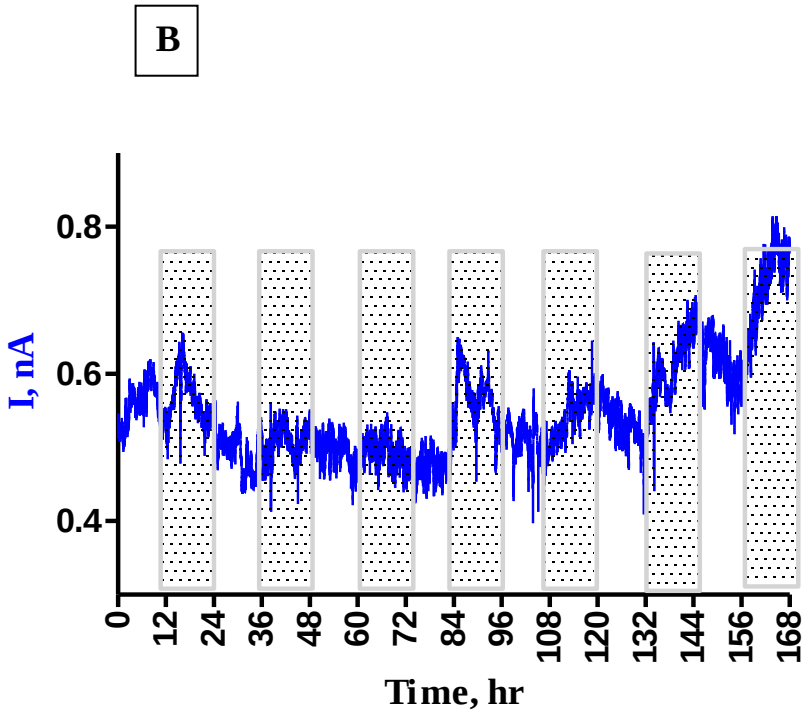

Figure 6.24: A time *vs.* current profile for (A) O_2 levels monitored by carbon paste electrodes (n = 3, SEM = 24.927 nA), and (B) NO levels recorded by NO sensors (n = 3, SEM = 0.104 nA) recorded over 168 hrs. The shaded region represents the dark phase from 07:00-19:00.

The figure above demonstrates the impact light reversal induces on striatal NO and O_2 levels over a 168 hr period showing the beginning of the light reversal experiment where the animals were exposed to light from 19:00–07:00 hr instead of their previously dark phase. It is clear, that both NO and O_2 levels demonstrate diurnal changes as observed previously, both recorded an increase between 07:00 – 19:00 and a decrease between 19:00-07:00. Therefore the circadian pattern remains unchanged however the diurnal changes are switched. Fillenz and O'Neill demonstrated that levels of motor activity was immediately disrupted after the reversal of the light/dark cycle and the pattern was re-established 8 days after light reversal (Fillenz and O'Neill, 1986). Interestingly, after 70 hrs the O_2 signal decreases and then remains stable with only small fluctuations observed over the 108-168 hr time period. Similarly for the NO data, the signal increases between 108-168 hr time period, however the diurnal changes are still evident; an increase in NO is observed between 07:00-19:00 during the dark phase and a decrease during the light period (19:00-07:00). Nitric oxide

synthase (NOS) plays an essential role in the synthesis of NO and acts as a mediator for many physiological processes, including mechanisms regulating biological clocks and circadian rhythms. Machado-Nils *et al.* demonstrates that an oscillation in iNOS activity and nNOS protein content occurs in the hippocampus of pigeons similar to experimental results shown in several brain regions in rodents (Machado-Nils *et al*., 2013). Clement and co-workers analysed the links existing between cortical release of NO and the NOS expression and activity in adult rats during baseline conditions, during a 24 hr paradoxical sleep deprivation (PSD) and during the subsequent recovery. The results demonstrated that during baseline conditions a marked circadian coupling exists between cortical release of NO and the NOS expression while a long-lasting disruption takes place during PSD and recovery (Clément *et al.*, 2004). Therefore the results above suggests that a homeostatic circadian regulation of the sleep-wake cycle takes place, the release of NO occurs phase-locked with the nNOS expression and activity.

In summary, these results demonstrate the effects light reversal induces on striatal NO and O_2 levels. These experiments show that NO and O_2 circadian patterns remain unaltered, however, the diurnal changes are switched an increase in NO and O_2 is observed at 07:00 and a decrease is recorded at 19:00. However, this investigation was performed in one animal with 3 carbon paste sensors and one animal with 3 NO sensors implanted in the striatum therefore, further studies are required in order to verify these results.

6.4: Conclusion

The initial aim of this chapter was to monitor the changes in NO and O_2 in a known animal model of PD. This investigation involved the administration of an acute (5 mg/kg) and chronic (0.1 mg/kg) dose of reserpine and to monitor the changes in NO and O_2 levels over long periods of time. It has been speculated that ROS and oxidative stress contribute to the pathogenesis of PD (Jenner and Olanow, 1996) and evidence of damage induced by oxidative stress has been discovered in both brain tissue from PD patients (Beal, 2002) and in pharmacological models such as reserpine (Bilska *et al*., 2007) (Spina and Cohen, 1989) and 1 methyl-4-phenyl-1,2,3,6-tetrahydropyrine (MPTP) (Obata, 2002). However, the results shown in this chapter postulate that O_2

and NO are not good markers of oxidative stress, particularly in this animal model of PD. No significance difference in NO or O_2 levels were observed after the administration of a single 5 mg/kg reserpine injection which was verified by AUC analysis where similar values were calculated for baseline and reserpine treatment.

The repeated administration of a sub-effective dose of reserpine has been identified as a progressive model of PD (Fernandes *et al.*, 2012). However, the changes in the O_2 levels were quantified after each of the 10 reserpine injections and no significant difference was observed, however a decrease in the total area was observed from the 8-10th injection which Fernanades *et al*. had speculated to be the period were oxidative stress occurs. Similarly, the NO levels were recorded continuously over a 20 day period and AUC analysis was performed to quantify any changes in NO observed as a result of the administration of each reserpine injection. Again no significant difference in the NO levels were found after the administration of the 10 reserpine injections. However, the NO levels decreased after the 7th injection and remained decreased following the 8th injection with a return to baseline levels after the 9th injection.

However, current literature does not recognise reserpine as a useful model of PD arguing the lack of construct validity. There is no nigral striatal dopaminergic cell degeneration observed in this model and thus it tends to be restricted to accessing novel approaches to symptomatic treatment (Duty and Jenner, 2011). Other drawbacks of this model include its inability to induce neurodegeneration and protein aggregation and its lack of specificity regarding dopaminergic neurotransmission. Also, motor performance, monoamine content and tyrosine hydroxylase staining are partially restored after treatment interruption (Leão *et al.*, 2015). This suggests that reserpine may lack validity as a PD model. The results in this chapter correlate with this suggestion in terms of determining the role of NO and O_2 in the manifestation of oxidative stress and its role in the pathogenesis of PD.

NO has been implicated in the regulation of sleep (Calabrese *et al.*, 2007) (Obal Jr and Krueger, 2003). Previous work by Kostin and co-workers utilising the same NO sensor monitored extracellular levels of NO across a spontaneous sleep-wake cycle. This research determined that the electrode generated currents were higher during the dark phase when implanted in the PF-LHA (Kostin *et al*., 2013). However, the results

observed in this research showed an opposing trend, the NO levels increased during the light phase and decreased during the dark phase. This same trend was observed by Cespuglio *et al*. when monitoring NO levels in the nRD however an opposing trend similar to Kostin's results was observed in the Cx (Cespuglio *et al*., 2012). Therefore, it can be postulated that diurnal NO changes are region specific. Similarly, diurnal O_2 changes were observed; striatal O_2 levels increased during the light period and decreased during the dark period when the animals were more active. Therefore, it can be expected that O_2 utilisation is higher resulting in a decrease in the O_2 signal. The changes in striatal NO and O_2 levels were quantified using AUC analysis over a 72 hr period and it was determined that no significant change was observed in the NO/O_2 levels between the day and night phases. This control baseline data was used to account for any changes attributed to the reserpine administration over a longer time period.

Finally, preliminary investigations of light reversal involving 2 animals (one with O_2 sensors and the other with NO sensors both implanted in the striatum) over a 168 hr period was performed. An increase in the NO signal was observed between 07:00-19:00 while a decrease was monitored between 19:00 and 07:00, irrespective of lights on or off. Similarly O_2 levels were monitored by carbon paste electrodes, the circadian rhythm an increase in O_2 observed between 07:00-19:00 and a decrease recorded between 19:00-07:00 was demonstrated for 60 hrs. However, after 60 hrs the O_2 signal decreased and remained almost stable with minor fluctuations between 108-166 hrs. Further investigations will have to be performed in order to verify these results.

Although this research remains inconclusive on the role of oxidative stress using NO and O_2 as markers of oxidative stress in this particular animal model of PD, other ROS such as H_2O_2 and O_2^- may provide previously undetermined information surrounding the etiology and pathophysiology of PD using this animal model. However, the baseline recorded data for both NO and O_2 levels in the striatum over extended periods of time provides a novel insight and foundation for further studies into the role of both species in the regulation of sleep.

6.5: References

Abílio V, Vera J, Ferreira L, *et al.* (2002) Effects of melatonin on orofacial movements in rats. *Psychopharmacology* 161: 340-347.

Antkiewicz-Michaluk L, Wąsik A, Możdżeń E, *et al.* (2015) Withdrawal from repeated administration of a low dose of reserpine induced opposing adaptive changes in the noradrenaline and serotonin system function: A behavioral and neurochemical *ex vivo* and *in vivo* studies in the rat. *Progress in Neuro-Psychopharmacology and Biological Psychiatry* 57: 146-154.

Arora V and Chopra K. (2013) Possible involvement of oxido-nitrosative stress induced neuro-inflammatory cascade and monoaminergic pathway: Underpinning the correlation between nociceptive and depressive behaviour in a rodent model. *Journal of Affective Disorders* 151: 1041-1052.

Barbosa RM, Lourenço CF, Santos RM, *et al.* (2008) Chapter Twenty - *In Vivo* Real-Time Measurement of Nitric Oxide in Anesthetized Rat Brain. In: Enrique C and Lester P (eds) *Methods in Enzymology.* Academic Press, 351-367.

Barzilay J, Grimm R, Cushman W, *et al*. (2007) Getting to Goal Blood Pressure: Why Reserpine Deserves a Second Look. *The Journal of Clinical Hypertension* 9: 591-594.

Bazzu G, Puggioni GGM, Dedola S, *et al.* (2009) Real-Time Monitoring of Brain Tissue Oxygen Using a Miniaturized Biotelemetric Device Implanted in Freely Moving Rats. *Analytical Chemistry* 81: 2235-2241.

Beal MF. (2002) Oxidatively modified proteins in aging and disease1,2. *Free Radical Biology and Medicine* 32: 797-803.

Betarbet R, Sherer TB and Greenamyre JT. (2002) Animal models of Parkinson's disease. *BioEssays* 24: 308-318.

Bilska A, Dubiel M, Sokołowska-Jez˙ewicz M, *et al.* (2007) Alpha-lipoic acid differently affects the reserpine-induced oxidative stress in the striatum and prefrontal cortex of rat brain. *Neuroscience* 146: 1758-1771.

Bolger FB, Bennett R and Lowry JP. (2011(a)) An *in vitro* characterisation comparing carbon paste and Pt microelectrodes for real-time detection of brain tissue oxygen. *Analyst* 136: 4028-4035.

Bolger FB and Lowry JP. (2005) Brain Tissue Oxygen: *In Vivo* Monitoring with Carbon Paste Electrodes. *Sensors* 5: 473-487.

Bolger FB, McHugh SB, Bennett R, *et al.* (2011(b)) Characterisation of carbon paste electrodes for real-time amperometric monitoring of brain tissue oxygen. *Journal of Neuroscience Methods* 195: 135-142.

Bowers D, Miller K, Mikos A, *et al.* (2006) Startling facts about emotion in Parkinson's disease: blunted reactivity to aversive stimuli. *Brain* 129: 3356-3365.

Brown FO, Finnerty NJ and Lowry JP. (2009) Nitric oxide monitoring in brain extracellular fluid: characterisation of Nafion®-modified Pt electrodes *in vitro* and *in vivo*. *Analyst* 134: 2012-2020.

Burlet S and Cespuglio R. (1997) Voltammetric detection of nitric oxide (NO) in the rat brain: its variations throughout the sleep-wake cycle. *Neuroscience Letters* 226: 131-135.

Cadenas E and Davies KJA. (2000) Mitochondrial free radical generation, oxidative stress, and aging1. *Free Radical Biology and Medicine* 29: 222-230.

Calabrese V, Mancuso C, Calvani M, *et al.* (2007) Nitric oxide in the central nervous system: neuroprotection versus neurotoxicity. *Nat Rev Neurosci* 8: 766-775.

Carlsson A, Lindqvist M and Magnusson TOR. (1957) 3,4-Dihydroxyphenylalanine and 5-Hydroxytryptophan as Reserpine Antagonists. *Nature* 180: 1200-1200.

Carvalho RC, Patti CC, Takatsu-Coleman AL, *et al.* (2006) Effects of reserpine on the plus-maze discriminative avoidance task: Dissociation between memory and motor impairments. *Brain Research* 1122: 179-183.

Caudle WM, Colebrooke RE, Emson PC, *et al.* (2008) Altered vesicular dopamine storage in Parkinson's disease: a premature demise. *Trends in Neurosciences* 31: 303-308.

Cespuglio R, Amrouni D, Meiller A, *et al.* (2012) Nitric oxide in the regulation of the sleep-wake states. *Sleep Medicine Reviews* 16: 265-279.

Chen CN, Chang KC, Lin RF, *et al.* (2016) Nitric oxide pathway activity modulation alters the protective effects of (−)Epigallocatechin-3-gallate on reserpine-induced impairment in rats. *Behavioural Brain Research* 305: 198-211.

Clément P, Sarda N, Cespuglio R, *et al.* (2004) Changes occurring in cortical NO release and brain NO-synthases during a paradoxical sleep deprivation and subsequent recovery in the rat. *Journal of Neurochemistry* 90: 848-856.

Cooper JA, Sagar HJ, Jordan N, *et al.* (1991) Cognitive impairment in early, untreated Parkinson's disease and its relationship to motor disability. *Brain* 114: 2095-2122.

Cunha AS, Matheus FC, Moretti M, *et al*. (2016) Agmatine attenuates reserpine-induced oral dyskinesia in mice: Role of oxidative stress, nitric oxide and glutamate NMDA receptors. *Behavioural Brain Research* 312: 64-76.

Dauer W and Przedborski S. (2003) Parkinson's Disease: Mechanisms and Models. *Neuron* 39: 889-909.

Dluzen DE, Bhatt S and McDermott JL. (2008) Differences in reserpine-induced striatal dopamine output and content between female and male mice: Implications for sex differences in vesicular monoamine transporter 2 function. *Neuroscience* 154: 1488-1496.

Duty S and Jenner P. (2011) Animal models of Parkinson's disease: a source of novel treatments and clues to the cause of the disease. *British Journal of Pharmacology* 164: 1357-1391.

El-Deab MS and Ohsaka T. (2003) Quasi-reversible two-electron reduction of oxygen at gold electrodes modified with a self-assembled submonolayer of cysteine. *Electrochemistry Communications* 5: 214-219.

Fernandes VS, Ribeiro AM, Melo TG, *et al.* (2008) Memory impairment induced by low doses of reserpine in rats: Possible relationship with emotional processing deficits in Parkinson disease. *Progress in Neuro-Psychopharmacology and Biological Psychiatry* 32: 1479-1483.

Fernandes VS, Santos JR, Leão AHFF, *et al.* (2012) Repeated treatment with a low dose of reserpine as a progressive model of Parkinson's disease. *Behavioural Brain Research* 231: 154-163.

Fillenz M and O'Neill RD. (1986) Effects of light reversal on the circadian pattern of motor activity and voltammetric signals recorded in rat forebrain. *The Journal of Physiology* 374: 91-101.

Finnerty NJ, Bolger FB, Pålsson E, *et al.* (2013(a)) An Investigation of Hypofrontality in an Animal Model of Schizophrenia Using Real-Time Microelectrochemical Sensors for Glucose, Oxygen, and Nitric Oxide. *ACS Chemical Neuroscience* 4: 825-831.

Finnerty NJ, O'Riordan SL, Brown FO, *et al.* (2012) *In vivo* characterisation of a Nafion®-modified Pt electrode for real-time nitric oxide monitoring in brain extracellular fluid. *Analytical Methods* 4: 550-557.

Finnerty NJ, O'Riordan SL, Lowry JP, *et al.* (2013(b)) Continuous Real-Time *in vivo* Measurement of Cerebral Nitric Oxide Supports Theoretical Predictions of an Irreversible Switching in Cerebral ROS after Sufficient Exposure to External Toxins. *Journal of Parkinson's Disease* 3: 351-362.

Francois J, Conway MW, Lowry JP, *et al.* (2012) Changes in reward-related signals in the rat nucleus accumbens measured by *in vivo* oxygen amperometry are consistent with fMRI BOLD responses in man. *NeuroImage* 60: 2169-2181.

Gandhi S and Abramov AY. (2012) Mechanism of oxidative stress in neurodegeneration. *Oxidative Medicine and Cellular Longevity* 2012.

Gołembiowska K and Dziubina A. (2012) The Effect of Adenosine A2A Receptor Antagonists on Hydroxyl Radical, Dopamine, and Glutamate in the Striatum of Rats with Altered Function of VMAT2. *Neurotoxicity Research* 22: 150-157.

Guo Z, Liu X and Huang H. (2015) Kinetics and Thermodynamics of Reserpine Adsorption onto Strong Acidic Cationic Exchange Fiber. *PLoS ONE* 10: e0138619.

Hafkenschiel JH, Sellers AM, King GA, *et al.* (1955) Preliminary Observations on the Effects of Parenteral Reserpine on Cerebral Blood Flow, Oxygen and Glucose Metabolism, and Electroencephalograms of Patients with Essential Hypertension. *Annals of the New York Academy of Sciences* 61: 78-84.

Heeringa MJ and Abercrombie ED. (1995) Biochemistry of Somatodendritic Dopamine Release in Substantia Nigra: An *In Vivo* Comparison with Striatal Dopamine Release. *Journal of Neurochemistry* 65: 192-200.

Hoffman JS and Domino EF. (1969) Comparative Effects of Reserpine on the Sleep Cycle of Man and Cat. *Journal of Pharmacology and Experimental Therapeutics* 170: 190-198.

Holmström N, Nilsson P, Carlsten J, *et al.* (1998) Long-term *in vivo* experience of an electrochemical sensor using the potential step technique for measurement of mixed venous oxygen pressure1. *Biosensors and Bioelectronics* 13: 1287-1295.

Jenner P and Olanow CW. (1996) Oxidative stress and the pathogenesis of Parkinson's disease. *Neurology* 47: 161S-170S.

Kealy J, Bennett R and Lowry JP. (2013) Simultaneous recording of hippocampal oxygen and glucose in real time using constant potential amperometry in the freely-moving rat. *Journal of Neuroscience Methods* 215: 110-120.

Kostin A, McGinty D, Szymusiak R, *et al.* (2013) Sleep-wake and diurnal modulation of nitric oxide in the perifornical-lateral hypothalamic area: Real-time detection in freely behaving rats. *Neuroscience* 254: 275-284.

Leão AHFF, Sarmento-Silva AJ, Santos JR, *et al.* (2015) Molecular, Neurochemical, and Behavioral Hallmarks of Reserpine as a Model for Parkinson's Disease: New Perspectives to a Long-Standing Model. *Brain Pathology* 25: 377-390.

Li J, Bravo DS, Louise Upton A, *et al.* (2011) Close temporal coupling of neuronal activity and tissue oxygen responses in rodent whisker barrel cortex. *European Journal of Neuroscience* 34: 1983-1996.

Loschen G, Azzi A, Richter C, *et al.* (1974) Superoxide radicals as precursors of mitochondrial hydrogen peroxide. *FEBS Letters* 42: 68-72.

Lowry JP, Boutelle MG and Fillenz M. (1997) Measurement of brain tissue oxygen at a carbon paste electrode can serve as an index of increases in regional cerebral blood flow. *Journal of Neuroscience Methods* 71: 177-182.

Lowry JP, Boutelle MG, O'Neill RD, *et al*. (1996) Characterisation of carbon paste electrodes in vitro for simultaneous amperometric measurement of changes in oxygen and ascorbic acid concentrations *in vivo. Analyst* 121: 761-766.

Lowry JP, Griffin K, McHugh SB, *et al.* (2010) Real-time electrochemical monitoring of brain tissue oxygen: A surrogate for functional magnetic resonance imaging in rodents. *NeuroImage* 52: 549-555.

Machado-Nils AV, de Faria LO, Vieira AS, *et al.* (2013) Daily cycling of nitric oxide synthase (NOS) in the hippocampus of pigeons (C. livia). *Journal of Circadian Rhythms* 11: 1.

Martin HL and Teismann P. (2009) Glutathione—a review on its role and significance in Parkinson's disease. *The FASEB Journal* 23: 3263-3272.

McHugh SB, Fillenz M, Lowry JP, *et al*. (2011) Brain tissue oxygen amperometry in behaving rats demonstrates functional dissociation of dorsal and ventral hippocampus during spatial processing and anxiety. *European Journal of Neuroscience* 33: 322-337.

Obal Jr F and Krueger J. (2003) Biochemical regulation of non-rapid-eye-movement sleep. *Frontiers in Bioscience: A Journal and Virtual Library* 8: d520-550.

Obata T. (2002) Dopamine efflux by MPTP and hydroxyl radical generation. *Journal of Neural Transmission* 109: 1159-1180.

Okano H, Masuda H and Ohkubo C. (2005) Effects of 25 mT static magnetic field on blood pressure in reserpine-induced hypotensive Wistar-Kyoto rats. *Bioelectromagnetics* 26: 36-48.

Olanow C and Tatton W. (1999) Etiology and pathogenesis of Parkinson's disease. *Annual Review of Neuroscience* 22: 123-144.

Ormonde DE and O'Neill RD. (1990) The oxidation of ascorbic acid at carbon paste electrodes. *Journal of Electroanalytical Chemistry and Interfacial Electrochemistry* 279: 109-121.

Pålsson E, Finnerty N, Fejgin K, *et al.* (2009) Increased cortical nitric oxide release after phencyclidine administration. *Synapse* 63: 1083-1088.

Rosenthal J and Page IH. (2012) *Arterial Hypertension: Pathogenesis, Diagnosis, and Therapy*: Springer New York.

Russell DM, Garry EM, Taberner AJ, *et al.* (2012) A fully implantable telemetry system for the chronic monitoring of brain tissue oxygen in freely moving rats. *Journal of Neuroscience Methods* 204: 242-248.

Santos JR, Cunha JAS, Dierschnabel AL, *et al.* (2013) Cognitive, motor and tyrosine hydroxylase temporal impairment in a model of parkinsonism induced by reserpine. *Behavioural Brain Research* 253: 68-77.

Schapira AH and Jenner P. (2011) Etiology and pathogenesis of Parkinson's disease. *Movement Disorders* 26: 1049-1055.

Sharma S, Moon CS, Khogali A, *et al.* (2013) Biomarkers in Parkinson's disease (recent update). *Neurochemistry International* 63: 201-229.

Spina MB and Cohen G. (1989) Dopamine turnover and glutathione oxidation: implications for Parkinson disease. *Proceedings of the National Academy of Sciences* 86: 1398-1400.

Stitzel RE. (1976) The biological fate of reserpine. *Pharmacological Reviews* 28: 179-208.

Venton BJ, Michael DJ and Wightman RM. (2003) Correlation of local changes in extracellular oxygen and pH that accompany dopaminergic terminal activity in the rat caudate–putamen. *Journal of Neurochemistry* 84: 373-381.

von Bohlen und Halbach O. (2005) Modeling Neurodegenerative Diseases *in vivo* Review. *Neurodegenerative Diseases* 2: 313-320.

Wisor JP, Gerashchenko D and Kilduff TS. (2011) Sleep-active neuronal nitric oxide synthase-positive cells of the cerebral cortex: a local regulator of sleep? *Current Topics in Medicinal Chemistry* 11: 2483-2489.

Wynne AM, Reid CH and Finnerty NJ. (2014) *In vitro* characterisation of ortho phenylenediamine and Nafion®-modified Pt electrodes for measuring brain nitric oxide. *Journal of Electroanalytical Chemistry* 732: 110-116.

Chapter 7
Conclusions

7.1 General Conclusions

The mammalian brain is a very complex organ that supports a wide range of functions including sensory input and processing, behavioural output or response, emotional response, memory and cognition. A number of techniques have been employed to determine the structure, metabolism and the role of neurochemicals in the brain. These include non-invasive techniques such as functional magnetic imaging (Austin *et al.*, 2003), spectroscopic analyses, positron emission tomography (Phelps, 2000) and invasive techniques including microdialysis (Miele and Fillenz, 1996) and Long Term *In-Vivo* Electrochemistry (LIVE) (O'Neill and Lowry, 2006). LIVE enables the in-situ detection of substances in the extracellular fluid (ECF). This technique involves the implantation of electrodes into specific brain regions, the application of a suitable potential and recording of the resulting Faradaic current which monitors the changes in the concentration of a variety of substances in the ECF with high temporal resolution over extended periods. This allows for the monitoring of analytes involved in neuronal signalling, drug actions and behaviours.

Electrochemical techniques have been utilised in the development of sensors for the detection of several electroactive species including oxygen (O_2) (Bolger and Lowry, 2005), nitric oxide (NO) (Brown and Lowry, 2003), ascorbic acid (AA) (Boutelle *et al*., 1989), dopamine (Robinson *et al*., 2003) and 5-hydroxytryptamine (5-HT) (Jackson *et al*., 1995). However, in order to extend this technique to detect electroinactive species such as glucose, choline, lactate and glutamate, biosensors have been developed. A biosensor is defined as a self-contained integrated device incorporating a biological recognition element in close proximity to an electrochemical transduction element (Wilson and Gifford, 2005) (Thévenot *et al.*, 2001). The development of biosensors has extended the pool of species which can be detected in the intact brain using LIVE. However, the electroactive compounds present in the ECF, tend to oxidise at similar potentials therefore, causing selectivity problems. The incorporation of permselective membranes has been utilised in the development of sensors, in order to improve the selectivity of the sensors by blocking other electroactive species (McMahon and O'Neill, 2005) (Lowry *et al.*, 1994). In addition, utilising this technique in the intact brain poses problems including; the composition of brain tissue can decrease the sensitivity of the sensor as a result of fouling (Garguilo and Michael, 1994) and restricted mass transport compared to the *in-vitro* environment (O'Neill, 1993). The primary aim of this thesis is the development of a biosensor

that can detect, with appropriate sensitivity and selectivity, the reactive oxygen species (ROS) superoxide (O_2^-) in the mammalian brain.

Electrochemical sensors for the detection of O_2^- have previously been developed by several research groups. Mesaros and coworkers have developed an amperometric O_2^- biosensor by the anodic polymerisation of pyrrole and concomitant immobilisation of superoxide dismutase (SOD) on Pt wire. The sensor was held at +700 mV, has a detection limit of 15 nM and a response time of 3-5 s (Mesároš *et al.*, 1998). Manning *et al.* designed a sensor by covalently attaching cytochrome c to a gold working electrode through surface modification with DTSSP (3,3'-dithiobis(sulfosuccinimidylpropionate)). The electrode was held at +100 mV and the detection limit was 10 nM (Manning *et al.*, 1998) (Manning and McNeil, 2011). Campanella *et al.* developed a O_2^- biosensor based on SOD which is physically entrapped in a kappa-carrageenan gel membrane (Campanella *et al*., 2000). The immobilised enzyme is then situated between the cellulose acetate membrane and a dialysis membrane and the whole assembly is fixed to the transducer by means of an O-ring. The Pt anode is then held at +650 mV with the sensor having a minimum detection limit of 0.01 mM and a response time ≤ 100 s.

Chapter 4 outlines the developmental steps undertaken to develop a sensitive and selective O_2^- biosensor for *in-vivo* neurochemical applications. The effect the addition of an immobiliser, stabilisers and cross-linkers were investigated in terms of their use in conjunction with the enzyme and their effect on the sensor's sensitivity and kinetic parameters. The immobilisation matrices utilised were both styrene and methyl methacrylate (MMA). It was determined that 5 layers of enzyme immobilised within these matrices was optimal for the biosensor design. The optimal enzyme unit of activity was determined to be a 200 U enzyme solution. The incorporation of a cross-linker GA, alongside PEI proved advantageous, however, the inclusion of the stabiliser BSA resulted in a significant decrease in the V_{max} current and K_m concentration recorded. These three components were extensively characterised in terms of their effect on the immobilisation of the enzyme until the optimal concentration and position in the layering process was determined for maximising O_2^- detection. The best design recorded was Sty-(SOD-0.5%GA-2%PEI)$_5$ which has a sensitivity of 0.91 ± 0.06 nA/µM , V_{max} of 15.98 ± 0.15 nA and a K_m concentration of 10.33 ± 0.27 µM (n = 17).

The aim of Chapter 5 was to determine an accurate and selective representation of current generated by the enzymatic dismutation of O_2^- at the Pt surface. Firstly, this chapter demonstrated that uric acid (UA) was generated as a by-product of the xanthine/XOD system.

This interferent molecule was successfully eliminated with the addition of the size exclusion polymer poly-*o*-phenylenediamine (PPD). PPD blocks access of larger interferent molecules such as AA and UA but smaller molecules such as H_2O_2 can permeate the layer (O'Brien *et al*., 2007) (Rothwell *et al.*, 2008), therefore the biosensor's signal is not compromised. This chapter also demonstrated that the spontaneous dismutation of O_2^- is taking place in the electrochemical cell generating H_2O_2. The production of H_2O_2 by the spontaneous dismutation of O_2^- was determined using catalase, a single 200 µL injection resulted in an instantaneous reduction in the electrochemical signal back to baseline. This was also verified using a Pt-Catalase biosensor whose design was based on a previously developed H_2O_2 biosensor (O'Brien *et al.*, 2007), where the signal was significantly reduced ($P < 0.0001$) when compared to the Pt-PPD sensor.

The contribution of this naturally occurring H_2O_2 is difficult to eliminate as H_2O_2 is permeable to the thin PPD layer. A dual sensor design can be employed and Section 5.3.8 shows this design in operation. The O_2^- biosensor described in this section consists of a pair of Pt electrodes, one with SOD immobilised on the electrode (O_2^- biosensor) and one without SOD (blank electrode). The H_2O_2 response of the blank sensor is lower than the SOD biosensor as this biosensor has SOD immobilised on the Pt surface which facilitates the enzymatic dismutation of O_2^- with the production of H_2O_2. Both sensors observe a signal from the spontaneous dismutation of H_2O_2 in the electrochemical cell, however, this response can be subtracted from the SOD biosensor to give the true response from the enzymatic dismutation of O_2^-. A O_2^- biosensor developed by McNeil and co-workers based on SOD-coated platinised activated carbon electrodes (PACE) (Pontie and Bedioui, 1999) utilised a similar subtraction method. The SOD-coated biosensor was polarised at +320 mV to estimate the H_2O_2 produced by the enzymatic disproportionation of O_2^- through its oxidation current and then a second electrode consisting of BSA coated PACE was incorporated to measure the natural disproportionation of O_2^- which was then subtracted from the combined current. Additionally, this chapter details advancements of the initial *in-vitro* characterisation determining the biosensor's limit of detection (LOD), response time and its ability to block interferences from electroactive species present in the ECF.

The initial aim of Chapter 6 was to monitor the changes in NO and O_2 in a known animal model of Parkinson's disease (PD). This investigation involved the administration of an acute (5 mg/kg) and chronic (0.1 mg/kg) dose of reserpine and to monitor the changes in NO and O_2

levels over long periods of time. It has been speculated that ROS and oxidative stress contribute to the pathogenesis of PD (Jenner and Olanow, 1996) and evidence of damage induced by oxidative stress has been discovered in both brain tissue from PD patients (Beal, 2002) and in pharmacological models such as reserpine (Bilska *et al*., 2007) (Spina and Cohen, 1989) and 1 methyl-4-phenyl-1,2,3,6-tetrahydropyrine (MTPT) (Obata, 2002). However, this chapter postulates that O_2 and NO are not good markers of oxidative stress particularly, in this animal model of PD. No significance difference in NO or O_2 levels were observed after the administration of a single 5 mg/kg reserpine injection which was verified by area under the curve (AUC) analysis which calculated similar values for animals treated with reserpine and the baseline.

The repeated administration of a sub-effective dose of reserpine has been identified as a progressive model of PD (Fernandes *et al.*, 2012). The changes in the O_2 levels were quantified after each of the 10 reserpine injections and no significant difference was observed. However, a decrease in the total area was observed from the 8-10th injection which Fernanades *et al*. had speculated to be the period were oxidative stress occurred. Similarly, the NO levels were recorded continuously over a 20 day period and AUC analysis was performed to quantify any changes in NO observed as a result of the administration of each reserpine injection. Again no significant difference in the NO levels were determined after the administration of the 10 reserpine injections. Similarly to O_2, the NO levels decreased after the 7th injection and remained decreased after the 8th injection with the levels returning to the baseline value after the 9th injection. However, current literature does not recognise reserpine as a useful model of PD arguing the lack of construct validity as no nigral striatal degeneration occurs (Duty and Jenner, 2011). The results obtained in this chapter correlate with this suggestion in terms of determining the role of NO and O_2 in the manifestation of oxidative stress and its role in the pathogenesis of PD

Finally, Chapter 6 shows preliminary investigations submitting 2 animals, one with O_2 sensors and the other with NO sensors both implanted in the striatum to light reversal to monitor the changes in NO and O_2 levels over a 168 hr period. An increase in the NO signal was observed between 07:00-19:00 while a decrease occurred between 19:00 and 07:00 irrespective of lights on or off. Similarly O_2 levels were monitored by carbon paste electrodes, the circadian rhythm (an increase in O_2 observed between 07:00-19:00 and a decrease recorded between 19:00-07:00) was demonstrated for 60 hrs. However, after 60 hrs the O_2 signal decreased and

remained almost stable with minor fluctuations between 108-166 hrs. Further investigations will have to be performed in order to verify these results.

This research demonstrates the development of a selective and sensitive O_2^- biosensor with a sub-second response time suitable for neurochemical monitoring of the target analyte. However, few reports exist of the monitoring of O_2^- *in-vivo*. Fabian *et al.* measured O_2^- *in-vivo* using a cytochrome c based platinised carbon electrode (Fabian *et al.*, 1995). This research demonstrated that this sensor was sensitive to changes in O_2^- levels and responsive to minute by minute changes in O_2^- levels during brain tissue injury and traumatic models of brain injury. Progression of this work would be a full *in-vivo* characterisation of this biosensor enabling therefore its use in neurochemical monitoring of O_2^- in various animal models of neurodegenerative diseases. This research remains inconclusive on the role of oxidative stress using NO and O_2 as markers of oxidative stress in this particular animal model of PD. Further work with this animal model involving the monitoring of other ROS such as H_2O_2 and O_2^- may provide previously undetermined information surrounding the etiology and pathophysiology of PD. NO has previously been speculated to be a regulator of sleep and preliminary results measured NO levels during light reversal and demonstrated that the circadian pattern remained unchanged, however, a switch in the diurnal changes was observed. Progression of this work would involve further investigations into the role NO plays in the regulation of sleep by monitoring the sleep-wake cycle in various brain regions including the hippocampus, prefrontal cortex, disruption of the sleep wake cycle by submitting animals to light reversal, determining the effects of sleep deprivation on NO levels, and investigating the effect the NO contribution has in the sleep impairments related to aging. Further work into the role of NO in sleep regulation could be investigated by the manipulation of NOS by administering local injections of NOS inhibitors and NOS donors such as L-NAME and L-NA and recording there effects on the NO signal observed during different sleep cycles.

7.2 References

Austin VC, Blamire AM, Grieve SM, *et al.* (2003) Differences in the BOLD fMRI response to direct and indirect cortical stimulation in the rat. *Magnetic Resonance in Medicine* 49: 838-847.

Beal MF. (2002) Oxidatively modified proteins in aging and disease1,2. *Free Radical Biology and Medicine* 32: 797-803.

Bilska A, Dubiel M, Sokołowska-Jez˙ewicz M, *et al.* (2007) Alpha-lipoic acid differently affects the reserpine-induced oxidative stress in the striatum and prefrontal cortex of rat brain. *Neuroscience* 146: 1758-1771.

Bolger FB and Lowry JP. (2005) Brain Tissue Oxygen: *In Vivo* Monitoring with Carbon Paste Electrodes. *Sensors* 5: 473-487.

Boutelle MG, Svensson L and Fillenz M. (1989) Rapid changes in striatal ascorbate in response to tail-pinch monitored by constant potential voltammetry. *Neuroscience* 30: 11-17.

Brown FO and Lowry JP. (2003) Microelectrochemical sensors for *in vivo* brain analysis: an investigation of procedures for modifying Pt electrodes using Nafion®. *Analyst* 128: 700-705.

Campanella L, Favero G, Persi L, *et al.* (2000) New biosensor for superoxide radical used to evidence molecules of biomedical and pharmaceutical interest having radical scavenging properties. *Journal of Pharmaceutical and Biomedical Analysis* 23: 69-76.

Duty S and Jenner P. (2011) Animal models of Parkinson's disease: a source of novel treatments and clues to the cause of the disease. *British Journal of Pharmacology* 164: 1357-1391.

Fabian RH, DeWitt DS and Kent TA. (1995) *In vivo* Detection of Superoxide Anion Production by the Brain Using a Cytochrome c Electrode. *Journal of Cerebral Blood Flow & Metabolism* 15: 242-247.

Fernandes VS, Santos JR, Leão AHFF, *et al.* (2012) Repeated treatment with a low dose of reserpine as a progressive model of Parkinson's disease. *Behavioural Brain Research* 231: 154-163.

Garguilo MG and Michael AC. (1994) Quantitation of choline in the extracellular fluid of brain tissue with amperometric microsensors. *Analytical Chemistry* 66: 2621-2629.

Jackson BP, Dietz SM and Wightman RM. (1995) Fast-scan cyclic voltammetry of 5-hydroxytryptamine. *Analytical Chemistry* 67: 1115-1120.

Jenner P and Olanow CW. (1996) Oxidative stress and the pathogenesis of Parkinson's disease. *Neurology* 47: 161S-170S.

Lowry JP, McAteer K, El Atrash SS, *et al*. (1994) Characterization of Glucose Oxidase-Modified Poly(phenylenediamine)-Coated Electrodes *in vitro* and *in vivo*: Homogeneous Interference by Ascorbic Acid in Hydrogen Peroxide Detection. *Analytical Chemistry* 66: 1754-1761.

Manning P and McNeil CJ. (2011) Electrochemical and optical sensing of reactive oxygen species: pathway to an integrated intracellular and extracellular measurement platform. *Biochemical Society Transactions* 39: 1288-1292.

Manning P, McNeil CJ, Cooper JM, *et al.* (1998) Direct, Real-Time Sensing of Free Radical Production by Activated Human Glioblastoma Cells. *Free Radical Biology and Medicine* 24: 1304-1309.

McMahon CP and O'Neill RD. (2005) Polymer−Enzyme Composite Biosensor with High Glutamate Sensitivity and Low Oxygen Dependence. *Analytical Chemistry* 77: 1196-1199.

Mesároš Š, Vaňková Ž, Grunfeld S, *et al.* (1998) Preparation and optimisation of superoxide microbiosensor. *Analytica Chimica Acta* 358: 27-33.

Miele M and Fillenz M. (1996) *In vivo* determination of extracellular brain ascorbate. *Journal of Neuroscience Methods* 70: 15-19.

O'Neill RD. (1993) Sensor-tissue interactions in neurochemical analysis with carbon paste electrodes *in vivo*. *Analyst* 118: 433-438.

O'Neill RD and Lowry JP. (2006) Voltammetry *In Vivo* for Chemical Analysis of the Living Brain. *Encyclopedia of Analytical Chemistry*. John Wiley & Sons, Ltd.

O'Brien K, Killoran S, O'Neill R, *et al.* (2007) Development and characterisation *in vitro* of a catalase-based biosensor for hydrogen peroxide monitoring. *Biosensors and Bioelectronics* 22: 2994-3000.

Obata T. (2002) Dopamine efflux by MPTP and hydroxyl radical generation. *Journal of Neural Transmission* 109: 1159-1180.

Phelps ME. (2000) Positron emission tomography provides molecular imaging of biological processes. *Proceedings of the National Academy of Sciences* 97: 9226-9233.

Pontie M and Bedioui F. (1999) Selective and sensitive electrochemical biosensing of superoxide anion production by biological systems: a short overview of recent trends. *Analusis* 27: 564-569.

Robinson DL, Venton BJ, Heien MLAV, *et al.* (2003) Detecting Subsecond Dopamine Release with Fast-Scan Cyclic Voltammetry *in Vivo*. *Clinical Chemistry* 49: 1763-1773.

Rothwell SA, Killoran SJ, Neville EM, *et al.* (2008) Poly (o-phenylenediamine) electrosynthesized in the absence of added background electrolyte provides a new permselectivity benchmark for biosensor applications. *Electrochemistry Communications* 10: 1078-1081.

Spina MB and Cohen G. (1989) Dopamine turnover and glutathione oxidation: implications for Parkinson disease. *Proceedings of the National Academy of Sciences* 86: 1398-1400.

Thévenot DR, Toth K, Durst RA, *et al.* (2001) Electrochemical biosensors: recommended definitions and classification1. *Biosensors and Bioelectronics* 16: 121-131.

Wilson GS and Gifford R. (2005) Biosensors for real-time *in vivo* measurements. *Biosensors and Bioelectronics* 20: 2388-2403.

Appendix

Oral Presentations

Doran,M.; *Development of a Biosensor for the In-Vivo Detection of Superoxide,* Postgraduate Research Day 2014, **Maynooth University**, (September 2014)

Doran,M; *Development of a Biosensor for the Neurochemical Monitoring of Superoxide*, 67th Irish Universities Chemistry Research Colloquium**, Maynooth University**, (June 2015)

Poster Presentations

Doran,M.; Finnerty,N.; Lowry, J. *Sleep Deprivation and Cellular Responses to Oxidative Stress: An Investigation of their Role in Neurological Disorders*, Irish Research Council Annual Symposium, **Dublin Convection Centre**, (September 2013)

Doran,M.; Finnerty,N.; Lowry, J. *The Role of Oxidative Stress in Sleep Deprivation and Neurological Disorders*, 3rd Plenary Meeting of the Research Data Alliance, **Croke Park Dublin**, (March 2014)

Doran,M.; Finnerty,N.; Lowry, J. *Development of an In-Vivo Biosensor for the Real-Time Detection of Superoxide,* 14th International Conference on Oxidative Stress, Redox Homeostasis and Antioxidants, **Paris**, (June 2014)

Doran,M.; Finnerty,N.; Lowry, J. *The Development of a Biosensor for Real-Time Monitoring of Brain Extracellular Superoxide*, Young Neuroscientists Symposium, **Trinity College Dublin**, (September 2014)

Doran,M.; Finnerty,N.; Lowry, J. *The Role of Oxidative Stress in the Manifestation of Parkinson's Disease,* 16th International Conference in Monitoring Molecules in Neuroscience, **Gothenberg, Sweden**, (May 2016)

Doran,M.; Finnerty,N.; Lowry, J. *Real-Time Monitoring of Oxidative Stress in a Model of Parkinson's Disease*, 68th Irish Universities Chemistry Research Colloquium, **University College Cork**, (June 2016)

Training Course Attended

In-Vivo Short Course in Neuroscience Techniques supported by the British Pharmacological and Physiological Society, **University of Glasgow and University of Strathclyde (June 2014)**